

Measurement and Control of Agglomeration for the Design of Crystalline Products

Lisa-Marie Terdenge

Measurement and Control of Agglomeration for the Design of Crystalline Products

Zur Erlangung des akademischen Grades eines
Dr.-Ing.
von der Fakultät Bio- und Chemieingenieurwesen
der Technischen Universität Dortmund
genehmigte Dissertation

vorgelegt von
Dipl.-Ing. Lisa-Marie Terdenge
aus
Recklinghausen

Tag der mündlichen Prüfung: 20. September 2016
1. Gutachter: Prof. Dr.-Ing. Gerhard Schembecker
2. Gutachter: Prof. Dr.-Ing. habil. Dr. h.c. Joachim Ulrich

Dortmund 2016

Bibliografische Information der Deutschen Nationalbibliothek

Die Deutsche Nationalbibliothek verzeichnet diese Publikation in der Deutschen Nationalbibliografie; detaillierte bibliografische Daten sind im Internet über <http://dnb.d-nb.de> abrufbar.

ISBN 978-3-8439-2891-5

© Verlag Dr. Hut, München 2016
Sternstr. 18, 80538 München
Tel.: 089/66060798
www.dr.hut-verlag.de

Die Informationen in diesem Buch wurden mit großer Sorgfalt erarbeitet. Dennoch können Fehler nicht vollständig ausgeschlossen werden. Verlag, Autoren und ggf. Übersetzer übernehmen keine juristische Verantwortung oder irgendeine Haftung für eventuell verbliebene fehlerhafte Angaben und deren Folgen.

Alle Rechte, auch die des auszugsweisen Nachdrucks, der Vervielfältigung und Verbreitung in besonderen Verfahren wie fotomechanischer Nachdruck, Fotokopie, Mikrokopie, elektronische Datenaufzeichnung einschließlich Speicherung und Übertragung auf weitere Datenträger sowie Übersetzung in andere Sprachen, behält sich der Autor vor.

1. Auflage 2016

Zusammenfassung

In Kristallisationsprozessen wird ein immenser Aufwand für Optimierung und Prozesskontrolle betrieben, um ein kristallines Produkt mit gewünschten Qualitätseigenschaften zu erhalten. Die Qualität, welche über die Kristallform und –größe sowie die Kristallgrößenverteilung (KGV) und Reinheit definiert wird, wird in erster Linie durch die Kristallisationsbedingungen festgelegt und beeinflusst den weiteren Downstream-Prozess. Die KGV zum Beispiel ist ein wichtiges Qualitätskriterium für die Filtrierbarkeit und Fließfähigkeit eines Produktes. Allgemein wird die KGV durch Kenngrößen wie die mittlere Kristallgröße d_{50} , die Breite der KGV d_{90} - d_{10} oder den Variationskoeffizienten charakterisiert. Allerdings liefern all diese Kenngrößen keine Information über die Partikelmorphologie oder den Anteil an Agglomeraten – im weiteren Verlauf als Agglomerationsgrad bezeichnet. Daher könnte das Auftreten von großen kristallinen Partikeln fälschlicherweise als Größenänderung durch Kristallwachstum interpretiert werden, obwohl Agglomerate vorliegen. Dieses Informationsdefizit über die Partikelmorphologie in der KGV kann, besonders wenn Agglomeration während der Fest-Flüssig-Trennung oder Trocknung auftritt und eine offline Messtechnik zur Bestimmung der KGV benutzt wird, zu einem falschen Verständnis des Kristallisationsprozesses führen. Generell kann es durch Agglomeration zu einer Verbreiterung der KGV kommen und etwaige Mutterlaugeneinschlüsse können eine geringere Reinheit bewirken. Um ein falsches Verständnis von Kristallisationsprozessen zu vermeiden und aufgrund der immer größer werdenden Reinheitsanforderungen in der Industrie spielt demzufolge die Erfassung und Lokalisierung von Agglomeration innerhalb der gesamten Kristallisationsprozesskette eine wichtige Rolle.

Daher wird in dieser Arbeit die Agglomerationsgradverteilung (AgV) als neues Qualitätskriterium eingeführt um eine quantitative Charakterisierung und Gegenüberstellung von kristallinen Produkten mit unterschiedlicher Morphologie zu ermöglichen. Um die AgV zu bestimmen wird ein Bildanalysetool basierend auf der Diskriminanzfaktoranalyse (DFA) für die Analyse von suspendierten sowie getrockneten Kristallen entwickelt. Die Identifizierung einer sogenannten Referenzdiskriminanzfunktion, d.h. eine Diskriminanzfunktion, welche innerhalb eines Stoffsystems übertragbar ist, ermöglicht dabei eine automatische und zeiteffiziente Klassifizierung der kristallinen Partikel. Durch den Einsatz der AgV können auf Basis einfa-

cher Experimente klare Aussagen darüber getroffen werden, ob ein Stoffsystem zur Agglomeration während der Kristallisation und/ oder des Downstream-Prozesses neigt.

Darüber hinaus wird das Agglomerationsverhalten von zwei Stoffsystemen, welche einen unterschiedlichen Kristallhabitus und d_{50} aufweisen, systematisch untersucht, um das Verständnis von Agglomerationsvorgängen zu verbessern und die Relevanz für ein ganzheitliches Prozessdesign hervorzuheben. Die Ergebnisse zeigen, dass die Kontrolle der Agglomeration während der Kristallisation und des weiteren Downstream-Prozesses essentiell ist, um Produktspezifikationen zu erreichen und so den Verlust von Chargen zu vermeiden.

Um Agglomeration im Verlauf der Kristallisation zu kontrollieren, wird die Begasungskristallisation – ein Verfahren zur Keimbildungsinitiierung – als vielversprechende Methode identifiziert. Durch Begasung lässt sich Agglomeration reduzieren, wodurch die Breite der KGV beeinflusst wird und eine höhere Reproduzierbarkeit im Vergleich zur Kühlungskristallisation ohne Begasung erreichbar ist. Agglomeration während der Trocknung kann mit einer hohen Konzentration an in der Mutterlauge gelösten Stoff nach der Kristallisation oder einer hohen Temperaturabhängigkeit der Löslichkeit in Verbindung gebracht werden. In diesem Fall wird, besonders wenn auf ein Waschen nach der Fest-Flüssig-Trennung verzichtet wird, die nach der Kristallisation erhaltene Produktqualität deutlich beeinträchtigt. Weiterhin zeigt die Evaluierung durch die AgV, dass ein finales Produkt – trotz ähnlicher Merkmale der KGV – höchst unterschiedlich sein kann. Demzufolge reicht eine Charakterisierung der Produktqualität anhand der KGV allein nicht aus. Für ein zuverlässiges Produktdesign ist die Quantifizierung von Agglomeration über die gesamte Prozesskette unerlässlich.

Abstract

In crystallization a high effort for optimization and process control is made to achieve the desired quality characteristics of the crystalline products. The quality, which is defined by the crystal form and size, as well as by the crystal size distribution (CSD) and purity, is primarily dominated by crystallization conditions, and affects further downstream processes. The CSD for example is an important quality criterion for filterability and flowability. In general, the CSD is characterized by characteristic values, like median crystal size d_{50} , width of CSD $d_{90}-d_{10}$, or the coefficient of variation CV. However, no information about the particle morphology or the amount of agglomerates – in the further course named as agglomeration degree – is given by these characteristic values. Hence, large crystalline particles may be interpreted as size change by crystal growth, although agglomerates exist. The lack of information about the particle morphology in CSD can lead to misunderstand the crystallization process, especially when agglomeration takes place during solid-liquid separation or drying, and an off-line CSD measurement technique is used. Through agglomeration the width of CSD might be broadened and mother liquor inclusions can lead to less purity. To avoid a misconception of crystallization processes and due to an increasing purity demand in industry, the detection and localization of agglomeration inside the whole crystalline process chain plays an important role.

Therefore, in this thesis the agglomeration degree distribution (AgD) is introduced as new quality criterion to allow a quantitative characterization and comparison of crystalline product batches with different morphology. To determine the AgD an image analysis tool based on discriminant factor analysis (DFA) is developed for the analysis of suspended and dry crystals. The identification of a so-called reference discriminant function, i.e. a discriminant function which is transferable within a material system, allows an automatic and time efficient classification of crystalline particles. By using the AgD clear statements whether a material system tends to agglomerate during crystallization and/or downstream process can be made on basis of simple experiments.

Furthermore, in order to increase the understanding of agglomeration and to provide insights into the relevance for holistic process design, the agglomeration behavior of two material systems, characterized by different crystal habit and d_{50} , is systematically investigated. The re-

sults show that the control of agglomeration during crystallization and the further downstream process is essential to reach product specifications and avoid loss of batches.

To control agglomeration during crystallization gassing crystallization – an induced nucleation method – is identified as a promising method. By gassing agglomeration is reduced, which affects the width of the CSD, and a higher reproducibility than for cooling crystallization without gassing is achievable. Agglomeration during drying can be associated with a high concentration of solute in the mother liquor after crystallization or a high temperature dependence of the solubility. Especially if washing after solid-liquid separation is omitted, the product quality obtained by crystallization is significantly affected. Moreover, the evaluation by the AgD indicates that the final product can be – despite similar characteristics of the CSD – highly different. Consequently, the characterization of the product quality by the CSD alone is insufficient and the quantification of agglomeration over the whole process chain is essential for reliable product design.

Content

Zusammenfassung	i
Abstract	iii
Declaration of Pre-Published Content	IX
List of Symbols and Abbreviations	XI
1. Introduction.....	1
1.1. Motivation	1
1.2. Objective and Scope	2
2. Basics and State of the Art	3
2.1. Crystallization.....	3
2.1.1. Solubility, Supersaturation, and Metastable Zone.....	3
2.1.2. Nucleation and Crystal Growth.....	4
2.1.3. Aggregation and Agglomeration	6
2.1.4. Control of Product Quality	8
2.2. Solid-liquid Separation and Washing.....	9
2.2.1. Filtration	10
2.2.2. Washing.....	12
2.3. Drying.....	14
2.3.1. Principles and Methods	14
2.3.2. Impact on Product Quality	17
3. Materials and Methods.....	19
3.1. Material Systems	19
3.1.1. L-Alanine/Water.....	19
3.1.2. Adipic acid/Water.....	20
3.2. Crystallization experiments	21
3.3. Filtration and Cake Washing.....	22
3.3.1. Development and Construction of new Filtration System	23
3.3.2. Selection and Addition of Wash Liquid.....	24
3.4. Drying.....	25
3.5. Analytical methods.....	26

3.5.1. Solubility measurements	26
3.5.2. Concentration profile and Metastable Zone Width	26
3.5.3. Crystal Size Distribution	27
3.6. Statistical Methods	28
3.6.1. Design of Experiments	28
3.6.2. Discriminant Factor Analysis	30
3.6.3. Factor Analysis	31
4. Quantification of Agglomeration.....	33
4.1. Introduction of Agglomeration Degree Distribution (AgD)	35
4.2. Development of Image Analysis Tool for Dry Crystals.....	37
4.2.1. Preparation.....	38
4.2.2. Multivariate Analysis	40
4.2.3. Evaluation.....	53
4.2.4. Application to the System Adipic Acid/Water.....	55
4.2.5. Comparison of material systems	58
4.3. Extension of Image Analysis Tool to Suspended Crystals.....	59
4.3.1. Sample Preparation and Image Recording	59
4.3.2. Reference Discriminant Functions	60
4.4. Summary.....	69
5. Material System I – L-Alanine/Water	71
5.1. Cooling Crystallization.....	71
5.2. Cake Washing.....	72
5.2.1. Wash Liquid Selection	73
5.2.2. Impact of Washing Parameters.....	76
5.3. Drying.....	80
5.3.1. Static Drying.....	81
5.3.2. Fluidized Bed Drying	84
5.3.3. Rotary Tube Drying.....	90
5.4. Summary.....	96
6. Material System II – Adipic Acid/Water	99
6.1. Cooling Crystallization.....	99
6.2. Cake Washing and Drying.....	101
6.2.1. Wash Liquid Selection	101

6.2.2. Impact of Downstream Conditions.....	103
6.3. Gassing Crystallization.....	107
6.3.1. Impact on Product Quality	108
6.3.2. Control of Product Quality	117
6.4. Summary.....	120
7. Conclusions and Outlook.....	121
A. Appendix	123
References.....	149
List of Figures.....	159
List of Tables.....	165
Curriculum Vitae.....	169

Declaration of Pre-Published Content

The content of this work was developed in the project “Technology platform: Innovative Downstream Processes” (FKZ0315520) financially supported by the Federal Ministry of Education and Research.

Parts of this work are already presented and published by the author, or are based on measurement data performed within the framework of student works supervised at the Laboratory of Plant and Process Design (Department of Biochemical and Chemical Engineering, TU Dortmund):

Chapter 2	2.1.4	Some parts of this section are published in	[B]
Chapter 3	3.3.1	The content of this section is published in	[A]
Chapter 4	4.1	Most parts of this section are published in	[A]
	4.2	Most parts of this section are published in The data acquisition was partially done by Stefan Heisel	[A] [b]
	4.3	Some parts of this section are published in	[B]
	4.3.2	The data in the paragraph “Adipic acid” are based on results performed by Jan A. Kossuch	[d]
Chapter 5	5.1	Most parts of this section are published in	[B]
	5.2	Most parts of this section are published in	[B]
	5.3.1	Most parts of this section are published in The crystalline product batches are produced by Britta Neugebauer	[B] [a]
Chapter 6	6.1	The data in this section are based on experimental results performed by Jan A. Kossuch	[d]
	6.2.1	The data in this section are based on experimental results performed by Manuela Horn	[c]
	6.3	The data in this section are based on experimental results performed by Jan A. Kossuch	[d]

Publications

[A] L.-M. Terdenge, S. Heisel, G. Schembecker, and K. Wohlgemuth: Agglomeration degree distribution as quality criterion to evaluate crystalline products. *Chemical Engineering Science*, 2015, 133, 157-169.

[B] L.-M. Terdenge and K. Wohlgemuth: Impact of agglomeration on crystalline product quality within the crystallization process chain. *Crystal Research and Technology*, 2016, 51, 513-523.

Data Acquisition and Programming in Framework of Student Work

[a] B. Neugebauer: Investigation of alternative drying methods in view of crystal size distribution, diploma thesis, TU Dortmund University, Dortmund, 2013.

[b] S. Heisel: Development of an image analysis tool of the determination of the agglomeration degree of crystalline products, bachelor thesis, TU Dortmund University, Dortmund, 2013.

[c] M. Horn: Impact of wash and drying parameters on the crystal size distribution and morphology, diploma thesis, TU Dortmund University, Dortmund, 2013.

[d] J.A. Kossuch: Influence of gassing crystallization on the agglomeration degree of crystalline products, master thesis, TU Dortmund University, Dortmund, 2015.

List of Symbols and Abbreviations

Abbreviations

AA	Adipic acid
AgD	Agglomeration degree distribution
Ag	Agglomeration degree
Ala	L-alanine
CSD	Crystal size distribution
DFA	Discriminant factor analysis
DoE	Design of experiments
MZW	Metastable zone width
RS	Stirring rate
ST	Static drying
SEM	Scanning electron microscopy
WS	Fluidized bed drying

Sub- and Superscripts

A	Agglomerates
c	Cake
C	Crossover crystals
dec	Decrease
eq	Equivalent
L	Liquid
nuc	Nucleation
m	Filter medium
ML	Mother liquor
s	Solid
S	Single crystals
sat	Saturation
W	Waste particles
WL	Wash liquid

Greek Symbols

α	Star value for central composite design in DoE	[-]
α	Specific cake resistance	[m/kg]
α	Efficiency of bimolecular collisions	[-]
β	Agglomerations kernel	[m ³ /s]
β	Regression coefficient	[-]
δAg	Deviation of the agglomeration degree	[-]
Γ	Discriminant criteria	[-]
κ	Cooling rate	[K/min]
η	Dynamic viscosity	[Pa·s]
φ	Correction factor of the MZW	[-]

Latin Symbols

A	Filtration area	[m ²]
A	Surface area for heat transfer	[m ²]
Ag	Agglomeration degree of the crystalline product batch	[%]
Ag _i	Agglomeration degree of value i	[-]
Ag _j	Agglomeration degree of particle fraction j	[-]
b _i	Discriminant coefficient	[-]
c	Concentration	[g/kg solvent]
$\Delta c_{\text{gassing}}$	Gassing supersaturation	[g/kg solvent]
ci	95 % confidence interval of DoE	[-]
d	Diameter	[μm]
d(Ag _i)	Equivalent diameter where AgD reaches the value i	[μm]
d ₅₀	Median crystal size	[μm]
d ₉₀ -d ₁₀	Width of crystal size distribution	[μm]
D	Discriminant function	[-]
f	Degree of freedom	[-]
G	Crystal growth rate	[$\mu\text{m/s}$]
h	Height of filter cake	[m]
k	Number of considered influence factors inside a DoE	[-]
k	Cake permeability	[m ²]
L	Crystal size	[μm]
m	Mass	[kg]
N	Particle density	[kg/m ³]

N	Number of experiments in DoE	[-]
n	Stirring rate	[rpm]
n_i	Number of particles of type i	[-]
n_0	Number of center point experiments in DoE	[-]
p	Pressure	[mbar]
PI	Performance index	[%]
PI_i	Specific performance index of group i	[%]
R	Resistance	[m ⁻¹]
SS_b	Dispersion between the groups	[-]
SS_w	Dispersion within the groups	[-]
sd	Standard deviation	[-]
T	Temperature	[K, °C]
T_{start}	Start temperature of cooling crystallization	[K, °C]
T_{end}	End temperature of cooling crystallization	[K, °C]
$T_{gassing}$	Temperature, where gassing starts	[K, °C]
t	Time	[s, min]
$\Delta t_{gassing}$	Gassing period	[s]
$\dot{V}_{gassing}$	Gas volume flow	[L/min, L/h]
t	Value of Students distribution in DoE	[-]
V	Volume	[m ³]
X_i	Characteristic variable	[-]
X	Moisture content	[-]
X	Effect of factor X in DoE	[-]
XX	Nonlinear effect of factor X in DoE	[-]
XY	Effect of factor interaction XY in DoE	[-]
\bar{x}	Mean value of sample	[-]
x_i	Influence of factor i in DoE	[-]
x_{ii}	Nonlinear influence of factor i in DoE	[-]
x_{ij}	Influence of factor interaction ij in DoE	[-]
\bar{x}_i	Mean value of influence factors in DoE	[-]
\bar{x}_{ij}	Mean value of factor interactions in DoE	[-]
y	Response in DoE	[-]
\bar{y}	Mean value of response in DoE	[-]

1. Introduction

1.1. Motivation

Crystallization is a widely used unit operation for separation, purification, and production of solid bulk chemicals or pharmaceuticals. The quality of crystalline products, which is defined by e.g. purity, crystal morphology, shape, size, and crystal size distribution (CSD), has to comply with custom requirements and requirements of the downstream process steps. Especially, if the target product is the solid generated, crystallization – as first unit operation of the process chain – is strongly interacting with solid-liquid separation, drying, and solid handling [1]. Consequently, quality characteristics like CSD, dominated by crystallization conditions first, specify the filterability, drying behavior, flowability, and formulation behavior of the final product [1–3]. Therefore, a high effort for control and design of the crystallization process is made to adjust e.g. the median crystal size d_{50} and width of the CSD d_{90} - d_{10} and to improve the downstream. In this context the control of the kinetic processes nucleation and growth, i.e. the control of the supersaturation profile during crystallization, is in focus of research. However, despite identical supersaturation profiles different CSDs can be obtained. Reasons for this are processes like agglomeration, or breakage and attrition. Agglomerates are assemblages of rigidly bounded crystals which are formed by crystalline bridges between two or more single crystals; i.e. agglomeration is a size-enlargement process which affects the morphology of the crystals. As consequence, uncontrolled agglomeration can lead to broad or bimodal CSDs [4–7] and mother liquor inclusions may reduce the purity so that, in reasons of an increasing purity demand in industry, the avoidance of uncontrolled agglomeration plays an important role also [8]. Furthermore, controlled agglomeration offers the opportunity to improve the filterability of small, needle-like crystals, to reduce dust in the process, or to avoid demixing during storage [9–11]. It has to be considered further that the desired product quality designed by crystallization can be changed by agglomeration during solid-liquid separation and drying also [11, 12]. Therefore, missing knowledge of product influencing processes like agglomeration within the overall process chain can lead to product batches out of specification, even if a high effort for optimization and process control was made for crystallization. Moreover, comprehensive process knowledge beyond crystallization offers the oppor-

tunity to obtain quality requirements which may not be directly achievable by crystallization. Hence, for reliable product design agglomeration has to be quantified and a holistic view of the unit operations crystallization, solid-liquid separation, and drying is required to allow an efficient process optimization [13]. However, the impact of further downstream processes is still poorly understood [3] and no specific guidelines for e.g. the avoidance of agglomeration during drying exist [14].

1.2. Objective and Scope

For the design of a crystallization process the CSD is an often utilized measure to evaluate the quality of a crystalline product, and the corresponding characteristic values like median crystal size d_{50} and width of CSD $d_{90}-d_{10}$ are used as responses. However, the characteristic values of the CSD do not deliver any information about the particle morphology or the amount of agglomerates inside the crystalline products; large crystalline particles may be interpreted as size change by crystal growth, although agglomerates exist. Therewith, first objective of this work is to develop a new quality criterion which delivers in addition to CSD information about the amount and distribution of agglomerates. The new quality criterion shall allow a quantitative characterization and comparison of crystalline product batches with different morphology also. It forms the basis to determine, whether crystals tend to agglomerate and whether agglomeration takes place during crystallization or in further downstream processing steps.

Furthermore, the impact of agglomeration during the downstream process on the final product quality should be analyzed. In this context the understanding of agglomeration processes should be increased to allow a synergistic process optimization of crystallization, solid-liquid separation, and drying to get the final product desired. Therefore, in this thesis the agglomeration behavior of two material systems is analyzed over the whole process chain. Key process parameters are systematically identified, and the impact of agglomeration on the CSD is recorded. The material systems chosen differ in morphology, median crystal size, and agglomeration behavior.

2. Basics and State of the Art

2.1. Crystallization

Crystallization is a thermal process used for separation or purification and describes the transformation of a liquid, gaseous, or amorphous substance into a crystalline solid. Thus, crystallization is a particle formation process also. Especially, if the target product is the generated solid, crystallization, as first unit operation of the process chain, is closely linked with solid-liquid separation, drying, and solid handling [1].

In literature crystallization is divided into solution and melt crystallization, whereby solution crystallization is subdivided in cooling, vacuum, evaporation, and anti-solvent crystallization [11, 15]. In the context of this thesis batch cooling crystallization is considered and applied only.

2.1.1. Solubility, Supersaturation, and Metastable Zone

Prerequisite for the applicability of cooling crystallization is a high temperature dependence of the solubility. The solubility of a substance specifies the maximum amount of a solid that can be dissolved in a solvent or solvent mixture and depends beside the temperature on the pressure. However, the pressure is normally negligible and the solubility can be depicted as solubility curve in dependence of the temperature (compare Figure 2.1). At the solubility curve the solution is called saturated, i.e. the chemical potentials of the liquid and solid phase are in thermodynamic equilibrium. The saturated solution can be characterized by the saturation temperature T_{sat} and the saturation concentration c_{sat} . [11, 16]

The state of solution on the right side of the solubility curve is denoted as undersaturated and on the left side as supersaturated. The supersaturation represents a deviation of the thermodynamic equilibrium and is the driving force of crystallization. In case of cooling crystallization the supersaturation is created by cooling of the solution. If the supersaturation is sufficiently high enough, the supersaturation curve is reached. At this critical supersaturation a solid phase is formed by nucleation and subsequently crystal growth occurs to achieve the thermodynamic equilibrium. [17]

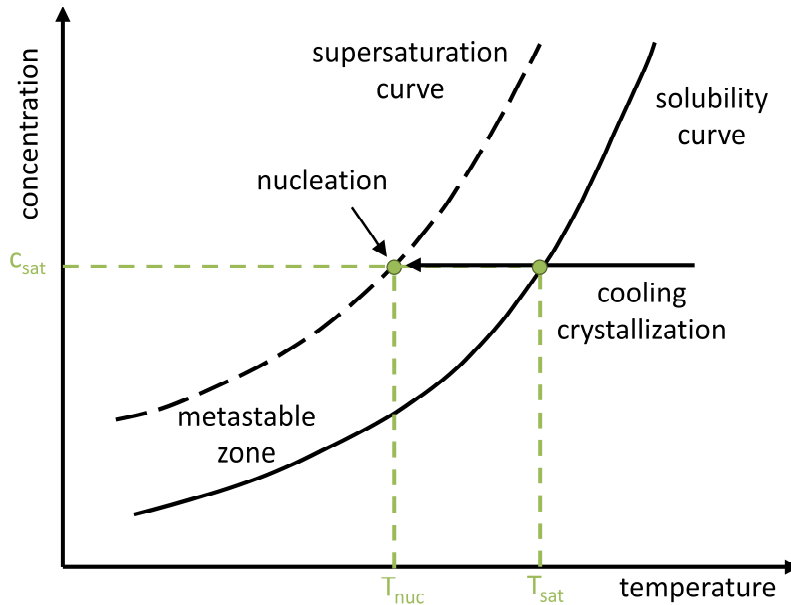


Figure 2.1: Solubility, supersaturation, and metastable zone

The region between the solubility and supersaturation curve is defined as metastable zone (see Figure 2.1) and can be characterized by the metastable zone width (MZW), the temperature difference of T_{sat} and T_{nuc} at which nucleation occurs. The MZW depends on the material system (e.g. solubility), plant properties (e.g. crystallizer volume), operation parameters – like thermal history of solution and cooling rate – as well as other influencing factors like the concentration of additives or impurities, and as demonstrated in the next section on the nucleation mechanism [11, 18].

2.1.2. Nucleation and Crystal Growth

Nucleation and crystal growth determine the crystallization process and therewith the interaction of both determines the characteristics of the crystalline product.

Nucleation dominates in regions of high supersaturation at the upper limit of the metastable zone and describes the process by which the formation of a solid phase is induced: the formation of nuclei [19]. Nuclei are molecule clusters of a critical size, i.e. thermodynamic stable clusters, which are capable to grow to crystals. Molecule clusters are formed in supersaturated solution by congregated molecules of the crystallizing solute. The number of molecules necessary for the formation of a nucleus is affected by the supersaturation, the nucleus shape, and the surface energy [20]. The higher the supersaturation the higher is the probability for nucleation. However, the critical supersaturation, which specifies as mentioned above the upper limit of the metastable zone, depends mainly on the mechanism of nucleation (see Figure 2.2) [21]. Generally, nucleation is divided into two main categories: primary and secondary

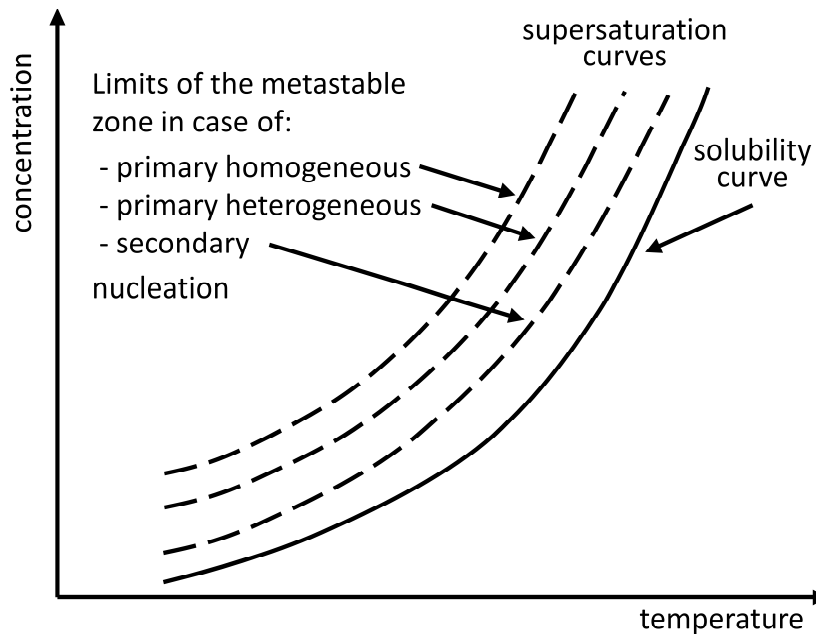


Figure 2.2: Limits of the metastable zone in dependence of the nucleation mechanism [8]

nucleation. Primary nucleation takes place in absence of intrinsic crystals and is subdivided into homogeneous and heterogeneous nucleation. Primary homogeneous nucleation defines the spontaneous induction of nucleation by thermal forces in absence of a foreign surface and needs therefore the highest supersaturation to occur. If foreign surfaces, like installations in the crystallizer, dust, or impurities, act as nucleation center the nucleation mechanism is called primary heterogeneous. Due to the present foreign surface the energy barrier for the formation of nuclei is decreased so that less supersaturation is required for nucleation than for primary homogeneous nucleation. However, since foreign surface is always present in real systems, homogeneous nucleation is merely a theoretic model. In case of secondary nucleation the supersaturation necessary is least, since nucleation is promoted by crystals of the crystallizing solute. Secondary nucleation is induced either in a targeted way by adding seed crystals or arises from crystal breakage and attrition after primary nucleation. Breakage and attrition occur due to crystal-crystal collisions or collisions of crystals with installations of crystallization equipment. Both phenomena lead to an increase of fines and irregular crystals. [17, 18, 21, 22]

After the first nuclei exist in solution simultaneous to nucleation **crystal growth** starts and both processes compete for molecules of the crystallizing solute. Crystal growth dominates at low levels of supersaturation and suppresses usually further nucleation [19].

$$G = \frac{dL}{dt} \quad (2.1)$$

The crystal growth rate G is defined as change of the crystal size L as function of time and can be mathematically expressed by equation (2.1). The process of crystal growth describes the mass transport of growth units (e.g. molecules) to the crystal surface and the incorporation of these growth units at so-called kink sites, trihedral corners on the crystal surface, in four steps: In the first step growth units are transferred by convection from the bulk phase into the diffusion layer around the crystal. The second step describes the diffusion through the layer and is followed by the adsorption of the growth unit on the crystal surface (third step). Subsequently, in the last step, the growth unit is incorporated into the crystal lattice. Each of these steps can be characterized by a difference of the chemical potentials, the driving force for crystal growth, whereby the slowest step determines the growth rate. If the diffusion from the bulk phase to the crystal surface is the rate limiting step the growth mechanism is diffusion-controlled, whereas a surface integration-controlled mechanism exists if the incorporation of the growth units into the crystal lattice is rate limited [17, 18, 21]. The shape and morphology of a crystal depends on the relative growth rates of the crystal surfaces, which are affected by internal factors, like defects in the crystal lattice, and external factors: temperature, supersaturation, solvent, and presence of impurities [18, 20, 22, 23]. Especially impurities can have a significant impact on the morphology of crystals, e.g. paracetamol changes in presence of metacetamol from an rhombic to a needle like habit [24].

2.1.3. Aggregation and Agglomeration

Although the size distribution and morphology of crystals is predominantly defined by the growth rate, processes like aggregation and agglomeration take a decisive role also. Aggregation and agglomeration are particle size enlargement processes, however their definitions are not standardized in literature. Nichols et al. [12] give a detailed review of different definitions. Both, aggregates and agglomerates are assemblages of single crystals or crystalline fragments, but the two assemblage processes differ in kind and strength of the binding behavior between the particles.

Like the vast majority, in this work aggregates are defined as over corners or edges loosely bounded crystals [12]. **Aggregation** can take place in under- and supersaturated solution. After the collision of two or more particles in suspension aggregates are formed by bonding forces, such as van der Waals or electrostatic forces [21]. A compilation of possible binding

mechanisms is given by Rumpf [25]. The bonding in aggregates is reversible and quite weak [26] and the cohesion of the aggregates depends highly on the hydrodynamic conditions in suspension. However, bonding forces like van der Waals or electrostatic forces matter for aggregates smaller than 10 μm only [15]. To form stable assemblages larger than 100 μm agglomerates have to be formed before desaggregation occurs [15].

Agglomerates are assemblages of rigidly bounded crystals which are characterized by crystalline bridges between them [12]. Since the bonding of the single crystals requires crystal growth, supersaturation is prerequisite for agglomeration. Generally, two main types of agglomeration are distinguished and can occur simultaneously during crystallization; primary and secondary agglomeration [16, 21]. Primary agglomeration describes the formation of polycrystals, dendrites, or twins by mal-growth and occurs either as consequence of the presence of impurities or of diffusion limitations in combination with high growth rates [27]. While for primary agglomeration a single crystal is the origin of the agglomeration process, secondary agglomeration arises out of the cementation of two or more in suspension aggregated single crystals, i.e. the collision and aggregation of crystals can be seen as preliminary stage for secondary agglomeration. A common way to describe the kinetic of secondary agglomeration is to calculate the temporal change of the particle density N in dependence of the efficiency of bimolecular collisions α and the agglomeration kernel β (see equation (2.2)) [11, 28].

$$\frac{dN}{dt} = \alpha \cdot \beta \cdot N^2 \quad (2.2)$$

The agglomeration kernel β , which describes the statistical collision probability, depends on the particle size and changes during the agglomeration process. For particles smaller than one micron the agglomeration mechanism is called orthokinetic and the agglomeration is promoted by the Brownian motion. In contrast, for an effective collision between particles larger than one micron a velocity gradient is necessary; this mechanism is called perikinetic.

In sum secondary agglomeration is affected by material system characteristics – the size, shape, density of particles in suspension, interaction between particles, the solvent, and the level of supersaturation – and hydrodynamic conditions, like the stirring intensity, which determines the collision probability, and the contact time between the particles available for the formation of a stable crystalline bridge [11, 21, 29]. Especially small crystals are prone to agglomerate [11, 21] and high supersaturations lead to agglomerates with strong crystalline bridges [11, 30–32]. Furthermore, from a certain point an increase of the stirring intensity promotes the breakage of agglomerates; in this way large agglomerates are disrupted by high shear forces leading to a maximum size of agglomerates in solution [15, 16, 32].

2.1.4. Control of Product Quality

The quality of a crystalline product is defined by characteristics like purity, crystal shape, form, and size, as well as crystal size distribution (CSD) and agglomeration degree (Ag). These characteristics have to comply with customer requirements and requirements of the following downstream process steps. Inter alia solid-liquid separation, drying, and solid handling are affected since the product quality – dominated by the crystallization conditions first – specifies the filterability, drying behavior, flowability, formulation behavior, and bioavailability of the final product [1, 14, 20, 22, 33, 34].

To reach the desired product quality and to obtain optimal initial conditions for the downstream in a reproducible way, crystallization control is essential. Otherwise, e.g. undesired fine, needle-like or flake shaped crystals and crystalline products with broad CSDs are produced, leading to bottlenecks in solid-liquid separation, washing, and drying [23, 33, 35, 36]. Furthermore, uncontrolled product quality influencing processes like attrition and agglomeration can result in product batches out of specification. Attrition leads to an increase of fines and by agglomeration the morphology of the crystals is affected leading to broader or bimodal CSDs also [4–7]. Further negative effects of agglomeration are that mother liquor inclusion might reduce the product purity and shelf life of e.g. drugs, and that a higher fragility of the product results [1, 37–39]. Therefore, with respect to an increasing purity demand in industry, avoiding spontaneous agglomeration plays an important role [8]. On the other hand controlled agglomeration delivers e.g. the possibility to design particle size, to enhance the filterability or flowability of the crystalline product, to reduce dust in the process, or to avoid demixing during storage [9, 10].

One strategy to control crystallization is to guarantee a reproducible start by induced nucleation. Uncontrolled, spontaneous nucleation at high supersaturation leads to the formation of a large number of crystals with a high surface area and therewith to varying crystalline products with broad CSDs, low bulk densities, and poor purity [19]. Hence, nucleation is a decisive step to reach the desired product quality. Common ways to control nucleation are seeding or the usage of ultrasound, i.e. sonocrystallization. In case of seeding spontaneous primary nucleation is avoided by the addition of seed crystals within the metastable zone [11, 40, 41], whereas for sonocrystallization nucleation is induced within the metastable zone by cavitation bubbles [42]. In contrast to seeding a major advantage of sonocrystallization is that nucleation control is provided without the need of seed crystals. Therefore, the time consuming, complex preparation of seed crystals [36] and the risk of contamination is avoided, making sonocrys-

tallization an interesting application for the production of pharmaceuticals and fine chemicals [43]. However, despite intensive research and first applications [7, 44–52] in industrial practice an economically affordable equipment has still to be designed to allow the use of ultrasound in large scale [7, 52]. Furthermore, the application of ultrasound leads to a temperature increase of the solution insonated so that the heat generated has to be removed [53]. An alternative induced nucleation method, which combines the sterile operation mode of sonocrystallization with a reduction of process energy required and a technically simpler setup regarding scale up, is gassing crystallization. Gassing crystallization was first applied in 1976 by the Henkell company for the production of sparkling wine [54] and was then investigated by Wohlgemuth further [6, 53, 55]. For gassing crystallization cavitation bubbles from sonocrystallization are replaced with gas bubbles of e.g. saturated synthetic air. Since for different organic material systems the metastable zone width (MZW) and the crystal size distribution (CSD) could be affected by gassing in a similar way than by sonocrystallization Wohlgemuth [53] concluded that the surface of the gas or cavitation bubbles act as nucleation center and a primary heterogeneous nucleation mechanism exists. Depending on the gassing parameters, means the start point of gassing - characterized by the temperature or supersaturation of the solution at which gassing is started -, the gas flow, and the gassing period, a different number of nuclei is induced, whereby the overall bubble surface area plays a decisive role [53]. Also first conclusions were drawn by Wohlgemuth [53] that gassing crystallization affects agglomeration, but no quantitative investigations were carried out yet.

Another strategy to meet crystalline product quality characteristics – but not investigated in the context of this thesis – is the control of crystal growth. By controlling the level of supersaturation during crystallization [33] high supersaturation is obviated to reduce secondary nucleation and promote crystal growth without e.g. dendritic growth or liquid inclusions [35]. A common way to regulate the supersaturation is to determine a special cooling profile via feedback control. However, this method is very complex and requires online analysis techniques to measure the change of concentration in solution [33, 56–58]. Therefore, e.g. parabolic, cubic, or quadratic cooling profiles are applied also to control the level of supersaturation [11, 17, 59].

2.2. Solid-liquid Separation and Washing

After crystallization – in the second step of the crystallization process chain – the crystalline product is first isolated from the mother liquor by solid-liquid separation. In this thesis the

suspended solid is defined as the target product. In such crystallization processes the solid-liquid separation is usually performed by cake forming filtration methods. According to the kind of driving force vacuum, pressure, and centrifugal filtration are distinguished [11, 16, 60]. Subsequently, remaining mother liquor can be removed by washing if necessary to enhance the product quality or to avoid quality changes during drying. In the following the principles of vacuum/ pressure filtration and washing are explained and the impact of both processes on the crystalline product quality is discussed.

2.2.1. Filtration

The principle of cake forming filtration involves the retention of solids (crystals) on the surface of a filter medium with pores smaller than the crystals in form of a filter cake, whereas the liquid (mother liquor) passes through the filter medium and is received as filtrate. For the permeation of the mother liquor a pressure difference Δp across the medium and the filter cake is required, which can be provided e.g. by a vacuum pump. The flow rate of the mother liquor dV/dt and therewith the filtration time depends beside Δp on the properties of the filtered slurry and the filtration setup and can be described by the modified Darcy's law [61] according to equation (2.3). Herein A is the filtration area, η the viscosity of the mother liquor, h the height of the filter cake, and k the permeability of the filter cake. Since h rises with the time for a constant filtration rate Δp has to be increased over time. Otherwise, in case of constant Δp the filtration rate decreases continuously. The impact of the cake height h and the permeability of the filter cake k on the filtration process can be expressed as cake resistance R_c . To consider the resistance of the filter medium $R_m = h_m/k_m$ also the cake resistance R_c in equation (2.3) can be substituted by the total resistance R (see equation (2.4)). However, R_m dominates at the beginning of filtration only and is often negligible after the formation of the filter cake. [62–64]

$$\frac{dV}{dt} = \frac{\Delta p \cdot A}{\eta} \cdot \frac{k}{h} = \frac{\Delta p \cdot A}{\eta} \cdot \frac{1}{R_c} \quad (2.3)$$

$$R = R_c + R_m \quad (2.4)$$

$$\alpha = \frac{R_c A}{cV} \quad (2.5)$$

The filterability of crystalline particles is commonly evaluated by an intrinsic measure, the specific cake resistance α (see equation (2.5)), which depends on the slurry concentration c , the volume of filtrate collected V , the filtration area A , and the cake resistance R_c . Therefore, α specifies figuratively the filterability of crystalline particles in dependence of the crystal

size, the density and shape of the crystals, as well as of the porosity of the cake formed [65]. As a rule, crystalline particles with a α value in the range between 10^7 m/kg and 10^8 m/kg are fast filtering, and values greater than 10^{10} m/kg characterize very slow filtering products like needles [62]. Moreover, the suspension density, the solvent composition, viscosity and velocity of the liquid affect the cake formation and therewith the resistance [66]. If the filtration rate has an impact on the packing of the filter cake the specific cake resistance is affected by the pressure difference also. The porosity of the filter cake might decrease due to the fact that small particles move into the gaps between larger ones or due to particle breakage. Such filter cakes are stated as compressible [60].

To improve the filterability of crystalline products filter aids can be added to the suspension to increase the porosity and permeability of the filter cake. Moreover, the size, size distribution, and form of the crystals can be changed by adjusting the product characteristics received by crystallization [11, 67]. For example Beck et al. showed that higher initial supersaturations during the precipitation of L-glutamic acid lead to crystals of different morphology and therewith to a change of the filterability [66]. Other strategies to influence the filterability by crystallization are the optimization of seeding and cooling conditions or the change of the solvent composition [68, 69]. In this context it has to be taken into account that the specific cake resistance is inversely proportional to the square of the particle size so that especially the fines in the product have a decisive impact on the filtration performance. Therefore, desirable characteristics for the crystalline product are large crystals. Moreover, crystals with an approximately spherical form and a narrow, monodisperse crystal size distribution are preferable to reach a high filter cake porosity which reduces the specific cake resistance also. [63]

As outcome of the filtration a wet filter cake with a specific content of residual mother liquor (moisture) is obtained. The residual mother liquor exists as capillary liquid in the pores of the filter cake, as adhering layer on the crystal surface, as “Zwickelfüssigkeit” in form of liquid bridges at the contact point between the crystals, and as inclusions in agglomerates [70]. The moisture content of crystal cakes varies after filtration from 5 % to 50 % [16] and depends on the pressure difference, the cake resistance, and the time of deliquoring. The larger the crystals and the narrower the CSD the lower the moisture content can be achieved [63]. However, a complete dehumidification of the filter cake is possible by thermic separation processes like drying only. To comply with purity requirements, especially in pharmaceutical or food production, washing is applied after solid-liquid separation.

2.2.2. Washing

Washing is performed mainly as an additional step of the process chain or as partial step of solid-liquid separation and can be very time consuming [71]. The main objective of washing is to remove the remaining mother liquor after solid-liquid separation out of the voids of the filter cake. Reasons for the removal can be to guaranty the desired purity by washing out mother liquor impurities or by-products, to recycle the mother liquor or other valuable components, to adjust the color of the final product, and – as applied in the context of this thesis – to avoid redissolution and agglomeration of the crystals during drying (compare section 2.3.2). [62, 64, 72–74]

Two main wash types are distinguished: reslurry and displacement washing which is denoted as cake washing also [8, 60, 62, 74, 75]. In case of reslurry wash the mother liquor is removed by dilution. For this purpose the cake is discharged from the filter and agitated together with the wash liquid in a vessel to a suspension. Afterwards, a second filtration step is accomplished. Cake washing is performed by feeding the wash liquid onto the top of the filter cake. The wash liquid flows through the cake, whereby the mother liquor is displaced. This flow can be realized by the same driving force used for filtration before. Thus, cake washing can be carried out in the existing filtration apparatus so that less additional equipment in contrast to reslurry washing is needed. The experimental effort is reduced and moreover, for cake washing in general, less wash liquid is required to reach the same washing efficiency [60]. As consequence in this study cake washing was chosen.

Under idealized conditions the wash liquid is driven in plug flow through the filter cake and the mother liquor is displaced (compare Figure 2.3) [60]. However, in reality the characteristics of the filter cake – porosity, homogeneity of the structure, height, compressibility, and moisture content – affect the efficiency [60, 76] so that a consistent formation of the filter cake during filtration is a key prerequisite to enable a reproducible cake washing. Due to the fact that the filter cake consists of non-uniform and dead-end pores, beside displacement, mixing and diffusion processes take place [64]. Furthermore, cake cracking can lead to channeling or bypassing effects. Especially for thin filter cakes channeling takes place and reduces the efficiency of cake washing [77]. Also inconsistent filter cakes with a non-uniform thickness lead to an uneven distribution of the wash liquid over the filter cake [77]. Hence, more

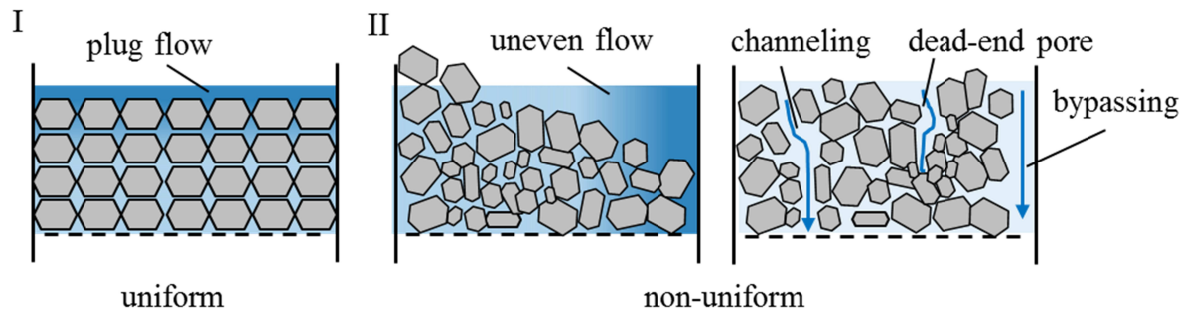


Figure 2.3: Impact of the filter cake formation on cake washing: (I) uniform filter cake under idealized conditions, (II) non-uniform filter cake under real conditions

wash liquid than the maximum volume of mother liquor in the filter cake, which corresponds to the total volume of the pores, is needed to remove the mother liquor.

Second prerequisite for an effective cake washing is a homogeneous dispersion of wash liquid over the surface of the filter cake. For example alternate plates, also known as washing plates, [78] or nozzles can be used to feed the wash liquid on the filter cake surface.

Furthermore, a suitable wash liquid has to be chosen accurately [8, 62, 71]. Criteria for the selection of a suitable wash liquid are:

- Solubility of impurities in wash liquid:
The solubility of the impurities should be high to dissolve them in the wash liquid and to avoid crystallization or precipitation of the impurity material inside the filter cake. [17]
- Solubility of crystalline product in wash liquid:
The solubility and temperature dependence of the solubility should be low for the crystalline product to ensure that redissolution of crystals during washing and drying at high temperatures is prevented also. To avoid product loss saturated wash liquids can be utilized to remove impurities [75]. However, it should be taken into account, that the usage of a strong antisolvent involves the risk of precipitation during washing. To avoid such impacts for the first wash cycle a mixture of wash liquid and crystallization solvent can be used. [62]
- Viscosity ratio between mother liquor and wash liquid:
The viscosity ratio of mother liquor (ML) to wash liquid (WL) η_{ML}/η_{WL} should be low to avoid “fingering”. Fingering means that the wash liquid flows in an inconsistent finger like stream through the filter cake. Due to a lower viscosity of wash liq-

uid in contrast to mother liquor the flow resistance in larger capillaries is decreased and smaller capillaries are insufficiently passed through [62, 76]. Furthermore, a low viscosity of the wash liquid can reduce the time of cake washing [17, 62].

- Miscibility of wash liquid and the mother liquor:

The miscibility of the wash liquid with the mother liquor, i.e. the solubility of the mother liquor in the wash liquid, should be high to avoid the building of streaks and to improve the efficiency of the washing process. The higher the miscibility the higher is the capacity of the wash liquid, i.e. less wash liquid is needed to displace the same amount of mother liquor. [17, 62]

2.3. Drying

In the last step of the crystalline process chain the crystals are dried to adjust the final moisture or solvent content of the product. Especially, in pharmaceutical or food industry legal requirements have to be complied [62]. Further objectives are to enhance or maintain the final form, habit, size, and size distribution of the crystals designed by crystallization, to control dust by particle design, and to reach a stable final crystalline product with a free flowing consistency for solid handling and storage [79]. Although drying is a common process for the production of e.g. pharmaceuticals, chemicals, or foods, holistic process knowledge is missing and no specific guidelines for the control of product quality influencing processes like agglomeration during drying exists [3, 14]; making drying to a “most complicated problem” [80] during quality control. Therefore, in the next sections the principle of drying is clarified, an excerpt of suitable drying methods for crystalline products is given, and the impact of drying on the quality of crystalline products is described to elucidate the relevance of holistic process optimization for reliable product design.

2.3.1. Principles and Methods

From the processing point of view drying is a thermal solid-liquid separation process. The solvent might surround the crystals, adhere to the crystal surface, or is bounded as solvate or hydrate inside the crystals. It is evaporated by heat energy either supplied by a carrier gas – air or inert gases –, or by hot surfaces, microwaves, and radiation [81]. The moisture content X , i.e. the ratio of liquid mass m_L to the mass of the dried solid m_S (see equation (2.6)), affects the overall drying time [62]. The temporal change of the moisture content is defined as drying

rate in equation (2.7) and depends on drying conditions like the temperature, humidity, air pressure, as well as the ratio of the mass of dry solid m_s to the available surface area A for heat transfer [81]. The surface area for heat transfer is affected by product properties like the crystal size distribution and the morphology of the crystals. It further depends on the drying method used [62].

$$X = \frac{m_L}{m_S} \quad (2.6)$$

$$\dot{m}_L = \frac{m_s}{A} \cdot \frac{dX}{dt} \quad (2.7)$$

The drying process can be characterized by drying curves (see Figure 2.4) and is divided into three stages. In the first stage (A to B in Figure 2.4) the system is preheated to the target drying temperature and the solvent starts to evaporate. The next stage between the points B and C is characterized by a constant drying rate and dominated by heat transfer, i.e. depends on the drying conditions and not on properties of the solid material. The free solvent around the solid material is completely evaporated until, at point C, the critical moisture content is reached. Finally, in the third stage (C to D) the drying rate decreases permanently with decreasing moisture content. Solvent that is present inside the pores of the solid or chemically bounded as solvate is removed until the equilibrium moisture content is reached. This stage of the drying process is mass transfer limited. [11, 62, 82, 83]

Based on the heat transfer mechanism drying methods can be categorized in principle into conductive and convective drying or hybrid forms of both methods. Moreover, radiant drying methods exist but are not considered in this thesis.

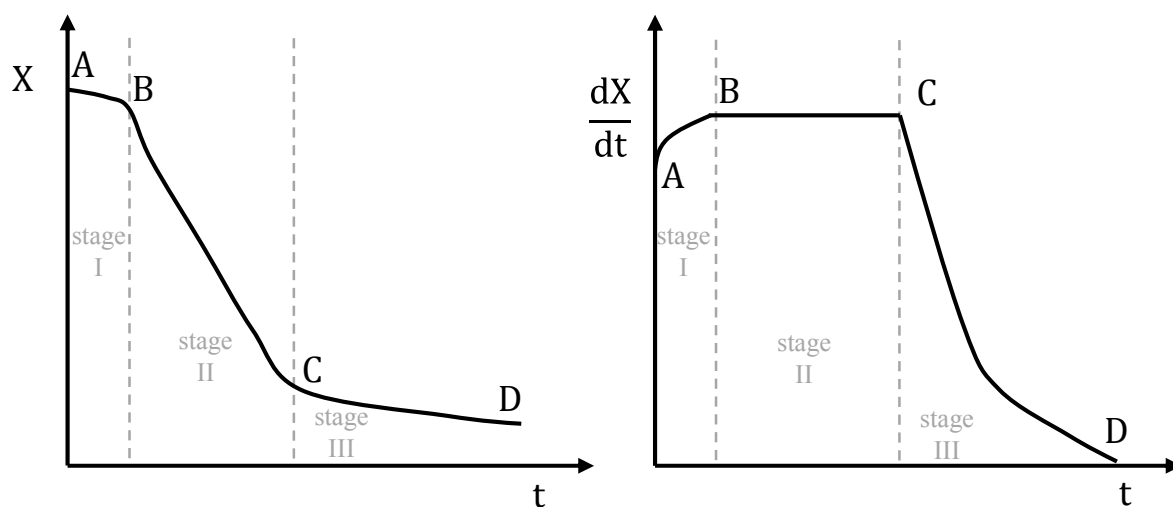


Figure 2.4: Drying curves: Moisture content in dependence of time (left), Drying rate in dependence of time (right); adapted from [82]

Conductive drying is a direct drying method. The heat transfer is provided by a heated surface which has contact to the feed material. Therefore, conductive drying is known as contact drying also. Often, conductive drying requires long drying times especially if the wet solid is dried in form of a static bed. In case of static conductive drying the drying rate decreases with the moisture content due to the fact that a barrier of dried solid material between the heated surface and the wet solids is built-up. To enhance the heat transfer the temperature difference between the heated surface and the solid bed can be increased or the surface area available for heat transfer can be enlarged by mixing.[81, 83]

Common apparatuses for conductive drying are tray dryers (static drying in an oven), agitated dryers, filter dryers, rotary tube or cone dryers, and tumble dryers [62].

In this thesis static and rotary tube drying are applied as conductive drying methods (compare section 3.4). On industrial scale the tube of a rotary tube dryer has a diameter of one to several meters and the length is five to eight times larger than the diameter [83]. Through a rotation around the longitudinal axis of the tube and lifting blades installed in the circumference of the tube a mixing of the feed material is achieved. Thus the surface area for heat transfer is enlarged and the drying rate is enhanced. The mixing conditions inside the tube and therewith particle-particle collisions, as well as the contact time between the particles, are affected by the rotational speed. The peripheral speed varies normally between 0.1 and 0.5 m/s [83].

In case of convective drying the heat transfer is performed by heated, unsaturated air or gas which flows through or over the wet solid. The solvent is vaporized and carried out of the process as humidity. Inter alia spray dryer, flash dryer, belt dryer, and fluidized bed dryer belong to convective drying techniques [83, 84].

In the context of this work fluidized bed drying is investigated as representative for convective drying. Fluidized bed dryers are used for fluidizable bulk solids consisting of powdery, crystalline, or short-fibred particles [85]. Despite several forms fluidized bed dryers are constructed out of the same components: a fluidized bed column, a distributor plate, a heater, a gas blower, and filter elements to separate the air or gas after usage from dust particles of the feed material [84].

The feed material is placed on the distributor plate which is passed through by heated air or gas supplied by the blower. The distributor plate ensures a homogeneous distribution of the air allowing a stable fluidization of the feed material. It has to be constructed in the way that feed material loss through the distributor plate is prevented even when the drying process is interrupted. In industry e.g. perforated plates, Conidur-plates, tissue- and sinter metal plates, or slit plates are used as distributor plates. [83]

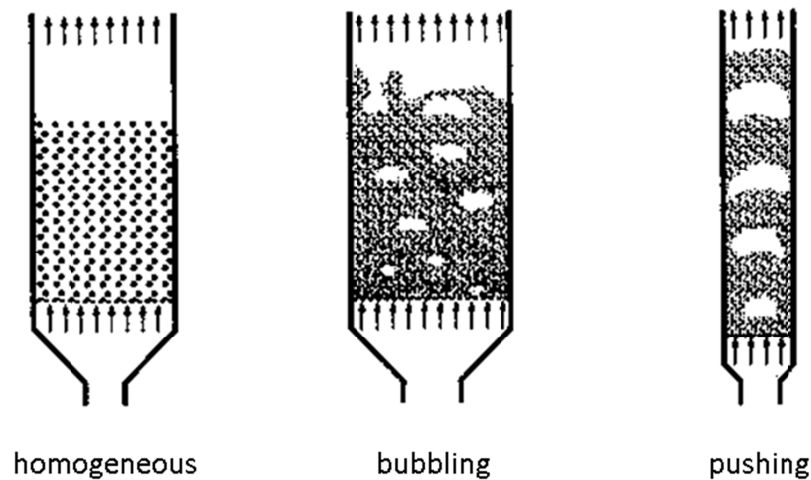


Figure 2.5: States of fluidized beds adapted from [86]

Beside the distributor plate, the fluidized state of the feed material depends on the air flow velocity, the particle size, and particle density [87–89]. When air flows through a static particle bed from a certain air flow velocity, the so-called minimum fluidization velocity, the incipient fluidization point is reached and the particles are fluidized in the air; i.e. the particles are held in suspension and a homogeneous fluidized bed is formed. As depicted in Figure 2.5 a homogenous fluidized bed is characterized by a uniform volume expansion, whereby the particles are classified by their weight. As a rule lighter particles are present in the upper regions of the fluidized bed and heavier ones in the lower regions. A further increase of the air velocity leads, in case of a feed material with a broad CSD, to the formation of an inhomogeneous fluidized bed. First instabilities of the fluidized bed can be observed as bubble formation inside the bed (bubbling fluidized bed). Afterwards, through the coalescence of the bubbles a fluent transition from the bubbling fluidized bed to a pushing fluidized bed takes place. [86, 89]

2.3.2. Impact on Product Quality

Drying can have a significant effect on the final product quality like e.g. on the purity or crystal size distribution (CSD) of the final crystalline product. The impact on the product quality depends on the material system, the initial conditions – like the moisture content –, and the drying method used. Effects such as attrition, breakage, overdrying, snowballing [3], or the formation of an unspecified polymorphic state [90] can occur. Drying can lead to partial or complete amorphization [11, 91]. Keey [92] describes a complete redissolution of wet crystals. Furthermore, agglomeration takes place during drying. Prerequisite for agglomeration is the presence of liquid bridges between crystals. These liquid bridges are formed by remaining

mother liquor or wash liquid after solid-liquid separation and can be destroyed or regenerated during agitated drying. During the drying process the concentration of solute in the remaining mother liquor increases permanently by evaporation of solvent and redissolution of product crystals, which creates supersaturation. Caused by the supersaturation crystalline bridges are formed by crystal growth and agglomeration results. For example lactose crystallized from mother liquor tends to lump and cake during drying [93]. Caking describes a fix connection of the whole crystalline product. Modugno et al. [93] showed that the crystal size, as well as the initial moisture content at the beginning of the drying process, have an significant impact on the caking of crystals. Especially small crystals are prone to agglomerate since more liquid bridges are formed per volume than for crystals of larger sizes increasing the cohesion necessary for agglomeration [93]. Negative effects of agglomeration are that mother liquor inclusion might lead to poorer product purity and a higher fragility of the product can be induced [38, 94]. Moreover, product characteristics designed by crystallization are changed. A broadening of the width of CSD by higher d_{90} values or a bimodal distribution is often caused by agglomeration [4, 5, 95, 96].

To avoid agglomeration during drying the mother liquor between the crystals of the wet filter cake has to be displaced entirely by washing, i.e. the solvent composition around the crystals has to be adjusted. In this context the solubility of the crystal material in the surrounded solvent is important to know to avoid redissolution of the crystals at high drying temperatures.

However, controlled wet agglomeration during drying known as granulation offers the opportunity for final particle design to control dust, to define and improve the flowability, or to avoid demixing during storage [9]. To promote agglomeration during drying binding liquids are sprayed onto the particles [97].

3. Materials and Methods

3.1. Material Systems

The “material system” defines the solute and solvent used for crystallization. In this thesis the agglomeration behavior of two organic material systems is analyzed, whereby in both cases water (ultrapure, 0.05 $\mu\text{S}/\text{cm}$, Millipore) was chosen as solvent. As solutes L-alanine (kindly provided by the Evonik Industries AG, $\geq 99.7\%$), and adipic acid (kindly provided by BASF SE, $\geq 99.7\%$) were considered. The selection of the solutes was made on basis of their differences in crystal size, morphology, and solubility behavior indicating a different agglomeration behavior also. In the following a short overview about L-alanine and adipic acid is given and the material systems are characterized.

3.1.1. L-Alanine/Water

L-alanine (2-aminopropanoic acid, $\text{C}_3\text{H}_7\text{NO}_2$) is a non-polar, aliphatic α -amino acid with a methyl group as side chain and is rated among the 20 proteinogenic amino acids. As a nonessential amino acid L-alanine can be synthesized by the human body. Industrially L-alanine can be produced e.g. biochemically from L-aspartic acid using immobilized *Pseudomonas dacunhae* cells or chemically from 2-chloropropionic acid and ammonia. Fields of application are e.g. the production of infusion solutions, cosmetics, and vitamin B6 or the usage as food additive. [98]

L-alanine is insoluble in nonpolar solvents, but highly soluble in water. The solubility of L-alanine in water is depicted in Figure 3.1 I and was measured by Wohlgemuth [53]. As can be seen in Figure 3.1 II L-alanine crystals from aqueous solution have an octahedral shape.

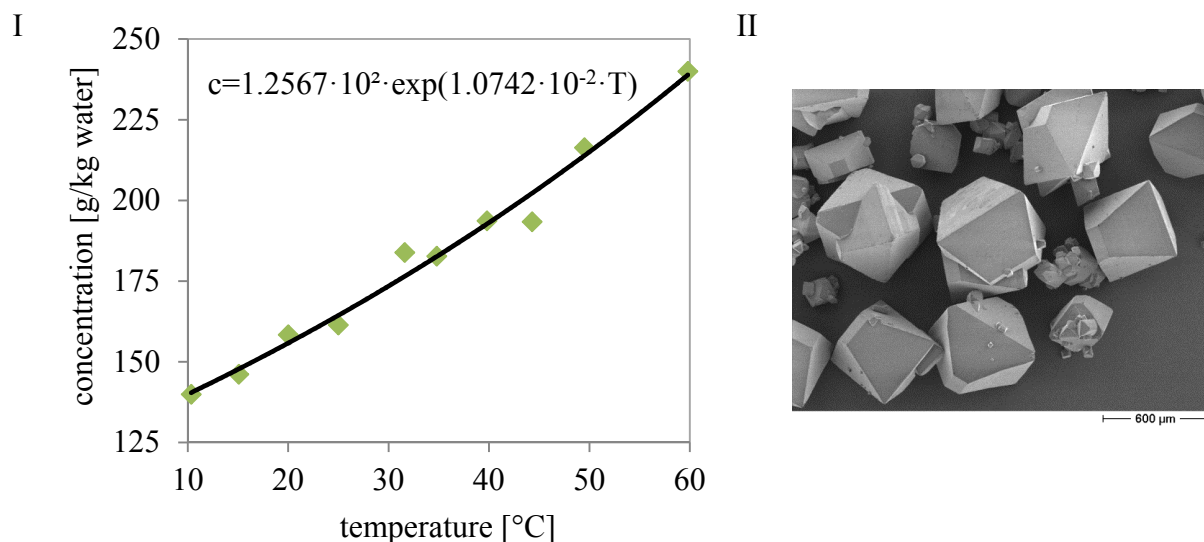


Figure 3.1: (I) Solubility of L-alanine in water [53], (II) SEM image of L-alanine crystallized out of water

3.1.2. Adipic acid/Water

Adipic acid (hexanedioic acid or 1,4-butanedicarboxylic acid, $C_6H_{10}O_4$) is an aliphatic dicarboxylic acid and is produced worldwide as large scale chemical. Per year around 2.5 million tons are produced. It is primarily used in plastic processing as precursor for the production of nylon 66, but is also utilized as excipient in drugs or in food production for e.g. flavoring [99]. The solubility of adipic acid in water was measured gravimetrically as described in Section 3.5.1 and is depicted in Figure 3.2 I. Adipic acid crystallizes from water as flat, elongated hexagonal, monoclinic plates [100] (compare Figure 3.2 II) strongly agglomerating [99, 101].

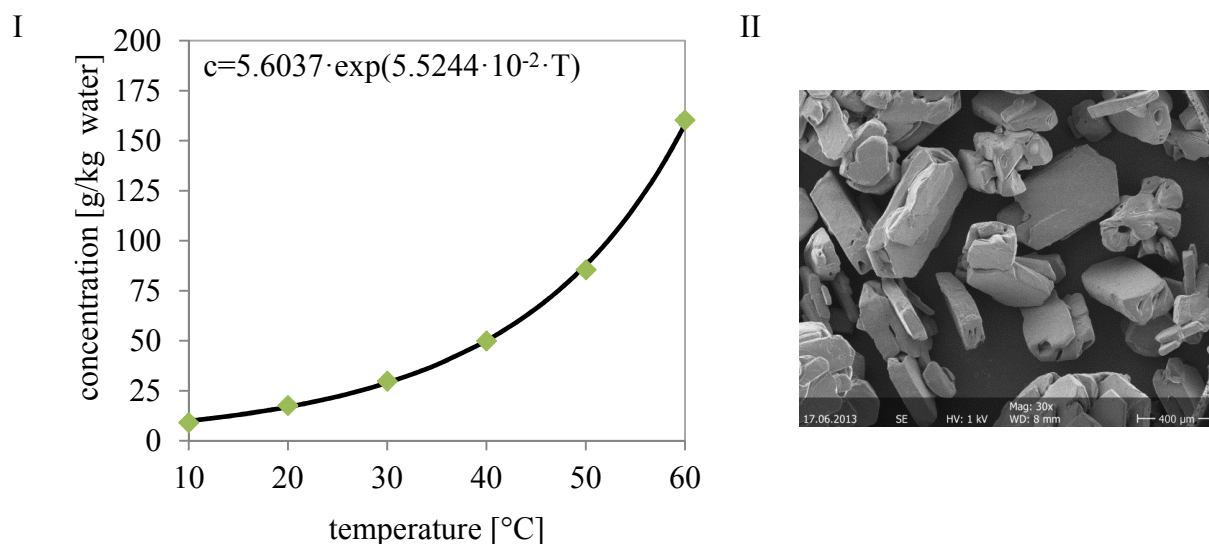


Figure 3.2: (I) Solubility of adipic acid in water, (II) SEM image of adipic acid crystallized out of water

3.2. Crystallization experiments

The batch cooling crystallization experiments with and without gassing were carried out in a double-jacket glass crystallizer with a volume of 1.2 L and a diameter of 100 mm. For cooling or heating tempered water was circulated through the jacket, connected to a thermostatic bath (HAAKE, Phoenix C25P). Through the top cover of the crystallizer the agitator and the measuring instruments were installed. The solution was homogenized with a four-pitched blade glass agitator with a diameter of 66 mm. The stirring velocity was generated by an electric drive (HEIDOLPH, RZR 2102). The temperature inside the crystallizer was controlled with a Pt100 temperature probe, which was connected to the thermostatic bath. For sampling a glass tube was installed near the Pt100. In case of gassing crystallization synthetic air (Air Liquide, $\geq 99.99\%$) was used. To avoid temperature changes inside the crystallizer, as well as the evaporation of solvent into the air bubbles, the synthetic air used for gassing passed a tempered with water filled washing bottle before it was introduced into the crystallizer. For the dispersion of the air bubbles a gassing ring with a diameter of 80 mm and 21 holes with a size of 0.5 mm on the upper side of the ring was installed 100 mm below the solution surface. For each crystallization experiment the crystallizer was filled with water and then solute material was added until the desired saturation concentration c_{sat} was reached. After that the solution was heated up to the start temperature T_{start} above the solubility limit within half an hour and then kept constant to ensure that all solute is dissolved. The subsequent crystallization was carried out from T_{start} with a linear cooling rate κ till the end temperature T_{end} was reached. In case of gassing crystallization the solution was treated with gas inside the metastable zone. During the gassing period the stirrer was switched off to ensure that the bubbles were not deformed.

The crystallization parameters were set depending on the investigations performed. Therefore, the information about the crystallization parameters investigated is given in each experimental section. Constant parameters, as well as the thermal history of the solution, are summed up for reasons of clarity for each material system in the appendix.

3.3. Filtration and Cake Washing

After crystallization the crystals were separated from the mother liquor by filtration. As mentioned in section 2.2 a consistent built-up of the filter cake – characterized by a flat surface without holes – is essential to guarantee that filtration and cake washing is done in a reproducible way. Otherwise, despite constant filtration and washing conditions, different starting conditions for drying are obtained. For the first experiments a commonly used filtration set up was used. It consisted of a porcelain Büchner funnel with a diameter of 70 mm, a 20-25 μm filter paper (WATMAN Grade 4), a 1 L side-arm flask, and a vacuum pump (VWR, model VP 86). The suspension was manually transferred from the crystallizer into the Büchner funnel. Since the volume of the Büchner funnel was less than the volume of the suspension the filtration was performed stepwise. To flush the crystallizer filtered mother liquor was used and then filtered again. In the following wash step, wash liquid was fed manually from a graduated cylinder on the filter cake. As can be seen in Figure 3.3 and Table 3.1 despite constant conditions of all process steps – crystallization, filtration, washing, and drying – highly different crystal size distributions (CSDs) were obtained for different batches after drying.

Since equal temperature and concentration profiles were arranged and measured during crystallization (compare Figure A.1 and Figure A.2) crystals were formed under the same kinetic conditions. Therefore, an impact during crystallization on the CSD was eliminated. However, the filtration set up used was dominated by manual working steps leading to an unreproducible, irregular build-up of the filter cake. Consequently, the low reproducibility of the CSD can be traced back to an inconsistent cake washing. Hence for further investigations a new filtration system was developed.

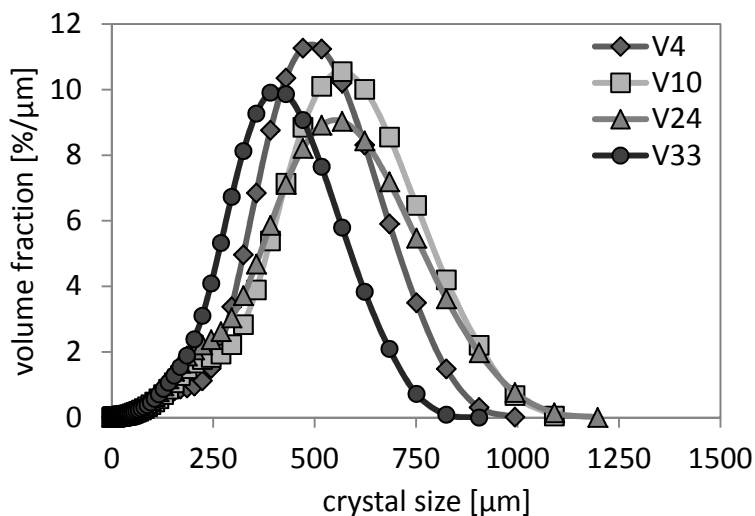


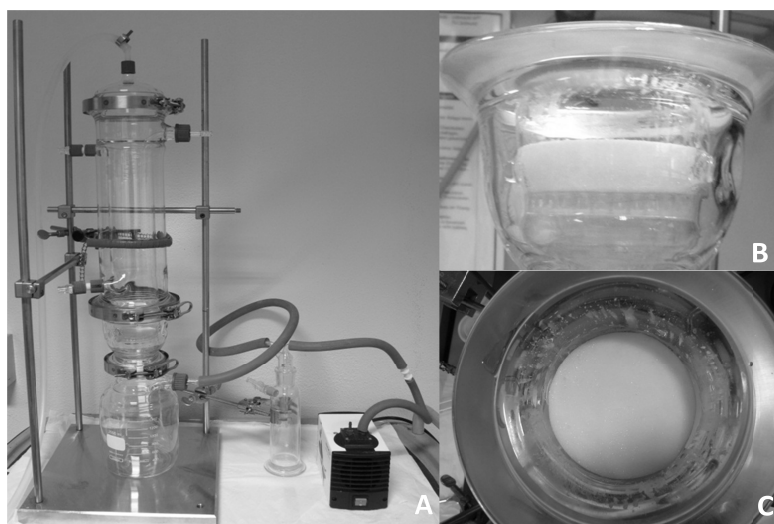
Figure 3.3: CSDs measured by laser diffraction of static dried L-alanine product batches filtered with Büchner funnel set up, produced under same conditions (listed in Table A.1 and Table A.3)

Table 3.1: Characteristic values of L-alanine product batches produced under same conditions for all process steps, filtered with Büchner funnel set up (cp. Figure 3.3)

	d_{10} [μm]	d_{50} [μm]	d_{90} [μm]	$d_{90}-d_{10}$ [μm]
V4	238	458	666	428
V10	199	507	756	557
V24	171	470	742	572
V33	176	370	565	389
Averaged	196 ± 26	451 ± 50	682 ± 76	486 ± 79

3.3.1. Development and Construction of new Filtration System

The self-constructed filtration system depicted in Figure 3.4 consists of a flask for the filtrate, a Büchner funnel like filtration unit with a 38.5 cm^2 glass frit of porosity four as filter medium, a cylindrical unit with a volume of 1.2 L above the filtration area, and a vacuum pump (VWR, VP 86). To avoid temperature influences during filtration the cylindrical unit is equipped with a double jacket for cooling or heating. Furthermore, due to the volume of 1.2 L above the filtration area the total amount of suspension from the crystallizer can be transferred at once to the filtration system by vacuum pumping before filtration starts. This sequential filtration allows a consistent filter cake build-up without manual influences which leads to a significantly improved reproducibility of the CSD (see Figure 3.5 and Table 3.2). Therefore, the Büchner funnel setup was replaced by the self-constructed filtration system and used for all experiments.

**Figure 3.4:** Self-constructed filtration system: (A) Overview, (B) Side view of filter cake, (C) Top view of filter cake

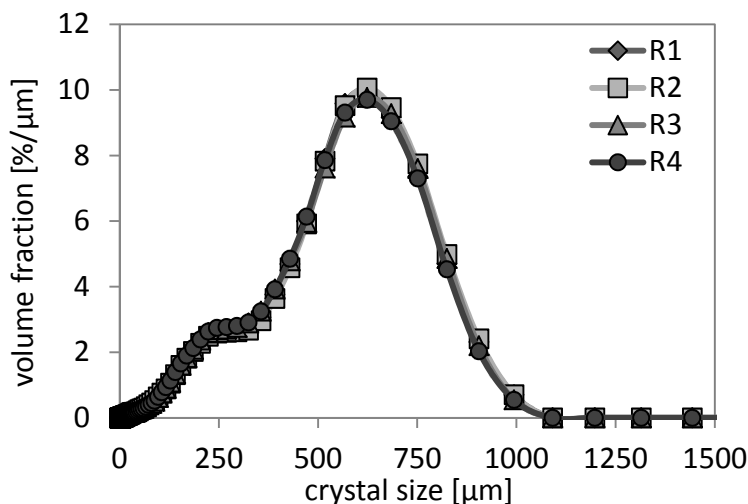


Figure 3.5: CSDs measured by laser diffraction of static dried L-alanine product batches filtered with the self-constructed filtration system depicted in Figure 3.4, produced under same conditions (listed in Table A.1 and Table A.3),

Table 3.2: Characteristic values of L-alanine product batches produced under same conditions for all process steps, filtered with the self-constructed filtration system (cp. Figure 3.5)

	d_{10} [μm]	d_{50} [μm]	d_{90} [μm]	$d_{90}-d_{10}$ [μm]
R1	151	507	705	554
R2	149	501	701	551
R3	149	511	705	556
R4	150	515	711	560
Averaged	150 ± 1	509 ± 5	705 ± 4	555 ± 3

3.3.2. Selection and Addition of Wash Liquid

Additionally to a homogeneous built-up of the filter cake, the selection of a suitable wash liquid and the addition of the wash liquid on the filter cake are decisive for an effective cake washing. In this thesis the focus of the cake washing lies on the displacement of the mother liquor between the crystals of the wet filter cake to reduce agglomeration during drying. Whereas, applications like the removal of by-products and impurities, or color removal were not taken into account. To select a suitable wash liquid for a material system the solubility of crystalline product in wash liquid, the miscibility of wash liquid and the mother liquor, and the viscosity ratio between mother liquor and wash liquid were considered. A detailed description of these criteria is given in section 2.2.2. The kinematic viscosity and density of the mother liquor after crystallization was measured at constant temperature with an Ubbelohde viscometer (capillary 1) and a pycnometer (Brand, 25 mL) to determine the dynamic viscosi-

ty. Furthermore, the water content of filtrate from each wash cycle was determined by Karl-Fischer (METTLER TOLEDO, V30) titration to evaluate the washout of mother liquor from filter cake.

To ensure a reproducible cake washing the addition of the wash liquid should allow a homogeneous penetration without filter cake deformation. Therefore, the addition of the wash liquid was performed with a full cone nozzle (MESTO, No. 1460). The moisture of the filter cake was adjusted via time. The filter cake was dehumidified for eight minutes after filtration, for three minutes between wash cycles, and for eleven minutes after washing. These times were determined during preliminary tests and ensured a dehumidification of the filter cake without shrinking or cracking.

3.4. Drying

To investigate the impact of drying on the quality of crystalline product batches three different drying methods were considered: static, fluidized bed, and rotary tube drying.

In case of static drying the crystals were dried in glass drying-cups with a diameter of 70 mm and height of 40 mm inside a ventilated oven (BINDER, series FD 53). For fluidized bed drying the fluid bed dryer TG 200 from Retsch with the three glass container attachment (container diameter 70 mm) was used. As third drying variant the rotary tube drying was investigated. Therefore, a self-constructed glass drying tube with a length of 3200 mm, a diameter of 750 mm, and five integrated rectangular baffles for mixing was used (compare Figure 3.6). Glass frits with a porosity of grade one, which were installed at both ends of the drying tube, ensured gas exchange and avoided product leakage. The drying tube was clamped in a rotating device and placed for temperature control in a ventilated oven (Heraeus, UT6120). The rotation was generated by an electric drive (WiseStir, HT50DX).

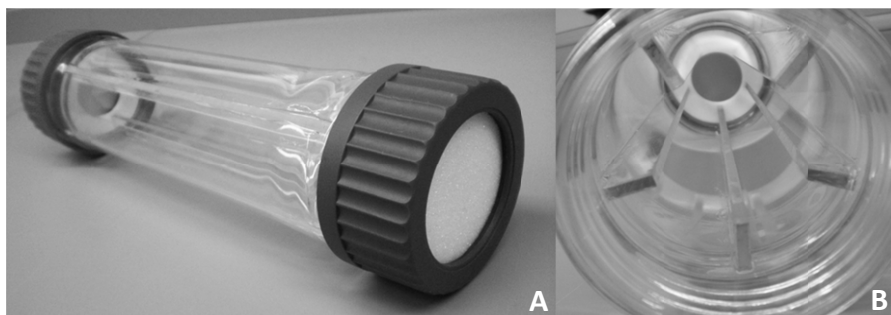


Figure 3.6: Self-constructed drying tube: (A) front view (B) interior view

3.5. Analytical methods

3.5.1. Solubility measurements

To determine the solubility of solids in different solvents gravimetric concentration measurements were carried out in a 300 mL double-jacket glass crystallizer or in 50 mL vessels with double-jacket. For temperature control Pt100 temperature probes connected with a thermostatic bath (Julabo, F25) were used. The crystallizer or vessel was filled with solvent and an excess of solid material. For sampling a glass tube was installed near the Pt100. The suspension was mixed in case of the crystallizer with a four-pitched agitator and in case of the vessels with a magnetic stirrer. For each measuring point the temperature was held constant for 48 h to reach equilibration before three samples of 2-3 mL were taken with a syringe via the glass tube. To avoid crystallization during sampling for temperatures higher than 35 °C the syringes were tempered at 50 °C in a ventilated oven. After sampling each sample was filtered through a 0.45 µm membrane. The solution received was weighed (m_{solution}), stored at 50 °C in a ventilated oven until the solvent was evaporated, and then the remaining solid was weighed (m_{solid}) again. The weighing was performed by a high precision scale (Mettler Toledo, XS205 DualRange) with an accuracy of 0.01 mg. Finally, the concentration of solid in the solvent was calculated according to equation (3.1). Herein, N stands for the number of samples taken.

$$c = \frac{1}{N} \sum_{i=1}^N \frac{m_{\text{solid},i}}{m_{\text{solution},i} - m_{\text{solid},i}} \quad (3.1)$$

3.5.2. Concentration profile and Metastable Zone Width

To characterize the crystallization process the concentration profile and the metastable zone width (MZW) were determined. The concentration profile was measured gravimetrically. For this purpose, at defined points in time two samples were taken out of the crystallizer during crystallization using the glass tube installed, and the corresponding temperature was noted. The concentration was determined following the method, described in the section above, for solubility measurements.

The MZW was determined as temperature difference according to equation (3.2) using the saturation temperature T_{sat} and the concentration profile measured. The concentration during crystallization stays first constant at saturation concentration c_{sat} . Then a rapid decrease of the

concentration and supersaturation profile can be observed, which marks the point of nucleation characterized by the nucleation temperature T_{nuc} and the limit of the MZW, respectively. Since the technique for the determination of the MZW is an indirect measurement method the correction factor φ was used to consider that nucleation can take place before concentration decreases measurably. The factor φ – determined by “naked eye”-measurements – depends on the material system and ensures that inside the MZW no crystals are present in solution.

$$\text{MZW} = \varphi \cdot (T_{\text{sat}} - T_{\text{nuc}}) \quad (3.2)$$

3.5.3. Crystal Size Distribution

Together with the purity and the habit of the final crystal product the crystal size distribution (CSD) is applied to characterize the product quality of crystalline product batches. Custom specifications like the median crystal size and the width of the CSD are determined by the characteristic diameters d_{50} , as well as the difference $d_{90}-d_{10}$, respectively. Since in this thesis the product quality of batches should be characterized after crystallization and drying only, the CSD was measured by off-line techniques.

During the first experiments laser diffraction analysis was applied. The measuring principle is based on the generation of diffraction patterns depending on the particle size. The size of each particle detected is given as diameter of a volume equivalent sphere. For the measurements a laser diffraction particle size analyzer (Beckman Coulter, LS 13320) in combination with the Tornado Dry Powder System was used. For suction of the dried sample the system was connected to a vacuum cleaner (Dyson, DC 29 allergy). The LS 13320 has a measurement range of 0.4 μm up to 2000 μm and offers a highly reproducible analysis of samples with a weight of around 25 g in a very short time (two minutes).

However, the laser diffraction analysis method is not suitable for all habits of crystals, especially the analysis of elongated or needle-like crystals is limited, and no information about the morphology of the crystals is provided. Therefore, in the further course of the work two image analysis techniques were used to provide not only the CSD but the morphology of the crystals also. Both methods determine the CSD out of the projection area of particles, i.e. the size corresponds to the diameter of an area equivalent circle; merely the image recording differs. Moreover, image descriptors – like the elongation – can be determined for each crystal to characterize the morphology.

Due to reasons of available equipment, first the so-called scanning image analysis technique for the characterization of dried crystalline product batches was developed. Herein the image

recording was performed by a transmitted light scanner (Epson, Perfection V750 Pro). Later, the scanning image analysis technique was adapted to allow the measurement of the CSD and morphology of crystals in suspension also. Therefore, instead of the transmitted light scanner the image analysis sensor QICPIC from Sympatec combined with the LIXELL module and a 2 mm cuvette was used. In contrast to the scanning image analysis technique the QICPIC image analysis technique can be used for the analysis of dried crystals as well as for crystals in suspension. The sample preparation and procedure for the measurement of the CSD and the morphology of the crystals via image analysis technique was developed in the context of the thesis and is therefore given in chapter 4 in detail.

3.6. Statistical Methods

3.6.1. Design of Experiments

Design of Experiments (DoE) allows investigating systematically in which way a specific change of input variables (influence factors) has an impact on output variables (responses). Through a goal-driven reduction of experiments time and costs are saved without impairing the significance of the results. The selection of a DoE depends on the aim of analysis, the number of influence factors investigated, and the available time. To investigate quantitatively the dependence of responses from k factors a central composite design is most suitable. The design is exemplarily depicted in Figure 3.7 for three factors and consists of a cube (black), a star (green), and a center point (red). The cube characterizes a full factorial design with 2^k experiments on two factor levels (-1, 1). By adding the star and the center point three additional factor levels ($-\alpha$, $+\alpha$, and 0) are realized so that nonlinear relations between the factors and responses can be identified. [102]

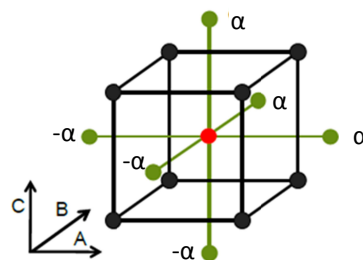


Figure 3.7: Central composite design for three factors (A, B, and C)

The total number of experiments N is calculated according to equation (3.3) and depends on the number of investigated factors k and the realizations of the center point experiments n_0 . By performing the center point experiments multiple times the standard deviation of the whole design can be defined so that all other experiments can be realized once only. [102]

As result of the central composite design a nonlinear regression model is obtained which describes the impact of the factors x_i , interactions x_{ij} , and nonlinearities x_{ii} on the response y (see equation (3.4)). The corresponding regression coefficients β_i , β_{ij} , and β_{ii} are calculated following equation (3.5) and (3.6) and specify the strength of the impact of the factors on the response. In these equations the variables \bar{x}_i , \bar{x}_{ij} , and \bar{y} are defined as mean values of the factors, factor interactions, and responses of all experiments performed. In case of an orthogonal design the regression coefficients are linear independent and the effect of a factor is twice the regression coefficient (effect= 2β). To increase the precision of the regression model significant factors, interactions, and nonlinearities are considered only. The significance is evaluated via the 95 % confidence interval ci (see equation (3.7)) using the standard deviation sd of the center points and the t -value of the Student's distribution which depends on the degree of freedom f of the center point experiments ($f=n_0-1$). An effect of a factor or of an interaction has a significant impact on one of the responses if the effect exceeds the confidence interval. Additionally, for the evaluation of a DoE significant effects are divided in positive and negative effects. A positive effect of a single factor X means that an increase of the factor X from level -1 to 1 increases the response, whereas for a negative effect a decrease of the response can be observed. Significant nonlinear effects XX indicate that the change of the factor X leads to a nonlinear change of the response. Hence, the response values in the respective factor range obtain a local minimum, a local maximum, or an asymptotic course. If a significant factor interaction XY is detected, the single factors X and Y are interdependent. [102]

To reach an orthogonal design the α -levels of the star have to be determined by equation (3.8). If factor levels of the star cannot be realized due to technical reasons, the factor levels can be centered to the face of the cube. These factor levels are called face-centered. However, in this case the resulting design is not orthogonal which leads to an overestimation of the nonlinear effect for the corresponding factor. Therefore, in case of face-centering the significance of nonlinear effects has to be treated with caution. [102]

To minimize random interferences of unknown influence factors the experiments of the DoEs have to be performed in randomized order.

$$N = N_{\text{cube}} + N_{\text{star}} + N_{\text{center point}} = 2^k + 2k + n_0 \quad (3.3)$$

$$y = \beta_0 + \sum_{i=1}^N \beta_i \cdot x_i + \sum_{i=1}^N \sum_{j=1}^N \beta_{ij} \cdot x_{ij} \quad (3.4)$$

$$\beta_i = \frac{\sum_{k=1}^N (x_{i,k} - \bar{x}_i)(y_k - \bar{y})}{\sum_{k=1}^N (x_{i,k} - \bar{x}_i)^2} \quad \beta_{ij} = \frac{\sum_{k=1}^N (x_{ij,k} - \bar{x}_{ij})(y_k - \bar{y})}{\sum_{k=1}^N (x_{ij,k} - \bar{x}_{ij})^2} \quad (3.5)$$

$$\beta_0 = \bar{y} + \sum_{i=1}^N \beta_i \cdot \bar{x}_i - \sum_{i=1}^N \sum_{j=1}^N \beta_{ij} \cdot \bar{x}_{ij} \quad (3.6)$$

$$ci = \pm \frac{2 \cdot sd \cdot t}{\sqrt{n_0}} = \pm \sqrt{4 \cdot \frac{\sum_{k=1}^{n_0} (y_k - \bar{y})^2}{n_0 \cdot (n_0 - 1)}} \cdot t \quad (3.7)$$

$$\alpha^2 = \frac{1}{2} \cdot (\sqrt{(N \cdot N_{\text{cube}})} - N_{\text{cube}}) \quad (3.8)$$

3.6.2. Discriminant Factor Analysis

The Discriminant Factor Analysis (DFA) – in literature also called discriminant function analysis or discriminant analysis – is a multivariate data analysis method and belongs to the class of structured testing algorithms. Here a short summary about the basic functionality of DFA is given, for detailed information see [103] or [104]. DFA is used to classify data sets on basis of characteristic variables X_i into two or more groups. In this thesis the method is used to differentiate between single crystals and agglomerates, whereby image descriptors like the circularity are used as characteristic variables (see chapter 4). Since DFA is a structured testing algorithm a training set has to be created first, i.e. a part of the data set has to be classified manually into groups. The principle of DFA is schematically depicted for two groups – displayed as red and blue dots – and two characteristic variables X_1 and X_2 in Figure 3.8.

As can be seen in Figure 3.8, neither the characteristic variable X_1 nor X_2 is suitable alone to separate the groups; the overlap is too large. Via DFA a linear combination of the characteristic variables X_i – a so-called discriminant function D – is identified by fitting the corresponding discriminant coefficients b_i (see equation (3.9)). The discriminant coefficients b_i are determined in such a way that the overlap between the groups is minimized leading to an maximal possible separation of the groups. Subsequently, the determined discriminant function can be used for the classification of the whole data set. [103]

To sum up the efficiency of the DFA classification depends on the training set and the characteristic variables selected. The better the training set maps the data set and the better the characteristic variables describe the difference of the objects, the more precise the classification with the discriminant function for the whole data set is.

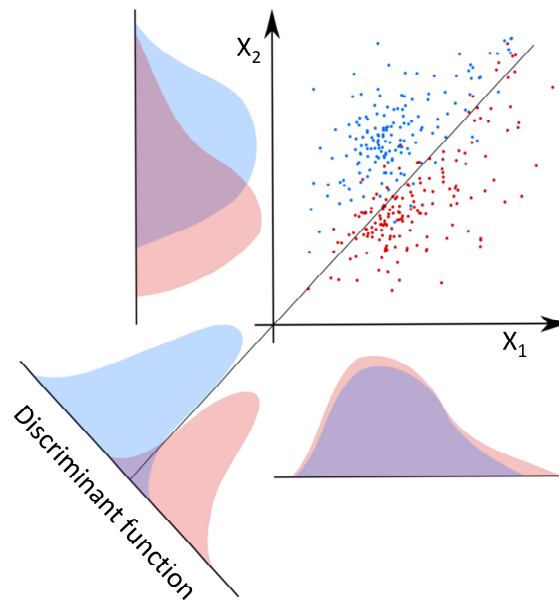


Figure 3.8: Schematic principle of Discriminant Factor Analysis (DFA) for two groups (displayed as blue and red dots) and two characteristic variables (X_1 , X_2) [105]

$$D = b_0 + \sum_{i=1}^N b_i \cdot X_i \quad (3.9)$$

3.6.3. Factor Analysis

The factor analysis is a statistical tool for the reduction or bundling of variables and is used for the detection of a correlation between variables. Strongly correlating variables are combined in groups, which are designated as factors also, so that slightly correlating variables can be separated from each other. To quantify the correlations between the variables correlation coefficients are calculated which allow the evaluation of the relationships between all variables. As result of the factor analysis a factor matrix (see Figure 3.9 I) is obtained by which the variables can be assigned to the factors (groups), i.e. for example all variables – in our case all image descriptors – which describe the expansion of an object are compiled. The maximum number of factors identified is equal to the number of variables considered.

I factor matrix				II rotated factor matrix			
variable	factors			variable	factors		
	1	2	3		1	2	3
A	0.939	-0.166	0.109	D	0.988		
B	-0.160	-0.789	-0.092	A	0.968		
C	0.184	0.829	-0.329	C		0.966	
D	0.947	-0.176	0.100	E		0.947	
E	0.232	0.909	-0.236	F			0.835
F	0.290	0.210	0.585	B			-0.731

Figure 3.9: Results of factor analysis: (I) factor matrix without processing, (II) with varimax algorithm rotated factor matrix, sorted by values, and an indicator threshold value of 0.5

To reduce the number of factors different extraction criteria can be considered. Here the Kraisser-criterion is used, i.e. the factors are extracted only if the corresponding Eigen-value is greater than one. The values inside the factor matrix are referred to as factor loading and are the correlation coefficients between the variables and the factors.

To facilitate the assignment of the variables to the factors it is useful to sort the factor loadings, to increase the indicator threshold value, and to rotate the factor matrix by using e.g. the varimax algorithm (see Figure 3.9 II). The rotated factor matrix is reached by the multiplication of the factor matrix with an orthogonal matrix. From a graphical view the rotation is comparable with an orthogonal rotation of the axis of a coordinate system, i.e. all point inside the loading space get new coordinates. Therefore the rotation can lead to higher differences of the factor loadings, i.e. the rotation facilitates the assignment of the variables to the factors.

[104]

In this thesis factor analysis will be used for the identification of suitable characteristic values (image descriptors) for the Discriminant Factor Analysis (DFA), i.e. per factor the image descriptor with the highest absolute factor loading is chosen (see chapter 4). For more information or mathematical background of factor analysis see [103, 104].

4. Quantification of Agglomeration

The crystal size distribution (CSD) is an important quality criterion to evaluate e.g. the filterability and flowability of crystalline products, and can be determined online, by e.g. Focus Beam Reflectance Measurement (FBRM), or off-line, after solid-liquid separation and drying, by e.g. sieving or laser diffraction measurements [15]. In general, the CSD measured is characterized afterwards by characteristic values, like median crystal size d_{50} or width of CSD $d_{90}-d_{10}$. However, no information about the particle morphology or the amount of agglomerates – in the further course named as agglomeration degree – is given by these characteristic values. Hence, large crystalline particles may be interpreted as size change by crystal growth, although agglomerates exist. Particular, several organic compounds like paracetamol [1, 10, 106], sucrose [1, 107], or adipic acid [55, 101] tend to agglomerate. The lack of information about the particle morphology in CSD can lead to misunderstand the crystallization process, especially when agglomeration takes place during solid-liquid separation or drying, and an off-line CSD measurement technique is used. To avoid a misconception of crystallization processes and due to an increasing purity demand in industry, the detection and localization of agglomeration plays an important role. Therefore, first aim of the thesis was to develop an automatic measurement method for the quantification of agglomerates. In this context the agglomeration degree distribution (AgD) of crystalline product batches is introduced to establish a new quality criterion, which delivers in contrast to CSD information about the amount and distribution of agglomerates (The definition of the AgD is given in section 4.1). The AgD and the corresponding characteristic values shall allow statements, whether crystals tend to agglomerate and whether agglomeration takes place during crystallization or further downstream processes. To determine the AgD, i.e. to differentiate between single crystals and agglomerates, image analysis in combination with Discriminant Factor Analysis (DFA) (compare section 3.6.2) is used.

In several previous studies the image analysis technique, developed by Pons et al. [108], was used successfully to describe crystalline particles by image descriptors, e.g. perimeter or area ratio. These results were combined with statistical multivariate data analysis, like Discriminant Factor Analysis (DFA) or Principal Component Analysis (PCA), to classify the crystalline particles. The image recording was realized off-line after drying using a microscope to

quantify the morphology of sucrose crystals [107] or to study the agglomeration behavior of paracetamol [1, 10, 109]. Online recording was implemented by Ferreira et al. [110], who investigated the influence of $MgCl_2$ on the morphology of NaCl in suspension and Blandin et al. [111], who used online image analysis to measure particle size distribution of salicylic acid. As multivariate data analysis DFA is primarily utilized [1, 107, 109, 110].

In literature crystalline particles are classified in different groups. In general, single crystals and agglomerates are distinguished, but according to the particular author's different subgroups of agglomerates are defined, e.g. Faria et al. [107] differentiate between small agglomerates, medium agglomerates, and large agglomerates. The performance of the discriminant function is expressed by the performance index PI, which describes the compliance between manual and automated classification. As outcome of the DFA an agglomeration degree, which is defined in various ways, can be determined. Faria et al. [107] established an agglomeration degree Ag_i , which is a measure of the complexity of each crystalline particle, and is calculated by the probabilities Pb_i of each particle to belong to groups like single crystals or large agglomerates. Also a number based agglomeration degree was used by Yu et al. [109]. This agglomeration degree is given by the ratio of agglomerates to all crystalline particles, considering the amount of medium agglomerates with a factor of 0.5.

In contrast to literature in this thesis a number-based agglomeration degree Ag of a crystalline product batch is calculated without factorial rating of particular groups. The main focus of the discriminant function validation lies on the transfer to other crystalline product batches of the same material system but produced under different conditions. The aim is to find an optimal discriminant function, a so-called reference discriminant function, which can be used for the classification of all crystalline product batches of the same material system, to avoid the time consuming manual creation of a training set for the AgD determination of each crystalline product batch. Therefore, the influences of the kind and amount of image descriptors used are investigated. The image analysis tool was developed for dried crystalline product batches of the material systems L-alanine/ water and adipic acid/ water first [112] and then extended for crystalline product batches in suspension. In the following the AgD , as well as the corresponding new characteristic values, are defined and explained (see section 4.1). In section 4.2 the image analysis tool developed for dried crystals is presented exemplarily for the material system L-alanine/ water first. Then the methodology is applied to the material system adipic acid/water. Afterwards, in section 4.3, the image analysis tool is extended to crystals in suspension.

4.1. Introduction of Agglomeration Degree Distribution (AgD)

The agglomeration degree distribution (AgD) describes the amount and distribution of agglomerates in a crystalline product batch, and is defined as a function of the crystal size d that fits the agglomeration degrees Ag_j for $j = [1, N]$ particle fractions using the least squares method. The number of particle fractions N depends on the particle size interval chosen. The agglomeration degree of the crystalline product batch Ag (see equation (4.1)) or the agglomeration degree of a particle fraction Ag_j (see equation (4.2)) is defined by the number of agglomerates to the number of crystals in the product batch or the particle fraction, respectively.

$$Ag = \frac{n_{\text{agglomerates}}}{n_{\text{crystals}}} \quad (4.1)$$

$$Ag_j = \frac{n_{\text{agglomerates},j}}{n_{\text{crystals},j}} \quad j=[1, N] \quad (4.2)$$

To get quantitative information about the AgD curve, and to allow the comparison of different crystalline product batches, similar to the often used characteristic values d_{10} , d_{50} , and d_{90} of CSD, as new characteristic measure $d(Ag_i)$ is introduced (compare Figure 4.1). $d(Ag_i)$ describes the crystal size d where the Ag reaches the value i . For example the characteristic value $d(Ag_{\text{max}})$ can be used to quantify the broadening of CSD by agglomeration processes, i.e. to identify whether big crystals are created by agglomeration or by crystal growth. Also the characteristic values $d(Ag_{\text{min}})$, $d(Ag_{0.5})$, and $d(Ag_{0.9})$ are calculated. An Ag_i of 0.5 or 0.9 means, that 50 % or 90 % of the crystalline particles are agglomerates. By means of these characteristic diameters it is possible to describe the progression of the AgD, i.e. the increase or decrease of agglomerates in dependence of crystal size. The curve progression of different AgDs can be divided into two sections. For the first section the span between $d=0 \mu\text{m}$ and $d(Ag_{0.5})$ represented by $d(Ag_{0.5})$ and for the second section the difference of $d(Ag_{0.9})$ and $d(Ag_{0.5})$ are used. As demonstrated in Figure 4.2 these descriptors allow to distinguish between different changes of the AgD. Less agglomeration shifts the AgD to lower Ag_j -values over the whole crystal size range (compare Figure 4.2 I) so that higher values for $d(Ag_{0.5})$ and for the difference $d(Ag_{0.9})-d(Ag_{0.5})$ are reached. Whereas, higher amounts of smaller agglomerates in combination with a lower amount of larger agglomerates results in lower values for $d(Ag_{0.5})$ and higher values for the difference $d(Ag_{0.9})-d(Ag_{0.5})$ (compare Figure 4.2 II).

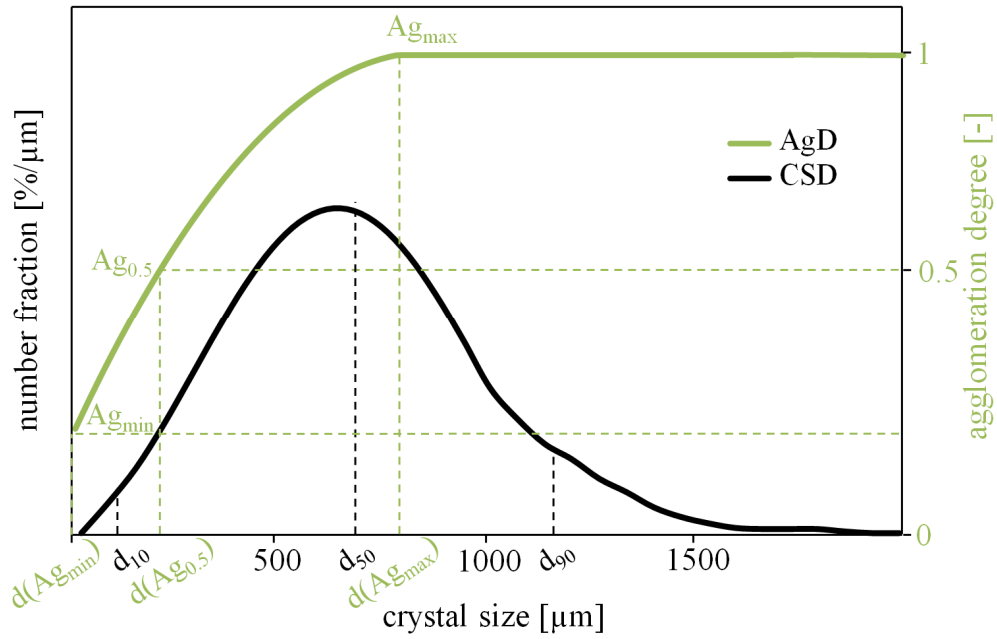


Figure 4.1: Schematic diagram of the agglomeration degree distribution (AgD) and crystal size distribution (CSD)

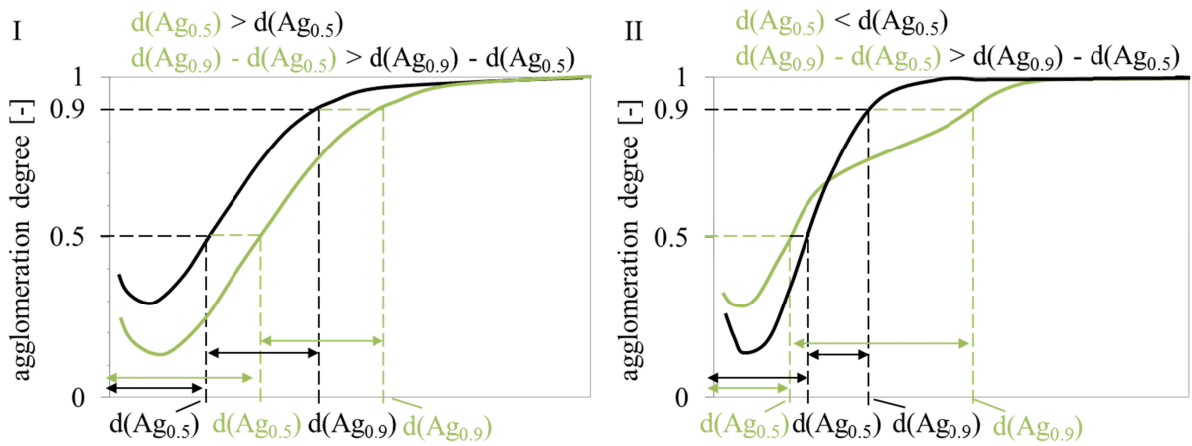


Figure 4.2: Characterization and comparison of AgDs by means of the characteristic values $d(Ag_{0.5})$ and $d(Ag_{0.9}) - d(Ag_{0.5})$

4.2. Development of Image Analysis Tool for Dry Crystals

The flow chart shown in Figure 4.3 gives an overview about the necessary steps for the determination of the agglomeration degree distribution (AgD) of a crystalline product batch. The procedure is divided into three subsections: Preparation, multivariate analysis, and evaluation. First – during preparation – images of a sample from the crystalline product batch are taken, and each crystal is characterized by several image descriptors. At second, if no reference discriminant function for the material system is available, Discriminant Factor Analysis (DFA) as multivariate analysis tool has to be applied to create the reference discriminant function for the material system. Otherwise, if a reference discriminant function already exists, the multivariate analysis is not necessary. In the last subsection – the evaluation – the reference discriminant function is used to classify automatically all crystalline particles of the sample, and the crystalline product batch is characterized by the AgD. The particular methods applied in each step are explained in the following subsections in detail.

For the development of the image analysis tool three statically dried crystalline product batches of L-alanine (Ala-1, Ala-2, Ala-3) and two statically dried crystalline product batches of adipic acid (AA-1, AA-2) are investigated. The crystalline products were produced in case of L-alanine by batch cooling crystallization and in case of adipic acid by gassing crystallization. The crystallization conditions were kept constant for all experiments (compare Table A.3 and Table A.6). The washing and drying parameters of all experiments are listed in Table 4.1. As wash liquids ethanol (Merk, absolute EMPLURA[®]) for L-alanine and acetonitrile (VWR, HPLC gradient grade $\geq 99.9\%$) for adipic acid were utilized. In the following for demonstration purposes data for the material system L-alanine/water are shown.

Table 4.1: Washing and drying parameters of the crystalline product batches investigated for the development of the image analysis tool

	Adipic acid		L-alanine		
	AA-1	AA-2	Ala-1	Ala-2	Ala-3
Cake washing					
Wash liquid temperature [°C]	20	-	12.5	5	5
Amount of wash liquid [mL]	70	-	35	50	20
Number of wash cycles [-]	3	-	2	1	1
Static drying					
Drying temperature [°C]	22	22	50	30	70
Layer thickness [cm]	2	2.1	1.35	0.9	0.9
Drying time [days]	1	1	2	1	1

4.2.1. Preparation

For image recording the crystalline product batch is fractionated with a rotary cone sample divider (Fritsch, Laborette 27) stepwise into 16 fractions. Afterwards, two of the fractions, in the following marked with “a” or “b” behind the name of the crystalline product batch listed in Table 4.1, are dispersed equally with a spatula on the glass surface of a transmitted light scanner (Epson, Perfection V750 PRO). Subsequently 2000 to 3000 crystalline particles are scanned as an A4 format 8-bit grayscale image with a resolution of 4800 dpi. For increasing the image quality the features unsharp mask filter and background lighting correction with level high are used in the Epson software (Epson scan). The TIF-File received is divided by MATLAB (MathWorks, Version R2010b) into 48 equal parts to reduce the file size for the image analysis. The image analysis is performed by the open source software ImageJ (Version 1.45s, Wayne Rasband, National Institute of Health, USA) in two steps:

In the first step primary (dimensioned) and secondary (dimensionless) image descriptors are determined (see Table A.7). Therefore, each 8-bit grayscale image is reduced to a binary image by using the threshold method *Yen*. After that the operation *Hole Filling* is used to fill out white areas, which are surrounded completely with black color. Furthermore, dust or blurred particles and particles, which have contact to the image border, are eliminated by the operations *Noise Elimination* and *Border Kill*. The limit of the *Noise Elimination* was set to a minimal projection area of 0.03 mm^2 , which was identified as limit to eliminate the majority of blurred particles. The minimal projection area of 0.03 mm^2 corresponds to an equivalent diameter of $200 \text{ }\mu\text{m}$, and leads to a size limitation for the measurement of the crystal size distribution and agglomeration degree distribution. After the operations *Noise Elimination* and *Border Kill* all remaining particles with an equivalent diameter larger than $200 \text{ }\mu\text{m}$ are identified, numbered, and described by their coordinates and boundary box.

To get further information about the crystalline particles, in the second step, grayscale parameters, which cannot be calculated from the binary images, are determined for each particle. For this purpose a single image is cut out for each particle from the grayscale images with MATLAB, using the determined coordinates and boundary boxes of the first step. Next the grayscale parameters area fraction, minimal grayscale value, mean grayscale value, and the standard deviation of grayscale values, described in Table A.7 (numbers 19-22), are determined for each single image using ImageJ again. As result of the preparation steps a data set with 22 image descriptors for each particle is obtained.

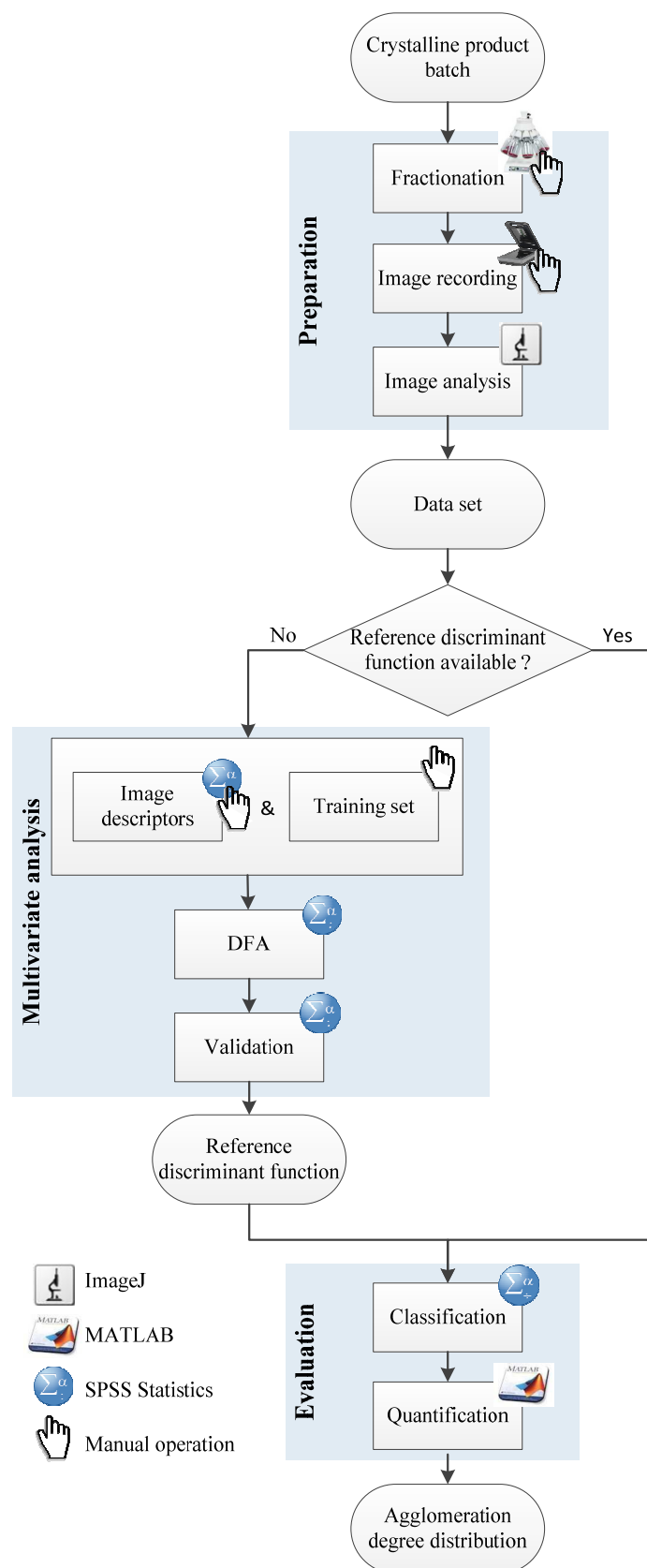


Figure 4.3: Flow chart to determine the AgD of a crystalline product batch

4.2.2. Multivariate Analysis

During multivariate analysis the data set of the previous preparation step is used to classify crystalline particles into groups like single crystals and agglomerates. Therefore, Discriminant Factor Analysis (DFA) is used. The analyses were performed with *SPSS Statistics* (IBM, Version 21). First of all, a part of the crystalline particles of the data set has to be classified manually to create a training set. In parallel, independent image descriptors from the data set have to be identified to find a linear combination of image descriptors that separates the particles of the training set with a minimal overlay of the defined groups. The best linear combination of the image descriptors is called discriminant function and can be used to classify automatically all particles of a data set. To avoid the time consuming manual classification step (creation of the training set) for each data set the aim of the discriminant function validation is to find a so-called reference discriminant function for the material system used. Consequently the multivariate analysis has to be performed only if no reference discriminant function for the material system is available. Otherwise, if a reference discriminant function for the material system already exists, this discriminant function can be used directly to classify all crystalline particles of the material system into groups like single crystals and agglomerates.

To assess the results of DFA the performance index PI (see equation (4.3)) and the specific performance indices PI_i (see equation (4.4)) are used, according to literature [107, 113]. However, no information about the agglomeration degree Ag (see equation (4.1)) is given by the performance indices. Hence, in contrast to literature, the assessment is made additionally by the percentage deviation of the agglomeration degree δAg (see equation (4.5)). δAg describes the deviation between the manually determined agglomeration degree Ag_{manual} and the by DFA calculated agglomeration degree $Ag_{\text{calculated}}$. In summary, a good classification result is reached if the results are characterized by high PI values and low δAg values.

$$PI = \frac{n_{\text{correctly classified particles}}}{n_{\text{total amount}}} \cdot 100 \% \quad (4.3)$$

$$PI_i = \frac{n_{\text{correctly classified particles of type i}}}{n_{\text{total amount of type i}}} \cdot 100 \% \quad (4.4)$$

$$\delta Ag = \frac{|Ag_{\text{calculated}} - Ag_{\text{manual}}|}{Ag_{\text{manual}}} \cdot 100 \% \quad (4.5)$$

Creation of a training set

A training set is needed to train the DFA and to assess the results of DFA by comparing manual and automatic classification. Consequently, the manual classification of the crystalline particles into groups, i.e. the composition of the training set, is the core of the DFA. The crystalline particles of L-alanine - as well as of adipic acid - can be distinguished depending on their morphology into four groups (see Figure 4.4, T1): Clearly identifiable single crystals (red), clearly identifiable agglomerates (blue), crossover crystals difficult to allocate to single crystals or agglomerates (green), and waste particles (orange). The group waste particles allows to exclude blurred elements, which have a projection area larger than 0.03 mm^2 (equivalent diameter larger than $200 \mu\text{m}$), like stains on the scanning surface as well as lint's from crystalline particles, to ensure that for the calculation of the agglomeration degree A_g (see equation (4.1)) crystalline particles are included only. These waste particles can be determined automatically by the image analysis software, and do not need any user input.

Since the manual classification of crossover particles strongly depends on the person performing, the question arises, which degree of detail is necessary to develop a good performing discriminant function. Therefore, to investigate the influence of the training set composition on the performance of DFA three different kinds of training sets (T1, T2, and T3) were considered, and their applicability for DFA was evaluated. The training sets differ in the amount of groups as well as in the classification of several crystalline particles, and are presented in Figure 4.4.

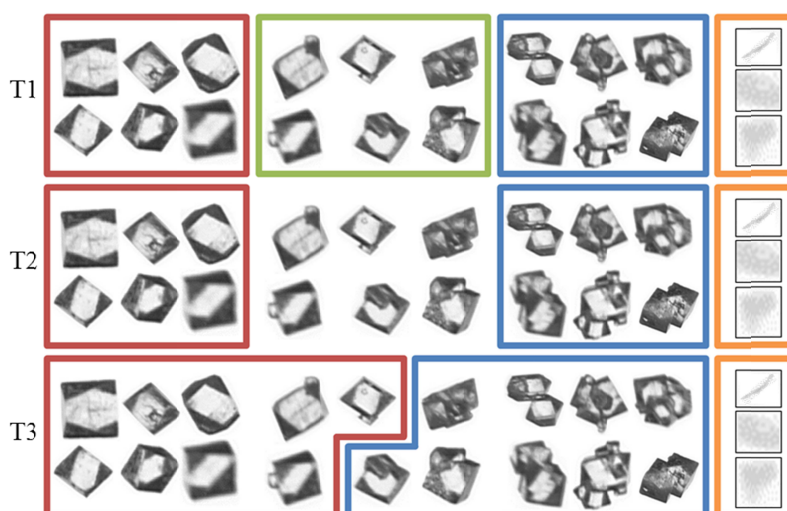


Figure 4.4: Composition of the training sets T1, T2, and T3: single crystals (red), crossover crystals (green), agglomerates (blue), and waste particles (orange)

The training set T1 is composed of all four groups mentioned before. The training set T2 is composed of three groups: Clearly identifiable single crystals (red), clearly identifiable agglomerates (blue), and waste particles (orange). Crossover crystals are not used in the training set T2 to reduce the number of groups, which have to be separated by DFA, as well as to reach a maximal difference between the groups' single crystals and agglomerates for the training of DFA. To assess the results of the discriminant function, which is determined based on the training set T2, the training set T3 has to be used as a so-called control group. Otherwise the potential benefit of the additional classification of the crossover crystals cannot be assessed. Therefore, training set T3 is composed of three groups like training set T2. But in this case all crystalline particles are assigned in single crystals (red), agglomerates (blue), and waste particles (orange). Crossover crystals consisting of two crystals only, one single crystal and a small crystal attached on the surface of the single crystal, are assigned to the group single crystals. All other crossover crystals are allocated to the group agglomerates. To allow an insight into the relative importance of the different particle groups the compositions of the training sets Ala-1a and Ala-2a are presented exemplarily in Table A.8.

To evaluate the applicability of the described training sets 1000 crystalline particles of the data sets Ala-1a and Ala-2b, respectively, were classified manually. The size of 1000 crystalline particles per training set shall ensure that the discriminant function is determined on the basis of a representative sample of the crystalline product batch. For the evaluation of the training set types T1, T2, and T3 image descriptors have to be selected parallel (see Figure 4.1). The results shown in this section are delivered by an iterative procedure. As image descriptors the equivalent diameter, the solidity, the elongation, the area fraction, and the standard deviation of grayscale values were used. This optimal set of image descriptors was determined following the methodology described in the next paragraph but not shown here for simplification reasons.

Table 4.2 shows exemplary the results of DFA for the data sets Ala-1a and Ala-2b. Beside the specific performance indices PI_i of the different groups and the performance index PI of the crystalline product batches, the percentage deviation of the agglomeration degree δAg is listed for the training sets T1, T2, and T3. In all cases a PI_w value of 100 % is reached for the group waste particles, and for increased values of the performance index PI decreased values of δAg are obtained. For both data sets the results, which are obtained with the training set T1, are characterized by a lower performance than the results of the training sets T2 and T3. Both, the values of the specific performance indices PI_i and the total performance index PI are lower, and the deviation of the agglomeration degree δAg is higher also.

Table 4.2: Results of DFA for the data sets Ala-1a and Ala-2b in dependence of the training sets (1000 particles) used; S: single crystals, C: crossover crystals, A: agglomerates, W: waste particles

Training set		PI _S [%]	PI _C [%]	PI _A [%]	PI _W [%]	PI [%]	δAg [%]
Ala-1a	T1	61.6	38.4	60.5	100	59.2	30.1
	T2	87.6	-	67.2	100	79.9	15.2
	T3	86.7	-	69.8	100	80.1	12.0
Ala-2b	T1	40.0	26.9	59.8	100	52.8	26.7
	T2	52.9	-	85.2	100	72.6	15.1
	T3	53.4	-	85.2	100	72.8	14.8

The values of the training sets T2 and T3 differ only slightly. The highest PI, as well as the lowest δAg, is reached with the training set T3.

The PI_W value of 100 % indicates that a separation of blurred particles is possible independent of the training set used. The correlation between PI and δAg can be explained due to the fact that a correct classification of the different crystalline particles has a direct influence on δAg (see equation (4.5)).

The analysis of the different training sets shows that the performance of the discriminant function depends on the kind of the training set used. With an increased number of groups the overlapping of the groups increases and the specific performance indices PI_i, as well as PI, decrease consequently. This can be seen especially for the crossover crystals of training set T1. Only 38.4 % (Ala-1a) or rather 26.9 % (Ala-2b) of the crossover crystals are classified correctly by DFA.

Due to the similarity of the results of the training sets T2 and T3 it should not make a big difference for the calculation of the agglomeration degree, i.e. the agglomeration degree distribution, whether the discriminant function of training set T2 or training set T3 is used. But in contrast to training set T3 the classification of training set T2 offers the advantage that the user has to assign clearly identifiable crystalline particles only making the composition of the training set T2 user-independent. Therefore, a training set composed of manually identified single crystals and agglomerates is sufficient to develop a good discriminant function. For further investigation the training set T2 was chosen using the advantage of a user-independent classification.

Selection of significant image descriptors

The choice of image descriptors plays - beside the creation of the training set - a decisive role for the performance of DFA, because they are used to characterize the crystalline particles for classification. Therefore, the objective of this subsection is to investigate the influence of the amount and kind of image descriptors used on the performance of DFA, as well as to evaluate if factor analysis (see section 3.6.3) offers a systematic and time efficient way for the selection of suitable image descriptors.

The 22 image descriptors, which are used in this study and described in Table A.7, are sorted by factor analysis for six different L-Alanine data sets. Table 4.3 shows the results. The image descriptors equivalent diameter (d_{eq}), elongation (Elong), and standard deviation of grayscale values (StdDev) are detected as being significant for all data sets. The solidity (Sol), the area fraction (%Area), as well as the NSwC are identified just in some cases, and the projection area (A) is detected for the data set Ala-1b only.

The results of Table 4.3 indicate that the number of image descriptors used for DFA can be reduced by factor analysis from 22 image descriptors to maximal seven image descriptors.

Due to the similar results for the different L-alanine data sets it can be assumed that, despite different downstream process parameters (compare Table 4.1), an overall correlation of image descriptors for crystalline product batches of a material system exists.

To proof the suitability of factor analysis as method for the selection of image descriptors different image descriptor sets were used, and the DFA results achieved were evaluated by comparing the results with DFA results of several combinations of image descriptors. In Table 4.4 an excerpt of all variants tested is given, sorted by the number of image descriptors used.

Table 4.3: Results of factor analysis for L- alanine data sets

Data set		Image descriptors				
Ala-1a	d_{eq}	Elong	StdDev		%Area	NSwC
Ala-1b	d_{eq}	Elong	StdDev			NSwC A
Ala-2a	d_{eq}	Elong	StdDev	Sol	%Area	
Ala-2b	d_{eq}	Elong	StdDev			NSwC
Ala-3a	d_{eq}	Elong	StdDev	Sol		
Ala-3b	d_{eq}	Elong	StdDev	Sol		

With d_{eq} : equivalent diameter, Elong: elongation, StdDev: standard deviation of grayscale values, Sol: solidity %Area: area fraction, A: projection area (for definition see Table A.7)

Table 4.4: Variants of image descriptor combinations (variant 3-6: combinations of factor analysis)

number of image descriptors	variant	selected image descriptors											Ala-1a		Ala-2a			
		d_{eq}	Circ.	Elong	Sol	Aspect ratio	Area ratio	Heywood	Wadell	FD	CBR	NSwC	%Area	StdDev	PI [%]	δAg [%]	PI [%]	δAg [%]
4	1	X	X	X		X									66.9	33.0	72.2	14.5
	2	X	X	X	X										62.7	44.0	63.0	41.2
	3		X	X								X	X		74.3	25.8	73.9	2.8
	4	X	X	X									X		74.1	31.1	68.2	42.5
5	5	X	X	X								X	X		79.9	14.2	81.3	6.3
	6	X	X	X							X		X		75.2	28.5	70.5	26.4
	7	X	X	X		X	X								66.9	33.0	72.2	14.5
	8	X	X	X		X		X							69.5	29.4	74.3	14.2
	9	X	X	X		X			X						73.9	23.9	71.0	14.2
7	10	X	X	X		X				X	X		X		79.0	16.7	81.9	12.3
	11	X	X	X		X				X		X	X		76.8	14.1	77.3	2.2
	12	X	X	X	X					X		X	X		80.2	14.8	82.3	4.7
8	13	X	X	X	X	X				X		X	X		80.0	13.8	81.7	4.4
	14	X	X	X	X	X				X	X		X		79.8	16.7	82.5	10.7
14	15	all secondary and grayscale image descriptors (numbers 8-22 Table A.7)											81.9	13.1	82.5	6.3		
22	16	all image descriptors											86.5	8.2	85.0	9.1		

The variants with the numbers three to six are combinations of the factor analysis results (compare Table 4.3). The other 12 variants are several combinations of image descriptors. For the identification of the other image descriptor combinations at first a preselection of promising image descriptors was done. From the primary image descriptors the equivalent diameter d_{eq} was chosen only, as a representative measure of the particle size. The other diameters like the minimal or maximal Feret diameter were used for the determination of secondary image descriptors only. The convex hull A_{convex} was excluded from the preselection also, due to the fact that the convex hull cannot be used alone to characterize a particle. Afterwards, different image descriptors were combined in an evolutionary way. For example in case of four image descriptors three image descriptors were set fixed, and the fourth image descriptor was varied. The excerpt of image descriptor combinations in Table 4.4 shows, for each number of image descriptors used the two or three combination identified with the highest PI and lowest δAg . Figure 4.5 shows the mean PI and the mean δAg for the data sets Ala-1a (blue) and Ala-2a (red) in relation to the number of image descriptors used for DFA. The mean values were calculated by the DFA results of the image descriptor combinations shown in Table 4.4. The results of the evolutionary combinations are illustrated as bars, and the mean values of the

factor analysis results are shown as diamonds. As described above, training sets of the type T2 with 1000 crystalline particles of the data sets were used to train the DFA first. For both data sets (Ala-1a and Ala-2a) it becomes obvious that with an increased number of image descriptors the mean PI increases and the mean δAg decreases, whereby in the range between seven and more image descriptors small changes occur only. Hence, the use of more than seven image descriptors does not lead to a considerable improvement. The image descriptor combinations identified by factor analysis deliver in contrast to the other combinations (four and five image descriptors) higher mean PI and lower mean δAg values, i.e. a classification with a higher performance. Moreover, it can be seen that with the factor analysis combinations of five image descriptors the same classification performance is achieved, as with the evolutionary combinations of seven image descriptors, despite a lower number of image descriptors used. Accordingly, factor analysis is a suitable method, which offers a systematic and time efficient selection of image descriptors for DFA.

However, the overall goal of the multivariate analysis is to find a reference discriminant function, which can be used for all crystalline product batches of a material system enabling a quick determination of the AgD. Consequently, for a final decision on an image descriptor combination the transfer potential of the resulting discriminant function to other data sets has to be validated (see next paragraph).

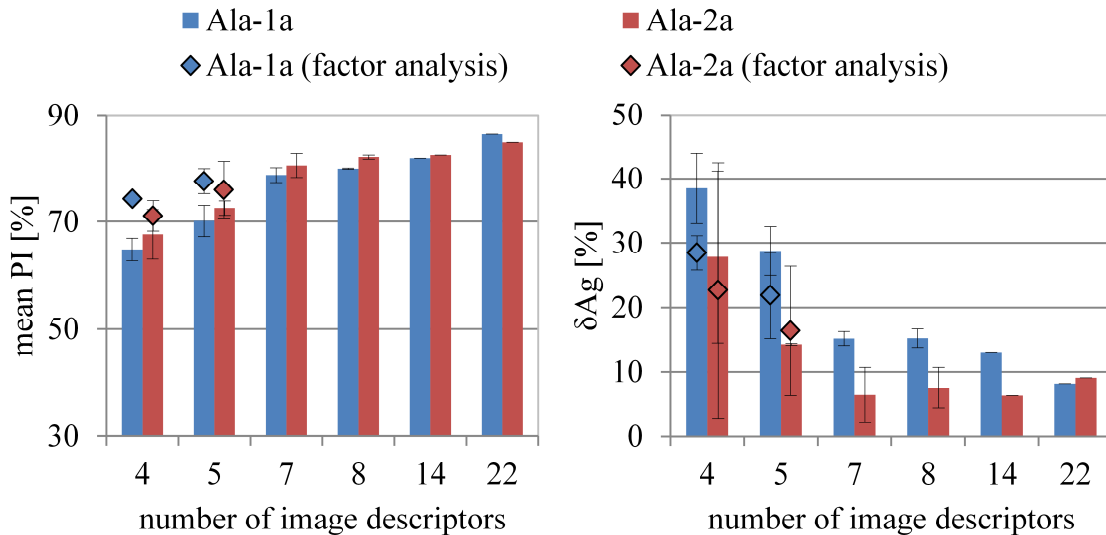


Figure 4.5: Influence of the number of image descriptors on mean PI (left) and mean δAg (right)

Validation of discriminant function

Aim of this paragraph is to find a reference discriminant function, which allows the classification of all crystalline particles of a material system, i.e. to find a discriminant function with a high transfer potential to other data sets. The use of a reference discriminant function avoids the time consuming manual classification of 1000 particles per data set (creation of the training set), and thereby reduces significantly the time for determining the AgD. The results depicted in Figure 4.5 have shown that the use of more than seven image descriptors does not lead to a considerable improvement of the classification performance for a training data set of L-alanine crystals out of water. Furthermore, it was shown that, for the same number of image descriptors used, combinations identified by factor analysis deliver higher classification performances. Assuming that the classification performance of a discriminant function, as a general rule, turned out worse for other data sets than for the training set, and following the hypothesis that discriminant functions with a high number of image descriptors have, due to a too special fitting to the training data set, a low transfer potential, the image descriptor combinations of variant 5 and variant 12 (see Table 4.4) were chosen to find a reference discriminant function for the material system L-alanine/water. Variant 5, identified by factor analysis, represents the variant with the best classification results of the combinations with four and five image descriptors, and variant 12 is the combination with the best classification results of the combinations with seven image descriptors. The transfer potential of a discriminant function depends, beside the image descriptors selected, on the training set used. Therefore, as training sets (type T2) 1000 crystalline particles of the data sets Ala-1a, Ala-2a and Ala-3a were used, and per variant of image descriptors and training set a discriminant function was determined by DFA. Afterwards, the discriminant functions were used for the classification of all data sets (Ala-1a, Ala-1b, Ala-2a, Ala-2b, Ala-3a, and Ala-3b) to evaluate their transfer potential.

Figure 4.6 and Figure 4.7 represent the classification results (PI and δ Ag) for variant 5 and variant 12 for all data sets classified. The results of the discriminant functions trained with the training set Ala-1a were plotted in blue, with the training set Ala-2a in red, and with the training set Ala-3a in green. For both variants a different trend of the results can be observed. In case of variant 12 the classification results show large fluctuations. As expected, when a discriminant function is used to classify a data set, which was used to set up the training set (marked by hatching), high PI values ($> 79\%$) and low δ Ag values ($< 16\%$) are reached in all cases.

If the same discriminant functions are used to classify a data set, which was produced with identical process parameters, the classification results are characterized by lower PI and higher δAg values than the classification results of the training set. E.g. data set Ala-1b is classified by using the training set Ala-1a with a PI of 53 % and a δAg of 62 %. The only exception is the classification of data set Ala-2b by the training set Ala-2a. In this case the PI values are nearly the same and the δAg increases in contrast to a value of 26 % only. For the transfer of the discriminant functions to data sets, which were produced with non-identical process parameters, two different kinds of classification results can be observed.

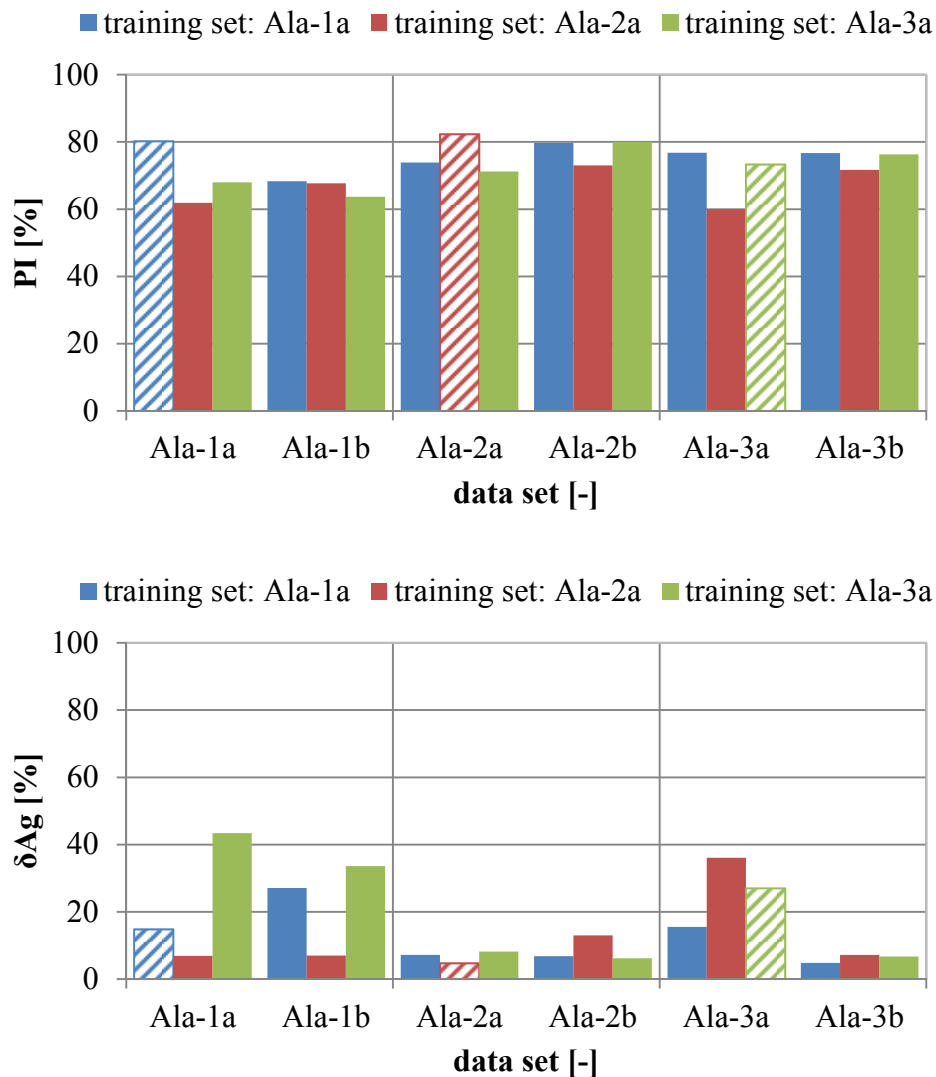


Figure 4.6: Transfer potential of variant 5 (5 image descriptors)

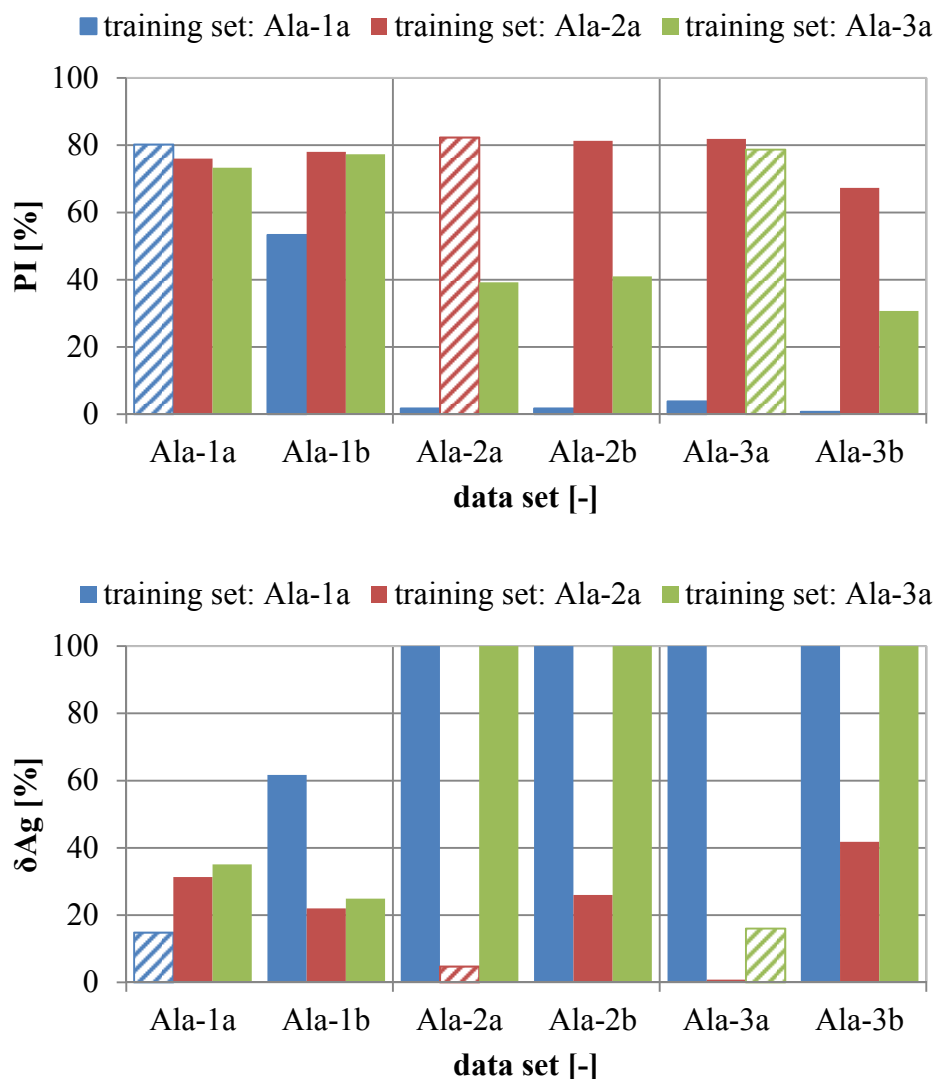


Figure 4.7: Transfer potential of variant 12 (7 image descriptors)

On the one hand for the classification of the data sets Ala-2a, Ala-2b, Ala-3a, and Ala-3b (training set: Ala-1a, blue bars) or of Ala-1a, Ala-1b, Ala-2a, and Ala-2b (training set: Ala-3a, green bars), respectively, PI values $< 60\%$ (training set: Ala-1a) and PI values $< 80\%$ (training set: Ala-3a) are achieved. In case of training set Ala-1a even PI values $< 4\%$ are calculated and high δAg -values up to 100% are recorded subsequently. On the other hand PI values of in average 70% and δAg values $< 40\%$ for all data sets are reached if the training set Ala-2a (red bars) is used.

Recapitulating, it can be pointed out that for variant 12 the training set used has a strong influence on the transfer potential of the discriminant functions. Comparing all training sets, the discriminant function with the training set Ala-2a shows the best classification results and the highest transfer potential to other data sets. But, due to δAg -values up to 40% (see data set Ala-3b) the discriminant function is not suitable as reference discriminant function for the L-

alanine/water system. The observed δAg -values of 100 % for data sets, which were produced with identical process parameters, clearly underline the low transfer potential. δAg -values of 100 % point out that all agglomerates are classified incorrectly by DFA. A correct classification with high PI-values and low δAg -values is achieved only if the training set is a part of the classified data set.

In case of variant 5 similar classification results can be observed for all data sets, independent of the training set used. PI-values between 60 % and 80 %, and δAg -values between 5 % and 43 % are reached. The discriminant function with the smallest range of variation is given with the training set Ala-1a (blue bars, PI: 68.3 % - 79.9 %; δAg : 4.8 % - 27.1 %). The small range of variation indicates that with the image descriptor combination of factor analysis (variant 5) discriminant functions with a high transfer potential to all data sets can be created. This means that in comparison to variant 12 the discriminant functions of variant 5 show a low influence of the training set on the transfer potential. Moreover, despite similar classification results for the training set of both variants (see Figure 4.6 and Figure 4.7, bars marked by hatching) the transfer potential of all discriminant functions of variant 5 is higher than for the discriminant functions of variant 12.

According to these observations, the hypothesis that the transfer potential of a discriminant function with a high number of image descriptors, due to a too special fitting to the training data set, is low seems to be correct. To verify this hypothesis the transfer potential of variant 13 (8 image descriptors), and variant 15 (14 image descriptors), which have shown in comparison to variant 5 and variant 12 classification performances in the same range (see Table 4.4), are investigated also. The classification results are given as supplementary artwork in Figure A.3 and Figure A.4. For both variants results similar to variant 12 are obtained. None of the discriminant functions can be used as reference discriminant function. However, in contrast to variant 5 none of the other investigated variants (12, 13, and 15) contain the equivalent diameter as image descriptor. Therefore, it has to be verified whether the poor transferability is caused by a too special fitting due to a high number of image descriptors used, or by the lack of the equivalent diameter, to confirm the hypothesis finally. Hence, variant 12 (seven image descriptors) and variant 13 (eight image descriptors) are extended by adding the equivalent diameter as an additional image descriptor. Afterwards, the extended variants – in the following referred to as variant 12+ and variant 13+ – are investigated on their transfer potential. The related classification results are shown in Figure A.3 and Figure A.4. For both variants similar classification results with PI values from 68 % to 84 % and δAg values between 4 % and 37 % are reached for all investigated data sets.

The comparison of the classification results of variant 12+ with variant 12 (compare Figure A.5 and Figure 4.7), as well as the comparison of variant 13+ with variant 13 (compare Figure A.6 and Figure A.3), indicates that by adding the equivalent diameter as additional image descriptor the transfer potential of all discriminant functions increases distinctly. Hence, the equivalent diameter is identified as an important image descriptor for the transfer potential.

In contrast to variant 5 (five image descriptors) none of the discriminant functions of variant 12+ and 13+ show a higher transfer potential than the discriminant function of variant 5 trained with the training set Ala-1a (see Figure 4.6, blue bars, PI: 68.3 % - 79.9 %; δAg : 4.8 % - 27.1 %). All discriminant functions of the variants 12+ and 13+ lead to classification results with δAg values greater than 31 % for data sets, which are not used as a training set. The higher δAg values arise from the fact that single crystals are classified with PI values over 90 %, whereas agglomerates are identified correctly to around 60 % only. In case of variant 5 the classification performance of both particle groups is in balance.

Although the comparison of variant 5 with the variants 12+ and 13+ demonstrates that the transfer potential of a discriminant function decreases with the number of image descriptors used, the comparison of the variants 12 and 12+, or 13 and 13+ respectively, indicates that a high number of image descriptors do not decrease the transfer potential in general. Therefore, the statement that the transfer potential of a discriminant function with a high number of image descriptors is low, due to a too special fitting to the training set, is not generally valid. Rather than the number of image descriptors used the selection of the right image descriptors, like the equivalent diameter, is crucial for the transfer potential. Furthermore, the comparison of all investigated variants shows that a discriminant function, which enables a high classification performance for a training data set, does not enable a high classification performance for other data sets of the same material system also. Therefore, the consideration of one crystalline product batch only is not sufficient to draw conclusions about the transfer potential of a discriminant function or the suitability of an image descriptor combination respectively.

In summary, it can be noted that the discriminant function with the highest transfer potential for the material system L-alanine/water is using the image descriptor combination variant 5, which was identified by factor analysis. Hence, factor analysis is a suitable method to select image descriptors for the creation of a reference discriminant function. Thereby, in contrast to the investigation of several combinations, image descriptors can be selected in a systematic and time efficient way. For the L-alanine/water system the discriminant function determined with the image descriptors of variant 5 and the training set Ala-1a was identified as reference discriminant function, and can be used to determine the AgD of all crystalline product batches

of the material system. The identified reference discriminant function includes four secondary image descriptors (elongation, solidity, area fraction, and standard deviation of grayscale values), which are dimensionless, and the equivalent diameter, a dimensional quantity, which is obviously the crucial image descriptor for the transferability. Why the equivalent diameter increases the transferability is uncertainly on basis of the available results, and needs to be further investigated. Nevertheless, the correlation between the equivalent diameter and probability for agglomeration can be explained by the fact that agglomeration is a size enlargement process, and agglomeration rates tend to increase with particle size [16]. During crystallization the probability for agglomeration increases with particle size, because large crystals spend a longer time in the solution during crystallization than smaller ones [107]. Also the probability for particle-particle collision, which is beside supersaturation a requirement for agglomeration, increases with crystal size [16]. However, this correlation does not mean that by the reference discriminant function identified particles with a specific equivalent diameter are classified automatically as agglomerates or single crystals. Limiting equivalent diameter values or regions, which are used to identify a crystalline particle as agglomerate or single crystal do not exist. The discriminant function used is a linear combination of the five image descriptors: elongation, solidity, area fraction, standard deviation of grayscale values, and the equivalent diameter. This means that the equivalent diameter has in combination with the other four image descriptors an influence on the group assignment of a crystalline particle only. To elucidate this fact various trace plots are given in Figure A.7, Figure A.8, and Figure A.9. Consequently, all steps of the subsection “multivariate analysis” (compare Figure 4.3) including the time-consuming, manual classification of 1000 crystalline particles for the creation of a training set can be omitted totally, and the time for the determination of the AgD is reduced by about one and a half hour.

4.2.3. Evaluation

In this subsection the reference discriminant function of a material system, estimated during multivariate analysis, is used to classify and quantify a crystalline product batch. First – in the classification step - the crystalline particles of the product batch are classified with the reference discriminant function to the groups single crystals, agglomerates, and waste particles. For the dry L-alanine crystals the discriminant function, which contains the image descriptors equivalent diameter, elongation, solidity, area fraction, and standard deviation of grayscale (Table 4.4, variant 5), trained with 1000 crystalline particles of the data set Ala-1a is used. This reference discriminant function classifies the crystalline particles of the data sets Ala-2 and Ala-3 with a PI of 77.5 % and a δAg of 4.8 %. The data sets Ala-2 and Ala-3 contain all crystals of the data sets Ala-2a and Ala-2b, or Ala-3a and Ala-3b respectively. Second – in the quantification step – the agglomeration degree Ag , the agglomeration degree distribution (AgD) and the CSD are calculated by the image analysis tool. As crystal size the equivalent diameter d_{eq} of the crystalline particles is used. Due to the image recording method used, the transmitted light scanning, it is possible to scan an image with crystalline particles in one plane only. As consequence crystalline particles smaller than 200 μm are recorded as blurred particles, which cannot be identified as single crystals or agglomerates. These particles are eliminated in the image analysis step by the operation *Noise Elimination* (see section 4.2.1) and the minimum crystal size for the analysis is limited to 200 μm . This limited value is traced back to the image recording method used only. By combining several focus plane images or by using another image recording method the detection limit of the crystal size can be reduced to smaller crystal sizes. Nonetheless, even with the limited crystal size range it is possible to characterize and compare crystalline product batches by their AgD, because the main part of the agglomerates usually are large crystals.

The AgD and CSD are calculated out of N particle fractions by fitting the agglomeration degrees Ag_j (see equation (4.2)), the number fractions or volume fractions of all particle fractions using the least squares method. Moreover, the curve progressions of the CSD and AgD are specified by characteristic values to allow a quantitative evaluation and comparison. The CSD is characterized by the median crystal size d_{50} and the width of the CSD $d_{90}-d_{10}$. For the AgD the characteristic values Ag_i and $d(Ag_i)$ are calculated (see section 4.1).

Figure 4.8 shows the calculated AgD curve (green line) and the CSD curve (black line) of the data sets Ala-2 (I) and Ala-3 (II). Furthermore, the Ag of the particle fractions are illustrated as green crosses. The corresponding characteristic values of the AgD and CSD curves are

listed in Table 4.5. For both analyses at least 5000 crystalline particles are investigated. The area fraction of all particles, which are smaller than 200 μm , amounts about 11.3 % for Ala-2 and about 17.8 % for Ala-3 (It should be noted that the values for the area fractions are approximate values only, due to the blurring of the particles).

For the crystalline product batch Ala-2 a median crystal size d_{50} of 297 μm and a width of CSD d_{90} - d_{10} of 291 μm can be observed. The Ag is 55.8 %. The AgD curve shows a minimum at 294 μm , and rises afterwards constantly to an Ag_{max} of 1 at 740 μm . Therefore, an Ag of 0.5 is reached two times, and shows that agglomerates exist mainly for crystal sizes smaller than 257 μm and larger than 331 μm . The $d(\text{Ag}_{\text{max}})$ of 740 μm indicates that the crystalline particles at this crystal size are all agglomerates, since Ag_{max} reaches the value 1.

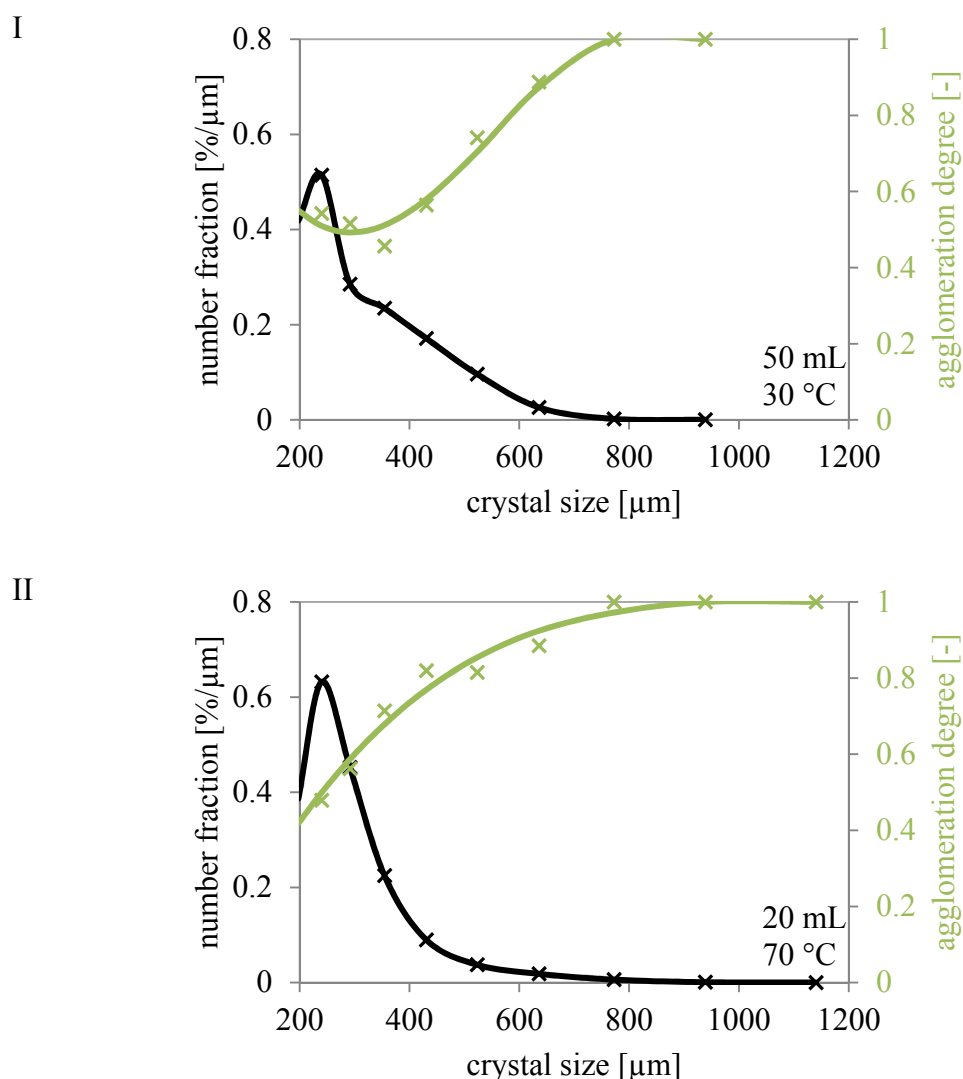


Figure 4.8: CSDs and AgDs of the crystalline product batches Ala-2 (I) and Ala-3 (II)

Table 4.5: Characteristic values of CSD and AgD for the crystalline product batches Ala-2 and Ala-3

		Ala-2	Ala-3
d_{10}	[μm]	208 \pm 1	210 \pm 0
d_{50}	[μm]	297 \pm 6	274 \pm 1
d_{90}	[μm]	499 \pm 5	430 \pm 7
$d_{90}-d_{10}$	[μm]	291	220
Ag_{max}	[-]	1 \pm 0	1 \pm 0
Ag_{min}	[-]	0.44 \pm 0.01	0.41 \pm 0.03
$d(Ag_{\text{max}})$	[μm]	740 \pm 2	938 \pm 8
$d(Ag_{\text{min}})$	[μm]	294 \pm 4	200 \pm 0
$d(Ag_{0.5})$	[μm]	257 \pm 6	331 \pm 8
Ag	[%]	55.8 \pm 0.5	56.6 \pm 0.3

The CSD curve of the crystalline product batch Ala-3 is characterized by a d_{50} of 274 μm and a $d_{90}-d_{10}$ of 220 μm . The Ag is 56.6 %. The AgD curve rises constantly from an Ag_{min} value of 0.41 at 200 μm to an Ag_{max} value of at 938 μm , i.e. the crystalline particles larger than 938 μm are agglomerates only.

The comparison of the AgD curves of the two crystalline product batches shows a different agglomeration degree distribution despite identical crystallization conditions, but very similar agglomeration degrees of the crystalline product batches (Ala-2: 55.8 %, Ala-3: 56.6 %). The AgD of Ala-3 meets the expectations. The Ag_i increases with crystal size, because the probability for agglomeration increases, since large crystals spend a longer time in the suspension during crystallization than smaller ones [107]. In contrast, the AgD of Ala-2 differs from the expected curve shape, and shows a different AgD than Ala-3. This indicates that the downstream conditions (see Table 4.1) have an impact on agglomeration behavior of material system L-alanine/water. However, for the verification of this hypothesis more than crystalline product batches have to be compared to allow clear conclusion about the impact of washing and drying parameters on the quality of L-alanine product batches. Therefore, detailed investigations regarding the agglomeration behavior within the crystalline process chain are given chapter 5.

4.2.4. Application to the System Adipic Acid/Water

The developed methodology of the image analysis tool was applied to the system adipic acid/water to proof the applicability to crystalline products with different morphology also. In contrast to L-alanine adipic acid crystals are platelet shaped (compare Figure 3.1 II and Figure 3.2 II). Probes of the crystalline product batches AA-1 and AA-2 are processed through the preparation steps fractionation, image recording, and image analysis (see section 4.2.1). Dur-

ing multivariate analysis training sets of the type T2 with 1000 crystalline particles are created, and factor analysis is used for the selection of image descriptors. As significant image descriptors the equivalent diameter, elongation, solidity, and minimal grayscale value are identified and used for DFA. The validation of the discriminant function shows that the discriminant function trained with 1000 crystalline particles of the crystalline product batch AA-2 is suitable as reference discriminant function for adipic acid/water. This discriminant function offers a high transfer potential: The training set AA-1 was classified with a PI of 93.1 % and a δAg of 1.3 %. Afterwards the crystalline product batches AA-1 and AA-2 were classified and quantified by their AgD and CSD (see Figure 4.9). The corresponding characteristic values are given in Table 4.6. The area fraction of particles below 200 μm amounts 3.1 % for AA-1 and 2.5 % for AA-2. (Again, it should be noted that the values for the area fractions are approximate values only, due to the blurring of the particles).

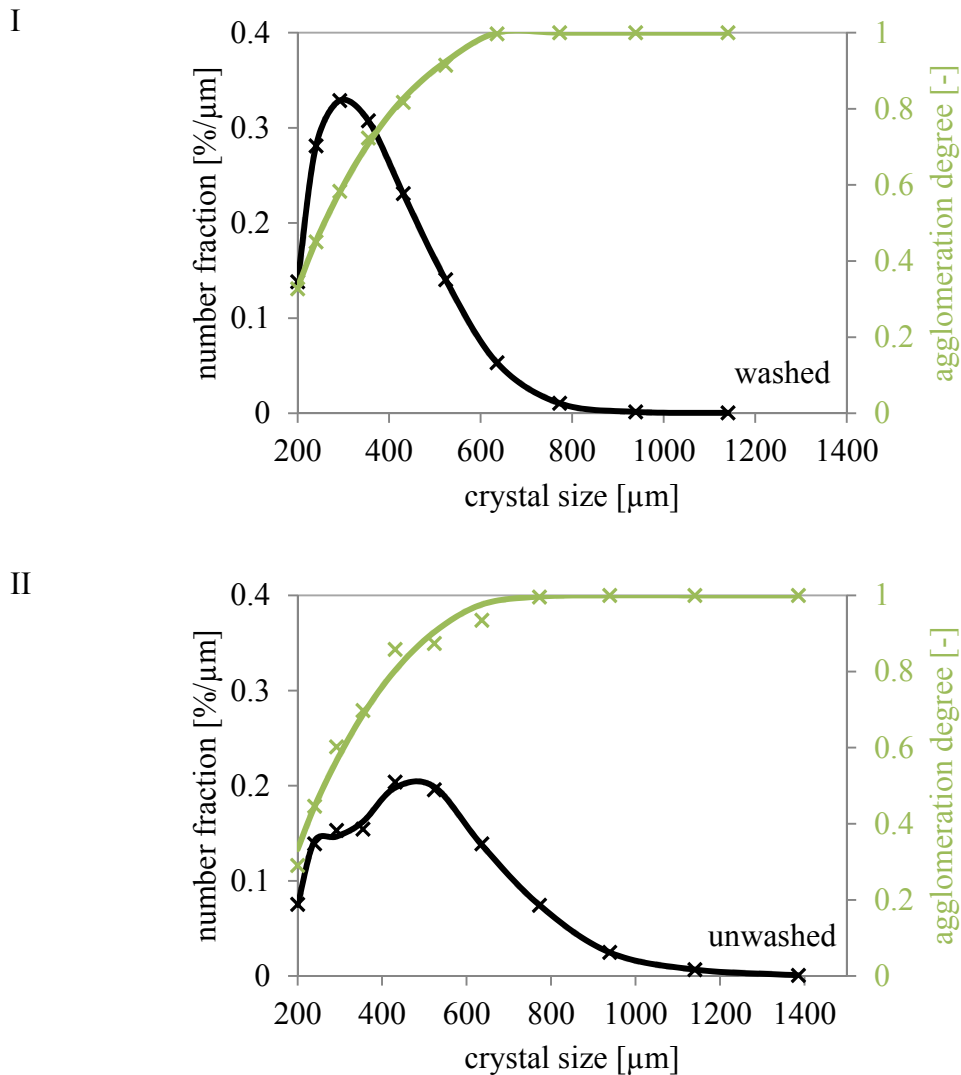


Figure 4.9: CSD and AgD of the crystalline product batches AA-1 (I) and AA-2 (II)

Table 4.6: Characteristic values of CSD and AgD for the crystalline product batches AA-1 and AA-2

		AA-1	AA-2
d_{10}	[μm]	236 \pm 1	210 \pm 1
d_{50}	[μm]	362 \pm 6	495 \pm 4
d_{90}	[μm]	556 \pm 5	774 \pm 5
$d_{90}-d_{10}$	[μm]	320	508
Ag_{max}	[-]	1 \pm 0	1 \pm 0
Ag_{min}	[-]	0.29 \pm 0.02	0.33 \pm 0.01
$d(Ag_{\text{max}})$	[μm]	685 \pm 4	938 \pm 3
$d(Ag_{\text{min}})$	[μm]	200 \pm 0	200 \pm 0
$d(Ag_{0.5})$	[μm]	258 \pm 1	263 \pm 3
Ag	[%]	70.9 \pm 0.3	81.6 \pm 0.1

The AgD curves rise constantly for crystals unwashed (AA-2) and crystals washed with acetonitrile (AA-1). For both crystalline products the Ag_{min} lies on the edge of the distribution at 200 μm . The Ag_i of 0.5 is reached at 258 μm (AA-1) and 263 μm (AA-2). The $d(Ag_{\text{max}})$ values differ with 685 μm for AA-1 and 938 μm for AA-2 in the same size range like the characteristic values d_{90} and $d_{90}-d_{10}$ of CSD. In comparison to AA-1, the CSD of AA-2 (d_{10} , d_{50} , d_{90}) is shifted and broadened to larger crystal sizes. The overall agglomeration degrees of the adipic acid products are calculated to 70.9 % for AA-1 and 81.6 % for AA-2.

The high agglomeration degrees of the adipic acid products show the strong tendency of adipic acid for agglomeration. The agglomeration degree of the crystalline product unwashed (AA-2) is higher than the agglomeration degree of the crystalline product washed with acetonitrile (AA-1). This may indicate that the shift to larger crystal size, as well as the broadening of the CSD, in case of AA-2 is a result of agglomeration during downstream processes, i.e. static drying, due to a missing washing step after filtration. The broadening by agglomeration during drying is especially visible for the size range between 938 μm ($d(Ag_{\text{max}})$) and 1490 μm (d_{max}). On the other hand, the constant increase of the AgD curves as well as the $d(Ag_{\text{min}})$ values at the edge of the distributions suggest that agglomeration takes place mainly during crystallization. However, to allow final conclusions about the agglomeration behavior for the material system adipic acid/water the AgD has to be recorded over the whole crystalline process chain. These investigations are shown in chapter 6.

4.2.5. Comparison of material systems

A comparison of the image descriptors identified for adipic acid/water and L-alanine/water shows a great similarity. In both cases the equivalent diameter, elongation, and solidity are used. However, for L-alanine the area fraction and standard deviation of grayscale values were identified in contrast to the minimal grayscale value used for adipic acid. The different selection of grayscale image descriptors can be explained by the different crystal morphology of the two material systems. The single crystals of L-alanine are characterized by a wide range of grayscale values. Due to the octahedral morphology a part of the single crystal is transmitted by light without refraction resulting in an area fraction, which is not black after thresholding. Whereas, the platelet shaped single crystals of adipic acid lie flat on the scanner surface, and are transmitted evenly, which results in minimal grayscale values.

In comparison to the system L-alanine/water the agglomeration degree of adipic acid product batches is with 81.6 % (AA-1) and 70.9 % (AA-2) higher than the agglomeration degree of the L-alanine product batches (Ala-2: 55.8 %, Ala-3: 56.6 %). As expected, the comparison shows that adipic acid tends more to agglomeration than L-alanine, which results in a broadened width of CSD. Furthermore, a comparison of all AgDs suggests, that agglomeration takes place for the material system adipic acid/water mainly during crystallization, whereas for the material system L-alanine/water the downstream conditions chosen influence the AgD more. Hence, cake washing has probably a higher effect on the AgD of a L-alanine product batch than on the AgD of an adipic acid product batch.

4.3. Extension of Image Analysis Tool to Suspended Crystals

To allow the measurement of the CSD, Ag, and AgD of crystalline product batches out of suspension after crystallization the origin image analysis tool developed for dried crystalline product batches (see section 4.2) was extended. The adaptations for the extension concern the sample preparation, the image recording, and the reference discriminant functions of the material systems.

4.3.1. Sample Preparation and Image Recording

A direct measurement of the slurry after crystallization by pumping it out of the crystallizer is not possible due to the high suspension density. Therefore, the slurry is filtered and washed immediately after filtration to avoid agglomeration or crystal growth by displacing the mother liquor in the voids of the filter cake. In case of the material system L-alanine/water as wash liquid 40 mL of an ethanol/water mixture (ratio 4/1) in the first wash step and 80 mL pure ethanol in the second wash step is used. For the material system adipic acid/ water the washing is performed two times with 70 mL at room temperature saturated adipic acid water. Afterwards, the filter cake is resuspended in 1 L wash liquid inside a separating funnel with a volume of 1 L. By placing the separating funnel over a rotary cone divider (Fritsch, Laborette 27) the filter cake is divided first into 8 samples. Next, two of the samples located opposite of one another are merged and transferred with 750 mL fresh wash liquid into the separating funnel. Then, the suspension is divided again into 8 samples, which contain around 2 g crystals and 125 mL wash liquid. Each of these 8 samples is used for image analysis, so that the CSD, Ag, and AgD are determined from one quarter of the filter cake. The setup of the measurement system for the image analysis of crystals in suspension is shown in Figure 4.10.

The image recording is performed by the QICPIC from Sympatec using the LIXELL module with a 2 mm cuvette. For dispersion of the samples a 1 L storage vessel with a diameter of 85 mm, equipped with four baffles and a four-pitched blade agitator, is used. The suspension is pumped by a peristaltic pump (Heidolph, pumpdrive 5201 with SP Quick), which is installed in front of the QICPIC, with 75 rpm from bottom to top through the cuvette. Long-term measurements, for which a crystal suspension is pumped in a closed loop through the measurement system, have shown that the peristaltic pump does neither cause breakage nor attrition.

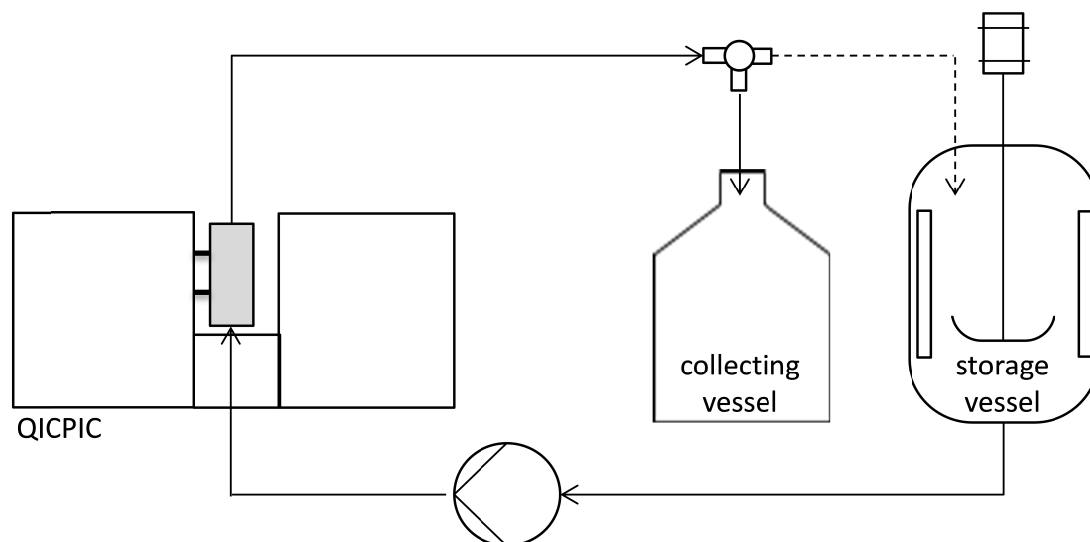


Figure 4.10: Setup of the measurement system for image recording of crystals in suspension using the QICPIC

For the measurement of each sample 800 mL wash liquid is filled into the storage vessel and pumped in a closed loop through the measurement system. Then, one of the fractionated samples is transferred to the ethanol solution and dispersed equally for 30 s by pumping the suspension in cycle. Afterwards, the three-way valve is positioned in the way that the suspension is pumped to a collecting vessel and no longer back to the storage vessel, and the image recording is started. This procedure ensures that each particle is measured once only. For the image recording a frame rate of 25 Hz is used and the stirring velocity of the storage vessel is reduced stepwise from 500 rpm to 50 rpm over the whole measurement time, because the fill level in the storage vessel decreases. The image recording is stopped when the whole suspension is pumped out of the storage vessel. As result of the image recording a black-and-white video is obtained, which is cut for the image analysis by MATLAB (MathWorks, Version R2010b) into frames. The images of the QICPIC allow a clear classification of particles larger than 80 μm , so that the limited crystal size range in contrast to the transmitted light scanner is broadened by about 120 μm .

4.3.2. Reference Discriminant Functions

Grayscale images as obtained with the transmitted light scanner cannot be taken with the QICPIC. Silhouettes of the crystals can be taken only, which results in a loss of crystal surface information. Therefore, grayscale image descriptors like the standard deviation of grayscale values and the minimal grayscale value, which have been used as variables in the reference discriminant function for the classification of dry crystalline product batches (see section 4.2.2 and 4.2.4), are not available. Additionally, in contrast to the classification of the dry

crystalline particles the group waste particles contains air bubbles (compare Figure A.10). Consequently, the existing reference discriminant function cannot be used for the classification of crystals in suspension. Therefore, for both material systems new reference discriminant functions have to be generated: First, training sets with around 1000 manually classified particles are created for three experiments and second new image descriptors – the number of concave points (nConc), the maximal concavity depth (MaxDepth), and the centroid distance (dCentroid) – are introduced to achieve reference discriminant functions with comparable classification performances although grayscale image descriptors are not available. The image descriptors MaxDepth and dCentroid were developed in cooperation with the chair of process systems engineering of professor Briesen at the Technische Universität München. The computation of all image descriptors is performed by MATLAB (MathWorks, Version R2010b). Concave points have been used in the past e.g. for the splitting of touching cells [114], the model-based segmentation of nuclei [115], and for dividing agglomerates into single crystals [116]. As depicted in Figure 4.11 a concave point corresponds to the concave edge of a crystal. To compute nConc for each point on the object boundary the minimal distance to the concave hull of the object (concavity depth) is determined. Furthermore, for each concave area a concave point is identified via a maximum of the concavity depth inside the concave area. The minimal concavity depth for the detection of a concave point is set to two pixels. The overall maximal concavity depth of the object standardized with the equivalent diameter defines the image descriptor MaxDepth. The image descriptor dCentroid is a circularity measure and is defined as standard deviation of the distances from the object boundary to the centroid of the object standardized with the average of the distances.

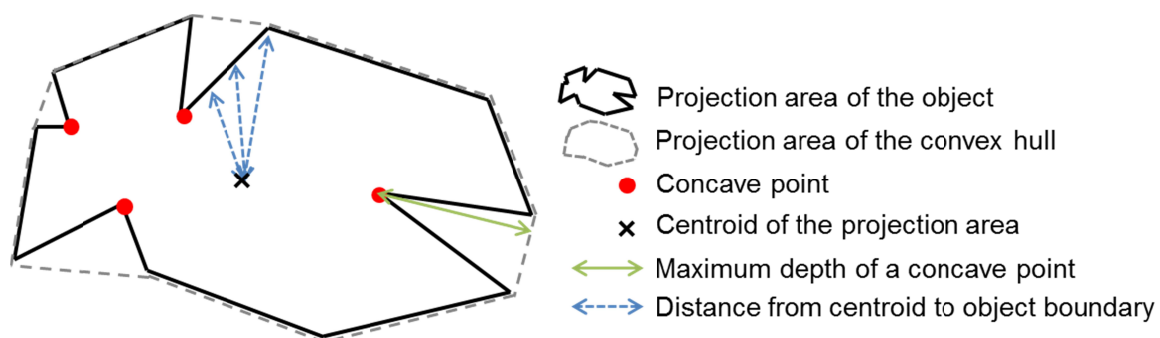


Figure 4.11: Schematic illustration of measures needed for the computation of the image descriptors number of concave points (nConc), maximal concavity depth (MaxDepth), and centroid distance (dCentroid) [119]

L-alanine/water

For the material system L-alanine/water the CSD, Ag, and AgD after crystallization is determined in this thesis for constant crystallization conditions (compare Table A.3) only. Nevertheless, the transfer potential of this discriminant function to two dried crystalline product batches Ala-ST and Ala-WS is validated. The compositions of all training sets investigated and the experimental conditions of the dried product batches are listed in Table 4.7.

First all image descriptors of the existing reference discriminant function except of the standard deviation of grayscale values was used. But without the standard deviation of grayscale values an unsatisfying classification result was reached: Although the training sets are classified in average with high PI-values of $81.1 \% \pm 2.8 \%$, the classification results show high δAg -values of $26.3 \% \pm 4.7 \%$. This indicates that the groups' single crystals and agglomerates cannot be accurately separated by the image descriptor combination chosen.

Hence, the standard deviation of grayscale values was substituted by the number of concave points so that the image descriptor combination tested next consists of elongation, solidity, area fraction, equivalent diameter, and number of concave points. Three discriminant functions were determined on basis of the training sets Ala-K1, Ala-ST, and Ala-WS. The training set Ala-K2 was used as test set¹ only. The classification results are summarized in Figure 4.12, whereby averaged values for Ala-K1 and Ala-K2 are given. The bars marked by hatching indicate the classification results of the training sets used for the determination of the discriminant function. With all discriminant functions transferable classification results with a better classification performance compared to the scanner discriminant function are reached.

Table 4.7: Composition of L-alanine trainings sets for QICPIC reference discriminant function

Training/ test set	number of particles			Σ
	single crystals	agglomerates	waste particles	
Ala-K1	386	586	18	990
Ala-K2	450	604	10	1064
Ala-ST	418	577	5	1000
Ala-WS	417	662	6	1085

Ala-ST: washing: 40 ml EtOH/water (4/1), 80 ml EtOH; static drying: 65 °C, 40 g
 Ala-WS: washing: 40 ml EtOH/water (4/1), 80 ml EtOH; fluidized bed drying:
 68 °C, 40 g, 28 m³/h

¹ Test set are training sets, which are used to evaluate the performance of a discriminant function only, i.e. a test set is not used to train a discriminant function.

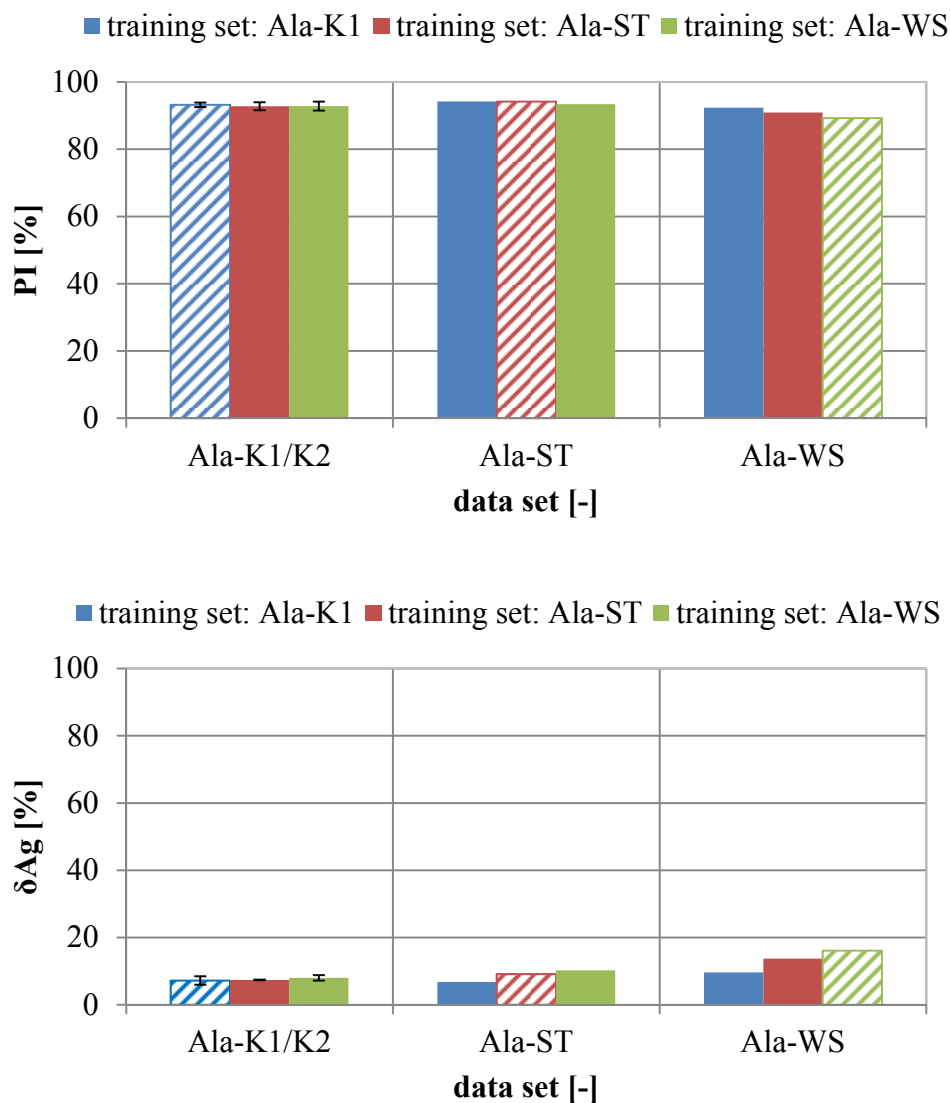


Figure 4.12: Transfer potential of the discriminant function using image descriptor combination: elongation, solidity, area fraction, equivalent diameter, and number of concave points for L-alanine crystals in suspension (compare Table 4.7)

In average the classification is performed with a PI of $92.6 \% \pm 1.5 \%$ and a δAg of $9.8 \% \pm 3.0 \%$. The discriminant function determined with the training set Ala-K1 delivers the best classification performance and is identified as reference discriminant function for L-alanine crystals in suspension. The training sets of the crystallization experiments Ala-K1 and Ala-K2 are classified with a PI of $93.2 \% \pm 0.7 \%$ and a δAg of $7.2 \% \pm 1.9 \%$ and the training sets of the drying experiments Ala-ST and Ala-WS with a PI of $93.3 \% \pm 0.9 \%$ and a δAg of $8.1 \% \pm 1.4 \%$.

Since in the further course of the thesis a comparison of the AgD after crystallization with AgDs after drying should be carried out (see section 5), it was investigated whether both reference discriminant functions (scanner and QICPIC) deliver comparable classification results.

Although the reference discriminant for the QICPIC – as indicated above – can be used for the classification of dried crystalline product batches as well, the scanning image analysis technique should be used for the classification of dried crystalline product batches further due to less effort regarding preparation and time. That's why the same dried crystalline product batch was fractionated and analyzed on the one hand with the transmitted light scanner and on the other hand after resuspension with the QICPIC. Since the image analysis of the dried crystalline product batches is limited to crystalline particles larger than 200 μm , this limited value of the crystal size was set for the analysis of the samples in suspension also. The results given in Table 4.8 and Figure 4.13 show that the AgDs, Ags, and the characteristics values of the CSDs are comparable but not identical. The AgD determined with the scanner lies slightly below the AgD determined with the QICPIC. Therefore, in case of the scanner a lower Ag is calculated also. These differences can be explained by the performances of the discriminant functions used. The scanner discriminant function shows with a PI of $77.4\% \pm 2.2\%$ and a δAg of $9.7\% \pm 4.3\%$ a lower performance than the QICPIC discriminant function. Since the δAg -value of the scanner discriminant function is higher, the deviation of the AgDs and Ag-values is the result of a lower correct classification of agglomerates.

Table 4.8: Characteristic values of the same crystalline product batch analyzed with the transmitted light scanner and the QICPIC; corresponding AgDs and CSDs are depicted in Figure 4.13

	Ag [%]	d_{10} [μm]	d_{50} [μm]	d_{90} [μm]	$d_{90}-d_{10}$ [μm]
scanner	57.1 ± 0.1	214 ± 2	285 ± 5	457 ± 8	243 ± 6
QICPIC	62.4 ± 0.4	207 ± 1	266 ± 1	443 ± 5	236 ± 6

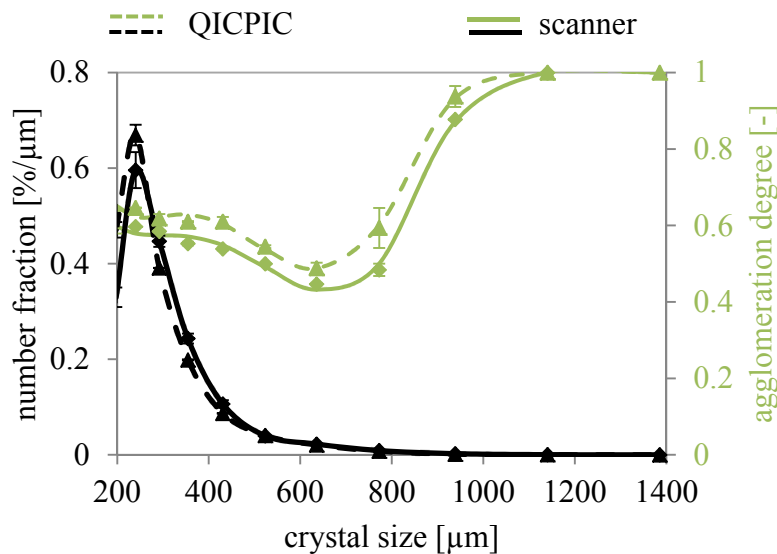


Figure 4.13: CSDs and AgDs of the same L-alanine crystalline product batch analyzed with the scanner (dried product) and the QICPIC (resuspended product)

Adipic acid/ water

The reference discriminant function for adipic acid crystals in suspension was generated to investigate the agglomeration behavior of adipic acid during gassing crystallization. Hence, for the creation of training and test sets² three different gassing crystallization experiments AA-G1, AA-G6, and AA-G9 were used. The composition of the corresponding training and test sets (fractionated samples of the crystalline products) is shown in Table 4.9. Herein the training sets are marked with an “a” behind the experimental name and test sets, with a “b”. The experimental conditions, which differ in terms of gas volume flow, gassing temperature, and stirring rate, are given in Table A.9. The experiments were chosen due to their difference in the width of the crystal size distribution d_{90} - d_{10} and median crystal size d_{50} (see Table A.9). It was assumed that the largest deviation of the crystal morphology exists for crystalline products with different CSDs so that the transferability of the discriminant function can be best assessed. The image descriptor combinations tested and listed in Table 4.10 have taken the reference discriminant function of the scanning image analysis technique as basis. The scanning reference discriminant function contains the equivalent diameter, elongation, solidity, and minimal grayscale as image descriptors (PI: 93.1 %, δAg : 1.3 %; compare section 4.2.4). The new image descriptor combinations listed in Table 4.10 were established by gradual addition of new image descriptors. Scope of the discriminant function validation in this paragraph is to identify a reference discriminant function for adipic acid crystals in suspension with a classification performance and transfer potential in the same order of magnitude as reached for the scanning image analysis.

Table 4.9: Composition of adipic acid (AA) trainings sets for QICPIC reference discriminant function; a: training set, b: test set

Training/ test set	number of particles			Σ
	single crystals	agglomerates	waste particles	
AA-G1a	195	808	7	1010
AA-G1b	174	814	12	1000
AA-G6a	251	749	9	1009
AA-G6b	261	733	27	1021
AA-G9a	153	846	6	1005
AA-G9b	167	833	20	1020

² Test set are training sets, which are used to evaluate the performance of a discriminant function only, i.e. a test set is not used to train a discriminant function.

To assess the classification performance and transferability of the image descriptor combinations each discriminant function was applied to the training and test sets, and the PI and δAg values were calculated. In the following for each image descriptor combination (D_{AA-0} – D_{AA-3}) the averaged classification results, summed up for reasons of clarity in Table 4.11 are discussed:

As first approach the **image descriptor combination D_{AA-0}** , which contains all image descriptors of the scanning reference discriminant function without the minimal grayscale value, was tested. The corresponding classification results are depicted in Figure A.11. In average PI-values of $80.5\% \pm 2.0\%$ and δAg -values of $7.4\% \pm 2.2\%$ were reached. The relative small standard deviations of the performance measurements (PI, δAg) denote that the image descriptor combination D_{AA-0} delivers transferable discriminant functions. However, in contrast to the scanning reference discriminant function lower PI and higher δAg -values are obtained so that the classification performance cannot be accepted. The specific performance indices, listed in Table 4.11 indicate that all waste particles are detected accurately (PI_W : $100\% \pm 0.0\%$), but the single crystals and agglomerates are classified to other groups also (PI_S : $78.1\% \pm 3.7\%$, PI_A : $82.3\% \pm 2.3\%$). To enhance the performance of the discriminant function it is helpful to know how the misclassified single crystals and agglomerates are distributed to the other groups. On basis of this information the image descriptor

Table 4.10: Image descriptor combinations of QICPIC discriminant functions tested for the material system adipic acid/ water; X indicates that the image descriptor is included in the combination

Variants	Image descriptors					
	d_{eq}	Sol	Elong	nConc	dCentroid	MaxDepth
D_{AA-0}	X	X	X			
D_{AA-1}	X	X	X	X		
D_{AA-2}	X	X	X	X	X	
D_{AA-3}	X	X	X	X	X	X

With d_{eq} : equivalent diameter, Sol: solidity, Elong: elongation, nConc: number of concave points, dCentroid: centroid distance, MaxDepth: maximal concavity depth (for definition see Figure 4.11)

Table 4.11: Averaged classification results for the image descriptor combinations D_{AA-0} – D_{AA-3} ; S: single crystals, A: agglomerates, W: waste

	PI [%]	δAg [%]	PI_S [%]	PI_A [%]	PI_W [%]
D_{AA-0}	80.5 ± 2.0	7.4 ± 2.2	71.8 ± 3.7	82.3 ± 2.3	100 ± 0
D_{AA-1}	81.7 ± 1.6	7.8 ± 2.2	75.2 ± 4.2	83.0 ± 2.0	100 ± 0
D_{AA-2}	84.3 ± 1.9	10.8 ± 1.9	86.3 ± 1.6	83.3 ± 2.5	100 ± 0
D_{AA-3}	89.8 ± 1.5	6.3 ± 2.0	6.3 ± 2.0	89.2 ± 1.9	100 ± 0

combination can be extended target-oriented to improve the separation of groups from one another. Therefore, the distribution of the particles on the three groups single crystals, agglomerates, and waste was calculated out of classification results (see Figure 4.14). The distribution of the single crystals is depicted as blue bars, of the agglomerates as red bars, and of the waste particles as green bars. The results indicate that $11.4\% \pm 4.9\%$ of the single crystals are assigned to the group agglomerates and $16.8\% \pm 5.0\%$ to the waste particles. The total percentage of misclassified agglomerates is slightly lower: $12.0\% \pm 1.6\%$ are assigned to the single crystals and $5.5\% \pm 1.9\%$ to the waste particles.

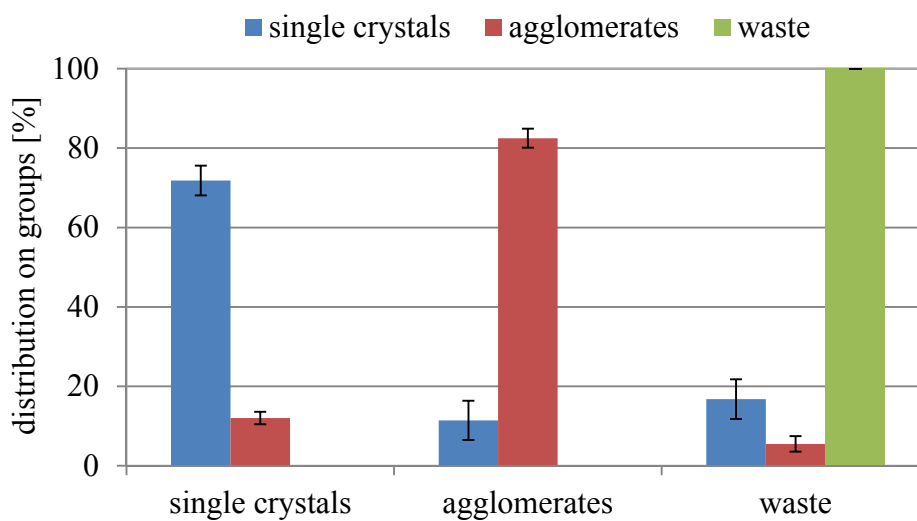


Figure 4.14: Averaged distribution of crystalline particles on the groups single crystal, agglomerates, and waste for the image descriptor combination D_{AA-0}

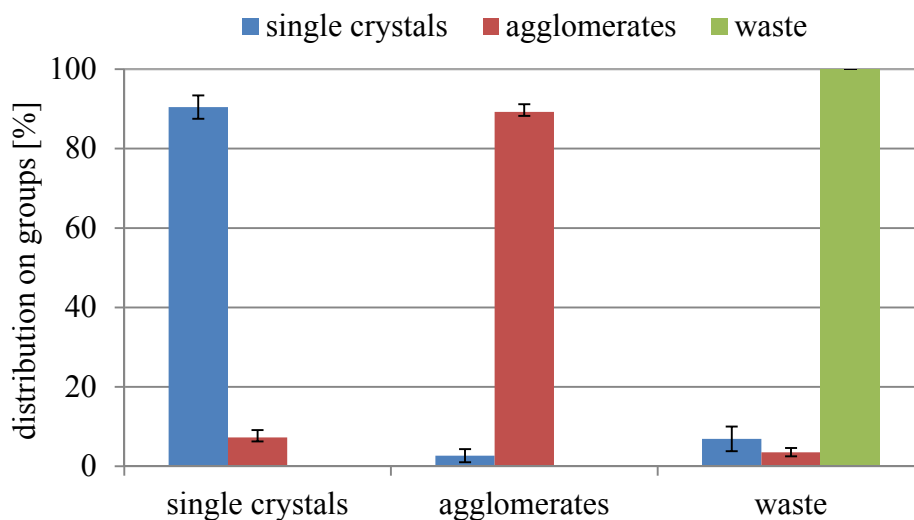


Figure 4.15: Averaged distribution of crystalline particles on the groups single crystal, agglomerates, and waste for the image descriptor combination D_{AA-3}

To enhance the separation between single crystals and agglomerates in the next step D_{AA-0} was extended by the image descriptor $nConc$ to the **image descriptor combination D_{AA-1}** ; for agglomerates normally more concave points are detected than for single crystals. The classification results, as well as the distribution of the particles to the groups, are depicted in Figure A.12 and Figure A.13. In comparison to D_{AA-0} the misclassification of single crystals to the group agglomerates is reduced by half to $7.2 \% \pm 2.7 \%$, whereas the rest of the distribution stays nearly constant. Thus, the overall classification performance is just slightly changed (PI: $81.7 \% \pm 1.6 \%$ and δAg : $7.8 \% \pm 2.2 \%$). Nevertheless, the classification of single crystals is enhanced by $nConc$ so that the image descriptor is retained inside the image descriptor combination.

Due to the fact that in average $17.6 \% \pm 5.3 \%$ of the single crystals are still assigned to the waste particles the image descriptor $dCentriod$, a circularity measure, was added to D_{AA-1} to allow a better differentiation between elongated single crystals and round bubbles. With the received **image descriptor combination D_{AA-2}** 11.1 % less single crystals are assigned to the group waste particles so that the specific performance index of the single crystals PI_S increases from $75.2 \% \pm 4.2 \%$ to $86.4 \% \pm 1.6 \%$ (see Figure A.14). However, $12.8 \% \pm 2.4 \%$ of the agglomerates are still mismatched to the group single crystals; leading to more single crystals detected than manually classified. As consequence the values for both performance measurements rise: The overall classification of D_{AA-2} is characterized in average by a PI-value of $84.3 \% \pm 1.9 \%$ and a δAg -value of $10.8 \% \pm 1.9 \%$ (compare Figure A.15).

Hence, to obtain a reference discriminant function with a classification performance in the same order of magnitude as reached for the scanning image analysis the separation of single crystals and agglomerates had to be further improved. Therefore, the image descriptor $MaxDepth$ was added to the **image descriptor combination D_{AA-3}** . As can be seen in Figure A.16 by adding $MaxDepth$ the classification performance is improved in averaged to a PI of $89.8 \% \pm 1.5 \%$ and a δAg of $6.3 \% \pm 2.0 \%$. The reason for this is that the mismatch of agglomerates to single crystals is reduced to $7.3 \% \pm 1.8 \%$ and furthermore still $2.7 \% \pm 1.7 \%$ of single crystals are detected as agglomerates (see Figure 4.15). Consequently, $MaxDepth$ is identified as suitable image descriptor.

Since out of all image descriptor combinations tested D_{AA-3} delivers a transferable discriminant function with comparable classification performance to the scanning discriminant function only, the discriminant function with the best classification performance and transferability is selected out of these ones: The reference discriminant function identified is based on the training set AA-G6a and classifies suspended adipic acid crystals with a PI of $90.5 \% \pm 1.5 \%$

and a δAg of $5.3 \% \pm 1.6 \%$ (see Figure A.16). The training set AA-G6a was created out of the crystalline product batch with a medium width of the CSD and a medium crystal size. It is assumed that the suitability of the training set AA-G6a arises out of the fact that in a CSD with a medium width and medium crystal size a broad range of crystal shapes exists and therefore the discriminant function can be trained in the best way.

4.4. Summary

The agglomeration degree distribution (AgD) of crystalline product batches was introduced as new quality criterion to quantify the amount and distribution of agglomerates. In comparison to the crystal size distribution (CSD) the AgD offers the advantage to distinguish between single crystals and agglomerates so that a differentiation between crystal growth and agglomeration is given. Therewith, crystalline product batches with different morphology can be quantitatively characterized or compared by its AgD and characteristic values of the AgD enable to evaluate whether the CSD is broadened by agglomeration or not.

To determine the AgD an image analysis tool based on Discriminant Factor Analysis (DFA) was developed and applied for two material systems with crystals of different morphology. Depending on the image recording method used crystalline product batches in suspension and dry crystalline product batches can be analyzed. In contrast to the transmitted light scanner the QICPIC system enables both the measurement of suspended and dried crystals. Core of the image analysis tool is a so-called reference discriminant function, which has to be identified for a material system first. The reference discriminant function allows an automatic classification of crystalline particles of the same material system without a time-consuming, manual classification step of about 1000 crystalline particles per crystalline product batch; i.e. in contrast to a normal discriminant function the reference discriminant function is transferable and does not need trained. To identify a reference discriminant function it has been shown that the creation of the training set, as well as the selection of image descriptors, play an essential role. In this context factor analysis turned out to be suitable for the selection of image descriptors. Furthermore, it was shown that the reference discriminant function of a material system has to be adapted if the image recording method is changed. Reasons for this are the availability of e.g. image descriptors and the orientation of particles during image recording.

5. Material System I – L-Alanine/Water

This chapter focuses on the investigation of the agglomeration behavior of the material system L-alanine/water within the crystallization process chain to increase the understanding of agglomeration and to provide insights with relevance for holistic process optimization. The influence of cake washing and drying on agglomeration is recorded. Three different drying methods are investigated systematically using Design of Experiments (DoE): Static drying, fluidized bed drying, and rotary tube drying. Main influencing process parameters are identified and the following questions are answered: “Where does agglomeration take place in the process?” and “How does agglomeration influence quality criteria like the CSD?”.

5.1. Cooling Crystallization

At first the crystal size distribution (CSD), agglomeration degree distribution (AgD), and overall agglomeration degree (Ag) of two crystalline product batches were measured after cooling crystallization. These measurements are used as reference point for the analysis of the agglomeration behavior, i.e. for comparison with measurements after drying to allow an evaluation of the impact of washing and drying on the product quality. The process parameters of the cooling crystallization experiments were set due to DoE based optimization by Wohlge-muth [53] to: cooling rate $\kappa=0.45$ K/min, $T_{\text{start}}= 60$ °C, $T_{\text{end}}= 10$ °C, saturation temperature $T_{\text{sat}}= 42.38$ °C, and stirring rate 300 rpm. The results of the experiments are depicted in Figure 5.1 and Table 5.1. To remind: Since a comparison of measurements after crystallization and drying should be carried out and the image analysis tool for dry crystals is limited to crystalline particles larger than 200 μm (see section 4.2.1) the presented results are referred to the crystal size range above 200 μm also.

The CSD after crystallization is characterized by a median crystal size of 270 μm , a width of 221 μm and exhibits for crystals larger than 350 μm a tailing in the distribution. The AgD first increases slightly in the size range from 200 μm to 400 μm from 0.2 to 0.3, stays then quasi-constant up to a size of 600 μm , and subsequently increases to a value of 0.9. In sum for the crystalline product an agglomeration degree (Ag) of 27.7 % is determined, which is relati-

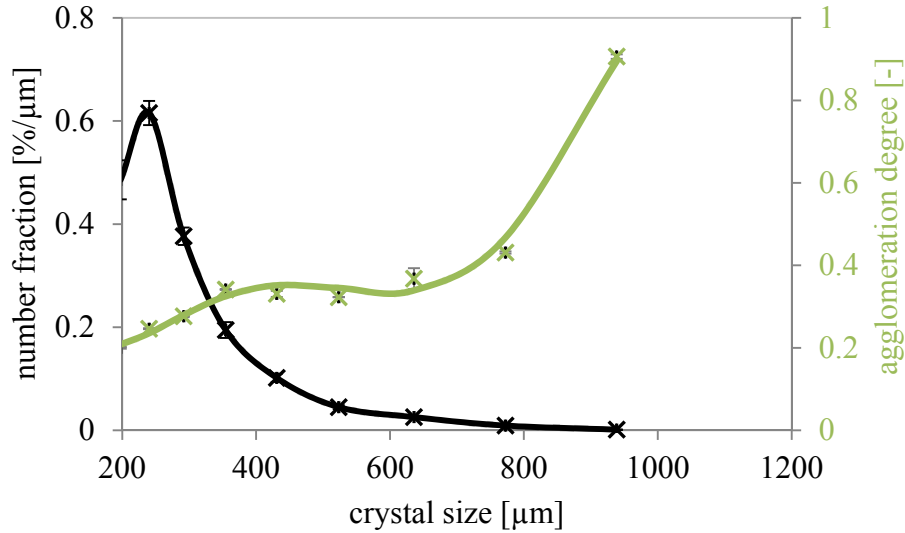


Figure 5.1: CSD and AgD of L-alanine/water measured directly after crystallization out of suspension with QICPIC (experimental conditions: $\kappa=0.45$ K/min, $T_{\text{start}}=60$ °C, $T_{\text{end}}=10$ °C, $T_{\text{sat}}=42.38$ °C, 300 rpm)

Table 5.1: Characteristic values of the L-alanine product batches directly after crystallization (cp. Figure 5.1)

	Ag [%]	d_{10} [μm]	d_{50} [μm]	d_{90} [μm]	$d_{90}-d_{10}$ [μm]
after crystallization	27.7 ± 0.2	206 ± 1	270 ± 6	427 ± 2	221 ± 2.5

vely low. According to expectations, the amount of agglomerates inside the CSD increases with the crystal size. Due to the fact that agglomeration is a size enlargement process, the probability to detect agglomerates is higher for larger crystalline particles. Furthermore, Faria et al. [107] describes that the probability for agglomeration during crystallization increases with the crystals size, because larger crystals spend a longer time in suspension than smaller ones. However, the curve progression of the AgD indicates that the observed tailing of the CSD is not caused by agglomeration only. Rather, the major part of the crystalline particles in the size range above 600 μm is constituted by single crystals. Therefore, a broadening of the CSD by the tailing could not be traced back to agglomeration only as probably expected without the information delivered by the AgD.

5.2. Cake Washing

At the end of the cooling crystallization at 10 °C a concentration of 147.24 g/kg water was measured, i.e. a high amount of solute remains in the mother liquor. Due to this high concentration the probability of agglomeration processes during drying is high also (compare section 2.3.2). During drying the concentration of solute in the remaining mother liquor in the voids between the crystals of the wet filter cake increases permanently by evaporation of the solvent. The higher the concentration, the higher is the amount of solute for the formation of

solid bridges, and the probability for the cementation of crystals rises. By cake washing after filtration the mother liquor inside the filter cake is displaced which might avoid agglomeration during drying.

To proof the assumption that the material system L-alanine/water has a strong tendency to agglomerate during drying the product quality of unwashed and washed crystalline product batches after drying are compared with the product quality reached directly after crystallization. For this purpose, first a suitable wash liquid is selected (see section 5.2.1) and afterwards washing experiments with a varied number of wash cycles and amount of wash liquid were carried out (see section 5.2.2).

5.2.1. Wash Liquid Selection

For the selection of a suitable wash liquid the following selection criteria are considered: solubility of L-alanine in the wash liquid, viscosity ratio between mother liquor and wash liquid, and miscibility of wash liquid and the mother liquor (compare section 2.2.2 and 3.3.2).

First, on basis of solubility data acetone, ethyl acetate, and ethanol are preselected. All these solvents are characterized by a low solubility of L-alanine at low and high temperatures (see Table A.10). The solubility of L-alanine is around thousand times lower than in water, so that a redissolution of L-alanine crystals during cake washing and drying is negligible, presupposed that the mother liquor is displaced entirely.

Subsequently, the washing efficiency, i.e. the potential of the solvents to displace the mother liquor out of the filter cake, is evaluated by the viscosity ratio and the miscibility or solubility of water in the wash liquid, respectively. As can be seen in Table 5.2 ethanol shows with a value of 1.4 a viscosity ratio in the range of one, whereas ethyl acetate followed by acetone show up to 2.5 times higher viscosity ratios. With an increasing viscosity ratio the effect of “fingering” during cake washing increases, and the washing efficiency decreases. Concerning

Table 5.2: Viscosity ratio, solubility of water, and wash results of potential wash liquids for the material system L-alanine/ water

	η_{ML}/η_{WL}^a [-]	Solubility of water ^b [g/100g solvent]	Water content after each wash cycle ^c [wt.-%]		
			1 th	2 nd	3 rd
Acetone	5.5	miscible	6.7	1.0	0.2
Ethyl acetate	3.9	3.3	2.3	1.6	0.9
Ethanol	1.4	miscible	7.8	0.9	0.3

a: at 10 °C, b: at 25 °C taken from [117], c: 40 mL solvent per wash cycle at 20 °C

the criterion miscibility it has to be considered that acetone and ethanol are both totally miscible with water, whereas the solubility of water in ethyl acetate is limited.

This means that the capacity of ethyl acetate is restricted and the washing efficiency is reduced by the formation of streaks. Thus, to wash out the same amount of mother liquor for ethyl acetate a higher amount is necessary than for ethanol and acetone. Nevertheless, under economic aspects a greater use of wash liquid can be economical if in sum the costs for purchase or recycling of the solvent are less. However, it has to be taken into account also that the time of the washing process rises with a higher amount of wash liquid. Since, in this study economic aspects are neglected, the washing efficiency of the solvents is evaluated for same amounts of wash liquid used per wash cycle. Ethanol is identified due to the low viscosity ratio and the unlimited miscibility with water as wash liquid with the greatest washing efficiency. To verify this, experiments in which the filter cake was washed three times with 40 mL acetone, ethanol, or ethyl acetate, respectively, were carried out. To characterize the washout of mother liquor from the filter cake after each wash cycle the water content of the filtrate was determined by Karl-Fischer titration (Mettler Toledo, V30).

After washing, the filter cake was dried statically at room temperature and images of the crystals were taken by scanning electron microscopy (SEM) (see Figure 5.2). Compared to unwashed crystals (A-B) washing with all wash liquids (C-H) prevents the formation of large agglomerates during drying. This leads to a softer consistency of the crystalline products. However, despite the low solubility of L-alanine in all solvents the crystals washed with acetone (C-D) and ethyl acetate (E-F) show rounded edges and rough surfaces due to partial dissolution of the crystals in the remaining mother liquor during drying. In contrast crystals washed with ethanol (G-H) show clear edges and smooth surfaces.

The results of the water content measurements are listed in Table 5.2 too. Herein the differences between the water contents after and before washing are shown. The calculated values seem to correlate with the viscosity ratios and the miscibility of the solvents with water. The washout of water from the filter cake after each wash cycle with ethanol is higher or nearly the same as the washout with acetone. In sum the highest water content is reached with ethanol followed by acetone and ethyl acetate. The low washing efficiency of ethyl acetate compared to acetone and the viscosity ratios determined can be reduced – as explained above – to the lower miscibility of ethyl acetate with water.

To sum up, ethanol was identified as suitable wash liquid for the material system L-alanine water and qualitative conclusions that agglomeration takes place during drying could be drawn from the SEM-images shown.

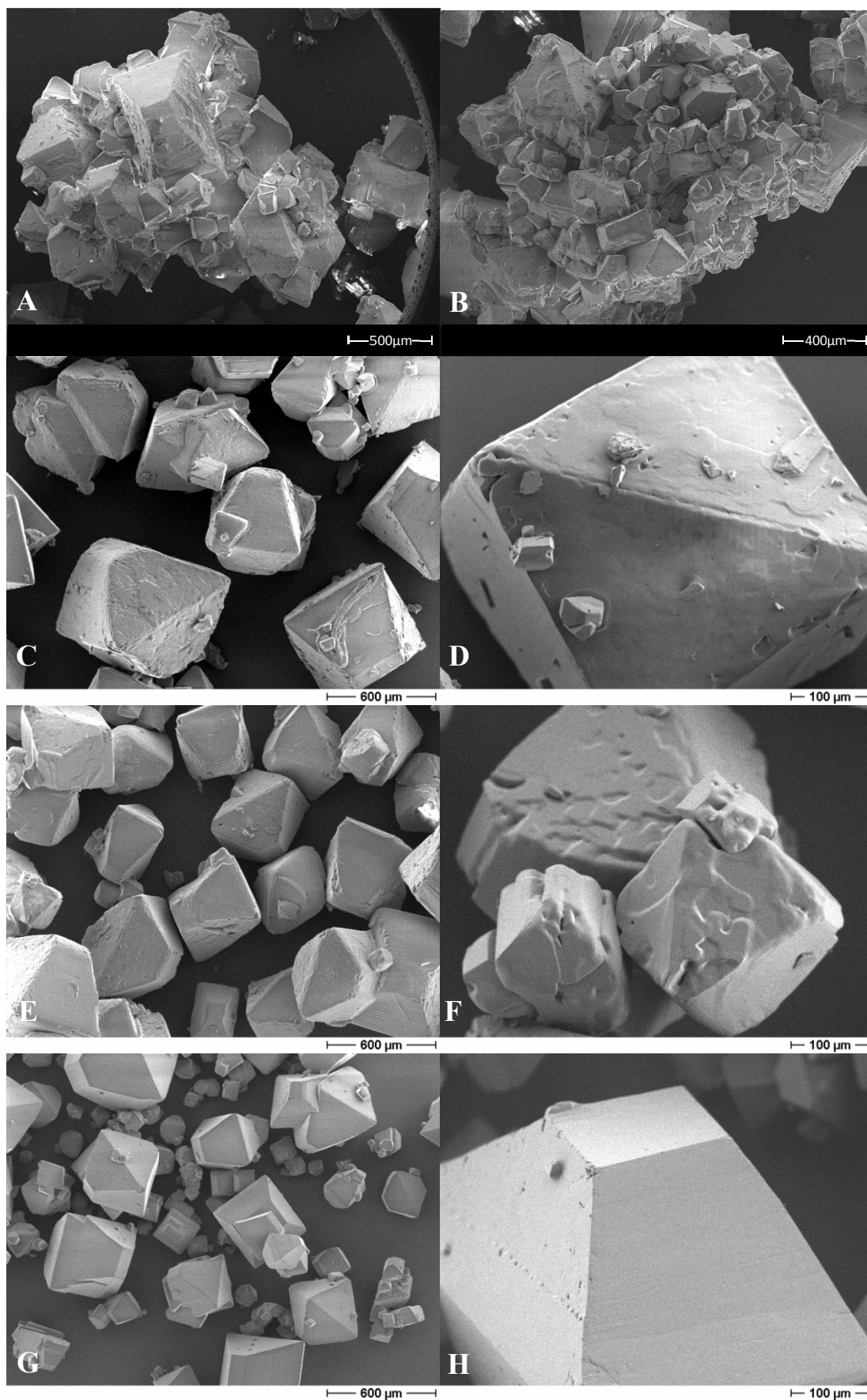


Figure 5.2: SEM images of statically dried L-alanine crystals: unwashed (A-B), washed with acetone (C-D), ethyl acetate (E-F), and ethanol (G-H); all crystal are dried under same conditions

5.2.2. Impact of Washing Parameters

To get quantitative information about the agglomeration of L-alanine crystals during drying and to investigate the influence of the washing parameters – number of wash cycles and amount of wash liquid – washing experiments were carried out with ethanol. To consider that ethanol may act as antisolvent posing the risk of precipitation during washing 40 mL of an ethanol/ water mixture with a volume ratio of 4/1 was used for the first wash cycle. For the ethanol/water mixture a solubility of 2.83 g/kg at 25 °C was measured gravimetrically, which is on the one hand around 14 times higher than the solubility in pure ethanol, and on the other hand 58 times lower than the solubility in water. Whenever a second wash cycle was performed, pure ethanol was used as wash liquid and the amount of pure ethanol added was varied between 20 mL and 80 mL. The crystallization and drying conditions were kept constant for all washing experiments. As drying methods static drying and fluidized bed drying were used. The drying temperature was set to 50 °C, the amount of feed material to 30 g, and - in case of fluidized bed drying - the volume flow to 31 m³/h.

The results of the washing experiments, in comparison to the results reached after crystallization, are summed up in Figure 5.3. The quality of the crystalline product batches is illustrated by the overall agglomeration degree (Ag) and the width of the CSD (d_{90} - d_{10}). As can be seen for static and fluidized bed drying nearly the same Ag and d_{90} - d_{10} values are obtained for unwashed and washed crystalline product batches. Also the corresponding

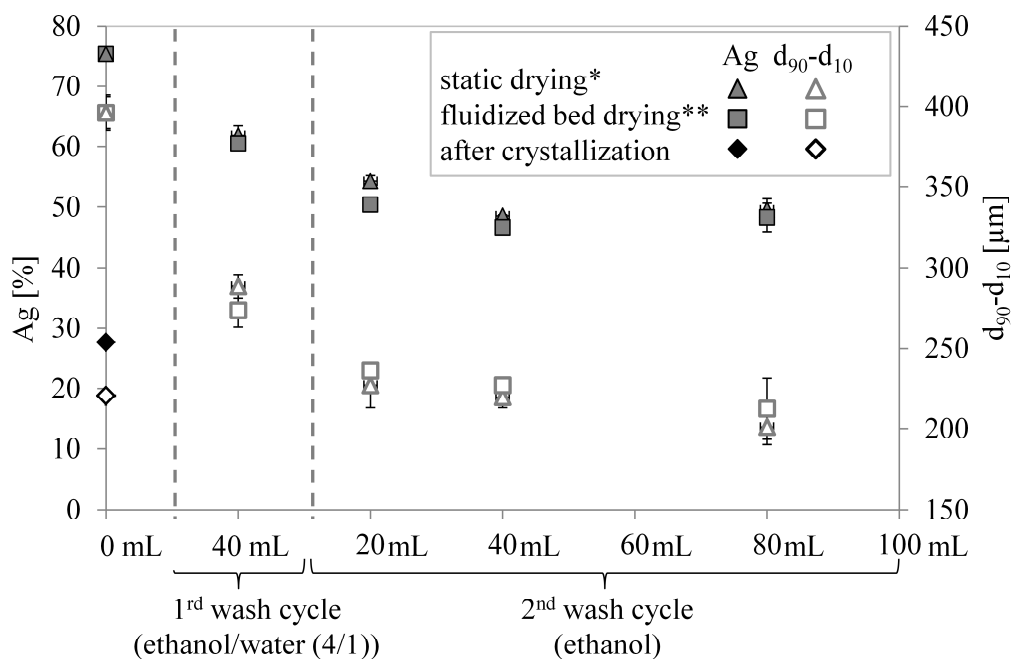


Figure 5.3: Ag and d_{90} - d_{10} of L-alanine crystalline product batches after crystallization and drying depending on the number of wash cycles and amount of wash liquid used (*50 °C, 30 g; **50 °C, 30 g, 31 m³/h)

agglomeration degree distributions (AgDs) and crystal size distributions (CSDs) exhibit the same trend independent of the drying method used. Therefore, the AgDs and CSDs of the crystalline product batches are shown here exemplarily for the experiments, which were dried statically (see Figure 5.4). The AgDs and CSDs of the crystalline product batches dried by fluidized bed drying are given in Figure A.17. In contrast to the product quality reached after crystallization the unwashed crystalline product batches after drying show significantly higher Ag-values of $75 \% \pm 0.6 \%$ and higher $d_{90-d_{10}}$ values of $396 \mu\text{m} \pm 11 \mu\text{m}$. The corresponding AgD for the static dried crystalline product batches, shown in Figure 5.4 I, indicates that the higher Ag and the broadening of the CSD can be traced back to agglomeration over the whole crystal size range.

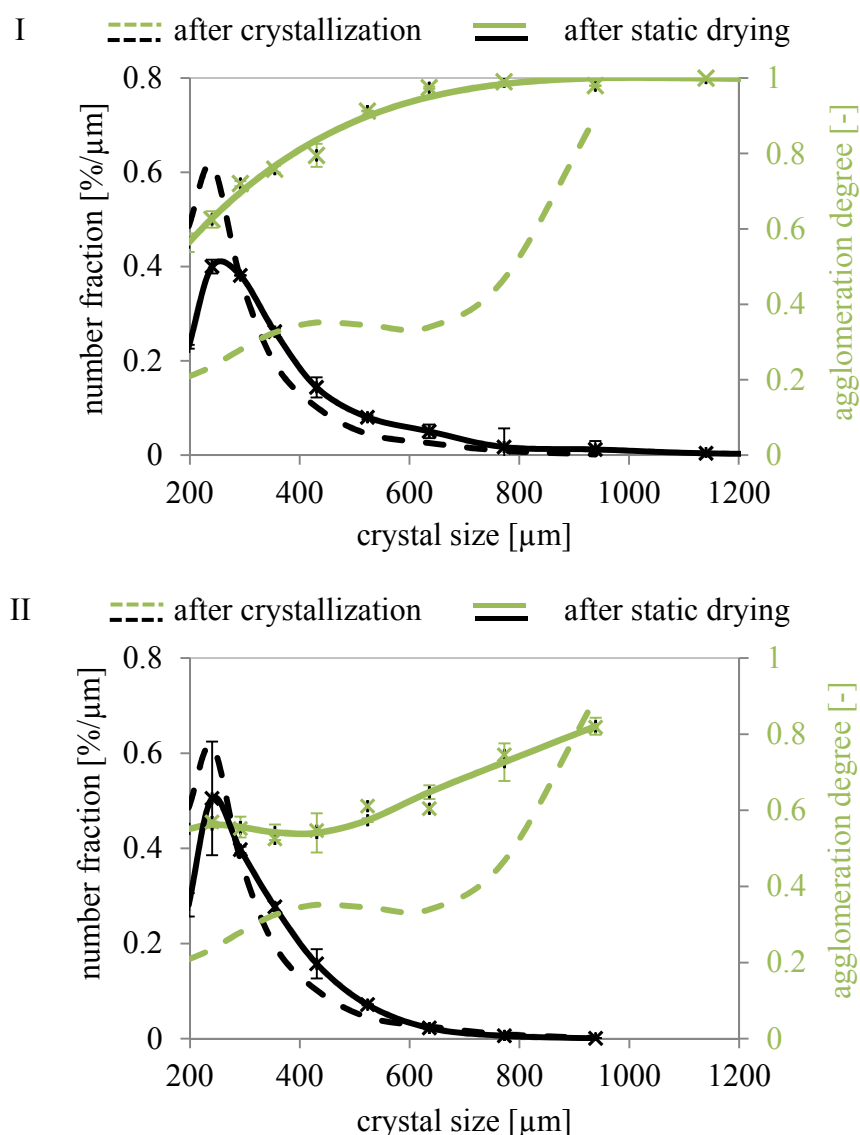


Figure 5.4-part 1: CSDs and AgDs after static drying ($50 \text{ }^\circ\text{C}$, 30 g) in comparison to the results after crystallization. I: unwashed; II: one wash cycle (40 mL ethanol/water ($4/1$)), III: two wash cycles (20 mL ethanol); IV: two wash cycles (40 mL ethanol)

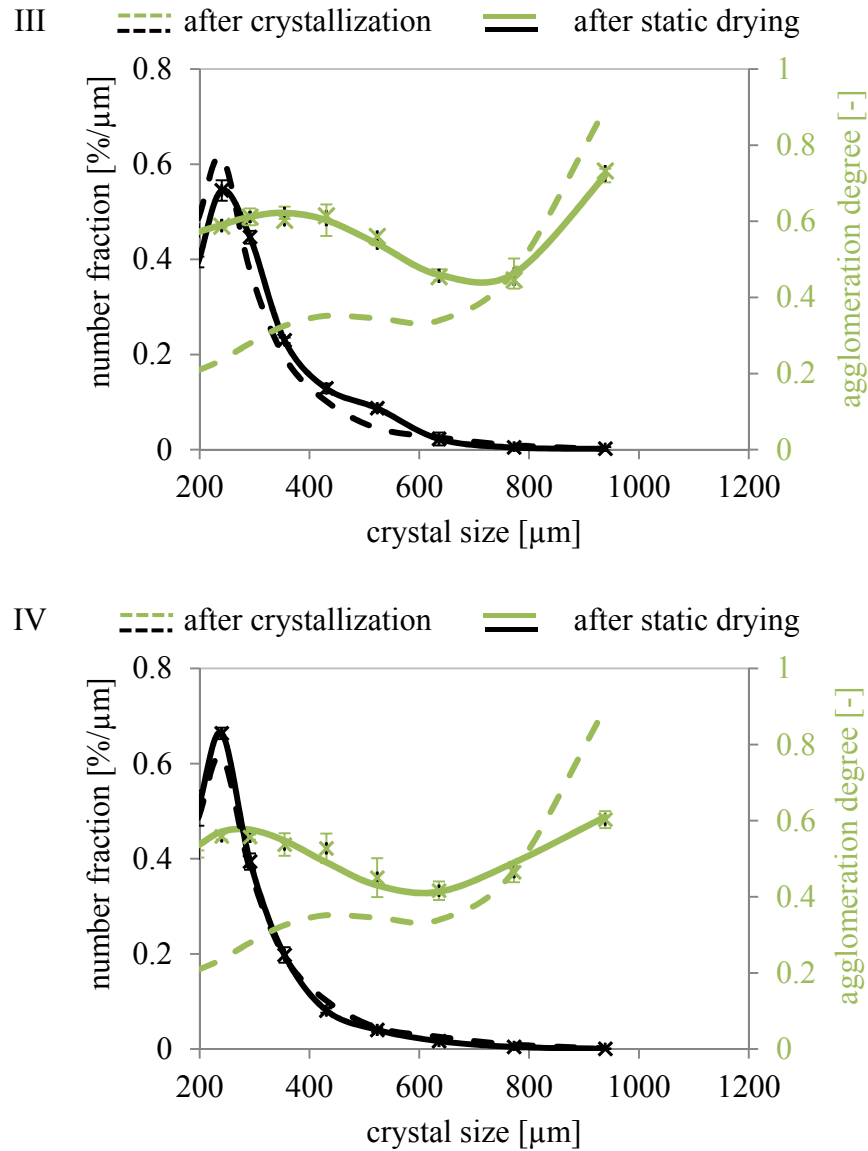


Figure 5.4-part 2: CSDs and AgDs after static drying (50 °C, 30 g) in comparison to the results after crystallization. I: unwashed, II: one wash cycle (40 mL ethanol/water (4/1)), III: two wash cycles (20 mL ethanol), IV: two wash cycles (40 mL ethanol)

In contrast to the AgD after crystallization the AgD after drying starts at 200 μm with an around three times higher agglomeration degree of the particle fraction, and is then characterized by an anti-logarithmic curve progression. The comparison shows that agglomeration - as assumed above - takes place strongly during drying and product characteristics like the width of CSD are affected. The small difference between the product qualities reached with the two drying methods can be traced back to the drying process of the unwashed crystalline product batches in the fluidized bed dryer. Instead of generating a fluidized bed the air flows through a bulk of material. Therefore, the drying characteristic, as well as the contact area between the crystals, seemed to be similar to static drying which results in similar product qualities.

The results of the washing experiments exhibit the following trends: Figure 5.3 indicates that the Ag and the width of the CSD are reduced by more wash cycles and a higher amount of wash liquid used. Up to an amount of 40 mL in the second wash cycle small differences in the product quality can be observed. The width of the CSD is nearly the same as after crystallization, but with around 48 % higher Ag-values are reached after drying, despite washing. The AgDs depicted in Figure 5.4 and Figure A.17 show that in accordance with the reduction of the Ag the formation of especially larger agglomerates can be prevented by using more wash cycles and a high amount of wash liquid. Due to the lower amount of larger agglomerates the d_{90} -values of the CSD is reduced and a narrower CSD is reached. Nevertheless, despite a higher amount of wash liquid higher agglomeration degrees in contrast to the AgD after crystallization are reached for small crystal sizes in the range between 200 μm and 400 μm . Therefore, the observed higher Ag-values of the crystalline product batches after drying are the result of a higher amount of smaller agglomerates. However, the higher amount of these small agglomerates does not have a strong impact on the d_{10} -value of the CSD, due to the high number of small particles and the lower limit for the analyzable crystal size. Consequently, in spite of higher Ag-values similar CSDs to the ones after crystallization are reached. The described agglomeration behavior can be traced back to the fact that with an increase of the number of wash cycles and the amount of wash liquid more mother liquor can be displaced out of the voids of the filter cake, whereby agglomeration is reduced. Furthermore, the solubility of L-alanine in both wash liquids is significantly lower than in water so that the redissolution of crystals during drying and thereby agglomeration is reduced as well. However, the mother liquor cannot be displaced entirely. Therefore, after a certain amount of wash liquid, in this case after the usage of 40 mL in the second wash cycle, an increase of the amount of wash liquid has a slight impact only. The specific resistance of a filter cake is inversely related to the permeability of the filter cake which influences the efficiency of cake washing [63]. The permeability of the filter cake depends on the size, size distribution, and shape of the crystals, which involves pores of different sizes inside the filter cake. By reducing the crystal size the permeability of the filter cake decreases [63]. Therefore, the permeability of the filter cake is lowered especially for regions with a high amount of small crystals. As result the filter cake is passed by the wash liquid inhomogeneously, caused by e.g. channeling through pores of larger size. This leaves mother liquor especially between small crystals, which explains the observed agglomeration tendency of small crystals during drying. Furthermore, the large specific surface area of small crystals involves a higher contact area allowing a higher amount of

mother liquor to attach. This results in strong liquid bridges [11] and a large contact area between small crystals, which promotes agglomeration of small crystals as well.

A comparison of the product qualities depicted in Figure 5.3 concerning the drying method used, suggests, that for washing experiments with two wash cycles a tendency for lower A_g -values exists if fluidized bed drying is used instead of static drying. After implementing a second wash cycle an expansion of the fluidized bed could be observed so that the lower A_g -values might be the result of a lower contact area between the crystals during fluidized bed drying. Since here the drying methods are compared at one condition only, a reliable comparison of the drying methods will not be possible until a systematic investigation is completed (see next section).

5.3. Drying

To investigate systematically the influence of drying on the quality of a crystalline product batch for each drying method – static, fluidized bed, and rotary tube drying – a Design of Experiment (DoE) was performed. For all drying methods the two factors, drying temperature and amount of feed material were considered. Additionally, in case of fluidized bed drying the air volume flow and in case of rotary tube drying the rotational speed was investigated. The factors and levels of the three DoE are shown in subsections 5.3.1 to 5.3.3 for static, fluidized bed, and rotary tube drying respectively. The center point experiments were realized six times ($n_0 = 6$) in case of static and fluidized bed drying, and four times ($n_0 = 4$) for rotary tube drying. Due to the different amount of center point experiments and factors different α -values were calculated (compare equation (3.8)). The α -value for static drying was calculated to ± 1.32 , whereas for fluidized bed drying an α -value of ± 1.52 , and for rotary tube drying an α -value of ± 1.41 was calculated. Caused by the different α -values, but also due to different setting options of the ventilated ovens, e.g. the temperature values of the experimental designs differ from each other. To quantify the impact of the factors on the product quality the overall agglomeration degree A_g , the median crystal size d_{50} , the characteristic diameters d_{10} and d_{90} , and the width of the crystal size distribution $d_{90}-d_{10}$ were used as responses in the experimental designs. The evaluation of the experimental designs was performed according to section 3.6.1. For all experimental designs the crystallization, filtration, and washing parameters, were kept constant. The filter cake was washed first with 40 mL of the ethanol/water mixture (ratio 4/1) and then with 80 mL ethanol. In the following the results of the experimental designs are discussed for each drying method separately.

5.3.1. Static Drying

Table 5.3 gives an overview on the factors and levels investigated in the experimental design for static drying. The results of the 14 experiments are given in detail in Table A.11. Out of these results the effects of the single factors, interactions, and nonlinearities as well as the 95 % confidence intervals (ci) were calculated for the responses Ag, d₁₀, d₅₀, d₉₀, and d₉₀-d₁₀ and listed in Table 5.4. Significant effects are highlighted in bold.

The drying temperature (A) and the amount of feed material (B), which corresponds to the layer thickness, have a linear effect on the responses Ag, d₉₀, and d₉₀-d₁₀. In addition, the insignificant interaction (AB) indicates that regarding the analyzed responses no interdependence between the drying temperature and the amount of feed material exists.

The agglomeration degree (Ag) is affected negatively by the drying temperature (A) and positively by the amount of feed material (B). The opposite effects can be observed on the width of the CSD (d₉₀-d₁₀). This means, that crystalline product batches dried at higher temperature are characterized by lower Ags and broader CSDs, whereas an increase of the amount of feed material leads to crystalline product batches with higher Ags and narrower CSDs. The characteristic diameter d₉₀ is influenced by the drying temperature and the amount of feed material in the same order of magnitude as d₉₀-d₁₀. Since, neither d₅₀ nor d₁₀ are affected significantly, a shift of the CSD to smaller or larger crystal sizes can be excluded. However, it should be taken into account that the insignificance regarding d₁₀ is probably caused by the limited analyzable size range. Hence, the influence on d₉₀-d₁₀ is traced back to changes of d₉₀ only.

Table 5.3: Factors (A-B) and levels investigated for static drying

Factor	Level				
	- $\alpha^{\#}$	-1	0	1	$\alpha^{\#}$
A Drying temperature [°C]	25	30	45	60	65
B Amount of feed material [g]*	20.2	25	40	55	59.8

*corresponds to different layer thickness, # $\alpha = \pm 1.32$

Table 5.4: Effects on the responses for static drying*

response	95 % ci	A	B	AA	BB	AB
Ag	± 5.08	-10.10	5.62	-1.61	2.07	2.15
d ₁₀	± 4.76	-0.11	-0.80	1.84	-1.03	1.50
d ₅₀	± 11.10	1.44	-3.46	9.27	-0.49	2.50
d ₉₀	± 23.68	24.66	-32.20	-12.79	11.32	-2.50
d ₉₀ -d ₁₀	± 21.44	24.76	-31.40	-14.63	12.35	-4.00

*A: drying temperature, B: amount of feed material, in bold: significant effects

The opposite effects on Ag and d_{90} - d_{10} indicate that changes of the d_{90} - d_{10} are caused by agglomeration. To elucidate this unexpected correlation the star experiments of the DoE are considered (see Figure 5.5). For star experiments one of the factors of DoE is varied only, whereas the other factor is constant on level zero.

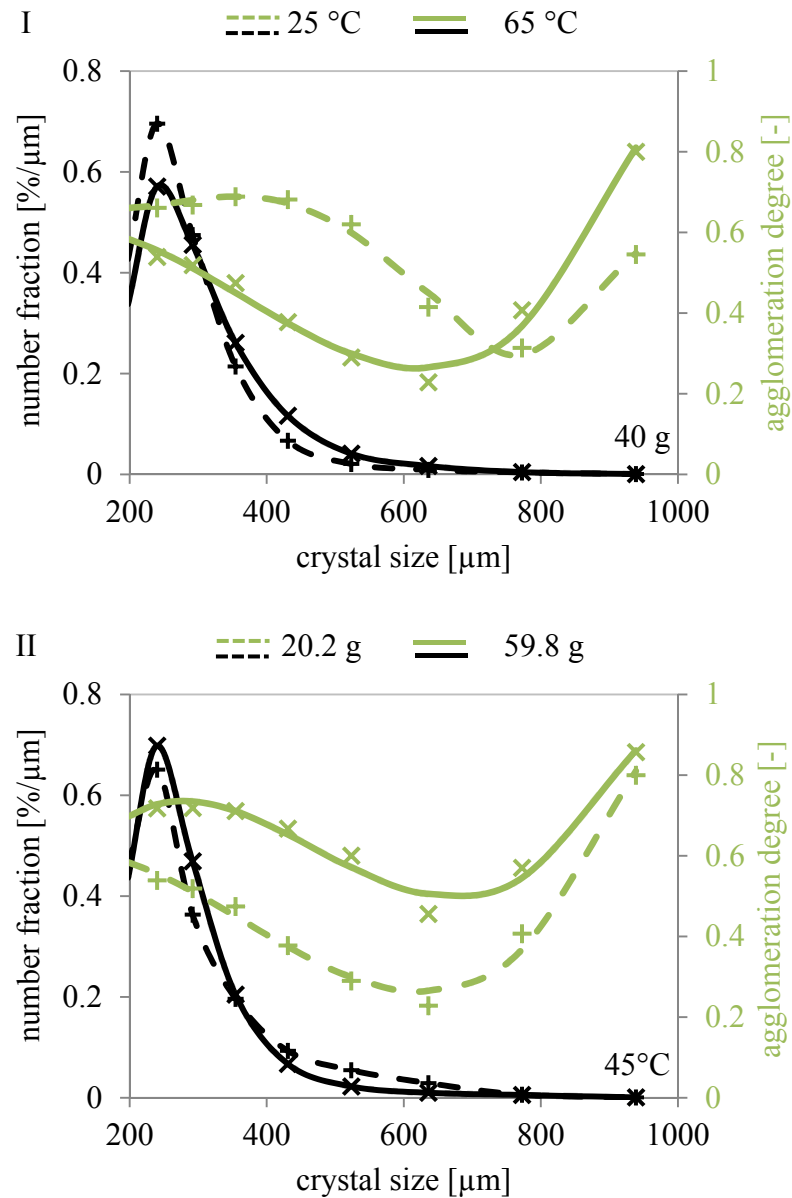


Figure 5.5: CSDs and AgDs of the star experiments of the DoE for static drying: (I) drying temperature, (II) amount of feed material

Table 5.5: Factor levels and responses of the star experiments depicted in Figure 5.5

		Figure 5.5 I		Figure 5.5 II	
		---	==	---	==
A	Temperature [°C]	25	65	45	45
B	Amount of feed material [g]	40	40	20.2	59.8
Responses	Ag [%]	66.4	47.4	49.6	70.6
	d ₁₀ [μm]	213	208	208	208
	d ₉₀ [μm]	385	439	476	390
	d ₉₀ -d ₁₀ [μm]	177	226	268	182

According to the star experiments in Figure 5.5 and the corresponding characteristic values of the crystalline product batches listed in Table 5.5, low drying temperatures, as well as a high amount of feed material, lead – except for the star experiments of the temperature in the range of large crystal sizes ($> 780 \mu\text{m}$) – to higher Ag_j -values of the AgDs over the whole crystal size range and thereby to higher Ag-values. The Ag of a crystalline product is a number based measure and is therefore mainly affected by the increase of agglomerates in the range between $200 \mu\text{m}$ and $300 \mu\text{m}$, because in this range, as indicated by the CSD, the largest amount of crystalline particles exists. Especially for the star experiments of the temperature (Figure 5.5 I) a considerable increase of crystalline particles within the crystal size range between $200 \mu\text{m}$ and $300 \mu\text{m}$ can be observed for lower drying temperatures. Since the corresponding AgD shows higher Ag_j -values in this crystal size range as well, the larger amount of particles can be traced back to agglomeration. It is assumed that these agglomerates are formed by the cementation of crystals smaller than $200 \mu\text{m}$ during drying, because neither breakage nor attrition was observed. Due to the limitation of the analyzable crystal size range to $200 \mu\text{m}$ no significant changes of the characteristic diameter d_{10} can be detected. But the value for d_{90} decreases because of the higher amount of crystalline particles in the crystal size range from $200 \mu\text{m}$ to $300 \mu\text{m}$ and nearly the same amount of large crystalline particles. In sum a narrower width of the CSD for crystalline product batches with a high Ag is obtained.

The impact of the drying temperature, as well as the amount of feed material, on agglomeration during static drying and thereby on the width of the CSD can be explained by the evaporation rate and the contact area between the crystals. The evaporation rate, which depends on the drying temperature, specifies the rate of supersaturation inside the solution between the crystals. Also during crystallization, the rate of supersaturation, provided by e.g. cooling or evaporation, is a highly influential parameter, which affects nucleation and crystal growth [11]. Therefore, it is not surprising that the evaporation rate during drying has a significant

influence the formation of crystalline bridges between the crystals. Fundamentally, for crystal growth a lower supersaturation than for nucleation is necessary. The lower the drying temperature, the lower is the evaporation rate during drying. Lower evaporation rates result in longer drying times and lower supersaturation, which promote the formation of stable crystalline bridges by crystal growth, i.e. agglomeration. The formation of more crystalline bridges by redissolution of the crystals during drying at higher drying temperatures can be excluded in our case because of the low temperature dependence of the solubility of L-alanine in ethanol (see section 5.2.1). The influence of the amount of feed material can be reduced partially to the rate of evaporation also. A higher layer thickness leads to a lower rate of evaporation. Furthermore, a higher contact area between the crystals is reached so that in sum the possibility for agglomeration increases.

5.3.2. Fluidized Bed Drying

The factor levels of the experimental design for fluidized bed drying are listed in Table 5.6 and the results of the 20 experiments are given in detail in Table A.12. The significant effects calculated of the drying temperature (A), amount of feed material (B), and volume flow (C) on the responses Ag , d_{10} , d_{50} , d_{90} , and $d_{90}-d_{10}$ are highlighted in bold in Table 5.7. The **agglomeration degree (Ag)** is significantly influenced by the drying temperature (A), which has a significant interaction (AC) with the volume flow (C). Hence, the drying temperature (A) and the volume flow (C) have to be considered together.

To evaluate the influence of the interaction (AC) on the Ag the contour plot depicted in Figure 5.6 I was calculated based on the regression model, given in equation (5.1).

Table 5.6: Factors (A-C) and levels investigated for fluidized bed drying. In brackets: Calculated factor values, which differ from the experimental values

Factor	Level				
	$-\alpha^{\#}$	-1	0	1	$\alpha^{\#}$
A Drying temperature [°C]	25 (22)	30	45	60	68
B Amount of feed material [g]	17.2	25	40	55	62.8
C Volume flow [m ³ /h]	13.7	18.7	28.0	37.4	42.4

$\alpha = \pm 1.52$

$$Ag = 51.52 - 3.10 \cdot x_A - 3.66 \cdot x_A x_C \quad (5.1)$$

$$d_{90} - d_{10} = 251.88 + 20.80 \cdot x_C + 23.75 \cdot x_A x_B \quad (5.2)$$

Table 5.7: Effects on the responses for fluidized bed drying*

response	95 % ci	A	B	C	AA
Ag	± 4.82	-6.21	-1.77	-0.95	1.47
d ₁₀	± 7.92	4.30	-8.25	-0.39	-2.93
d ₅₀	± 23.37	10.99	-16.44	6.14	-4.42
d ₉₀	± 45.36	14.27	-20.41	41.21	-2.31
d ₉₀ -d ₁₀	± 39.88	9.98	-12.16	41.61	0.62
response	BB	CC	AB	AC	BC
Ag	0.74	-2.19	0.42	-7.33	-3.48
d ₁₀	6.13	-0.77	1.00	3.00	0.50
d ₅₀	14.13	-2.26	10.25	8.75	-1.25
d ₉₀	38.24	14.08	48.50	16.00	1.00
d ₉₀ -d ₁₀	32.11	14.86	47.50	13.00	0.50

*A: drying temperature, B: amount of feed material C: volume flow;
in bold: significant effects, effects with grey background plotted in
Figure 5.6

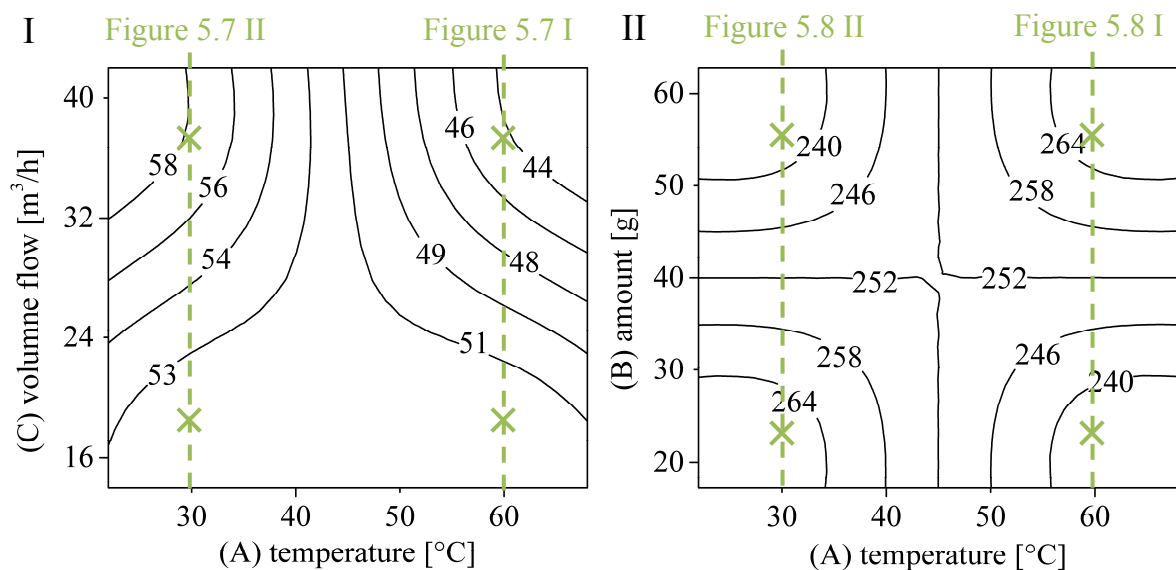


Figure 5.6: Contour plots for the significant factor interactions of fluidized bed drying: (I) interaction (AC) for Ag [%], (II) interaction (AB) for d₉₀-d₁₀ [µm]; constant factor on level minus one

Due to the negative single effect of the drying temperature (A), the Ag decreases with the temperature for constant volume flows (C). The drying temperature determines the evaporation rate during drying. For higher drying temperatures, higher evaporation rates are reached, which reduces the formation of stable crystalline bridges by crystal growth (compare results section 5.3.1). The contour lines in Figure 5.6 I demonstrate that a rising volume flow (C) leads to a reduction of the Ag in combination with high drying temperatures (> 45 °C), whereas in combination with lower drying temperatures (< 45 °C) higher Ag are reached. To

explain these results in more detail the CSDs and AgDs of the crosses are displayed in Figure 5.7 I and II. The CSDs measured are all similar whereby the AgDs are highly different. As depicted in Figure 5.7 I the overall Ag is decreased with an increasing volume flow due to lower amounts of small and large agglomerates. The volume flow (C) inter alia determines, like the drying temperature, the drying time. Moreover, the formation and behavior of the fluidized bed, i.e. the height and therewith the contact area and contact time between the crystals is affected. High drying temperatures in combination with an increased volume flow reduces the contact area and time between the crystals and therewith the possibility for agglomeration due to an earlier expansion of the fluidized bed. In contrast at lower drying temperatures the evaporation rate is lowered resulting in high drying times and a later expansion of the fluidized bed. This increases the possibility for agglomeration, especially the formation of smaller agglomerates caused by the higher contact area of small crystals. In turn, as can be seen in Figure 5.7 II for higher values of the volume flow the formation of larger agglomerates consisting of smaller agglomerates is reduced which results in a higher amount of smaller agglomerates.

Regarding the **crystal size distribution (CSD)** the results of the DoE listed in Table 5.7 indicate that the characteristic diameters d_{10} and d_{90} , as well as the width of CSD ($d_{90}-d_{10}$) are significantly affected by fluidized bed drying, whereas no influence on the median crystal size (d_{50}) exists. The volume flow (C) has a positive significant effect on $d_{90}-d_{10}$, i.e. the lower the volume flow the narrower is the CSD. The lower the volume flow, the smaller is the expansion of the fluidized bed so that the contact time between the crystals is extended and the agglomeration probability rises as well. The progression of the AgDs of the star experiments for the volume flow (available as in Figure A.18) confirms that for a low volume flow a higher amount of small agglomerates within the size range between 200 μm and 300 μm exists.

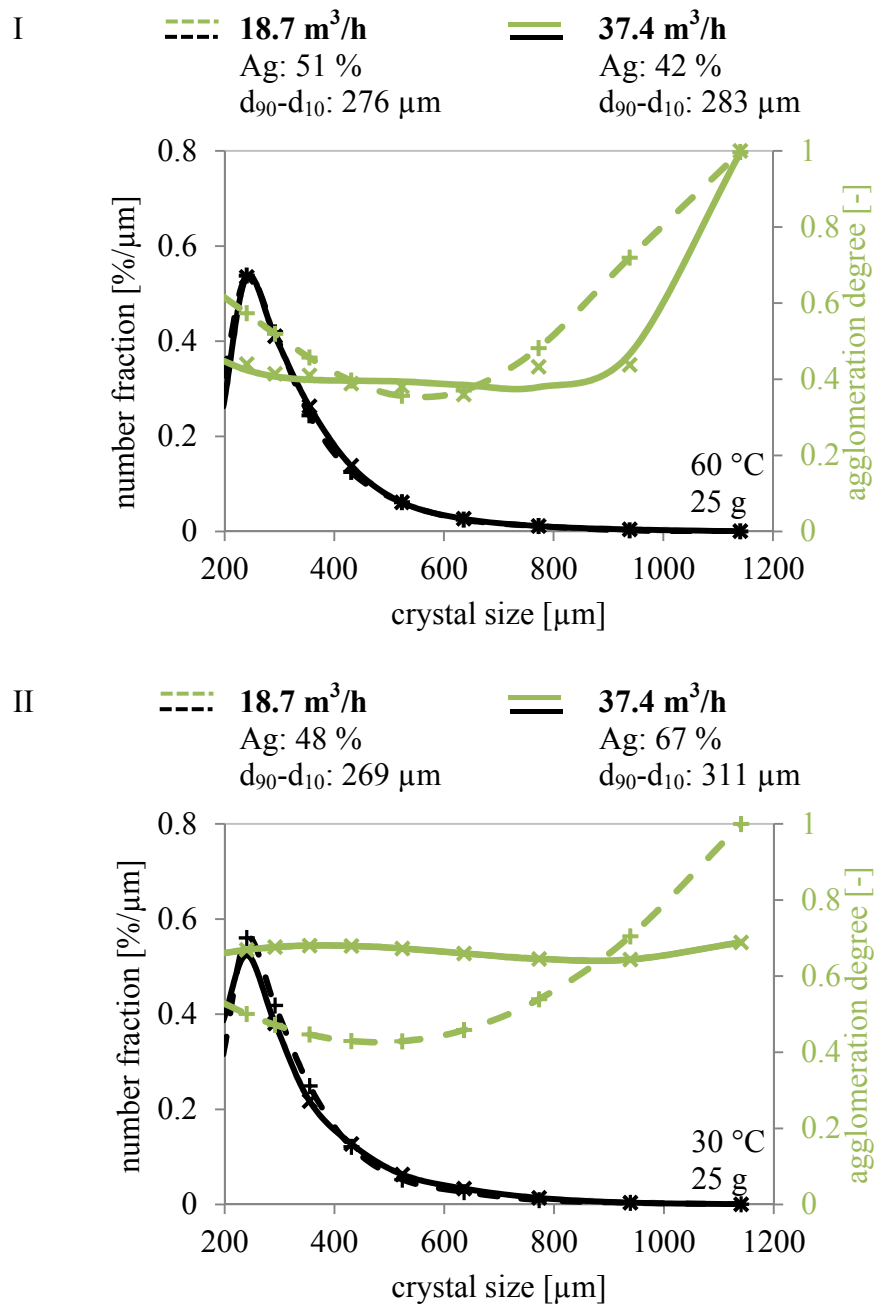


Figure 5.7: CSDs and AgDs of crystalline product batches after fluidized bed drying: variation of the volume flow at (I) high temperature (60 °C) and (II) low temperature (30 °C)

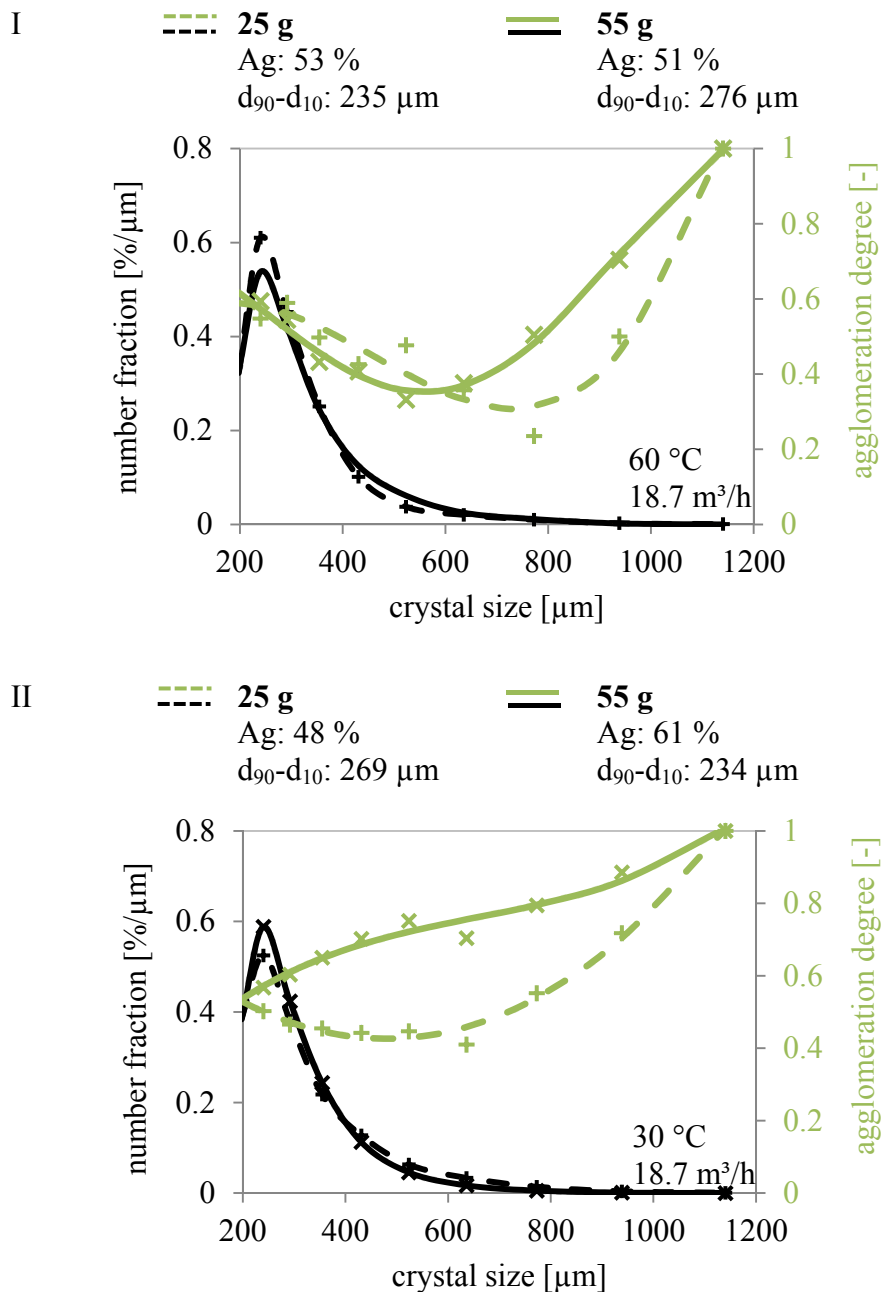


Figure 5.8: CSDs and AgDs of crystalline product batches after fluidized bed drying: variation of the amount of feed material at (I) high temperature (60 °C) and (II) low temperature (30 °C)

As described in section 5.3.1, it is assumed that the higher amount of small agglomerates can be traced back to the cementation of crystalline particles smaller than 200 μm . This leads to a reduction of the d_{90} -value and therewith to a narrower CSD. Furthermore, the interaction (AB) of the drying temperature (A) and the amount of feed material (B) has a significant effect on $d_{90}-d_{10}$. Therefore, both factors have to be considered in dependence of each other. The respective contour plot is shown in Figure 5.6 II and was calculated by the regression model given in equation (5.2). Since a significant effect of the interaction (AB) on the charac-

teristic diameter d_{90} in the same order of magnitude exists the width of CSD is influenced by changes of d_{90} mainly. As depicted in the contour plot in Figure 5.6 II for low temperatures (30 °C) the CSD is narrowed with a rising amount of feed material (B). For higher temperatures (60 °C) the opposite effect on the width of CSD is observed. According to the crosses in Figure 5.6 II, Figure 5.8 I and II depicts the AgDs and CSDs of crystalline product batches dried at different levels of amount of feed material (B) for a drying temperature of 60 °C and 30 °C, respectively. The curve progressions of the CSDs in Figure 5.8 I and II elucidate that a narrower CSD, reached by the variation of the drying temperature (A) or the amount of feed material (B), leads to a higher amount of agglomerates, especially a higher amount of small agglomerates and vice versa. This trend was observed during static drying also (compare section 5.3.1). Hence, the changes of the width of CSD ($d_{90}-d_{10}$) in the contour plot of the interaction (AB) can be traced back to agglomeration even though the interaction (AB) has no significant effect on Ag. The amount of feed material (B) determines, like the volume flow (C), the formation and behavior of the fluidized bed. With rising amount of feed material (B) the collision probability between the crystalline particles rises. Moreover, the amount of feed material (B) determines, like the drying temperature (A), the moment of the expansion of the fluidized bed; the higher the amount of feed material (B), the later the expansion of the fluidized bed occurs. In sum the probability for agglomeration rises with higher amounts of feed material (B) due to the larger contact area and longer contact time between the crystals. In contrast, as mentioned above, a higher drying temperature (A) reduces the agglomeration probability, i.e. the formation of stable crystalline bridges by higher evaporation rates. Therefore, in combination with a lower amount of feed material (25 g), a lower amount of large agglomerates is formed (compare Figure 5.8 I), which results in a higher amount of smaller agglomerates and a narrower CSD respectively. However, with the increase of the amount of feed material (B) the fluidized bed is expanded later and the collision probability rises so that larger agglomerates are formed despite the high drying temperature (see Figure 5.8 II).

Although, for fluidized bed drying no opposite significant effects of the single factors and interactions on the Ag and $d_{90}-d_{10}$ exist - as shown before for static drying – the evaluation of the DoE demonstrates that the width of the CSD is influenced by agglomeration in the same way.

5.3.3. Rotary Tube Drying

The factors and levels of the experimental design for rotary tube drying are denoted in Table 5.8 and the results of all 18 experiments are given in Table A.13. Table 5.9 shows the effects of the single factors, interactions, and nonlinearities as well as the 95 % confidence intervals (ci) regarding the responses Ag , d_{10} , d_{50} , d_{90} , and $d_{90}-d_{10}$. Significant effects are given in bold. The **agglomeration degree (Ag)** is significantly affected by all factors investigated. For the amount of feed material (B) a significant, negative nonlinear effect (BB) exists so that the Ag runs through a maximum. Due to the fact that the drying temperature (A) shows a significant interaction (AB) with the amount of feed material (B), both factors have to be considered together. The corresponding contour plot is depicted in Figure 5.9 I and was calculated with the regression model given in equation (5.3).

Table 5.8: Factors (A-C) and levels investigated for rotary tube drying

Factor	Level				
	$-\alpha^{\#}$	-1	0	1	$\alpha^{\#}$
A Drying temperature [°C]	30	34	45	56	60
B Amount of feed material [g]	25	29	40	51	55
C Rotational speed [rpm]	15.7	21.7	36.4	51.1	57.1

$\alpha = \pm 1.41$

Table 5.9: Effects on the responses for rotary tube drying*

response	95 % ci	A	B	C	AA
Ag	± 4.28	1.63	1.80	0.46	1.91
d_{10}	± 25.85	2.15	4.88	-8.18	-5.67
d_{50}	± 64.31	-14.11	3.21	-29.12	-7.25
d_{90}	± 54.30	-23.49	8.52	-24.68	-38.42
$d_{90}-d_{10}$	± 42.24	-25.64	3.64	-16.50	-32.75
response	BB	CC	AB	AC	BC
Ag	-8.84	-3.54	5.08	-7.88	-1.58
d_{10}	13.83	-15.67	-3.00	10.50	-1.00
d_{50}	-0.25	-53.75	-14.75	45.75	-8.75
d_{90}	-41.42	-52.42	-8.25	69.75	17.25
$d_{90}-d_{10}$	-55.25	-36.75	-5.25	59.25	18.25

*A: drying temperature, B: amount of feed material C: rotational speed; in bold: significant effects, effects with grey background plotted in Figure 5.9

$$Ag = 56.43 - 4.42 \cdot x_B^2 + 2.54 \cdot x_A x_B - 3.94 \cdot x_A x_C \quad (5.3)$$

$$d_{90} - d_{10} = 363.58 - 27.63 \cdot x_B^2 + 29.63 \cdot x_A x_C \quad (5.4)$$

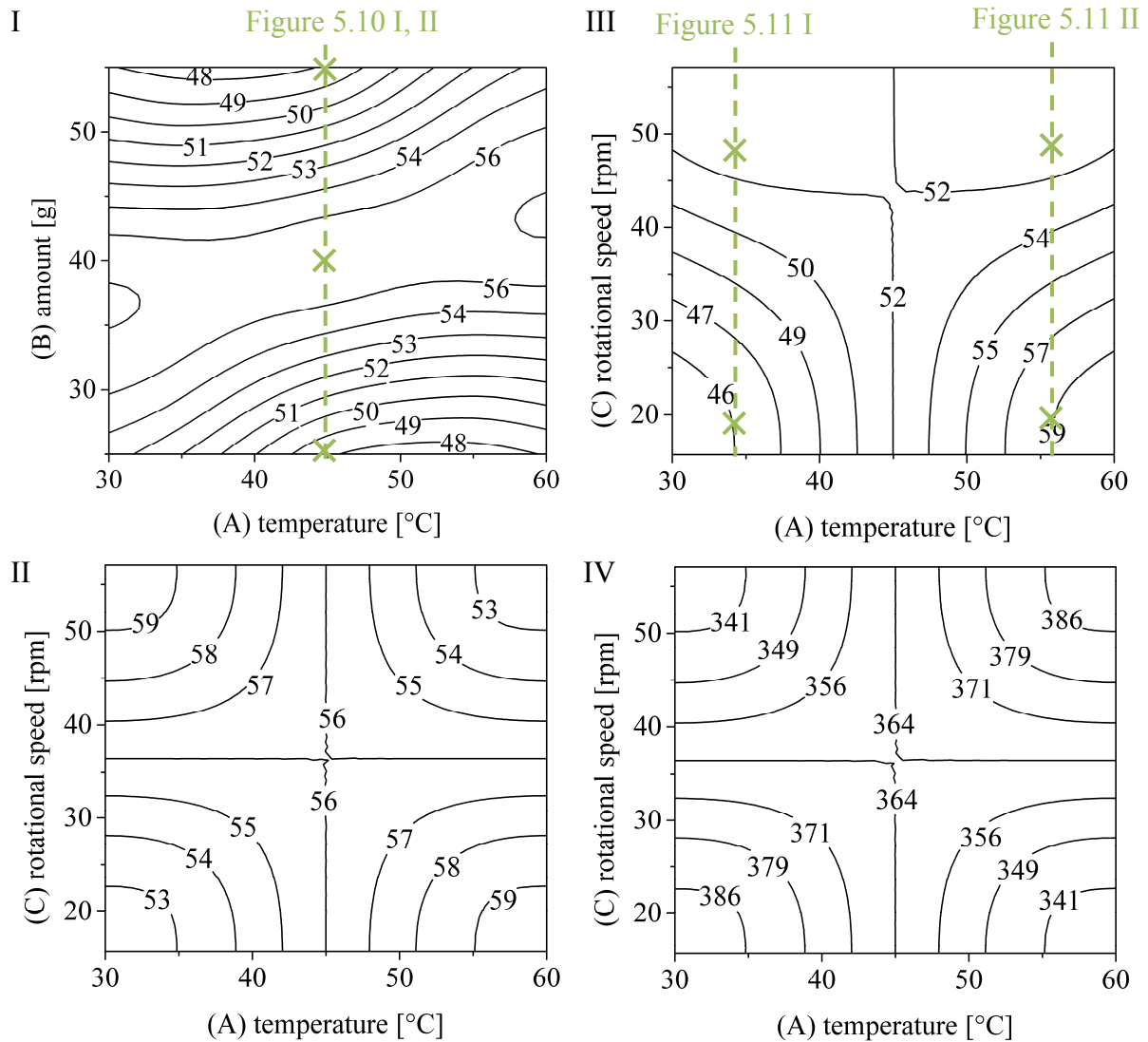


Figure 5.9: Contour plots for the significant factor interactions of rotary tube drying: (I-III) Ag [%], (IV) $d_{90} - d_{10}$ [μm]; (I, II, IV) constant factor on level zero; (III) constant factor on level one

As can be seen in Figure 5.9 I for a rising amount of feed material (B) the agglomeration degree Ag goes through a maximum. With a rising amount of feed material the collision probability and contact time between the crystals, as well as the drying time, increases so that more crystalline bridges are formed leading to more or larger agglomerates. To validate this assumption Figure 5.10 I and II display the CSDs and Ag Ds of the star experiments of the amount of feed material (solid lines) and the center point experiments (dashed lines) for comparison. The results elucidate that an increase of the amount of feed material from 25 g to

40 g leads to a higher amount of smaller agglomerates and the formation of a few larger agglomerates (see Figure 5.10 I); in sum a higher Ag is reached. It is assumed that the higher possibility for the agglomeration of small crystals is traced back to an inhomogeneous washing of the filter cake (see section 5.2.2) which leads to remaining mother liquor especially between small crystals. For a further increase of the amount of feed material from 40 g to 55 g (Figure 5.10 II) a reduction of the amount of smaller agglomerates can be observed, whereas a significantly higher amount of larger agglomerates exists. Moreover, a shift of the CSD to larger crystal sizes occurs. This indicates that the larger agglomerates formed are consisting of smaller agglomerates, which results in an overall lower Ag. Therefore, the nonlinear influence of the amount of feed material is traced back to a higher agglomeration tendency despite a lower overall Ag is reached.

The contour lines in Figure 5.9 I indicate that the influence of the drying temperature on the Ag depends on the amount of feed material. On the one hand for low amounts of feed material a reduction of the Ag with a rising drying temperature can be observed. This influence of the drying temperature was observed for static as well as fluidized bed drying also (compare sections 5.3.1 and 5.3.2). Due to a higher evaporation rate at high temperature the formation of stable crystalline bridges by crystal growth is avoided leading to the formation of fewer agglomerates. On the other hand for high amounts of feed material the increase of the drying temperature leads to higher Ag-values. This effect can be reduced to the evaporation rate as well. By increasing the drying temperature the effect of the amount of feed material (BB) means the cementation of smaller agglomerates to larger agglomerates is reduced due to the higher evaporation rate and a higher Ag is reached.

Furthermore, for the Ag a significant interaction (AC) between the drying temperature (A) and the rotational speed (C) exists. An increase of the rotational speed improves of the mixing inside the rotary tube. Hence, the drying time is reduced, but collisions of the crystals are more likely to happen. Nevertheless, the collisions do not result in agglomerates since the contact time between the crystals is too short. Therefore, with an increase of the rotational speed fewer agglomerates are formed. To make this assumption explicit the contour plot of the interaction (AC) for d_{90} - d_{10} calculated with the constant factor on level zero (amount of feed material (B) = 40 g) is depicted in Figure 5.9 II.

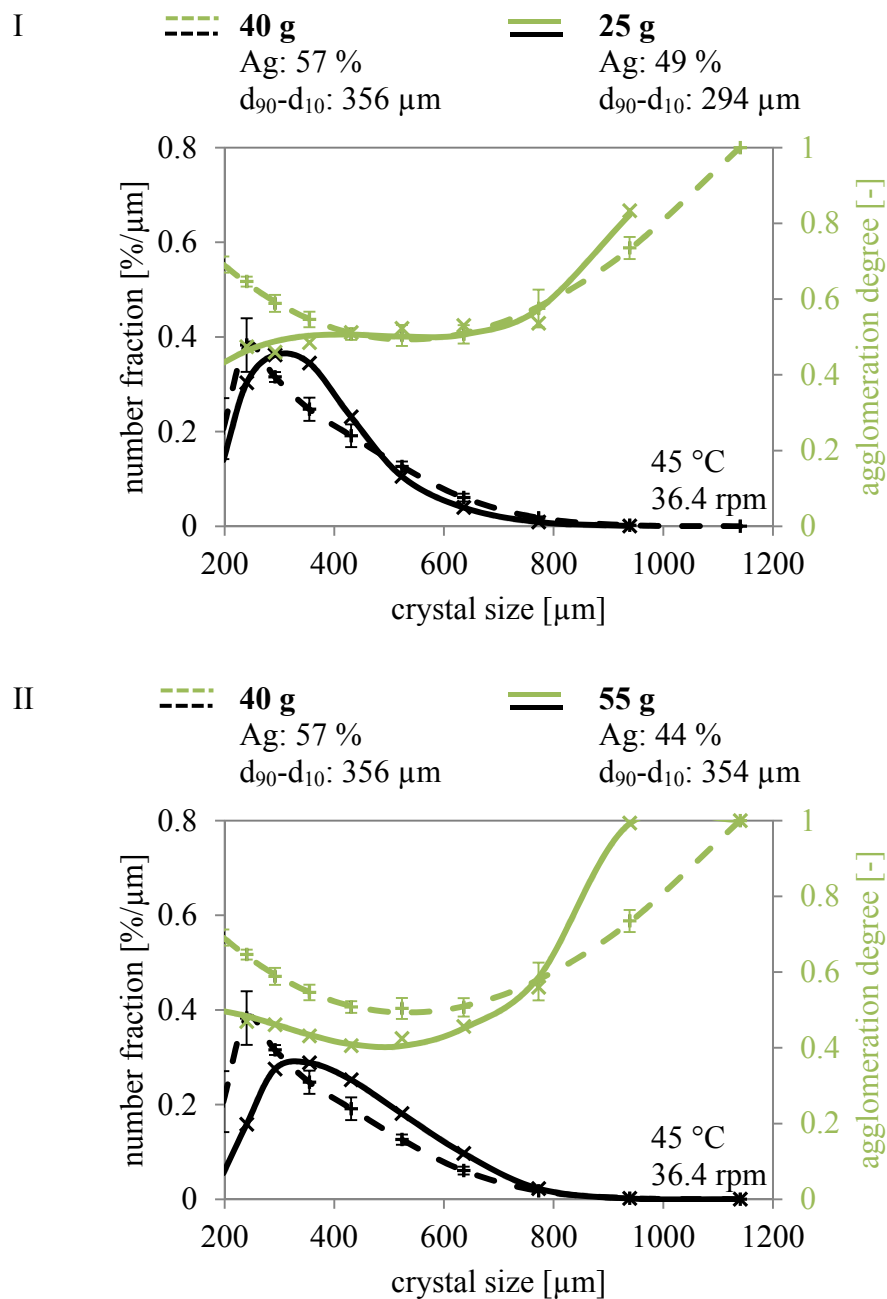


Figure 5.10: CSDs and AgDs of crystalline product batches after rotary tube drying: comparison of center point experiments (dashed lines) with the star experiments (solid lines) of the amount of feed material (I) - α , (II) + α

However, on basis of these contour lines a verification with experimental data out of the DoE is without further ado not possible because not all combinations of factor levels were experimentally investigated. The star experiments of the rotational speed cannot be used, because neither a significant effect of the single factor (C) nor a significant effect of the nonlinearity (CC) was detected. Moreover, as explained above a significant interaction between the temperature (A) and the amount of feed material (B) exists. Consequently, for the variation of the rotational speed (C) at a constant level of the temperature (A) the influence of the amount of

feed material (B) has to be considered also. Therefore, the contour plot calculated with the constant factor on level one (amount of feed material (B) = 51 g) is given for the interaction AC additionally in Figure 5.9 III to allow verification with experimental data. The contour lines of the Ag depicted in Figure 5.9 III show that an increase of the rotational speed (C) at low drying temperatures leads to higher Ag, whereas at high drying temperatures lower Ag-values are reached. The AgDs of the corresponding experiments depicted in the Figure 5.11 I and II elucidate the assumption that an increase of the rotational speed leads to less agglomerates. As can be seen in Figure 5.11 I a higher rotational speed leads to the disruption of large agglomerates, which are composed of several single crystals or smaller agglomerates, so that a higher amount of smaller agglomerates is detected; this results in a higher overall Ag. At higher drying temperatures (see Figure 5.11 II) with a rising rotational speed the agglomeration is reduced over the whole crystal size range leading to lower Ag-values due to the higher evaporation rate.

Regarding the **crystal size distribution (CSD)** the amount of feed material (B) has a significant nonlinear effect (BB) on the width of CSD (d_{90} - d_{10}). The single factor is insignificant and no significant interactions exist so that d_{90} - d_{10} runs through a maximum. The nonlinear effect of the amount of feed material (BB) on the width of the CSD is traced back to the different distribution of agglomerates inside the CSD. Thus the whole discussion shows that both has to be considered together. First, an increase of the amount of feed material leads to a broadening of the CSD ($294 \mu\text{m} \rightarrow 356 \mu\text{m}$). According to Figure 5.10 I, where the CSD and AgD of the center point experiments (dashed line) are depicted in comparison to the star experiment for the amount of feed material at low factor level (solid line), lower d_{10} and higher d_{90} values are achieved due to a higher amount of small and large agglomerates. Then, a further increase of the amount of feed material promotes the formation of larger agglomerates out of smaller agglomerates leading to a shift of the CSD to larger crystal sizes so that the width of the CSD stays nearly constant on $355 \mu\text{m}$ (see Figure 5.10 II).

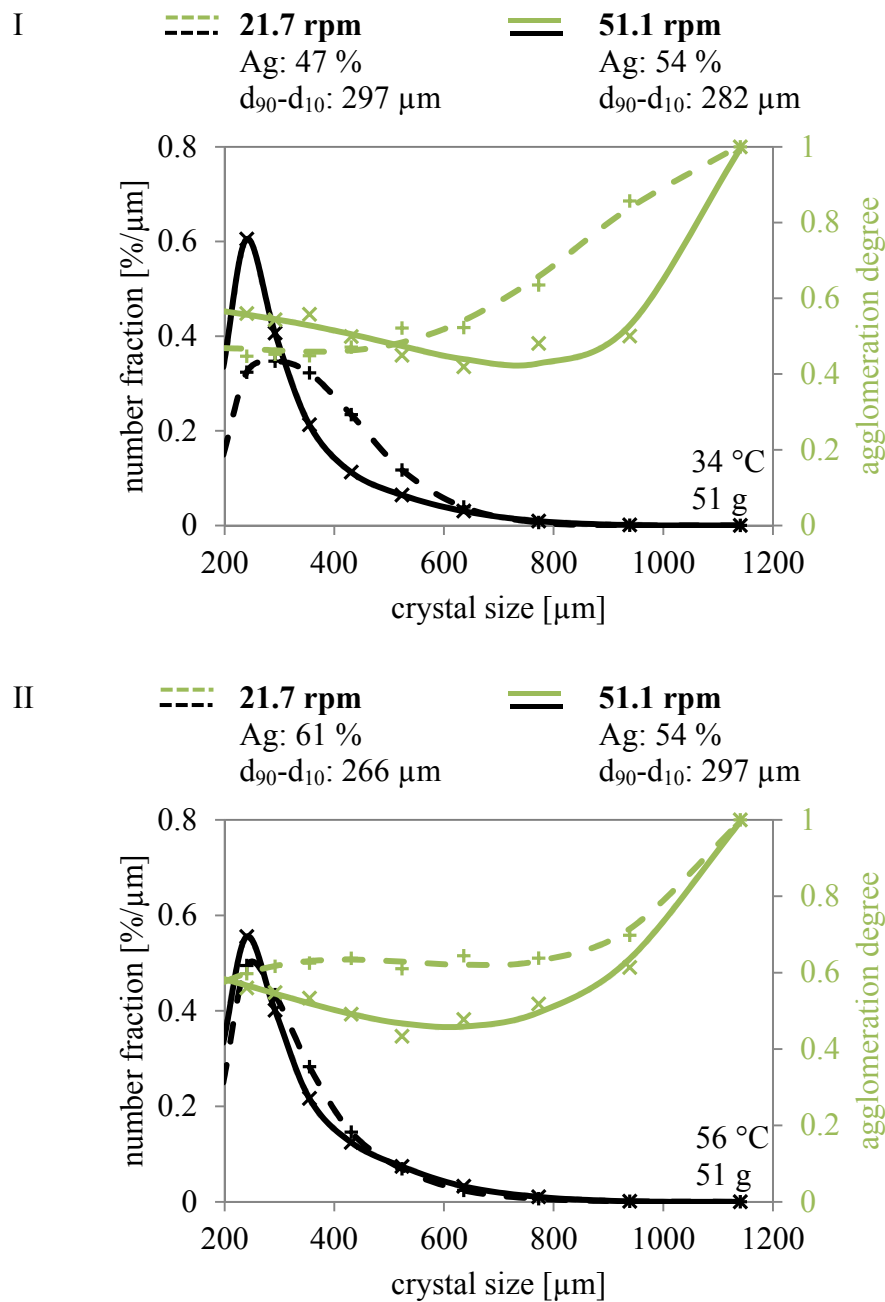


Figure 5.11: CSDs and AgDs of crystalline product batches after rotary tube drying: variation of the rotational speed at (I) low temperature (34 °C) and (II) high temperature (56 °C)

Finally, the width of the CSD ($d_{90}-d_{10}$) is significantly affected by the interaction (AC) of the drying temperature (A) and the rotational speed (C). Since a significant interaction (AC) in the same kind of magnitude exists for the characteristic diameter d_{90} a narrowing or broadening of the CSD can be reduced to changes of d_{90} mainly. The contour plot of the interaction (AC) regarding $d_{90}-d_{10}$ is given in Figure 5.9 IV and was calculated based on the regression model given in equation (5.4). Here, again, the comparison with the contour plot for the Ag of

the interaction (AC) (see Figure 5.9 II) shows that a narrow CSD is correlated with a high Ag, whereas a broad CSD is correlated with a low Ag. The evaluation of the interaction (AC) regarding the Ag has shown that a higher Ag is traced back to a lower amount of larger agglomerates and a higher amount of smaller agglomerates respectively. Therefore, a narrower CSD is traced back to a high amount of smaller agglomerates, which causes a reduction of the d_{90} -value. In contrast a broadening of the CSD is mainly correlated with a higher amount of larger agglomerates.

5.4. Summary

The agglomeration behavior of the material system L-alanine/ water within the crystalline process chain was investigated. To quantify the agglomeration the agglomeration degree (Ag) and the agglomeration degree distribution (AgD) of crystalline product batches were determined after crystallization in suspension and after drying. The influence of cake washing was recorded and the influence of three different drying methods (static, fluidized bed, and rotary tube drying) on agglomeration was systematically investigated using DoE. Finally, the impact of agglomeration on the crystal size distribution (CSD) was analyzed.

Figure 5.12 summarizes the experimental results of all investigations, whereby the width of CSD (d_{90} - d_{10}) is plotted against the overall agglomeration degree (Ag).

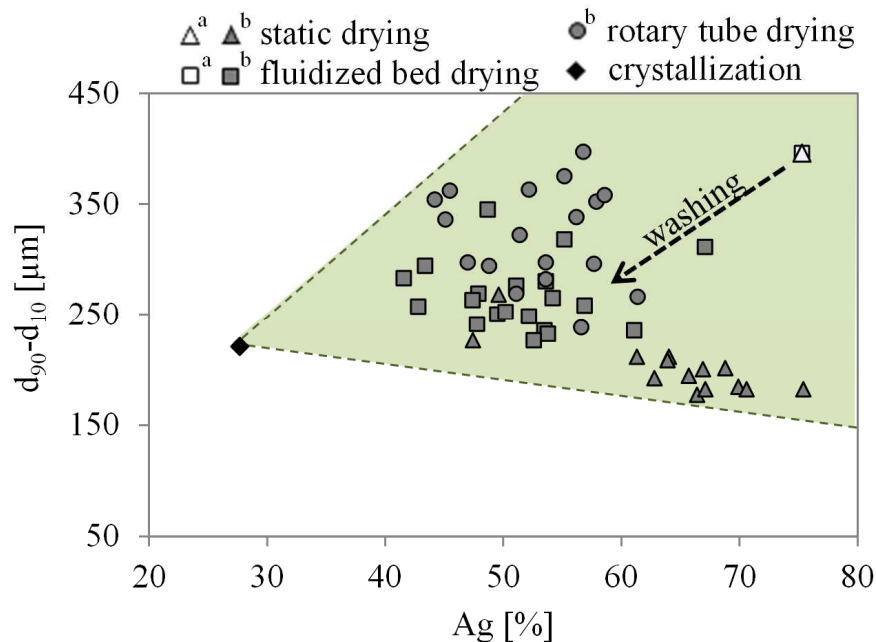


Figure 5.12: Ag and d_{90} - d_{10} of L-alanine crystalline product batches after crystallization, static drying, fluidized bed drying, and rotary tube drying (a: unwashed, b: washed with 40 mL ethanol/water (4/1) and 80 mL ethanol)

After crystallization the crystalline product is characterized by a relatively low A_g of less than 30 %. The corresponding A_gD has shown that the tailing of the CSD could not be traced back to agglomeration only. The comparison of the A_g over the whole crystalline process chain elucidates the requirement for holistic process optimization. Agglomeration takes place for the material system L-alanine/water mainly during drying especially if washing after filtration is omitted so that the product quality achieved by crystallization is significantly worsened. The A_g of the dried material without washing is increased up to 75 %. Along with the higher A_g a broadening of the CSD due to a higher amount of agglomerates over the whole analyzed crystal size range (compare section 5.2.2) was observed. As reason for agglomeration during drying a high concentration of solute in the mother liquor after crystallization was identified. Therefore, to preserve the product quality after crystallization cake washing after filtration is essential to reduce agglomeration during drying. However, the data points of the drying experiments demonstrate that the drying method and the drying conditions affect the A_g and therewith the width of the CSD as well. The evaluation of the DoEs (sections 5.3.1, 5.3.2, and 5.3.3) has shown that for all drying methods agglomeration is affected by the drying temperature and the amount of feed material. The effect of the drying temperature is traced back to the evaporation rate and the effect of the amount of feed material to the larger contact area or collision probability. The averaged overall agglomeration degree of static dried crystalline product batches $\overline{A_g}_{\text{static}}$ is with 64 % around ten percent higher than the averaged values reached after fluidized or rotary tube drying ($\overline{A_g}_{\text{fluidized bed}}$: 52 %, $\overline{A_g}_{\text{rotary tube}}$: 53 %). Due to the given additional influence factors, means the volume flow or the rotational speed, the contact time between the crystals can be shortened. Therefore, in contrast to static drying the formation of crystalline bridges and therewith the formation of agglomerates is reduced. Corresponding to the influence of agglomeration on the width of CSD the data points of all washed crystalline product batches after drying indicate that a trend between the A_g and $d_{90}-d_{10}$ exists: The lower the A_g the broader is the CSD, and vice versa. The A_g as a number-based measure is mainly affected by high amounts of small agglomerates. Conversely, larger agglomerates, which are composed of several smaller agglomerates, decrease the overall A_g and lead in turn to broader CSDs. To conclude, the investigations show impressively that an evaluation of the CSD of a product batch alone is insufficient since despite same characteristics of the CSD the final product can be highly different due to different agglomeration behavior.

6. Material System II – Adipic Acid/Water

As second material system adipic acid/ water was investigated regarding its agglomeration behavior. The material system was chosen because of the known tendency of adipic acid to agglomerate during crystallization [99, 101]. To confirm quantitatively that the material system adipic acid/ water is prone to agglomerate more during crystallization than during drying, the overall agglomeration degree (Ag) and the agglomeration degree distribution (AgD) were recorded over the crystallization process chain using the QICPIC image analysis technique (compare section 4.3). Subsequently, the effect of gassing crystallization (compare section 2.1.4) on the agglomeration behavior of adipic acid was systematically investigated using Design of Experiments (DoE) to proof if gassing crystallization is a promising method to control the product quality in terms of agglomeration. To remind: The performed image analysis for the determination of the Ag, AgD, and CSD is limited to crystalline particles larger than 80 μm (see section 4.3). Therefore, all results presented are referred to the crystal size range above 80 μm .

6.1. Cooling Crystallization

Cooling crystallization experiments with a saturation temperature T_{sat} of 50 $^{\circ}\text{C}$ and a stirring rate of 210 rpm were carried out from 60 $^{\circ}\text{C}$ with a cooling rate κ of 0.3 K/min till a temperature of 10 $^{\circ}\text{C}$ was reached. During crystallization every five minutes until 40 $^{\circ}\text{C}$ and then every ten minutes two samples were taken out of the crystallizer to measure gravimetrically the concentration profile and the absolute supersaturation profile which was computed from the difference of the concentration profile to the corresponding saturation concentrations (see Figure A.19). To provide comparability of cooling crystallization experiments with and without gassing the gassing ring was installed but unused. Thus, the agglomeration degree distribution (AgD), crystal size distribution (CSD), and the belonging characteristic values (see Figure 6.1 and Table 6.1) measured directly after crystallization out of suspension with the QICPIC are suitable as reference to evaluate the impact of the further downstream process, as well as the impact of gassing, on the crystalline product quality.

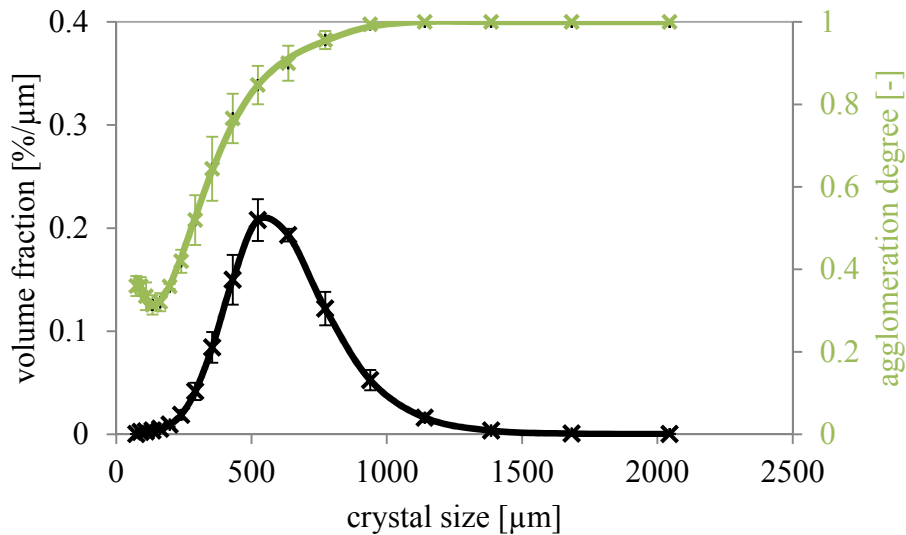


Figure 6.1: CSD and AgD of adipic acid/water measured directly after crystallization out of suspension with QICPIC (experimental conditions: $\kappa = 0.3$ K/min, $T_{\text{start}} = 60$ °C, $T_{\text{end}} = 10$ °C, $T_{\text{sat}} = 50$ °C, 210 rpm)

Table 6.1: Characteristic values of adipic acid product batches directly after crystallization (cp. Figure 6.1)

	Ag [%]	$d(\text{Ag}_{\text{max}})$ [μm]	d_{10} [μm]	d_{50} [μm]	d_{90} [μm]	$d_{90}-d_{10}$ [μm]
AA-K1	61.1	1035	405	632	954	549
AA-K2	67.9	916	375	575	873	498
AA-K3	63.1	1079	396	610	908	512
Averaged	64.0 ± 3.5	1010 ± 84	392 ± 15	606 ± 29	912 ± 41	520 ± 26

After cooling crystallization the adipic acid product batch is characterized by a CSD with a d_{50} of $606 \mu\text{m} \pm 29 \mu\text{m}$ and a $d_{90}-d_{10}$ of $520 \mu\text{m} \pm 26 \mu\text{m}$; whereby the width of the CSD is broadened in the range of large crystals by a tailing. The overall agglomeration degree Ag is with $64 \% \pm 3.5 \%$ relative high and demonstrates the tendency of adipic acid to agglomerate during crystallization. The corresponding AgD curve measured after cooling crystallization runs through a minimum at $135 \mu\text{m} \pm 8.8 \mu\text{m}$ and then rises constantly until at $1010 \mu\text{m} \pm 84 \mu\text{m}$ an Ag_i of one is reached. Therefore, the broadening of the CSD is the result of the formation of large agglomerates. The minimum inside the AgD can be traced back to fragments of broken agglomerates. These fragments are counted, due to their irregular form, as agglomerates and are the consequence of crystal-crystal collisions or collisions of crystals with internals of the crystallizer like the stirrer. In other respects the progression of the AgD, i.e. the increase of agglomerates with the crystal size, meets the expectations. The probability for agglomeration increases, since large crystals spend a longer time in the suspension during crystallization than smaller ones [107].

6.2. Cake Washing and Drying

After cooling crystallization the mother liquor has a concentration of 11.75 g/kg, i.e. 13.24 % of the initially solved mass of adipic acid remains in the mother liquor only. Consequently, the amount of solute for the formation of solid bridges is limited and the probability of agglomeration during drying seems to be rather low. However, the solubility of adipic acid in water depends strongly on the temperature (compare Figure 3.2) so that redissolution during drying at higher temperatures might have an influence on the agglomeration tendency. Therefore, agglomeration during drying cannot be excluded and the impact of the downstream conditions – regarding washing and drying – was investigated after the selection of a suitable wash liquid.

6.2.1. Wash Liquid Selection

For the selection of a wash liquid a solvent screening regarding the solubility of adipic acid was performed on basis of literature data extended by own measurements regarding the temperature range available. The solubility data of all solvents considered are given in comparison to the solubility in water in Figure A.20. To avoid redissolution of crystals during washing and drying the solubility of adipic acid in the wash liquid at low and high temperatures should as be low as possible (compare section 2.2.2). Therefore, the solvents acetonitrile, diethyl ketone, ethyl acetate, and butyl acetate (Figure A.20, blue symbols) – which all show a low solubility of adipic acid – are preselected. To evaluate the suitability of the four remaining solvents the viscosity ratio and solubility of water in the solvents are used as further selection criteria (compare section 2.2.2). Both criteria give information about the wash efficiency³ of the solvents: the viscosity ratio specifies the tendency for “fingering” and the solubility of water the capacity of the solvent. To reduce the probability of “fingering” during cake washing the viscosity ratio of the wash liquid should be low and to avoid the formation of streaks the solubility of water in the solvent should be high. The viscosity ratios and solubility data of the preselected solvents are listed in decreasing order regarding both criteria in Table 6.2. On the one hand acetonitrile exhibits with a value of 3.46 the highest viscosity ratio, but it is the only solvent totally miscible with water. On the other hand butyl acetate has with 1.62 the lowest viscosity ratio, but with 1.64 g/100g solvent the lowest solubility of water too. Ethyl acetate and diethyl ketone are characterized by middle viscosity ratios and solubility charac-

³ Potential of the solvents to displace the mother liquor out of the filter cake

teristics. As can be seen both criteria rank the solvents in opposite direction. To determine the most important criterion, the filter cake was washed after filtration with 30 mL acetonitrile, ethyl acetate, diethyl ketone, and butyl acetate respectively, and the water content after filtration was measured by Karl-Fischer titration to investigate the amount of water displaced. To remind: as described for the material system L-alanine/ water in section 5.2.1 the wash efficiency is evaluated in context of this thesis for same amounts of solvents only. The results of the water content measurements listed in Table 6.2 show that the solubility of water in the solvent is the determining criterion for the wash efficiency. Although acetonitrile has the highest viscosity ratio of all solvents a ten times higher water content in the filtrate is reached compared to butyl acetate. Since for ethyl acetate and diethyl ketone non-acceptable wash results are reached as well, acetonitrile is identified as wash liquid for the material system adipic acid/ water.

Table 6.2: Viscosity ratio, solubility of water, and wash results of potential wash liquids for the material system adipic acid/ water

	η_{ML}/η_{WL} ^a [-]	Solubility of water [g/100g solvent]	Water content of filtrate ^d [wt.-%]
Acetonitrile	3.46	miscible ^b	11.34
Ethyl acetate	2.92	3.3 ^b	4.29
Diethyl ketone	2.66	2.31 ^c	3.24
Butyl acetate	1.62	1.64 ^b	1.23

a: at 10 °C, b: at 25 °C taken from [117], c: at 25 °C taken from [118]

d: one wash cycle with 30 mL solvent at 22 °C

6.2.2. Impact of Downstream Conditions

To determine the amount of acetonitrile necessary to displace almost entirely the mother liquor (water) out of the voids of the filter cake further **wash experiments** were carried out. Each experiment was realized two times. The filter cake was washed one, two, or three times with 70 mL acetonitrile and the amount of washed out water was measured by Karl-Fischer titration. The results of these experiments are depicted in Figure 6.2 in comparison to the experimental result reached with acetonitrile in the section before (washing with 30 mL acetonitrile); whereby the percentage of water displaced with regard to the moisture content of the filter cake after filtration is plotted against the number of wash cycles. As assumed, the amount of water displaced rises the more acetonitrile is used for cake washing and the data points form an asymptotic curve progression: An increase from 30 mL to 70 mL acetonitrile (one wash cycle) leads to an increase of water displaced from $79.4 \% \pm 8.3 \%$ to $88.6 \% \pm 2.1 \%$. By washing the filter cake two times with 70 mL acetonitrile the percentage of water displaced increases to $94.3 \% \pm 3.2 \%$; whereas a third wash cycle (3x 70mL) causes no noticeable changes. Furthermore, it becomes obvious that the reproducibility of the cake washing is given from a certain amount of acetonitrile only (compare 1x 30 mL with 1x 70 mL). The enhancement of the reproducibility can be traced back to the reason that for low volumes of wash liquid the filter cake is incompletely penetrated especially if – as in case of 30 mL acetonitrile – the ratio of the filter cake volume and the volume of wash liquid is smaller than one. Thus changes of the filter cake structure have a large impact on the displacement of the mother liquor. The asymptotic curve progression can be traced back to the structure of the

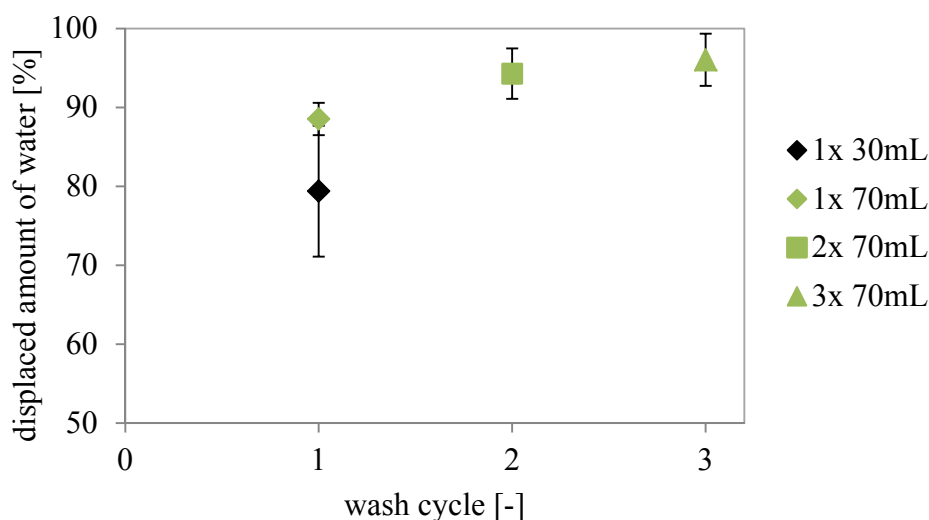


Figure 6.2: Impact of the amount of acetonitrile used for cake washing on the displacement of water out of the filter cake

filter cake too; e.g. dead-end or inaccessible pores avoid an entire displacement of the mother liquor. Since the results of the wash experiments have shown that a filter cake washing with three wash cycles leads to a slightly higher amount of water displaced only, for further experiments the filter cake was washed two times with 70 mL acetonitrile.

After specifying the washing conditions the agglomeration behavior of adipic acid during drying was investigated to verify the hypothesis formulated at the beginning of chapter 6.2 that the probability of agglomeration during drying is rather low and agglomeration takes place rather at high temperatures. Therefore, **drying experiments**, with and without washing at low (22 °C) and high temperature (50 °C), were carried out. As drying method static drying was chosen because this method bears the highest risk for agglomeration due to the permanent contact of the crystals. To measure the AgD and CSD samples of the crystalline product batches were resuspended in 1 L saturated acetonitrile and analyzed with the QICPIC. The experimental conditions and characteristic values measured of all experiments are listed in Table A.14. Figure 6.3 shows the AgDs and CSDs of the crystalline product batches dried at 22 °C in comparison to the results measured directly after crystallization (dashed lines). As can be seen, independent of the washing conditions the same curve progression and characteristic values of the AgD and CSD is reached; whereby in comparison to the results measured after crystallization a slight difference regarding the AgD exists only: The AgDs measured after drying do not pass a minimum and the maximum agglomeration degree Ag_{max} of one is reached in average at 720 μm ; i.e. in comparison to the results measured after crystallization an Ag-values of one are achieved around 290 μm before. The Ag after drying is with $58\% \pm 1.7\%$ in average lower than after crystallization (Ag: $64.0\% \pm 3.5\%$). This can be explained by the number-based characteristic of the Ag. During drying small agglomerates cement together and larger agglomerates are formed, which reduce the total number of agglomerates in the crystalline product batch and therewith the Ag. Nevertheless, the results show – as assumed above – that agglomeration takes place slightly during drying at low temperature only.

The experimental results of the crystalline product batches dried at 50 °C are illustrated in Figure 6.4. The AgD and the CSD are comparable with the results of the product batches dried at 22 °C and show therewith slight deviations to the results measured after crystallization only (see Figure 6.4 I). However, larger deviations are observed for the crystalline product batch unwashed. As can be seen in Figure 6.4 II the AgD curve of the unwashed product batch rises with a slope comparable to the AgD measured after crystallization, but the AgD is shifted with an exception for small crystal sizes to higher Ag_j -values and the $d(Ag_{max})$ is

reached at $622\ \mu\text{m}$ at a clearly smaller crystal size. Therefore – as indicated by the overall agglomeration degree Ag of $66.0\ \% \pm 2.9\ \%$ also – more agglomerates are detected inside the CSD than after crystallization and it can be concluded that the corresponding CSD is broadened to a width of $610\ \mu\text{m} \pm 20\ \mu\text{m}$ as a consequence of agglomeration during drying.

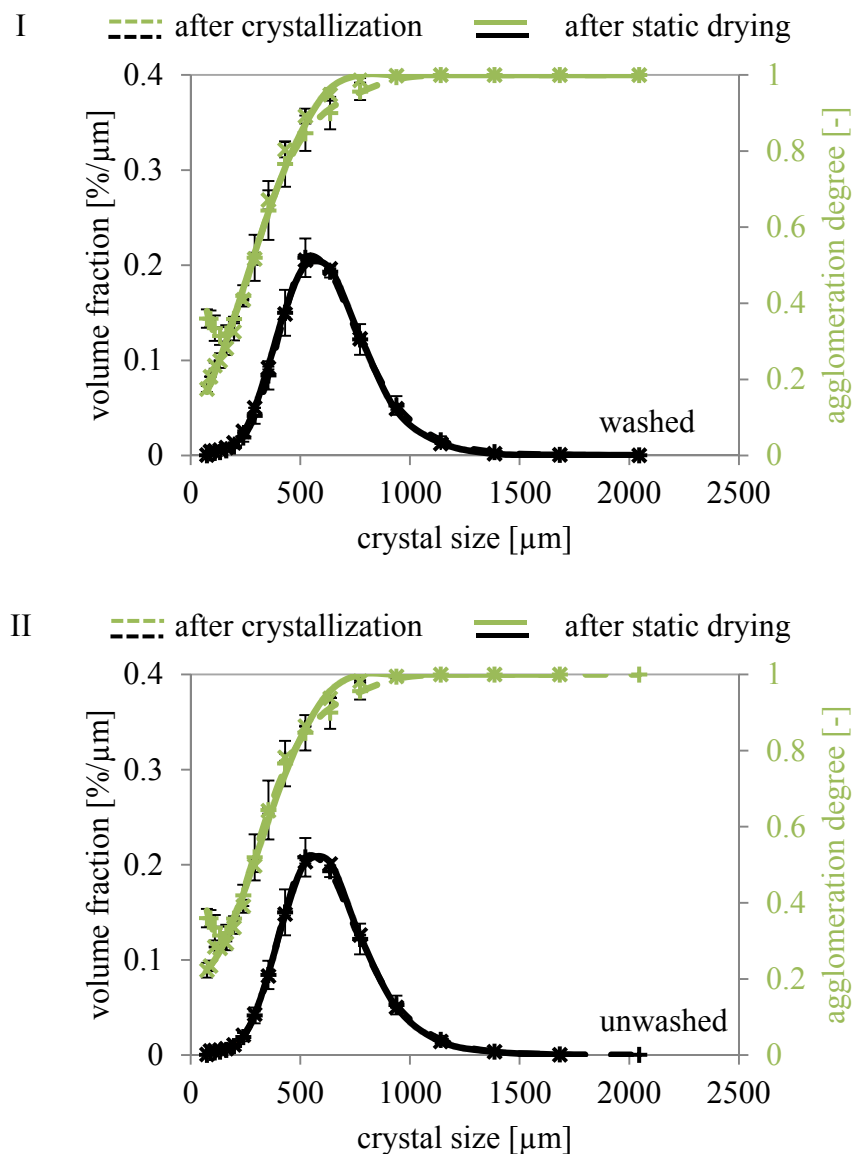


Figure 6.3: CSDs and AgDs after static drying at $22\ ^\circ\text{C}$ in comparison to the results after crystallization measured with QICPIC. I: AA-ST1, two wash cycles with $70\ \text{mL}$ acetonitrile each; II: AA-ST2, unwashed; corresponding characteristic values are denoted in Table 6.1 and Table A.14

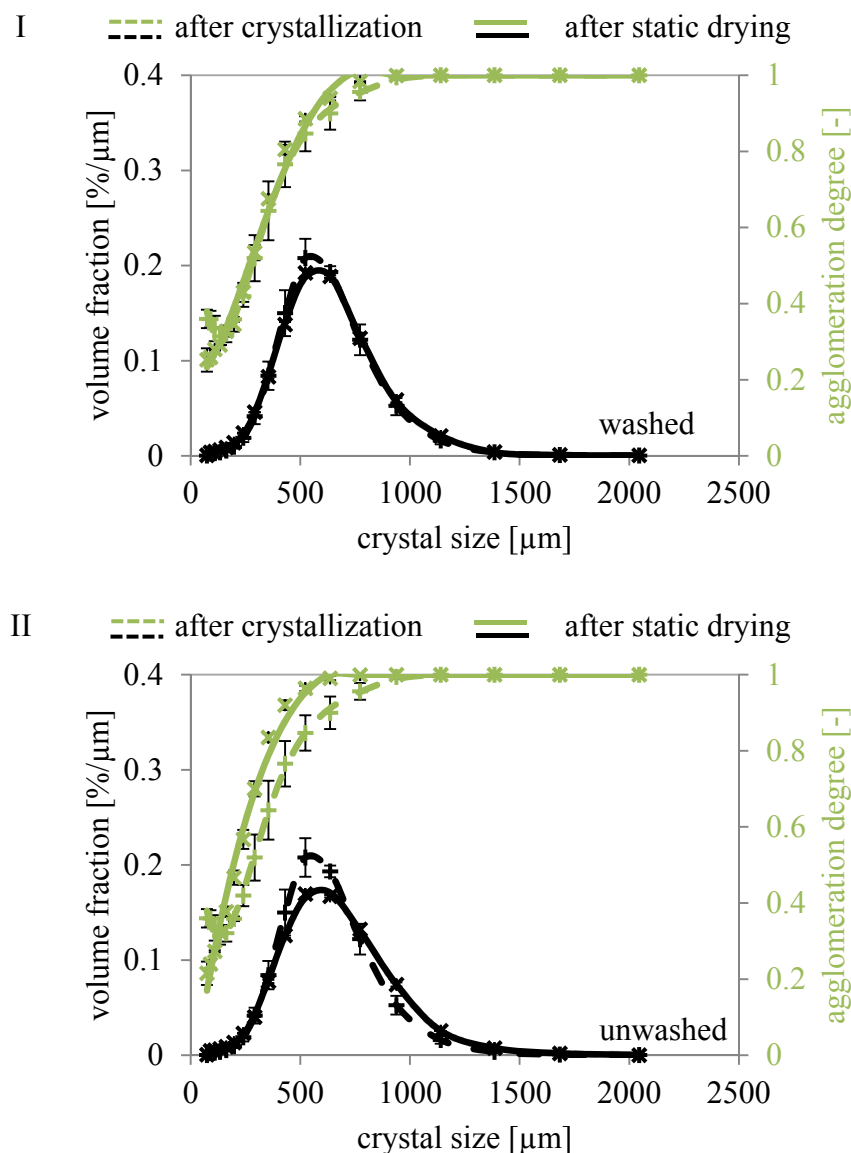


Figure 6.4: CSDs and AgDs after static drying at 50 °C in comparison to the results after crystallization measured with QICPIC. I: AA-ST3, two wash cycles with 70 mL acetonitrile each; II: AA-ST4, unwashed; corresponding characteristic values are denoted in Table 6.1 and Table A.14

To sum up the results of the drying experiments verify that agglomeration during drying takes place for the material system adipic acid water at high temperatures only. At lower temperatures the remaining mass of adipic acid solved in the mother liquor is too low to promote agglomeration in a way that the characteristic values of the crystalline product batch, like the width of the CSD, are affected significantly. On the other hand at higher temperatures the amount of solute increases since the solubility of adipic acid in water increases with the temperature. As consequence redissolution takes place and more agglomerates are formed. However, by washing the mother liquor can be displaced by acetonitrile. In this solvent adipic acid has a low solubility at high temperatures and agglomeration is avoided.

6.3. Gassing Crystallization

In the previous sections it was shown that agglomeration takes place mainly during crystallization. Therefore, crystallization is identified as decisive process step to control the quality of adipic acid product batches. As mentioned in section 2.1.4 a common way to control crystallization processes is the induction of nucleation. In this context gassing crystallization turned out to be an innovative and suitable method to control crystallization processes and first conclusions that gassing crystallization affects agglomeration were drawn by Wohlgemuth [53]. However, no quantitative investigations have been carried out yet regarding agglomeration. Therefore, a central composite Design of Experiments (DoE) was used to investigate systematically the impact of gassing inside the metastable zone on the product quality of adipic acid product batches. The center point experiments were realized six times and four factors were considered: The gas flow \dot{V}_{gassing} , the gassing period $\Delta t_{\text{gassing}}$, and the point of gassing, means the gassing temperature T_{gassing} or gassing supersaturation $\Delta c_{\text{gassing}}$, respectively, as well as the stirring rate. The stirring rate was chosen as test variable additionally to the three gassing parameters, since the relation between the stirring rate and agglomeration during crystallization was already mentioned in literature [11, 16, 19]. Therefore, the effects identified regarding the stirring rate can be used to verify the results of the DoE. During the gassing period the stirrer was switched off to ensure that the air bubbles were not deformed. All other crystallization parameters were set as described in section 6.1 and kept constant. To ensure orthogonality the α -level of the star experiments was calculated to be ± 1.719 . Table 6.3 shows the factor levels investigated; the whole experimental design is denoted in Table A.15.

The gas flow (A) is varied between the lowest volume flow, which ensures an even escape of gas out of the gassing ring, and the maximum measurable volume flow. The maximal gassing period (B) is set to 120 seconds because continuous gassing should not be performed. To set the start point of gassing (C) the metastable zone width (MZW) of the material system was determined first on basis of the concentration profiles measured during cooling crystallization without gassing and shown in Figure A.19. From the measured concentration profiles the averaged nucleation temperature T_{nuc} was determined to $45.72 \text{ }^\circ\text{C} \pm 0.08 \text{ }^\circ\text{C}$. The MZW was calculated according to equation (3.3) in section 3.5.2 to $4.28 \text{ K} \pm 0.08 \text{ K}$; whereby the factor φ was determined to one since no crystals were present in solution. Based on this result, the start point of gassing (C) was defined. To ensure that gassing is applied in supersaturated solution a distance of 0.5 K to the saturation temperature (T_{sat} : $50 \text{ }^\circ\text{C}$) was chosen leading to the lowest gassing temperature of $46 \text{ }^\circ\text{C}$. This temperature range for gassing is rather narrow so

Table 6.3: Factors (A-D) and levels investigated for gassing crystallizations of adipic acid

Factor			Level				
			- $\alpha^{\#}$	-1	0	1	$\alpha^{\#}$
A	Gas flow	[L/h]	200	367	600	833	1000
B	Gassing period	[s]	10	33	65	97	120
C*	Gassing temperature/	[°C]	46	46	47.75	49.5	49.5
	Gassing supersaturation	[g/kg]	17.6	17.6	10.4	2.4	2.4
D	Stirring rate	[rpm]	120	158	210	262	300

[#] calculated α -value due to orthogonality: ± 1.719 ; *face-centered

that in case of five factor levels the step size would have been too small to assess interactions between the gassing period (B) and the values of the factor gassing temperature/ supersaturation (C). Therefore, the gassing temperature was selected face-centered. In addition to the gassing temperature levels the corresponding levels of the gassing supersaturation are given in Table 6.3. Since the gassing supersaturation represents the driving force for induced nucleation by gassing, the gassing supersaturation is used instead of the gassing temperature in the following to evaluate the impact of the start point of gassing on the product quality. The range of the stirring rate (D) is selected in such a way that the “90 % layer thickness criterion” is fulfilled and the formation of a thrombus is minimized; the level of the center point experiment was set in accordance with the stirring rate of the cooling crystallization experiments without gassing to 210 rpm (compare section 6.1).

As responses the agglomeration degree of the crystalline product batch (Ag), the characteristic diameter $d(\text{Ag}_{0.5})$ of the AgD, and the difference of the characteristic diameters $d(\text{Ag}_{0.9})$ and $d(\text{Ag}_{0.5})$ were used. The results of the 30 experiments are listed up in Table A.16.

6.3.1. Impact on Product Quality

The effects of the single factors, interactions, and nonlinearities as well as the 95 % confidence intervals (ci) of the DoE regarding the responses overall agglomeration degree (Ag), agglomeration degree distribution (AgD) - characterized by $d(\text{Ag}_{0.5})$ and $d(\text{Ag}_{0.9})-d(\text{Ag}_{0.5})$ -, median crystal size (d_{50}), and width of the crystal size distribution ($d_{90}-d_{10}$) are listed in Table 6.4. Significant effects are given in bold.

As can be seen for the Ag, the AgD, and $d_{90}-d_{10}$ significant single effects exist for the gassing supersaturation (C) and the stirring rate (D). Regarding $d_{90}-d_{10}$ for these factors significant interactions (AC, AD, BC, and BD) exist between the gas flow (A) and the gassing period (B). Furthermore, the gas flow (A) has an significant single effect on $d(\text{Ag}_{0.9})-d(\text{Ag}_{0.5})$, but

since no significant single effect regarding $d(\text{Ag}_{0.5})$ was identified, the single effect of the gas flow (A) on $d(\text{Ag}_{0.9})-d(\text{Ag}_{0.5})$ is neglected. Moreover, it becomes obvious that the median crystal size d_{50} is significantly changed by the stirring rate (D) only. The only significant non-linear effect appears to be the gassing supersaturation (CC). However, this effect has to be treated with caution due to the face-centering. The face-centering leads to an overestimation of the effect CC for all responses [102]. Therefore, the significance of CC has to be checked carefully. With rising supersaturation larger molecule clusters are present in solution and the probability for nucleation increases. Consequently, a higher number of nuclei is induced for higher gassing supersaturations than for lower ones. Since the supersaturation in the metastable zone increases quasi-linear (compare Figure A.19) the number of nuclei increases most probably proportional to the gassing supersaturation chosen. A nonlinear impact of the gassing supersaturation is realistic only if for the star experiment with a gassing supersaturation of 2.4 g/kg (all other factors on level zero) nucleation cannot be induced by gassing due to the fact that supersaturation is too low. However, shortly after gassing small crystals were present in solution. Hence, the nonlinear effect of the gassing supersaturation (CC) can be related to the face-centering and stated as insignificant.

Based on the significant effects identified regression models were formed for the responses. Herein all significant factors and factor interactions were considered. The variables x_i represent the factor levels of the respective factor i and the regression coefficients are the half of the effects. Equations (6.1) and (6.2) represent the regression models for Ag and $d_{90}-d_{10}$, the most important responses for product quality. We abstained from representing the regression model for d_{50} since the stirring rate (D) is identified as influence factor only. In the following all remaining significant effects of the factors are analyzed in detail.

Table 6.4: Effects of factors, factor interactions, and nonlinearities on the responses for gassing crystallization of adipic acid/ water*

response	95 % ci	A	B	C	D	AA	BB	CC	DD	AB
Ag	± 3.44	-0.05	-1.16	-6.32	3.46	1.99	1.41	8.37	0.87	1.76
d(Ag _{0.5})	± 32.01	-9.09	8.13	32.24	-50.54	-16.96	-7.45	-38.99	-10.56	-7.34
d(Ag _{0.9})-d(Ag _{0.5})	± 57.09	57.91	24.93	100.98	81.68	-24.44	-26.37	-96.19	-6.13	-19.54
d ₅₀	± 57.60	-3.64	4.95	28.11	-71.06	-11.62	-10.27	-2.00	33.73	0.63
d ₉₀ -d ₁₀	± 25.63	-4.50	10.21	49.67	-74.64	-0.69	-3.06	-63.89	24.36	7.00

response	95 % ci	AC	AD	BC	BD	CD	ABC	ABD	BCD	ACD
Ag	± 3.44	0.29	-0.39	-2.31	-2.19	1.49	0.16	0.79	-1.84	-0.39
d(Ag _{0.5})	± 32.01	-6.46	8.79	4.19	10.45	-30.49	-10.24	-3.34	2.84	1.94
d(Ag _{0.9})-d(Ag _{0.5})	± 57.09	17.76	-21.39	22.19	18.29	53.24	-10.31	-12.76	48.96	-3.81
d ₅₀	± 57.60	-24.88	23.63	2.13	8.63	-9.38	-5.38	-25.38	2.63	25.13
d ₉₀ -d ₁₀	± 25.63	32.75	40.00	58.25	38.00	12.25	44.25	-7.00	-21.75	13.25

*A: gas flow, B: gassing period, C: gassing supersaturation, D: stirring rate; in bold: significant effects, effects with grey background plotted in Figure 6.7

$$Ag = 61.3 - 3.2 \cdot x_C + 1.7 \cdot x_D \quad (6.1)$$

$$d_{90} - d_{10} = 522 + 25 \cdot x_C - 37 \cdot x_D + 16 \cdot x_A x_C + 20 \cdot x_A x_D + 29 \cdot x_B x_C + 19 \cdot x_B x_D + 22 \cdot x_A x_B x_C \quad (6.2)$$

Effects on Ag and AgD

The **gassing supersaturation (C)** has a negative linear effect on Ag, but we have to take into consideration that the supersaturation is high for low factor levels and low for high factor levels (compare factor levels depicted in Table 6.3) This means that the higher the gassing supersaturation the higher is the Ag of a crystalline product batch. As described above more nuclei are induced if gassing is applied at higher supersaturation. The nuclei grow to crystals and compete for the same amount of adipic acid molecules solved in solution. As consequence the growth of each crystal is reduced leading to smaller crystals. These smaller crystals are more prone to agglomerate than larger ones [11, 21]. Furthermore, high supersaturation leads to agglomerates with strong crystalline bridges [11, 30, 31]. In Figure 6.5 I experimental data are representatively given for experiments at low (2.4 g/kg) and at high supersaturation (17.6 g/kg); all other factors are constant. As can be seen gassing at high supersaturations results in an increase of all Ag_j values so that the changes of the Ag can be correlated with the increase of agglomerates over the whole crystal size range. The effect of the gassing supersaturation (C) on the responses $d(Ag_{0.5})$ and $d(Ag_{0.9})-d(Ag_{0.5})$ quantifies the impact on the progression of the AgD (compare section 4.1). As listed in Table 6.4 for both responses of the AgD – $d(Ag_{0.5})$ and $d(Ag_{0.9})-d(Ag_{0.5})$ – positive linear effects are detected. Accordingly, for higher gassing supersaturations lower values for $d(Ag_{0.5})$ and $d(Ag_{0.9})-d(Ag_{0.5})$ are achieved. This corresponds to an increase of agglomerates over the whole crystal size range and the impact of the gassing supersaturation (C) depicted exemplarily in Figure 6.5 I is confirmed for all experiments.

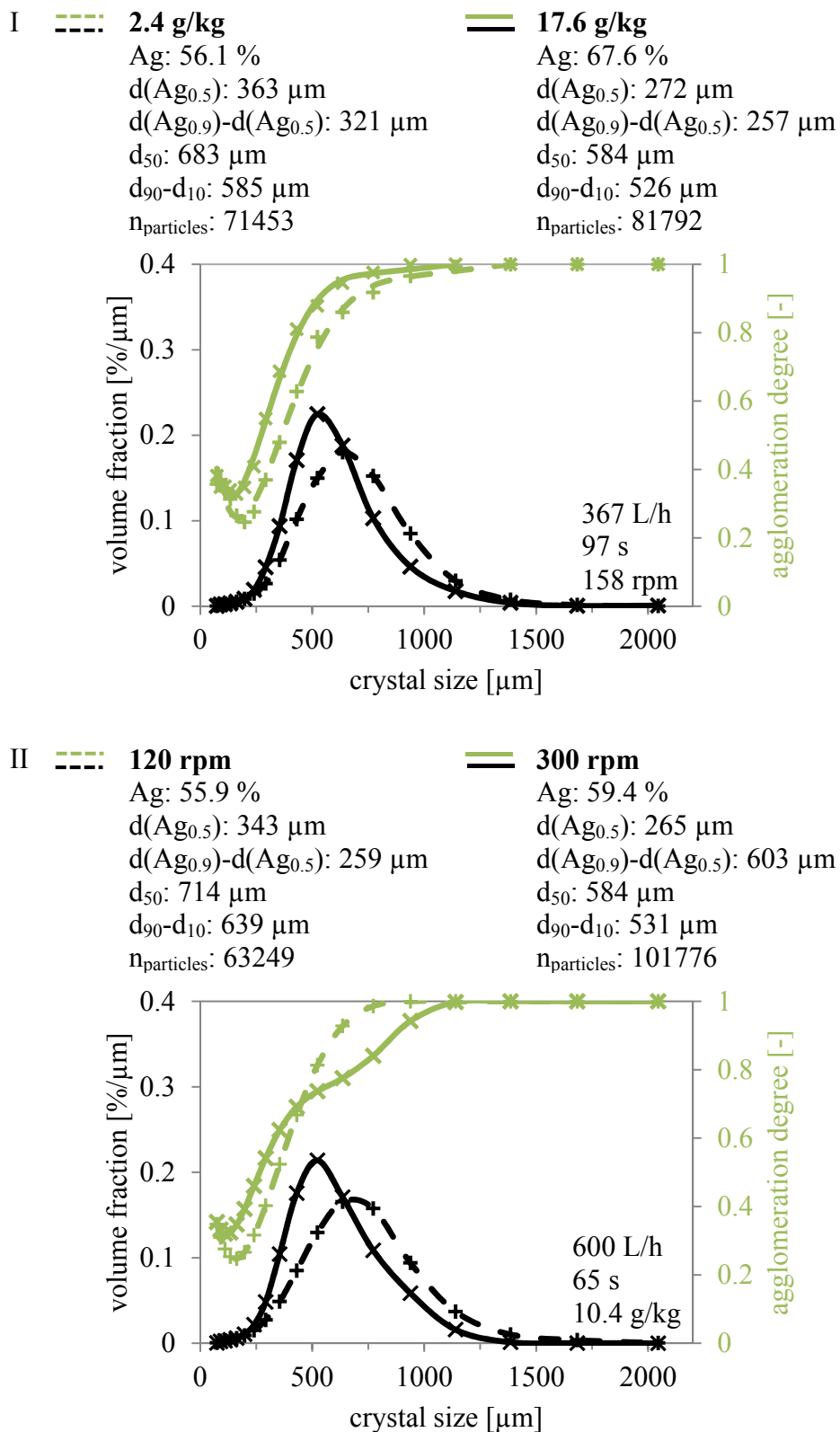


Figure 6.5: CSDs and AgDs of adipic acid product batches: (I) impact of gassing supersaturation, (II) impact of stirring rate

The **stirring rate (D)** shows a small positive linear effect on the overall agglomeration degree (Ag). This means the faster the stirring rate the higher is the Ag. The stirring intensity affects primarily the mixing of the solution and thereby crystal growth and agglomeration. On the one hand higher stirring rates lead to more particle-particle collisions so that the probability of crystals sticking together increases. On the other hand the contact time between the crystals is shortened so that time for the formation of crystalline bridges is limited. Additionally, more collisions of particles with installations occur which promotes desaggregation and breakage of agglomerates formed. Especially, large agglomerates are disrupted by high shear forces leading to a maximum size of agglomerates in solution [16]. Since the Ag is a number based measure both, the formation of more agglomerates and the breakage of larger agglomerates into smaller fragments of agglomerates, results in an increase of the Ag. To prove whether an increase of the stirring rate (compare Table 6.3) leads to more agglomerates in general, or to breakage of large agglomerates, the impact of the stirring rate on the AgD is analyzed using the responses $d(Ag_{0.5})$ and $d(Ag_{0.9})-d(Ag_{0.5})$. The linear effects on $d(Ag_{0.5})$ and $d(Ag_{0.9})-d(Ag_{0.5})$ regarding the stirring rate are opposed; the effect on $d(Ag_{0.5})$ is negative and the effect on $d(Ag_{0.9})-d(Ag_{0.5})$ is positive. This means that for higher stirring rates AgDs with a higher slope in the range of smaller crystal sizes and a lower slope in the range of larger crystal sizes are achieved. As can be seen in Figure 6.5 II, where the AgDs and CSDs of the star experiments of the stirring rate are depicted, the changes in the progression of the AgD correspond to a higher number of smaller and a lower number of larger agglomerates. Furthermore, the number of crystalline particles analyzed is with 101,776 particles at 300 rpm significantly higher than at 120 rpm (63,249 particles). These counts underpin the fact additionally; since due to sample preparation the mass of particles was approximate the same. To sum up the impact of the stirring rate on the Ag can be related to the breakage of especially large agglomerates.

Effects on CSD

The effects calculated in Table 6.4 show that the CSD, represented by the responses d_{50} and $d_{90}-d_{10}$, is significantly affected by the gassing parameters and the stirring rate.

In case of the width of the CSD ($d_{90}-d_{10}$) seven significant effects are identified. As depicted in Figure 6.6 changes of $d_{90}-d_{10}$ are caused by changes of d_{90} only, the diameter d_{10} stays nearly constant around 390 μm . Therefore, changes of the CSD by secondary nucleation or attrition are negligible and crystal growth, agglomeration, or breakage is decisive.

The **gassing supersaturation (C)** has a positive linear effect on d_{90} - d_{10} . Furthermore, two significant factor interactions exist; the interaction (AC) with the **gas flow (A)** and the interaction (BC) with the **gassing period (B)**. Therefore, the impact of the gassing supersaturation (C) has to be considered together with the other two gassing parameters. To analyze these interactions the contour plots depicted in Figure 6.7 I and II were created based on the respective regression model (see equation (6.2)). For higher gassing supersaturation (C) (compare factor levels in Table 6.3) the width of the CSD is narrowed when gas flow (A) and gassing period (B) are kept constant. As described for the Ag, gassing at higher supersaturation results in a higher number of smaller crystals. Despite the strong tendency of small crystals to agglomerate more single crystals have to grow together, i.e. more crystalline bridges have to be formed, to reach agglomerates of the same size. However, the increased competition for adipic acid molecules solved in solution reduces not only the growth of each crystal, but limits the formation of crystalline bridges also so that less large agglomerates result. Hence the characteristic diameter d_{90} decreases and a narrower CSD is achieved (compare Figure 6.6).

Since the contour lines of both interactions are very similar the gas flow (A) and the gassing period (B) have depending on the gassing supersaturation (C) the same influence on d_{90} - d_{10} . Both, the gas flow and the gassing period determine the total number of gas bubbles provided and therewith the foreign surface area available to induce nucleation. Merely the time, in which the foreign surface area is provided, is changed. It is assumed that the larger the surface area is, the higher is the possibility to induce nucleation.

For low gas flows and low gassing periods d_{90} - d_{10} values are obtained in the same order of magnitude as for cooling crystallization without gassing independent of the gassing supersaturation. This indicates that a minimal gas volume flow and a minimal gassing period exist to provide enough foreign surface area to induce nucleation and explains that the impact of the gassing supersaturation (C) increases with rising gas flows and gassing periods. At low gassing supersaturation (2.4 g/kg) an increase of the gas flow or the gassing period, i.e. an increase of the foreign surface area, results in a broadening of the CSD. With an increase of the foreign surface area nucleation is induced at low supersaturation so that fewer nuclei are created than without gassing. Consequently a lower number of crystals grow to larger crystalline particles, which results in higher d_{90} values. In contrast, at high gassing supersaturation (17.6 g/kg) an increase of the foreign surface area narrows the CSD. Due to the high supersaturation more nuclei are induced than without gassing, which results in a high number of crystals. Therefore, as described above the competition for adipic acid molecules increases, less large crystalline particles are formed, and d_{90} decreases.

For the **stirring rate (D)** a negative linear effect and significant interactions (AD, BD) with the **gas flow (A)** and the **gassing period (B)** exist regarding d_{90} - d_{10} . Furthermore, the stirring rate (D) is the only significant factor determining the **median crystal size (d_{50})**.

Since neither for the gas flow (A) nor for the gassing period (B) significant single effects are identified, and the effects of the interactions AD and BD have nearly the same order of magnitude, the contour plots of the interactions (see Figure 6.7 III and IV) are identical. This underlines that the gas flow (A) and the gassing period (B) are influencing the CSD as mentioned above by the foreign surface area provided.

The contour lines indicate that for constant gas flows and gassing periods higher stirring rates go along with a narrower d_{90} - d_{10} . This relation is mentioned in literature also [11] and is in accordance with the effect of the stirring rate on the Ag described above. Higher stirring rates cause the breakage of large agglomerates which creates smaller crystals so that d_{90} and d_{50} decrease also (compare Figure 6.5 II).

Moreover it can be seen that the influence of the stirring rate on d_{90} - d_{10} is reduced the higher the gas flow or the longer the gassing period is. Since for all experiments the stirrer was turned off during gassing (compare section 6.3) an impact of the stirring rate on the foreign surface area by deformation of gas bubbles can be excluded so that the interaction between the stirring rate and the gas flow or the gassing period must take place after nucleation. Therefore, independent of the stirring rate more nuclei are induced the larger the foreign surface area is. As result a high number of small crystals is present in solution. Less large crystals and agglomerates are formed, d_{90} - d_{10} is narrowed, and the effect of the stirring rate is reduced because less large agglomerates can break. For low stirring rates (< 210 rpm) an increase of the foreign surface area results in a narrower CSD. Breakage is reduced because of low shear forces, but the higher number of crystals leads to less large crystalline particles. In contrast for high stirring rates (> 210 rpm) a broadening of the CSD is observed. Despite a slower growth of each crystal the crystalline particles formed are larger than the fragments of destroyed agglomerates so that d_{90} increases.

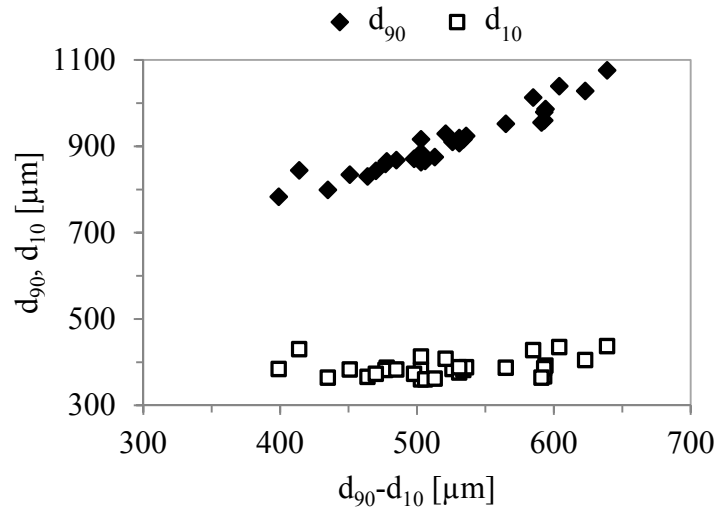


Figure 6.6: Correlation between the width of the CSD ($d_{90}-d_{10}$) and the characteristic diameters d_{10} and d_{90} of all data points of the DoE

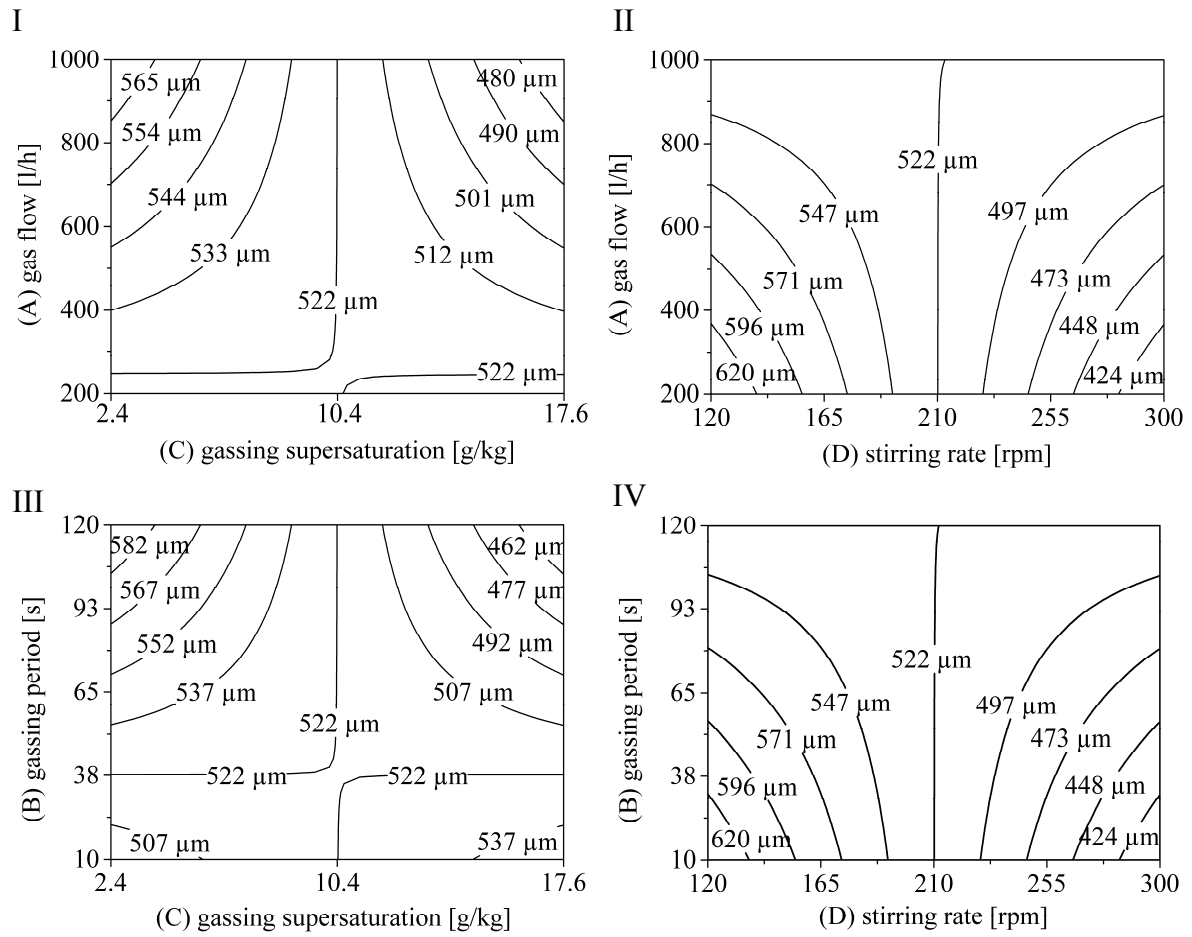


Figure 6.7: Contour plots for the significant factor interactions for $d_{90}-d_{10}$: (I) interaction (AC), (II) interaction (BC), (III) interaction (AD), (IV) interaction (BC); all other factors constant on level zero

6.3.2. Control of Product Quality

The results of the DoE indicate that the product quality of a crystalline product batch, characterized by the overall agglomeration degree (Ag) and width of the crystal size distribution (d_{90} - d_{10}) can be affected by gassing, whereby all gassing parameters exhibit a significant effect. Furthermore, the stirring rate is a decisive factor. Now it shall be proven whether it is possible to control the product quality regarding Ag and d_{90} - d_{10} using the regression models in equations (6.1) and (6.2). As can be seen in Figure 6.8, where the width of the CSD (d_{90} - d_{10}) for all factor level combinations of the DoE is plotted against the Ag, a correlation between Ag and d_{90} - d_{10} seems to exist. Low Ag-values go along with broad CSDs, whereas with an increasing Ag the CSD is narrowed. As described in the section before broad CSDs are characterized by a higher amount of large agglomerates than narrower ones. Since the Ag is a number-based measure higher Ag-values are reached when smaller agglomerates, which are formed probably out of fewer crystals than larger agglomerates, are present in a crystalline product batch. The correlation between Ag and d_{90} - d_{10} has to be kept in mind for the control of the product quality. If the aim is a narrow CSD, a high Ag and therewith maybe a lower purity has to be accepted. Using the excel solver the factor level combinations for a crystalline product batch with a minimal d_{90} - d_{10} (high Ag) and a minimal Ag (broad CSD) were identified within the ranges investigated for the DoE. Since the Ag is affected by the gassing supersaturation and the stirring rate only the gas flow and the gassing period were chosen in the way that a maximal broad CSD is covered also. Afterwards for each of the both factor level combinations two gassing experiments were performed to assess the prediction of the regression models. The factor levels identified, as well as predicted and experimental results of the responses, are listed in Table 6.5.

Table 6.5: Factor levels and results of the responses d_{90} - d_{10} and Ag for product quality control

Factor	Level	Value for min d_{90} - d_{10}	Level	Value for min Ag
A Gas flow	$-\alpha$	200 [L/h]	$-\alpha$	200 [L/h]
B Gassing period	$-\alpha$	10 [s]	$-\alpha$	10 [s]
C Gassing supersaturation	$-1/\alpha$	17.6 [g/kg]	$1/\alpha$	2.4 [g/kg]
D Stirring rate	α	300 [rpm]	$-\alpha$	120 [rpm]
Predicted results	Ag:	67.4 [%]	Ag:	55.2 [%]
	d_{90} - d_{10} :	331 [μ m]	d_{90} - d_{10} :	714 [μ m]
Experimental results	Ag:	67.3±0.4 [%]	Ag:	58.2±0.7 [%]
	d_{90} - d_{10} :	423±8 [μ m]	d_{90} - d_{10} :	602±19 [μ m]

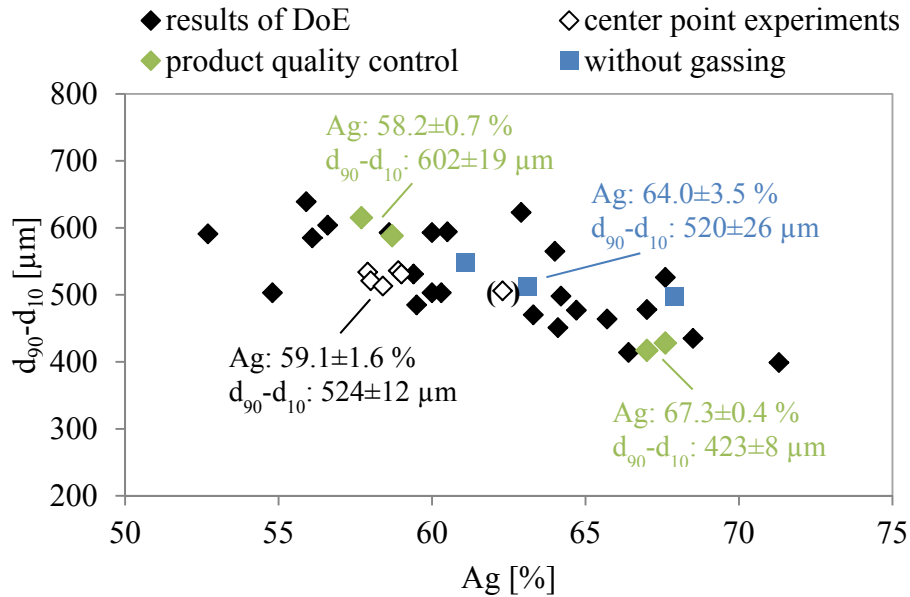


Figure 6.8: Experimental results for d_{90} - d_{10} and Ag of all experiments

Regarding the Ag the predicted results demonstrate a high level of conformity with the experimental results. The experimental value for the minimal Ag differs with $58.2 \pm 0.7\%$ only 3 % from the calculated value. The corresponding calculated Ag (67.4%) of the minimal d_{90} - d_{10} lies within the standard deviation of the experimental determined Ag ($67.3 \pm 0.4\%$). For the prediction of d_{90} - d_{10} higher deviations are observed. Both calculated results exhibit a deviation of around $100\ \mu\text{m}$ to the experimental values of d_{90} - d_{10} . In sum the predicted range of d_{90} - d_{10} ($383\ \mu\text{m}$) is around $200\ \mu\text{m}$ larger than the corresponding experimental one ($179\ \mu\text{m}$). However, in comparison to all experimental d_{90} - d_{10} values of the DoE the d_{90} - d_{10} values touch the lower end of the result space. The high deviation between the predicted and experimental values for d_{90} - d_{10} might be explained by the fact that a minor shift of the volume fraction based CSD has a strong impact on d_{90} . Nevertheless, the prediction of both regression models seems to be sufficiently accurate to control the agglomeration degree (Ag) and the width of CSD (d_{90} - d_{10}) of adipic acid crystalline product batches.

Finally, we wanted to investigate whether induced nucleation by gassing leads to an improved reproducibility of the product quality. Therefore, the results of the three cooling crystallization experiments without gassing (stirring rate at 210 rpm (factor level zero)) are compared with the center point experiments (all factors on level zero) and with the experiments which were performed to assess the regression models (factor levels listed in Table 6.5). The Ag and d_{90} - d_{10} values of all these experiments are depicted in Figure 6.8. As can be seen the dispersion of Ag and d_{90} - d_{10} is clearly higher for cooling crystallization experiments without gassing than for the gassing crystallization experi-

ments one outlier – highlighted in Figure 6.8 by brackets – is observed for the center point experiments only. This outlier cannot be explained. Results of retries were always comparable to the other center point experiments. Nevertheless, the outlier was considered inside the DoE to take random interferences of unknown influence factors into account. Consequently, it can be pointed out that the reproducibility of the center point experiments can be improved by gassing due to induced nucleation which additionally facilitates the control of the product quality.

In contrast to cooling crystallization without gassing a higher degree of freedom for gassing crystallization is available to adjust A_g and $d_{90}-d_{10}$ due to additional process parameters (gas flow, gassing period, and gassing supersaturation). Since the stirring rate (D) was investigated as factor of the DoE the corresponding results (compare Figure 6.8) cannot be used for a direct comparison with the crystallization experiments without gassing at medium stirring rate (factor level zero). To enable a comparison independent of the stirring rate and to identify ranges adjustable by gassing for A_g and $d_{90}-d_{10}$ the regression model was used. The stirring rate factor level was set to zero (center point conditions) and the minimal and maximal values of the A_g and $d_{90}-d_{10}$ were calculated by using the corresponding regression models (compare equations (6) and (7)). The predicted results are listed in Table 6.6 and indicate that by gassing crystalline product batches with lower A_g s (down to 58.1 %) and narrower or broader CSDs ($355 \mu\text{m} \leftrightarrow 689 \mu\text{m}$) can be achieved than for cooling crystallization without gassing ($64.0 \pm 3.5 \%$, $520 \pm 26 \mu\text{m}$). However, we would like to call attention to the fact that the predicted span of the $d_{90}-d_{10}$ values has to be treated with caution. As shown above for the prediction of $d_{90}-d_{10}$ (compare Table 6.5) deviations of around $100 \mu\text{m}$ exists so that the predicted span from $355 \mu\text{m}$ to $689 \mu\text{m}$ is probably narrower in reality. Nevertheless, the statement that by gassing narrower or broader CSDs can be reached, seems to be reasonable.

Table 6.6: Adjustable range for A_g and $d_{90}-d_{10}$ of gassing crystallizations in comparison of cooling crystallization results without gassing at 210 rpm

	$d_{90}-d_{10}$ [μm]	A_g [%]
without gassing	520 ± 26	64.0 ± 3.5

with gassing (predicted)		
MIN	355^*	58.1^{**}
MAX	689^{**}	64.5^*

*1000 L/h, 120 s, 17.6 g/kg; **1000 L/h, 120 s, 2.4 g/kg

6.4. Summary

The agglomeration behavior of the material system adipic acid/ water was investigated. Therefore, the agglomeration degree (Ag) and the agglomeration degree distribution (AgD) were recorded over the crystallization process chain using the QICPIC image analysis technique. The crystalline product batch reached after crystallization shows a relative high overall agglomeration degree of 64 %, which confirmed that adipic acid tends to agglomerate during crystallization. For cake washing acetonitrile was selected as wash liquid and wash conditions were identified, which guarantee a nearly complete displacement of mother liquor. The analysis of product batches after static drying has indicated that the product quality is affected by agglomeration during drying if cake washing was omitted at high drying temperatures only. Therefore, it was concluded that agglomeration takes place mainly during crystallization and the further downstream process has a rather low impact on the product quality. As consequence crystallization was identified as decisive process step to control the quality of adipic acid product batches. Therefore, gassing crystallization, as induced nucleation method, was systematically investigated by DoE in terms of the possibility to control the agglomeration behavior of adipic acid crystals during crystallization. The gassing supersaturation, the gas flow, the gassing period, and the stirring rate were considered as process parameters and the impact on the Ag, AgD, and CSD was grasped. It has been shown that gassing crystallization affects agglomeration and therewith the width of the crystal size distribution (d_{90} - d_{10}). High Ag values go along with narrow d_{90} - d_{10} and vice versa. In comparison to cooling crystallization without gassing a better reproducibility was achieved. Therefore, gassing crystallization seems to provide a promising method to control agglomeration during crystallization and therewith the product quality of crystalline product batches. Nevertheless, the stirring rate plays a decisive role also.

7. Conclusions and Outlook

First objective of this work was to develop a new quality criterion which delivers quantitative information about the amount and distribution of agglomerates. The second focus was to increase the understanding of agglomeration processes and to provide insights into the relevance of holistic process optimization. Therefore, the agglomeration behavior of two material systems was analyzed over the whole crystalline process chain.

The investigations within this thesis clearly show that an evaluation of the crystal size distribution (CSD) of a product batch alone is insufficient since despite same characteristics of the CSD the final product can be highly different due to different agglomeration behavior. Regardless of quantifying agglomeration misconception of the crystallization process is possible. Therefore, the agglomeration degree distribution (AgD) – introduced in this thesis in combination with the overall agglomeration degree Ag – as new quality criterion should be used in addition to CSD for quality evaluation to allow a quantitative characterization and comparison of crystalline product batches with different morphology. For an efficient and reliable product design it is crucial to identify whether crystals are prone to agglomerate and in which process step agglomeration takes predominantly place. Thus the CSDs and AgDs of a product batch after crystallization and drying have to be compared. In addition, a high concentration of solute in the mother liquor after crystallization or a high temperature dependency of the solubility can be an indication for agglomeration during drying. Afterwards, the identified process steps have to be further investigated.

If agglomerates are formed during crystallization the adjustment of the stirring rate and the induction of nucleation play a decisive role to control agglomeration. Using gassing crystallization as induced nucleation method improves the reproducibility of the product quality. To avoid the formation of large agglomerates, i.e. to produce product batches with narrow CSD, a high stirring rate in combination with low gassing supersaturation and gas flow, and a short gassing period should be chosen.

If the crystals are more prone to agglomerate in the further downstream, cake washing after filtration is essential to avoid agglomeration during drying and preserves the product quality designed by crystallization. However, prerequisite for an effective cake washing is the selection of a suitable wash liquid. A preselection of solvents can be performed based on the solu-

bility of the crystalline product in solvent, the viscosity ratio between mother liquor and solvent, and the solubility of mother liquor in the solvent. Promising solvents for cake washing are characterized by a low solubility of the crystalline product at low and high temperatures, a low viscosity ratio, and a high solubility of the mother liquor. Furthermore, the drying method used has a significant impact on the agglomeration behavior. To reduce agglomeration the time for the formation of crystalline bridges has to be shortened, i.e. the contact area and contact time between the crystals has to be decreased. Consequently, dynamic drying methods like fluidized bed drying are preferable to classic static drying methods.

To conclude, for a target-oriented, reliable product design a holistic view on the whole crystalline process chain is crucial, whereby the control of agglomeration process is decisive.

For further research it should be noted that one lack regarding the quantification of agglomeration is still existing: Neither the AgD nor the Ag deliver information about the amount of single crystals bounded as agglomerates. As consequence the number-based characteristic of the Ag leads to the unexpected effect that low Ag-values are correlated with broad CSDs. To overcome this lack of information, the image analysis tool developed should be adapted in an appropriate manner. Research work in this direction was already performed by Kovacevic et al. [116]. Moreover, alternative approaches like neural networks can be tested to enhance the classification performance and the selection of image descriptors, as well as the composition of the training sets should be further systemized. In this context it might be of interest if an image descriptor combination exists for the classification of agglomerates and single crystals independent of the material system. Since, the impact of gassing has indicated that nucleation affects the agglomeration behavior during crystallization it should be proven whether agglomeration takes place mainly shortly after nucleation or during the further crystallization process also. Therefore, the AgD shall be measured during the crystallization process itself. To realize this, the measurement system of the QICPIC has to be adapted by a heated flow cell and a bypass system to adjust the suspension density.

A. Appendix

Material and Methods

Table A.1: Filtration/washing* and drying conditions of CSDs depicted in Figure 3.3 and Figure 3.5 of static dried L-alanine product batches

Wash liquid	T _{wash liquid} [°C]	V _{wash liquid} [mL]	N _{wash cycle} [-]	T _{drying} [°C]	Layer thickness [cm]
ethanol	12.5	35	2	50	1.35

*dehumidified for eight minutes after filtration, for three minutes between wash cycles, and for eleven minutes after washing

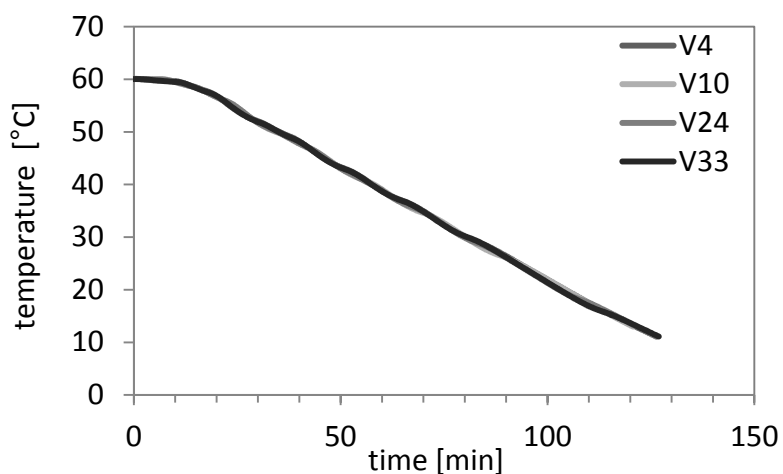


Figure A.1: Corresponding cooling profiles of crystallization to the CSDs depicted in Figure 3.3 of static drying crystalline product batches

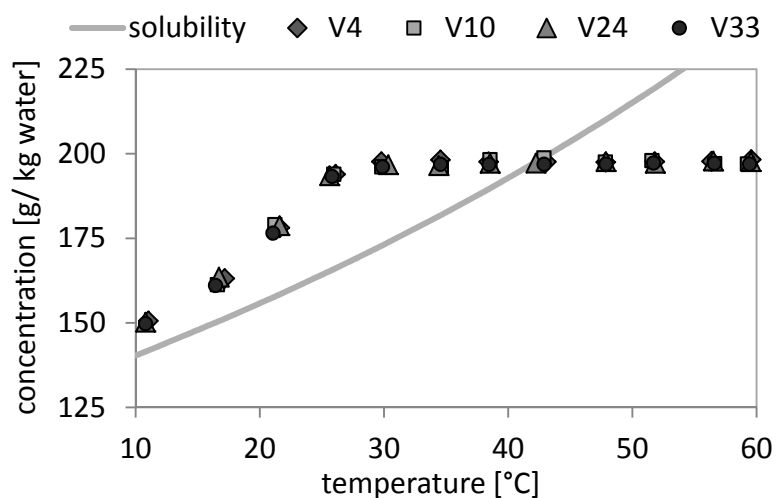


Figure A.2: Corresponding concentration profiles of crystallization to the CSDs depicted in Figure 3.3 of static drying crystalline product batches

L-Alanine/Water

Table A.2: Thermal history of L-alanine/water crystallizations

T_{start} [°C]	T_{end} [°C]	t [hh:mm:ss]
20.00	20.00	12:00:00
20.00	60.00	00:30:00
60.00	60.00	05:30:00
60.00	03.00	02:06:40

Table A.3: Constant crystallization conditions of the material system L-alanine/water

T_{sat} [°C]	c_{sat} [g/kg water]	T_{start} [°C]	T_{end} [°C]	κ [K/min]	n [rpm]
42.38*	197.89	60.00*	10.00	0.45*	300

*DoE optimized values taken from Wohlgemuth (2012)

Adipic acid/Water

Table A.4: Thermal history of the adipic acid/water crystallizations

T_{start} [°C]	T_{end} [°C]	t [hh:mm:ss]
20.00	20.00	12:00:00
20.00	60.00	00:30:00
60.00	60.00	03:30:00
60.00	03.00	03:10:00

Table A.5: Constant crystallization conditions of the material system adipic acid/water

T_{sat} [°C]	c_{sat} [g/kg water]	T_{start} [°C]	T_{end} [°C]	κ [K/min]
50.00	88.73	60.00	10.00	0.30

Quantification of Agglomeration

Table A.6: Constant gassing crystallization conditions of the adipic acid crystalline product batches AA-1 and AA-2

T_{sat} [°C]	c_{sat} [g/kg water]	T_{start} [°C]	T_{end} [°C]	κ [K/min]	T_{gassing} [°C]	$\Delta t_{\text{gassing}}$ [s]	\dot{V}_{gassing} [L/min]
50.00	88.73	60.00	10.00	0.30	49	16	37

Table A.7-part 1: Primary (numbers 1-8), secondary (numbers 9-18), and grayscale image descriptors (numbers 19-22)

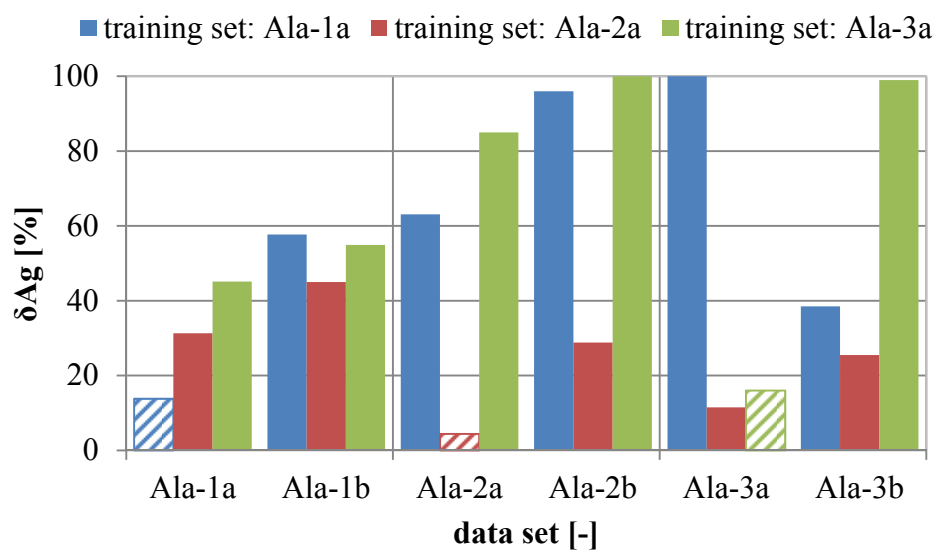
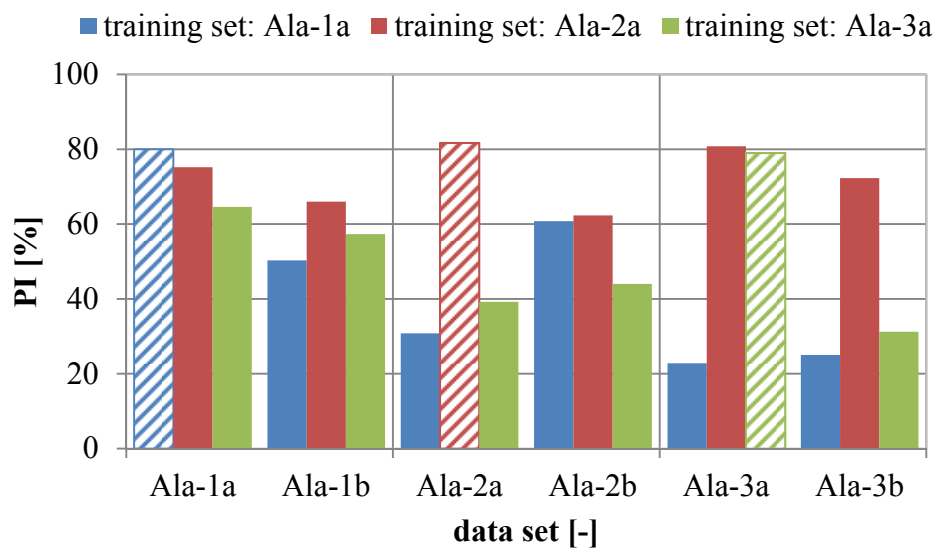
Number	Image descriptor	Symbol	Unit	Explanation
1	Projection area	A	[mm ²]	Area, which is surrounded by the perimeter. [111]
2	Convex hull	A _{convex}	[mm ²]	Area, which is surrounded by a convex bounding polygon. [106]
3	Perimeter	P	[mm]	Length of the outside particle boundary. [111]
4, 5	Feret diameter	F _{min} , F _{max}	[mm]	Shortest (F _{min}), longest (F _{max}) distance between two points on the particle boundary.
6, 7	Ellipse axis	L, B	[mm]	Major (L) and Minor (B) axis of the best fitting ellipse, with a right angle between the axes. [111]
8	Equivalent diameter	d _{eq}	[mm]	Diameter of a coextensive circle.
9	Circularity	Circ	[-]	Similarity of a particle with a circle. Circ = $4\pi A/P^2$ [111]
10	Elongation	Elong	[-]	Ratio of maximal to minimal Feret diameter, which is a measurement for the symmetric dimension of a particle. Elong = F_{max}/F_{min}
11	Solidity	Sol	[-]	Ratio of projection area to convex hull. Sol = A/A_{convex}
12	Aspect ratio	AR	[-]	Ratio of longest distance between two points on the particle boundary (F _{max}) to diameter of a coextensive circle. AR = F_{max}/d_{eq}
13	Area ratio	Area ratio	[-]	Ratio between major and minor axis of the best fitting ellipse. Area ratio = L/B

Table A.7 -part 2: Primary (numbers 1-8), secondary (numbers 9-18), and grayscale image descriptors (numbers 19-22)

Number	Image descriptor	Symbol	Unit	Explanation
14	Modified Heywood area ratio	Heywood	[-]	Ratio between the projection area A and rectangle with a length of $F_{\max}(\theta)$ and a width of $F_{\max}(\theta+90^\circ)$ [112]. Instead of $F_{\max}(\theta)$ and $F_{\max}(\theta+90^\circ)$ the ellipse axes L and B are used. Heywood = A/BL
15	Modified Wadell sphericity	Wadell	[-]	Squared ratio between the diameter of a volume equivalent sphere d_v and the equivalent diameter d_{eq} [113]. Due to 3d dimensions are not available, the volume of the particles are described approx. by an ellipse, which z-dimension is described by the average of the ellipse axes L and B. $\text{Wadell} = \left(\frac{d_v}{d_{eq}} \right)^2 = \left(\frac{\sqrt[3]{4BL(B+L)}}{d_{eq}} \right)^2$
16	Fractal dimension	FD	[-]	With the imageJ function "BoxCount" calculated slope of the function that relates the log(box count) to the negative log(box size). The "Box Counting" is a procedure, which analyses an object systematically by laying a series of grids of decreasing caliber (box size) over the object, and recording the box count needed to cover the object boundary for each box size. [111,114]
17	Convex box ratio	CBR	[-]	Ratio between convex hull A_{convex} and the ellipse axes L and B. $\text{CBR} = A_{\text{convex}}/BL$
18	NSwC	NSwC	[-]	Modified parameter NS developed by Podczec et al. (1997) [115]. NS combines three conventional shape descriptors, which describe the difference to a square, a circle, and a triangle as well as the elongation with the number of characteristic corners of the shape C. The parameter C was neglected in this study. $\text{NSwC} = (2AP/F_{\max}BL) - (4A^2/\pi BL^3)$
19	Area fraction	%Area	[%]	Percentage of the projection area A, which is not black after thresholding, because the grayscale values lies below the threshold. [111]
20	Minimal grayscale value	Min	[-]	Minimal grayscale value of an image. [111]
21	Mean grayscale value	Mean	[-]	Average grayscale value of an image. [111]
22	Standard deviation of grayscale values	StdDev	[-]	Standard deviation of the average grayscale value. [111]

Table A.8: Composition of the training sets Ala-1a and Ala-2a

training set	number of			
	single crystals	agglomerates	crossover crystals	waste particles
Ala-1a	283	501	203	13
Ala-2a	370	477	150	3

**Figure A.3:** Transfer potential of variant 13 (8 image descriptors)

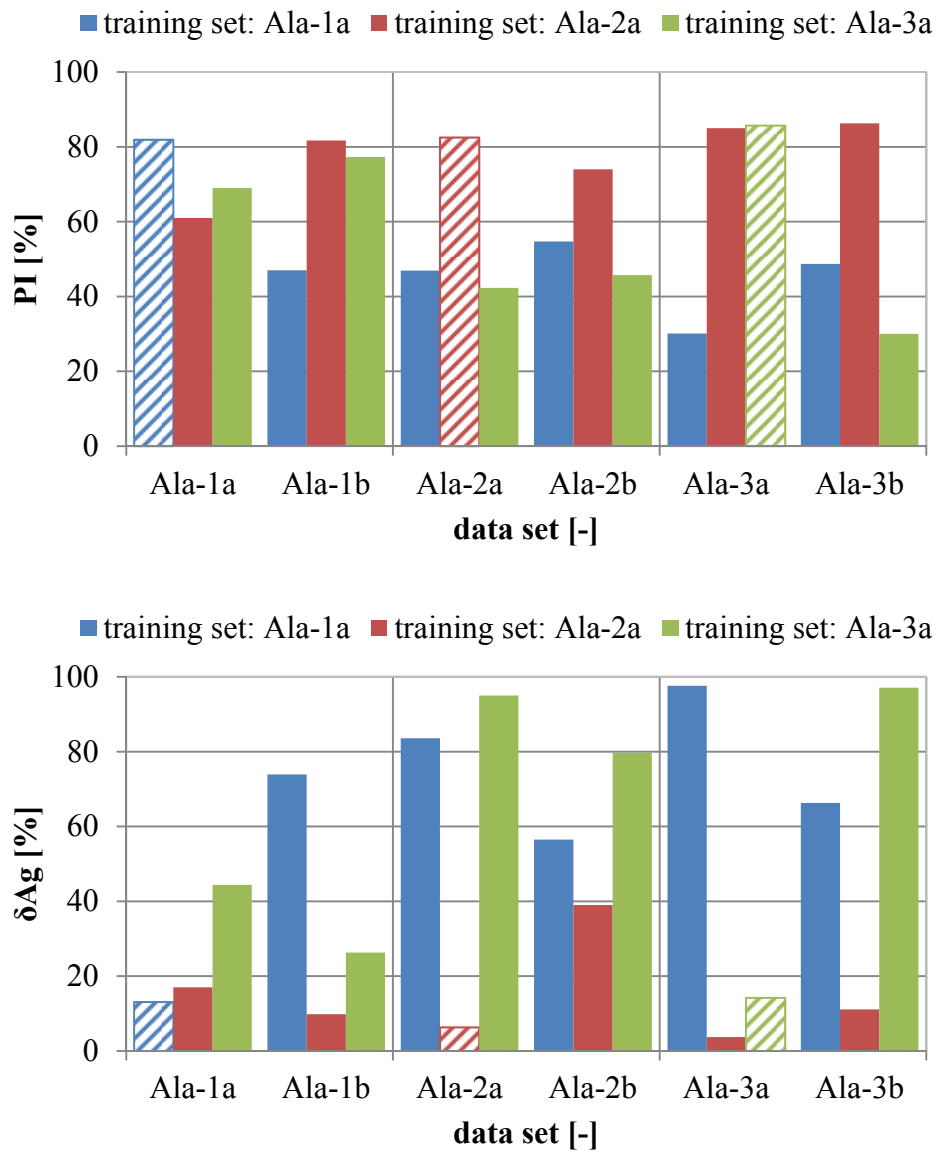


Figure A.4: Transfer potential of variant 15 (14 image descriptors)

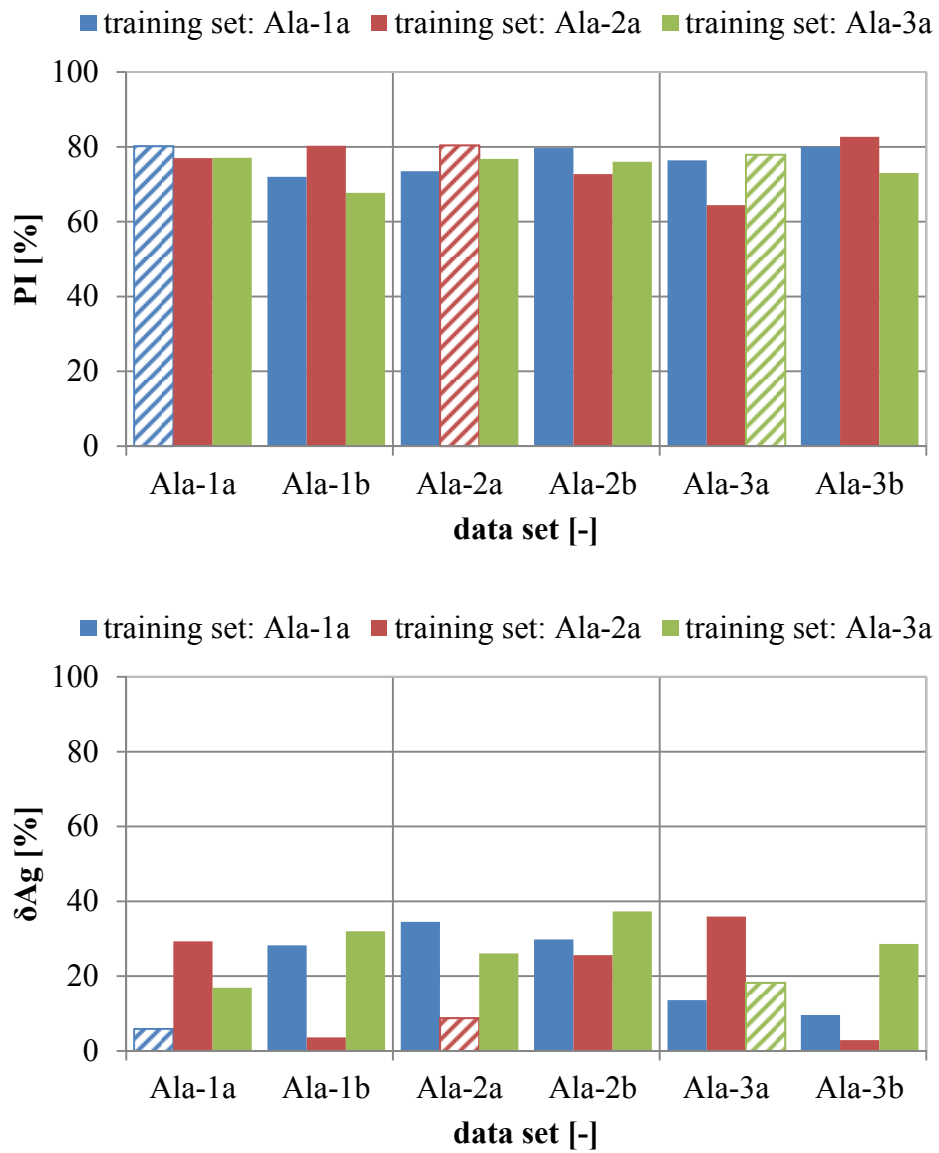


Figure A.5: Transfer potential of variant 12+ (8 image descriptors); the + indicates that the image descriptors of the variant is extended by the equivalent diameter d_{eq}

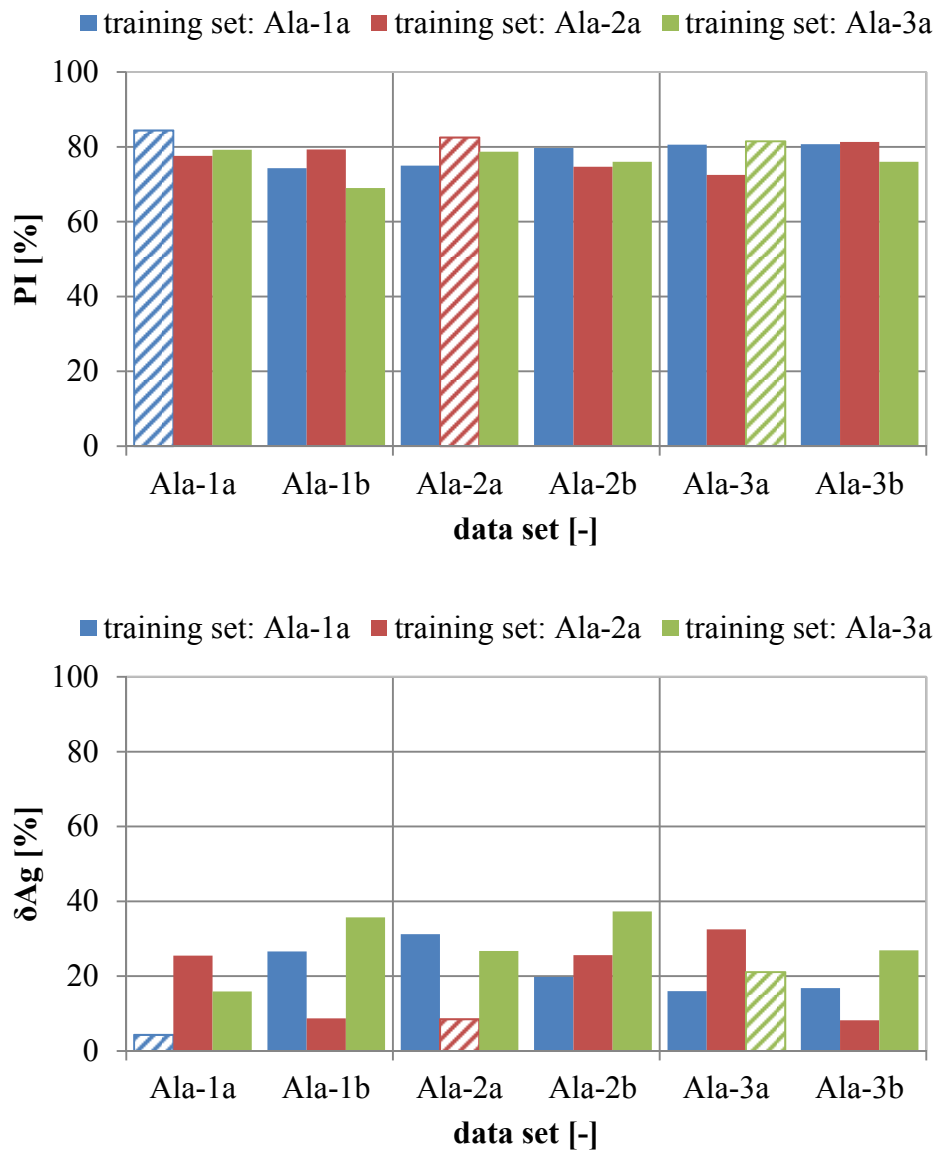


Figure A.6: Transfer potential of variant 13+ (9 image descriptors); the + indicates that the image descriptors of the variant is extended by the equivalent diameter d_{eq}

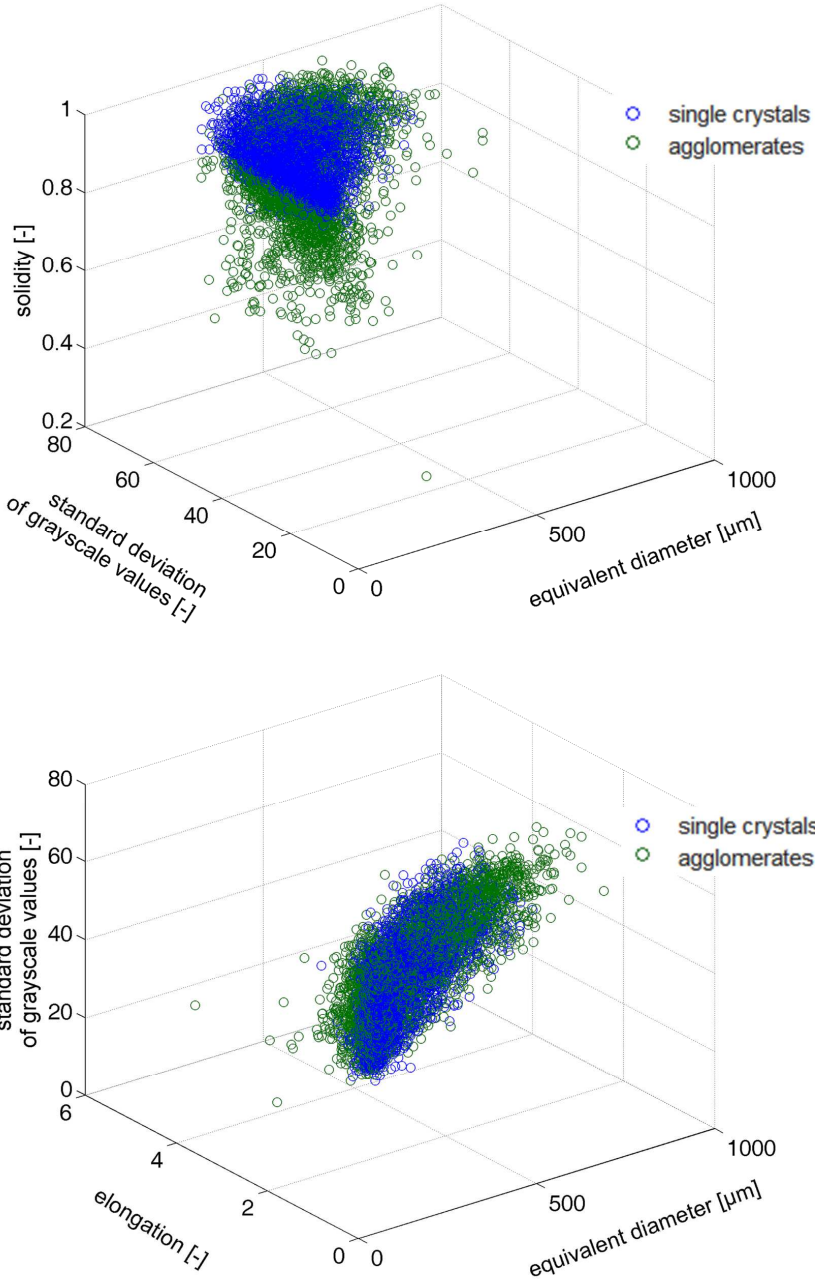


Figure A.7: Classification results of the crystalline product batch Ala-2 depicted as trace plots for the image descriptors equivalent diameter, elongation, standard deviation of grayscale values, and equivalent diameter, solidity, standard deviation of grayscale values

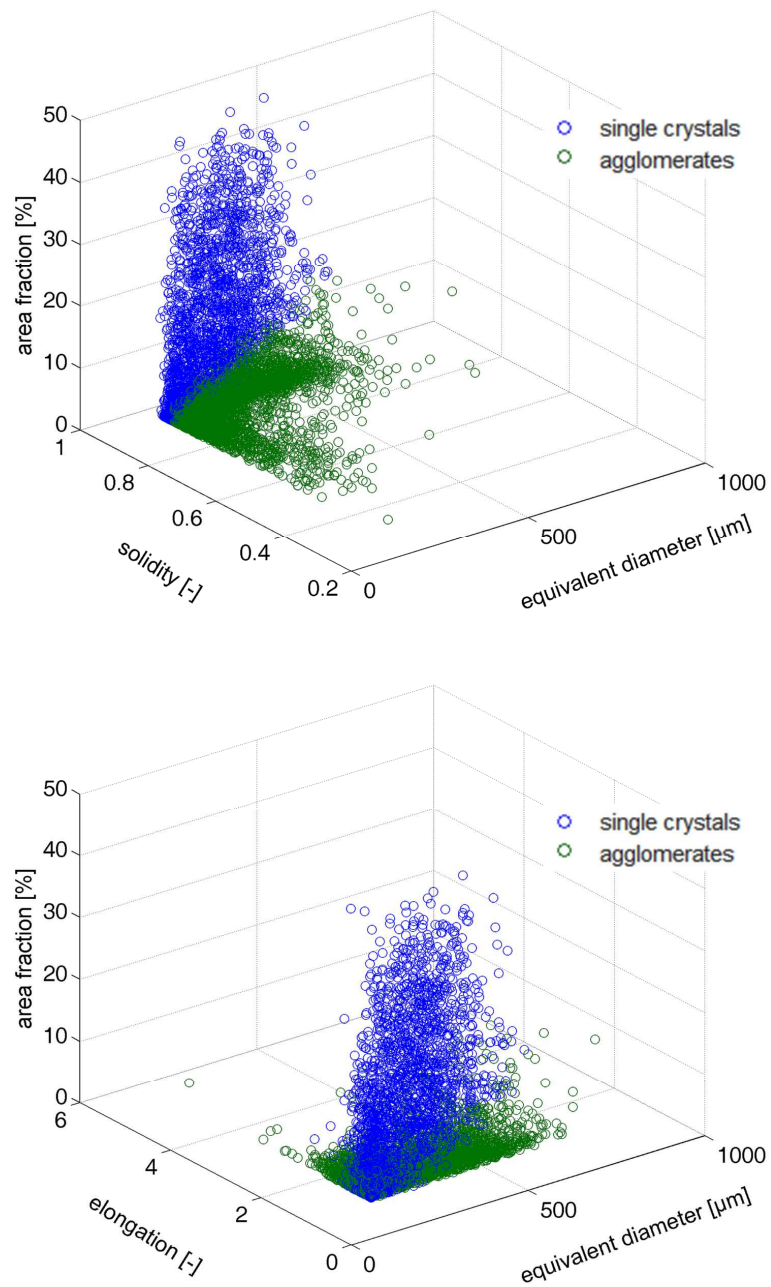


Figure A.8: Classification results of the crystalline product batch Ala-2 depicted as trace plots for the image descriptors equivalent diameter, elongation, area fraction, and equivalent diameter, solidity, area fraction

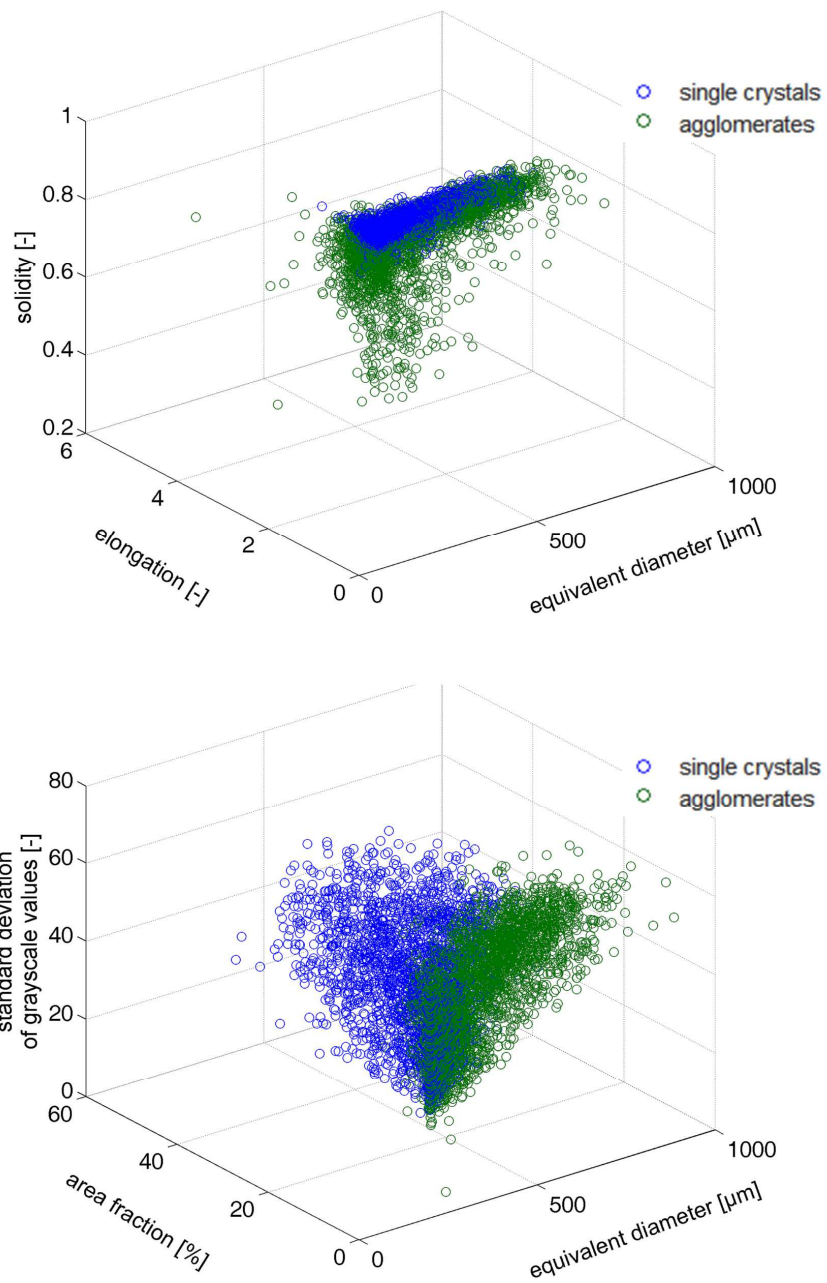


Figure A.9: Classification results of the crystalline product batch Ala-2 depicted as trace plots for the image descriptors equivalent diameter, elongation, solidity and equivalent diameter, area fraction, standard deviation of grayscale values

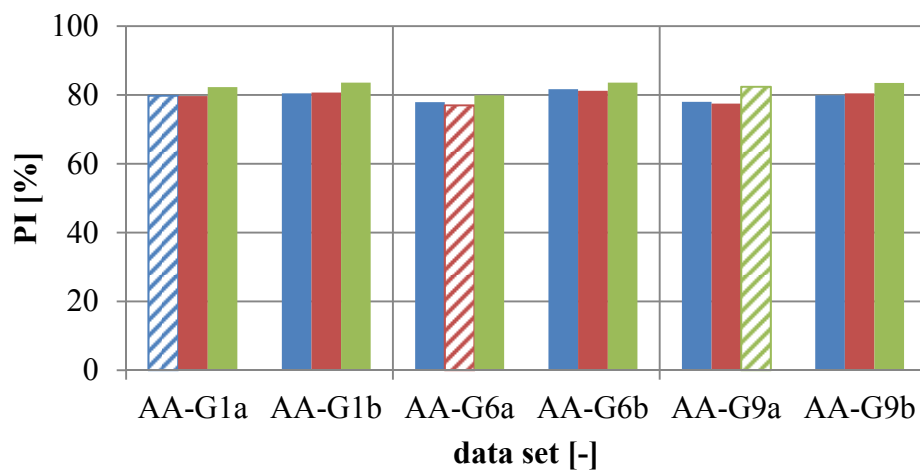


Figure A.10: Images of single crystals, agglomerates, and waste particles recorded with the QICPIC for the material system adipic acid/ water [119]

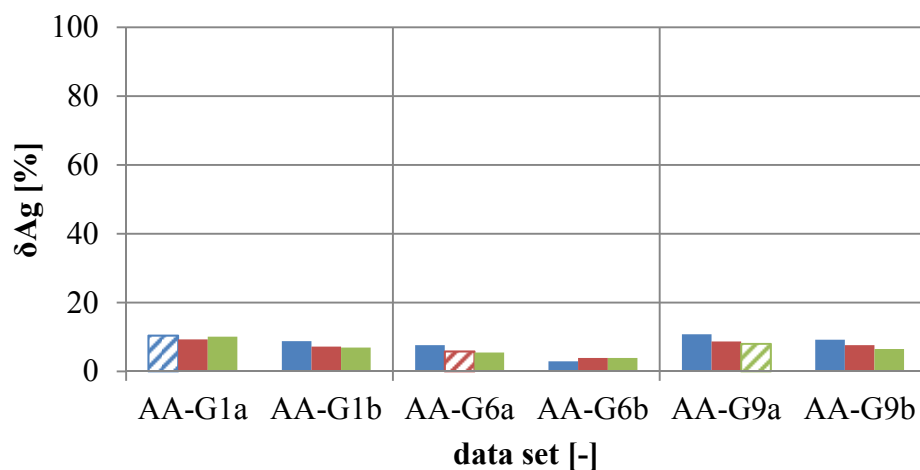
Table A.9: Gassing experiments of the material system adipic acid/ water used for the creation of the training sets listed in Table 4.9

			AA-G1	AA-G6	AA-G9
factors	Gas flow	[l/h]	367	833	367
	Gassing period	[s]	33	33	33
	Gassing temperature	[°C]	46	49.5	46
	Stirring rate	[rpm]	158	158	262
CSD	d ₅₀	[μm]	632	602	532
	d ₉₀ -d ₁₀	[μm]	623	503	435

■ training set: AA-G1a ■ training set: AA-G6a ■ training set: AA-G9a



■ training set: AA-G1a ■ training set: AA-G6a ■ training set: AA-G9a

**Figure A.11:** Transfer potential for variant D_{AA}-0 with an average PI: 80.5 % ± 2.0 % and δAg: 7.4 % ± 2.2 %

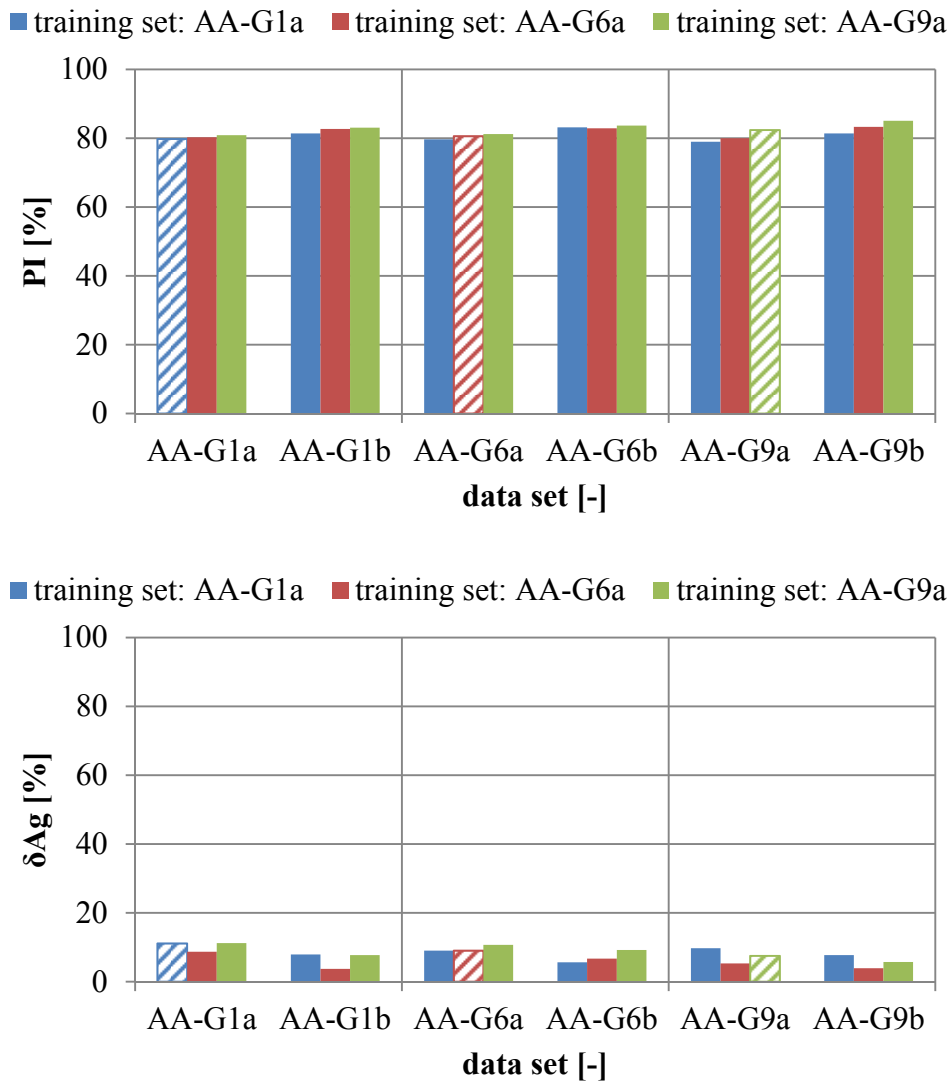


Figure A.12: Transfer potential for variant D_{AA-1} with an average PI: $81.7 \% \pm 1.6 \%$ and δAg : $7.8 \% \pm 2.2 \%$

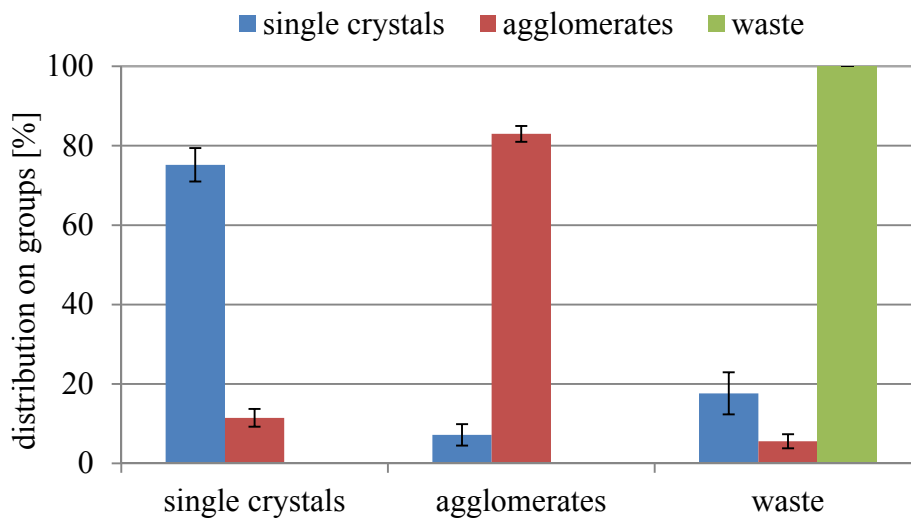


Figure A.13: Averaged distribution of crystalline particles on the groups single crystal, agglomerates, and waste for the image descriptor combination D_{AA-1}

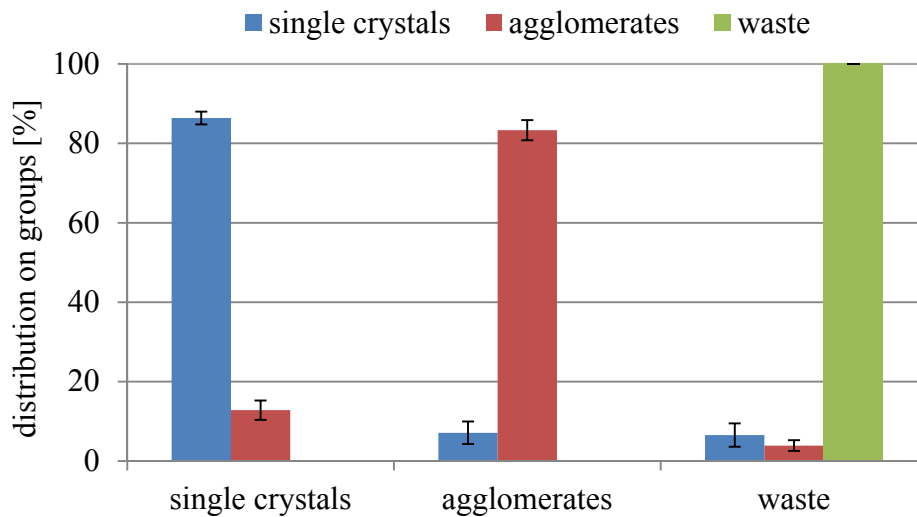


Figure A.14: Averaged distribution of crystalline particles on the groups single crystal, agglomerates, and waste for the image descriptor combination D_{AA-2}

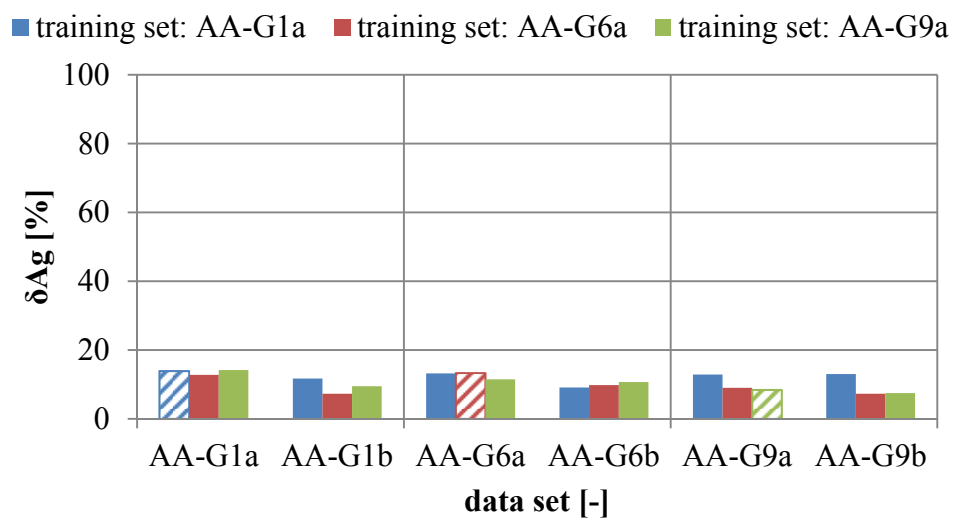
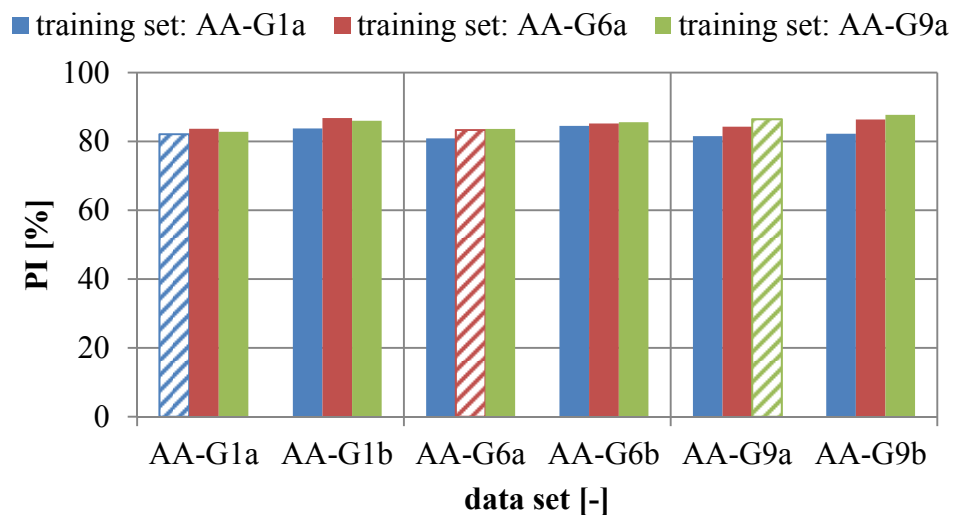


Figure A.15: Transfer potential for variant D_{AA-2} with in average PI: $84.3 \% \pm 1.9 \%$ and δAg : $10.8 \% \pm$

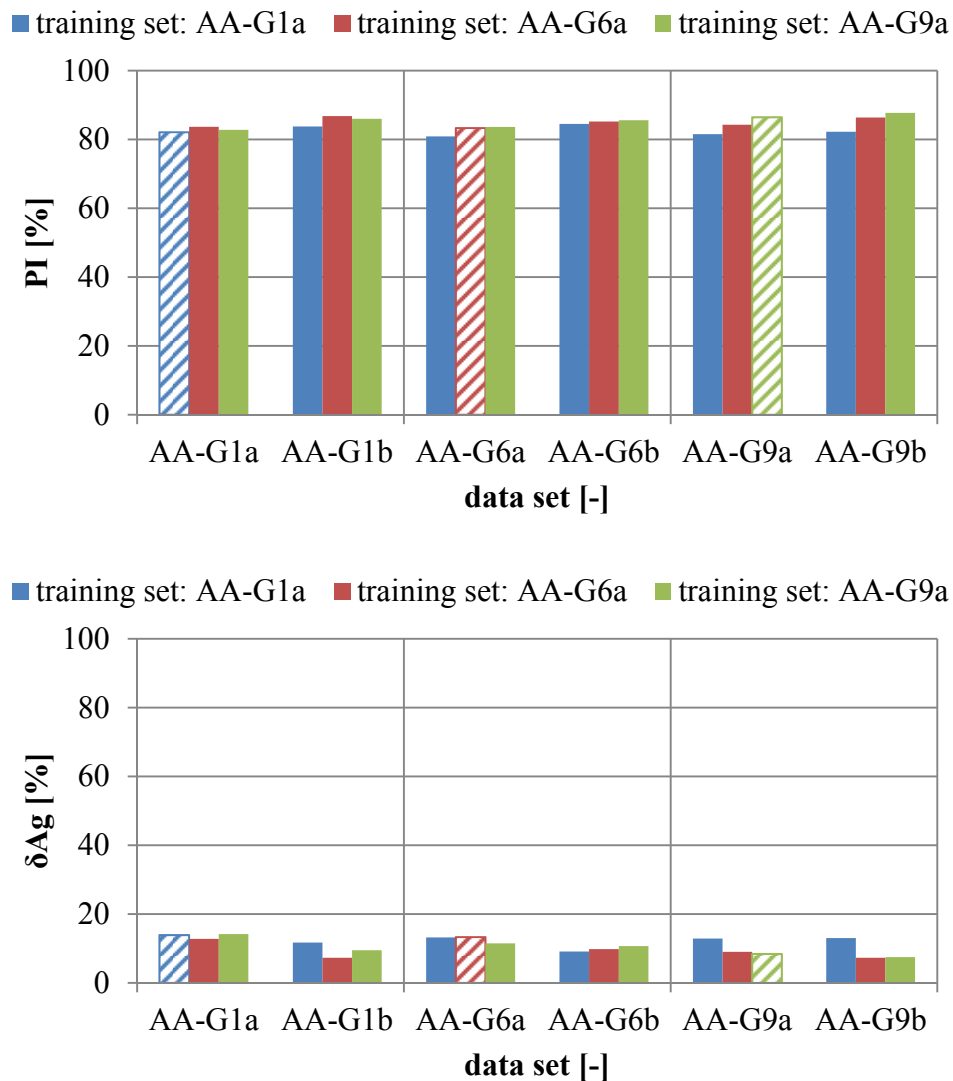


Figure A.16: Transfer potential for variant D_{AA-3} with an average PI: $89.8 \% \pm 1.5 \%$ and δAg : $6.3 \% \pm 2.0 \%$

Material System I – L-Alanine/Water

Table A.10: Solubility of L-alanine in different solvents measured two times

	T [°C]	c [g/kg solvent]
Acetone	12.88	$5.88 \cdot 10^{-3} \pm 1.36 \cdot 10^{-4}$
	42.15	$8.82 \cdot 10^{-2} \pm 9.99 \cdot 10^{-3}$
Ethyl acetate	13.61	$1.23 \cdot 10^{-1} \pm 1.25 \cdot 10^{-2}$
	59.80	$1.45 \cdot 10^{-1} \pm 8.82 \cdot 10^{-3}$
Ethanol	13.47	$2.86 \cdot 10^{-2} \pm 7.22 \cdot 10^{-5}$
	56.89	$5.84 \cdot 10^{-2} \pm 4.87 \cdot 10^{-4}$

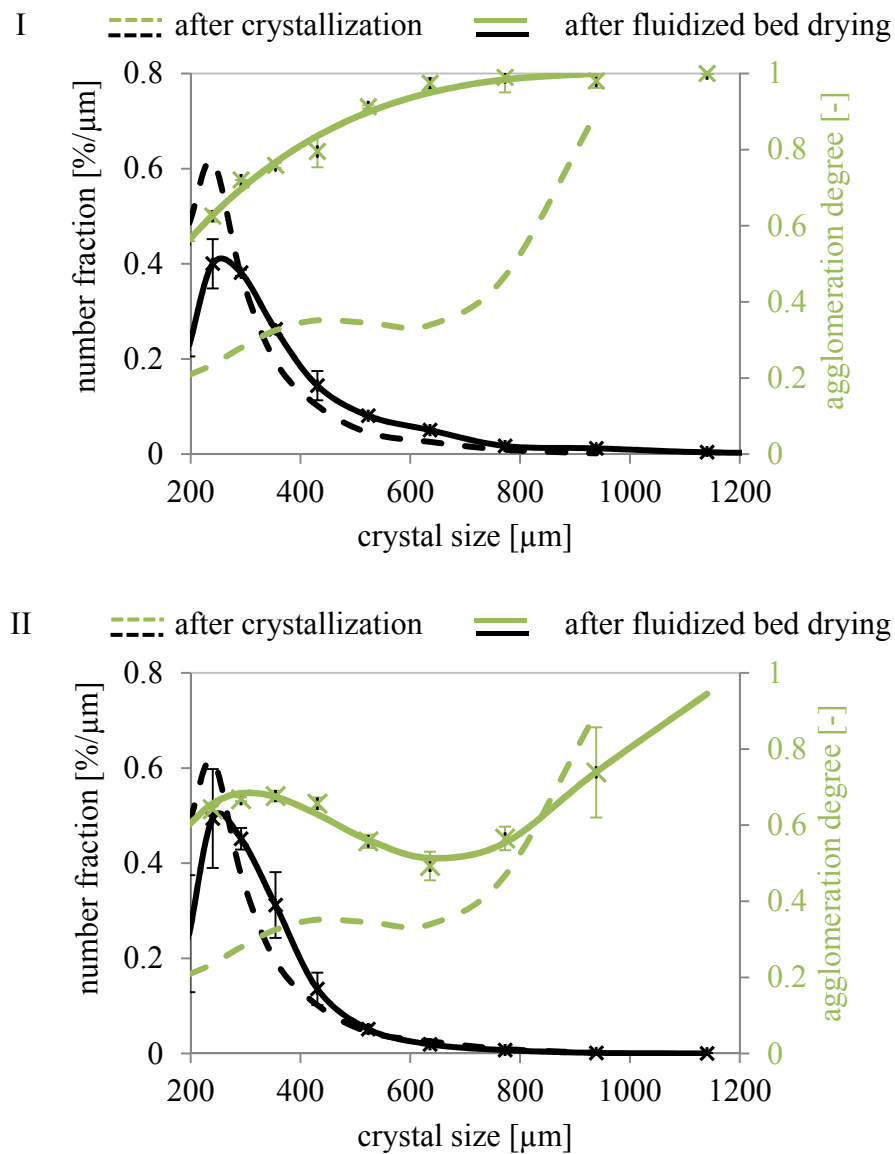


Figure A.17-part 1: CSDs and AgDs after fluidized bed drying (50 °C, 30 g, 31 m³/h) in comparison to the results after crystallization. I: unwashed, II: on wash cycle (40 mL ethanol/water (4/1)), III: two wash cycles (20 mL ethanol), IV: two wash cycles (40 mL ethanol)

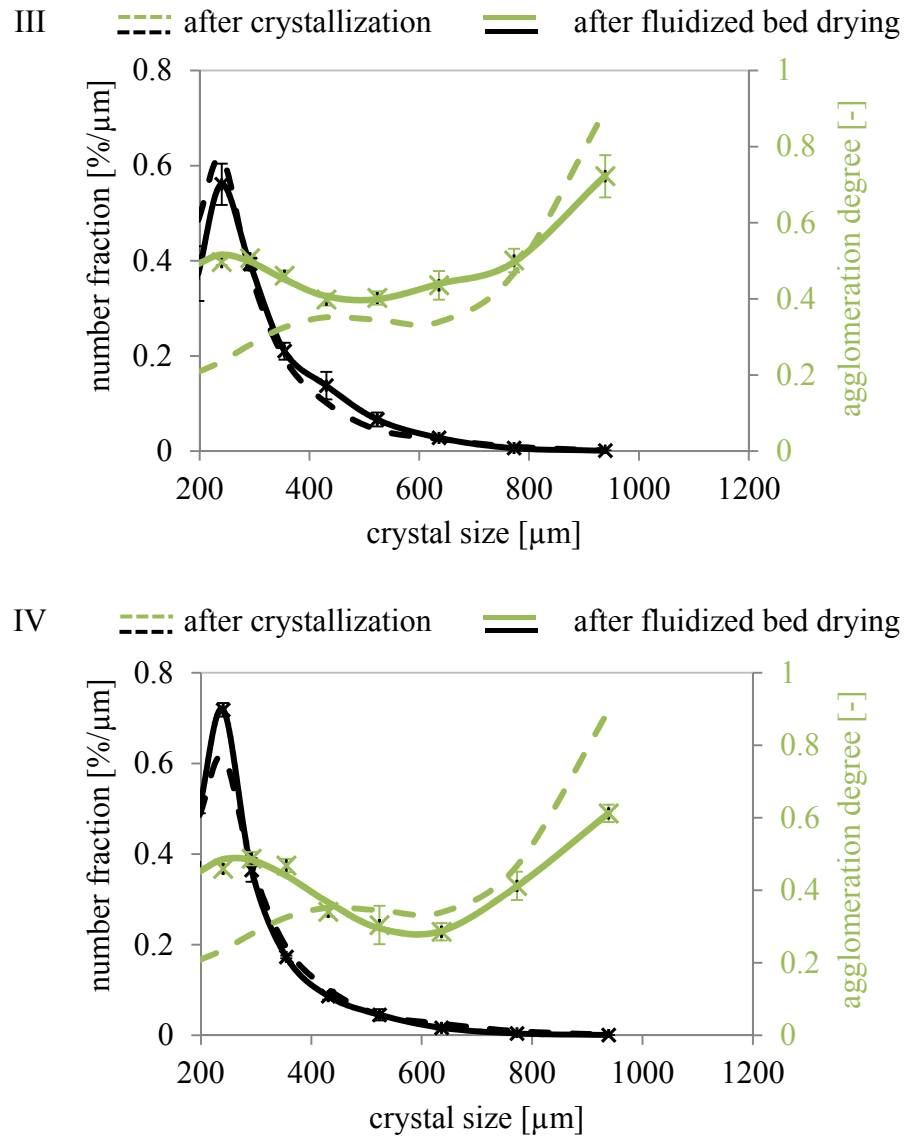


Figure A.17-part 2: CSDs and AgDs after fluidized bed drying (50 °C, 30 g, 31 m³/h) in comparison to the results after crystallization. I: unwashed, II: on wash cycle (40 mL ethanol/water (4/1)), III: two wash cycles (20 mL ethanol), IV: two wash cycles (40 mL ethanol)

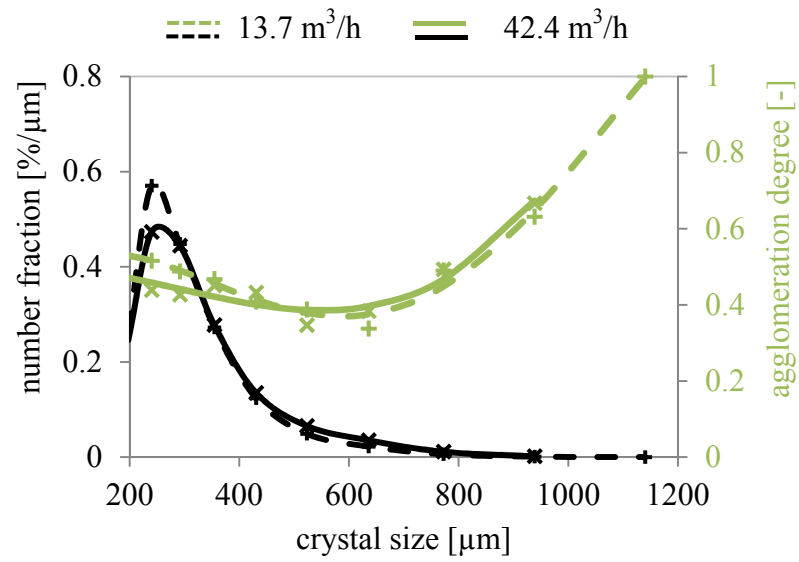


Figure A.18: CSDs and AgDs after fluidized bed drying: star experiments for the volume flow

Table A.11: Experimental design and results for static drying (L-alanine/ water)

systematic no.	experiment no.	(A) T_{drying} [°C]	(B) m_{drying} [g]	Ag [%]	d_{10} [μm]	d_{50} [μm]	d_{90} [μm]	$d_{90}-d_{10}$ [μm]
1	Ala-ST2	60	25	66.9	206	258	406	200
2	Ala-ST4	60	55	65.7	206	256	400	194
3	Ala-ST8	30	25	75.4	211	271	393	182
4	Ala-ST10	30	55	69.9	208	264	392	184
5	Ala-ST14	65	40	47.4	213	285	439	226
6	Ala-ST7	25	40	66.4	208	265	385	177
7	Ala-ST12	45	59.8	70.6	208	265	390	182
8	Ala-ST3	45	20.2	49.6	208	268	476	268
9	Ala-ST11	45	40	64.0	206	255	417	211
10	Ala-ST5	45	40	68.8	207	263	408	201
11	Ala-ST9	45	40	67.1	205	254	387	182
12	Ala-ST1	45	40	62.8	210	270	402	192
13	Ala-ST6	45	40	61.3	212	264	423	211
14	Ala-ST13	45	40	63.9	208	264	416	208

Table A.12: Experimental design and results for fluidized bed drying (L-alanine/ water)

systematic no.	experiment no.	(A) T_{drying} [°C]	(B) m_{drying} [g]	(C) \dot{V} [m ³ /h]	Ag [%]	d_{10} [μm]	d_{50} [μm]	d_{90} [μm]	$d_{90}-d_{10}$ [μm]
1	Ala-WS13	60	55	37.4	48.7	215	305	560	345
2	Ala-WS8	60	55	18.7	51.1	213	290	489	276
3	Ala-WS12	60	25	37.4	41.6	216	296	499	283
4	Ala-WS2	60	25	18.7	53.5	214	284	449	235
5	Ala-WS1	30	55	37.4	56.9	207	272	465	258
6	Ala-WS18	30	55	18.7	61.1	210	280	445	235
7	Ala-WS6	30	25	37.4	67.1	209	289	520	311
8	Ala-WS10	30	25	18.7	47.9	214	289	483	269
9	Ala-WS16	68	40	28	49.5	218	302	468	250
10	Ala-WS5	25	40	28	50.2	212	286	464	252
11	Ala-WS9	45	62.8	28	42.8	211	285	468	257
12	Ala-WS3	45	17.2	28	55.2	240	346	558	318
13	Ala-WS17	45	40	42.4	43.4	218	303	512	294
14	Ala-WS15	45	40	13.7	47.8	217	290	458	241
15	Ala-WS4	45	40	28	52.2	218	298	466	248
16	Ala-WS7	45	40	28	53.6	215	291	495	280
17	Ala-WS11	45	40	28	54.2	215	300	480	265
18	Ala-WS14	45	40	28	53.8	207	267	439	232
19	Ala-WS19	45	40	28	52.6	209	281	435	226
20	Ala-WS20	45	40	28	47.4	212	289	475	263

Table A.13: Experimental design and results for rotary tube drying (L-alanine/ water)

experiment no.	sequence no.	(A) T_{drying} [°C]	(B) m_{drying} [g]	(C) RS [rpm]	Ag [%]	d_{10} [μm]	d_{50} [μm]	d_{90} [μm]	$d_{90}-d_{10}$ [μm]
Ala-D1	15	34	29	21.7	45.5	235	360	597	362
Ala-D2	3	34	29	51.1	56.6	210	274	448	238
Ala-D3	18	56	29	21.7	51.1	219	305	488	269
Ala-D4	16	56	29	51.1	45.1	225	348	561	336
Ala-D5	4	34	51	21.7	47.0	230	348	527	297
Ala-D6	6	34	51	51.1	53.6	213	282	495	282
Ala-D7	5	56	51	21.7	61.4	218	301	484	266
Ala-D8	7	56	51	51.1	53.6	212	289	509	297
Ala-D9	14	45	40	15.7	52.2	223	343	586	363
Ala-D10	9	45	40	57.1	51.4	218	305	540	322
Ala-D11	13	30	40	36.4	56.8	221	393	618	397
Ala-D12	8	60	40	36.4	57.7	240	348	536	296
Ala-D13	10	45	25	36.4	48.8	234	347	528	294
Ala-D14	2	45	55	36.4	44.2	266	408	620	354
Ala-D15	11	45	40	36.4	56.2	230	351	568	338
Ala-D16	17	45	40	36.4	55.2	234	374	609	375
Ala-D17	12	45	40	36.4	57.9	216	325	568	352
Ala-D18	1	45	40	36.4	58.6	216	326	574	358

Material System I – Adipic acid/Water

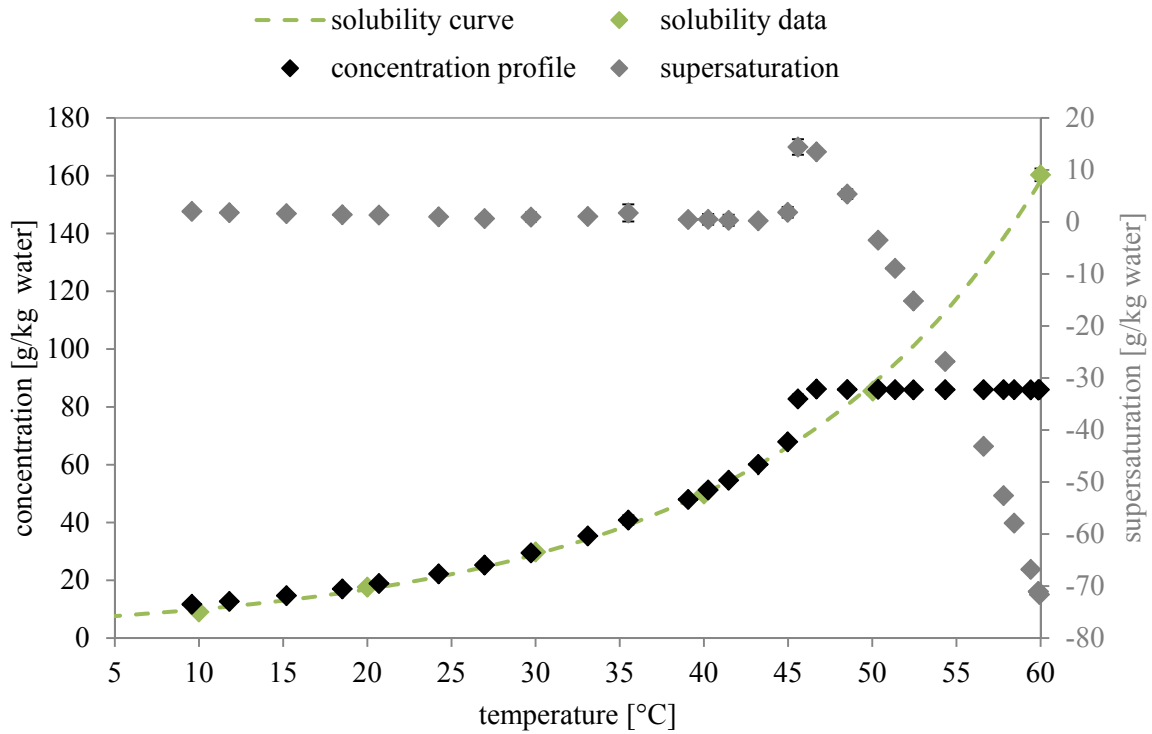


Figure A.19: Solubility and averaged concentration as well as supersaturation profile of cooling crystallizations without gassing of adipic acid in water (experimental conditions: $\kappa = 0.3$ K/min, $T_{\text{start}} = 60$ °C, $T_{\text{end}} = 10$ °C, $T_{\text{sat}} = 50$ °C, 210 rpm)

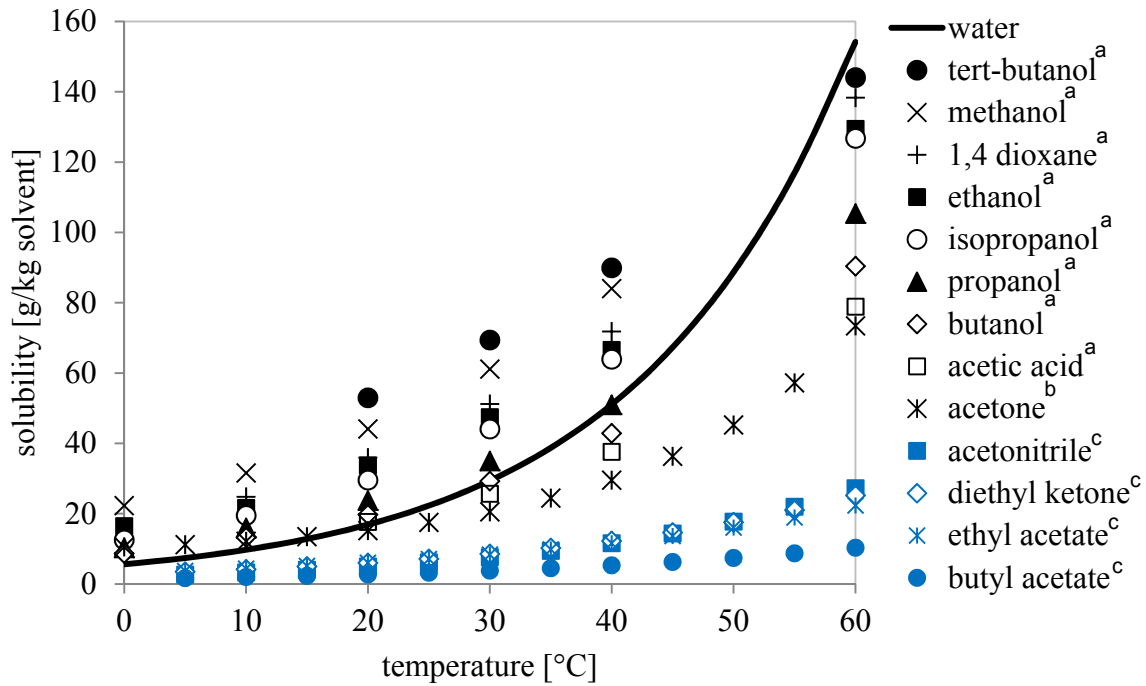


Figure A.20: Solubility of adipic acid in different solvents; extended data taken from a: [120], b: [121], and c: [122]

Table A.14: Experimental conditions and characteristic values of adipic acid product batches realized two times and analyzed after static drying with QICPIC (cp. Figure 6.3 and Figure 6.4)

		AA-ST1	AA-ST2	AA-ST3	AA-ST4
Downstream conditions					
Amount of wash liquid	[ml]	70	-	70	-
Number of wash cycles	[-]	2	-	2	-
Drying temperature	[°C]	22	22	50	50
Characteristic values					
Ag	[%]	58.2±1.0	58.9±2.1	60.2±0.1	66.0±2.9
d(Ag _{max})	[µm]	703±40	743±28	720±14	622±0
d ₁₀	[µm]	376±0	389±6	384±1	390±0
d ₅₀	[µm]	600± 5	606±2	616±5	647±5
d ₉₀	[µm]	882±11	893±2	938±1	1000±20
d ₉₀ -d ₁₀	[µm]	506±11	505±2	554±2	610±20

Table A.15: Experimental design for gassing crystallization (adipic acid/ water)*

experiment no.	sequence no.	(A) \dot{V}_{gassing} [L/h]	(B) $\Delta t_{\text{gassing}}$ [sec]	(C) T_{gassing} [°C]	(D) RS [rpm]
AA-G1	20	367	33	46	158
AA-G2	28	833	33	46	158
AA-G3	6	367	97	46	158
AA-G4	2	833	97	46	158
AA-G5	17	367	33	50	158
AA-G6	8	833	33	50	158
AA-G7	9	367	97	50	158
AA-G8	26	833	97	50	158
AA-G9	4	367	33	46	262
AA-G10	22	833	33	46	262
AA-G11	13	367	97	46	262
AA-G12	19	833	97	46	262
AA-G13	1	367	33	50	262
AA-G14	21	833	33	50	262
AA-G15	24	367	97	50	262
AA-G16	3	833	97	50	262
AA-G17	29	200	65	48	210
AA-G18	11	1000	65	48	210
AA-G19	25	600	10	48	210
AA-G20	18	600	120	48	210
AA-G21	30	600	65	46	210
AA-G22	15	600	65	50	210
AA-G23	12	600	65	48	120
AA-G24	10	600	65	48	300
AA-G25	16	600	65	48	210
AA-G26	14	600	65	48	210
AA-G27	7	600	65	48	210
AA-G28	23	600	65	48	210
AA-G29	27	600	65	48	210
AA-G30	5	600	65	48	210

* T_{sat} : 50 °C, κ : 0.3 K/min

Table A.16: Experimental results of the DoE for gassing crystallization (adipic acid/ water)

experiment no.	Ag [%]	d(Ag _{0.5}) [μm]	d(Ag _{0.9})-d(Ag _{0.5}) [μm]	d ₁₀ [μm]	d ₅₀ [μm]	d ₉₀ [μm]	d ₉₀ -d ₁₀ [μm]
AA-G1	62.9	303	308	405	632	1028	623
AA-G2	64.0	277	311	387	602	952	565
AA-G3	67.6	272	257	384	584	910	526
AA-G4	66.4	274	379	430	637	844	414
AA-G5	56.6	355	292	435	701	1039	604
AA-G6	54.8	349	471	382	602	885	503
AA-G7	56.1	363	321	428	683	1013	585
AA-G8	60.5	312	353	392	605	986	594
AA-G9	68.5	255	272	364	532	799	435
AA-G10	64.1	265	377	383	570	834	451
AA-G11	67.0	262	297	387	567	865	478
AA-G12	71.3	255	247	384	546	783	399
AA-G13	65.7	253	384	366	547	830	464
AA-G14	64.7	259	426	382	576	859	477
AA-G15	59.5	278	461	383	582	868	485
AA-G16	60.0	258	530	367	571	960	593
AA-G17	60.0	297	366	360	559	863	503
AA-G18	58.6	292	442	386	605	979	593
AA-G19	64.2	271	323	373	572	871	498
AA-G20	52.7	346	479	364	596	955	591
AA-G21	63.3	283	328	373	572	843	470
AA-G22	60.3	310	447	413	628	916	503
AA-G23	55.9	343	259	437	714	1076	639
AA-G24	59.4	265	603	376	584	907	531
AA-G25	62.3	290	371	360	553	866	506
AA-G26	57.9	309	441	382	587	916	534
AA-G27	58.0	334	386	408	625	929	521
AA-G28	58.4	322	391	362	564	875	513
AA-G29	58.9	316	429	388	604	924	536
AA-G30	59.0	303	396	388	607	919	531

References

- [1] Z. Yu, J. Chew, P. Chow, R. Tan, Recent Advances in Crystallization control, *Chemical Engineering Research and Design* 85 (2007) 893–905.
- [2] A. Ferreira, N. Faria, F. Rocha, J. Teixeira, Using an Online Image Analysis Technique to Characterize Sucrose Crystal Morphology during a Crystallization Run, *Industrial & Engineering Chemistry Research* 50 (2011) 6990–7002.
- [3] A. Lekhal, K.P. Girard, M.A. Brown, S. Kiang, B.J. Glasser, J.G. Khinast, Impact of agitated drying on crystal morphology: KCl-water system, *Powder Technology* 132 (2003) 119–130.
- [4] D. Binev, A. Seidel-Morgenstern, H. Lorenz, Study of crystal size distributions in a fluidized bed crystallizer, *Chemical Engineering Science* 133 (2015) 116–124.
- [5] J.-M. Kim, S.-M. Chang, K.-S. Kim, M.-K. Chung, W.-S. Kim, Acoustic influence on aggregation and agglomeration of crystals in reaction crystallization of cerium carbonate, *Colloids and Surfaces A: Physicochemical and Engineering Aspects* 375 (2011) 193–199.
- [6] K. Wohlgemuth, A. Kordylla, F. Ruether, G. Schembecker, Experimental study of the effect of bubbles on nucleation during batch cooling crystallization, *Chemical Engineering Science* 64 (2009) 4155–4163.
- [7] G. Ruecroft, D. Hipkiss, T. Ly, N. Maxted, P.W. Cains, Sonocrystallization: The Use of Ultrasound for Improved Industrial Crystallization, *Organic Process Research & Development* 9 (2005) 923–932.
- [8] F. Ruslim, B. Hoffner, H. Nirschl, W. Stahl, Evaluation of pathways for washing soluble solids, *Chemical Engineering Research and Design* 87 (2009) 1075–1084.
- [9] R. Polke, W. Herrmann, K. Sommer, Charakterisierung von Agglomeraten, *Chemie Ingenieur Technik* 51 (1997) 283–288.
- [10] E.M. Alander, M.S. Uusi-Penttilä, A.C. Rasmuson, Characterization of paracetamol agglomerates by image analysis and strength measurement, *Powder Technology* (2003) 298–306.

-
- [11] W. Beckmann (Ed.), *Crystallization: Basic concepts and industrial application*, 1st ed., Wiley-VCH Verlag, Weinheim, 2013.
- [12] G. Nichols, S. Byard, M.J. Bloxham, J. Botterill, N.J. Dawson, A. Dennis, V. Diart, N.C. North, J.D. Sherwood, A review of the terms agglomerate and aggregate with a recommendation for nomenclature used in powder and particle characterization, *Journal of Pharmaceutical Sciences* 91 (2002) 2103–2109.
- [13] T.A. Bell, Challenges in the scale-up of particulate processes - an industrial perspective, *Powder Technology* 150 (2005) 60–71.
- [14] D.J. am Ende (Ed.), *Chemical engineering in the pharmaceutical industry: R&D to Manufacturing*, John Wiley & Sons, New Jersey, 2011.
- [15] G. Hofmann, *Kristallisation in der industriellen Praxis*, Wiley-VCH Verlag, Weinheim, 2004.
- [16] A. Jones (Ed.), *Crystallization Process Systems*, Butterworth-Heinemann, Oxford, 2002.
- [17] J.W. Mullin, *Crystallization*, 4th ed., Butterworth-Heinemann, Oxford, 2001.
- [18] N. Rodriguez-hornedo, D. Murphy, Significance of controlling crystallization mechanisms and kinetics in pharmaceutical systems, *Journal of Pharmaceutical Sciences* 88 (1999) 651–660.
- [19] E.L. Paul, H.-H. Tung, M. Midler, Organic crystallization processes, *Powder Technology* 150 (2005) 133–143.
- [20] M.A. Lovette, A.R. Browning, D.W. Griffin, J.P. Sizemore, R.C. Snyder, M.F. Doherty, Crystal Shape Engineering, *Industrial & Engineering Chemistry Research* (2008) 9812–9833.
- [21] A. Mersmann, *Crystallization technology handbook*, 2nd ed., Marcel Dekker AG, New York, 2001.
- [22] A.Y. Lee, A.S. Myerson, Particle Engineering: Fundamentals of Particle Formation and Crystal Growth, *MRS Bulletin* 11 (2006) 881–886.
- [23] N. Variankaval, A.S. Cote, M.F. Doherty, From form to function: Crystallization of active pharmaceutical ingredients, *AIChE Journal* 54 (2008) 1682–1688.

-
- [24] B.A. Hendrickson, D.J. Grant, P. Meenan, D.A. Green (Eds.), Incorporation of structurally related Substances into paracetamol (acetaminophen) crystals, *Crystal Growth of Organic Materials. Conference Proceedings Series*, American Chemical Society, Washington DC, 1996.
- [25] H. Rumpf, Grundlagen und Methoden des Granulierens, *Chemie Ingenieur Technik* 30 (1958) 144–158.
- [26] H. Schubert, Principles of agglomeration, *Chemie Ingenieur Technik* 51 (1979) 266–277.
- [27] A.G. Walton, The formation and properties of precipitates, Wiley-VCH Verlag, New York, 1967.
- [28] M.v. Smoluchowski, Versuch einer mathematischen Theorie der Koagulationskinetik kolloider Lösungen, *Zeitschrift für Physikalische Chemie* 92 (1917) 129–168.
- [29] M. Brunsteiner, A.G. Jones, F. Pratola, S.L. Price, S.J.R. Simons, Toward a Molecular Understanding of Crystal Agglomeration, *Crystal Growth & Design* 5 (2005) 3–16.
- [30] F. Pratola, S. Simons, A.G. Jones, A Novel Experimental Device for Measurement of Agglomerative Crystallization Forces, *Chemical Engineering Research and Design* 80 (2002) 441–448.
- [31] J. Wójcik, A. Jones, Particle disruption of precipitated CaCO₃ crystal agglomerates in turbulently agitated suspensions, *Chemical Engineering Science* 53 (1998) 1097–1101.
- [32] P. Synowiec, A.G. Jones, P. Ayazi Shamlou, Crystal break-up in dilute turbulently agitated suspensions, *Chemical Engineering Science* 48 (1993) 3485–3495.
- [33] P. Barrett, B. Smith, J. Worlitschek, V. Bracken, B. O'Sullivan, Des O'Grady, A Review of the Use of Process Analytical Technology for the Understanding and Optimization of Production Batch Crystallization Processes, *Organic Process Research & Development* 9 (2005) 348–355.
- [34] M.R. Abu Bakar, Z.K. Nagy, A.N. Saleemi, C.D. Rielly, The Impact of Direct Nucleation Control on Crystal Size Distribution in Pharmaceutical Crystallization Processes, *Crystal Growth & Design* 9 (2009) 1378–1384.
- [35] J. Ulrich, C. Strege, Some aspects of the importance of metastable zone width and nucleation in industrial crystallizers, *Journal of Crystal Growth* 237-239 (2002) 2130–2135.

-
- [36] E. Aamir, Z.K. Nagy, C.D. Rielly, Evaluation of the Effect of Seed Preparation Method on the Product Crystal Size Distribution for Batch Cooling Crystallization Processes, *Crystal Growth & Design* 10 (2010) 4728–4740.
- [37] R. David, J. Villermaux, P. Marchal, J.-P. Klein, Crystallization and precipitation engineering—IV. Kinetic model of adipic acid crystallization, *Chemical Engineering Science* 46 (1991) 1129–1136.
- [38] P. Marchal, R. David, J.P. Klein, J. Villermaux, Crystallization and precipitation engineering—I. An efficient method for solving population balance in crystallization with agglomeration, *Chemical Engineering Science* 43 (1988) 59–67.
- [39] M. Fujiwara, Shan Cho, Paracetamol crystallization using laser backscattering and ATR-FTIR spectroscopy: metastability, agglomeration and control, *Crystal Growth & Design* 2 (2002) 363–370.
- [40] A. Warstat, J. Ulrich, Seeding during Batch Cooling Crystallization – An Initial Approach to Heuristic Rules, *Chemical Engineering & Technology* 29 (2006) 187–190.
- [41] N. Kubota, N. Doki, M. Yokota, A. Sato, Seeding policy in batch cooling crystallization, *Powder Technology* 121 (2001) 31–38.
- [42] Hem, Stanley, L., The effect of ultrasonic vibrations on crystallization processes, *Ultrasonics Sonochemistry* 5 (1967) 202–207.
- [43] L.J. McCausland, P.W. Cains, Martin P. D., Use the Power of Sonocrystallization for Improved Properties: High-intensity sound initiates nucleation and helps to control crystal size and habit to yield products that better meet users specifications, *Chemical Engineering Progress* 97 (2001) 56–61.
- [44] A. Abbas, M. Srour, P. Tang, H. Chiouc, H.K. Chan, J.A. Romagnoli, Sonocrystallization of sodium chloride particles for inhalation, *Chemical Engineering Science* 62 (2007) 2445–2453.
- [45] R.D. Dennehy, Particle Engineering Using Power Ultrasound 1, *Organic Process Research & Development* 7 (2003) 1002–1006.
- [46] H. Li, H. Li, Z. Guo, Y. Liu, The application of power ultrasound to reaction crystallization, *Ultrasonics Sonochemistry* 13 (2006) 359–363.
- [47] M. de Luque Castro, F. Priego Capote, Ultrasound-assisted crystallization (sonocrystallization), *Ultrasonics Sonochemistry* 14 (2007) 717–724.

-
- [48] L.J. McCausland, P.W. Cains, Ultrasound to make crystals, *Chemistry and Industry* (2003) 15–17.
- [49] E. Miyasaka, Y. Kato, M. Hagiwara, I. Hirasawa, Effect of ultrasonic irradiation on the number of acetylsalicylic acid crystals produced under the supersaturated condition and the ability of controlling the final crystal size via primary nucleation, *Journal of Crystal Growth* 289 (2006) 324–330.
- [50] O. Narducci, A.G. Jones, E. Koungoulos, Continuous crystallization of adipic acid with ultrasound, *Chemical Engineering Science* 66 (2011) 1069–1076.
- [51] C. Virone, H. Kramer, G.M. van Rosmalen, A.H. Stoop, T.W. Bakker, Primary nucleation induced by ultrasonic cavitation, *Journal of Crystal Growth* 294 (2006) 9–15.
- [52] Z. Zhang, D.-W. Sun, Z. Zhu, L. Cheng, Enhancement of Crystallization Processes by Power Ultrasound: Current State-of-the-Art and Research Advances, *Comprehensive Reviews in Food Science and Food Safety* 14 (2015) 303–316.
- [53] K. Wohlgemuth, *Induced Nucleation Process during Batch Cooling Crystallization*, Schriftenreihe Anlagen- und Prozesstechnik 5, Dr. Hut, München, 2012.
- [54] O.H. Rhein, DE-OS 2 438 627, 1967.
- [55] K. Wohlgemuth, F. Ruether, G. Schembecker, Sonocrystallization and crystallization with gassing of adipic acid, *Chemical Engineering Science* 65 (2010) 1016–1027.
- [56] V. Liotta, V. Sabesan, Monitoring and Feedback Control of Supersaturation Using ATR-FTIR to Produce an Active Pharmaceutical Ingredient of a Desired Crystal Size, *Organic Process Research & Development* 8 (2004) 488–494.
- [57] Z.K. Nagy, R.D. Braatz, Advances and New Directions in Crystallization Control, *Annual Review of Chemical and Biomolecular Engineering* 3 (2012) 55.
- [58] Z.K. Nagy, G. Fevotte, H. Kramer, L.L. Simon, Recent advances in the monitoring, modelling and control of crystallization systems, *Chemical Engineering Research and Design* 91 (2013) 1903–1922.
- [59] H. Takiyama, Supersaturation operation for quality control of crystalline particles in solution crystallization, *Advanced Powder Technology* 23 (2012) 273–278.
- [60] L. Svarovsky (Ed.), *Solid-Liquid Separation (Fourth Edition)*, Butterworth-Heinemann, Oxford, 2001.

-
- [61] H. Darcy, *Les Fontaines Publiques de la Ville de Dijon*, Dalmont, Paris, 1856.
- [62] S. Murugesan, P.K. Sharma, J.E. Tabora, *Design of Filtration and Drying Operations: in Chemical Engineering in the Pharmaceutical Industry: R&D to Manufacturing* (ed D. J. am Ende), John Wiley & Sons, Inc., Hoboken, NJ, USA (2010).
- [63] R. Wakeman, The influence of particle properties on filtration, *Separation and Purification Technology* 58 (2007) 234–241.
- [64] W.G.C.A. Siegfried Ripperger, "Filtration, 1. Fundamentals," in: *Ullmann's Encyclopedia of Industrial Chemistry*, 2011, accessed 11 May 2012.
- [65] W.L. McCabe, J.C. Smith, P. Harriott, *Unit Operations of Chemical Engineering*, 7th ed., McGraw-Hill, New York, 2005.
- [66] R. Beck, A. Häkkinen, D. Malthe-Sørensen, J.-P. Andreassen, The effect of crystallization conditions, crystal morphology and size on pressure filtration of l-glutamic acid and an aromatic amine, *Separation and Purification Technology* 66 (2009) 549–558.
- [67] B. Koglin, Einfluß der Agglomeration auf die Filtrierbarkeit von Suspensionen, *Chemie Ingenieur Technik* 56 (1984) 111–117.
- [68] H.B. Matthews, J.B. Rawlings, Batch crystallization of a photochemical: Modelling, control and filtration, *AIChE Journal* 44 (1998) 1119–1127.
- [69] A. Häkkinen, K. Pöllänen, M. Karjalainen, J. Rantanen, M. Louhi-Kultanen, L. Nynström, Batch cooling crystallization and pressure filtration of sulphathiazole: the influence of solvent composition, *Biotechnology & applied biochemistry* 41 (2005) 17–28.
- [70] D. Redeker, K.-H. Steiner, U. Esser, Das mechanische Entfeuchten von Filterkuchen, *Chemie Ingenieur Technik* 55 (1983) 829–839.
- [71] B. Hoffner, B. Fuchs, J. Heuser, Washing Processes for Disperse Particulate Systems - Process Spectrum and Aspects for the Process Choice, *Cemical & Engineering Technology* 27 (2004) 1065–1071.
- [72] A. Tomiak, Theoretical recoveries in filter cake reslurrying and washing, *AIChE Journal* 19 (1973) 76–84.
- [73] L. Cisternas, J. Cueto, R. Swaney, Flowsheet synthesis of fractional crystallization processes with cake washing, *Computers & Chemical Engineering* 28 (2004) 613–623.

-
- [74] F. Ruslim, H. Nirschl, W. Stahl, P. Carvin, Optimization of the wash liquor flow rate to improve washing of pre-deliqouered filter cakes, *Chemical Engineering Science* 62 (2007) 3951–3961.
- [75] F. Ruslim, J. Fleischer, H. Nirschl, U. Peuker, Filterkuchenwäsche zur Aufreinigung löslicher kristalliner Feststoffpartikel, 2006, accessed 15 May 2013.
- [76] F. Hardekopf, Experimentelle und theoretische Untersuchungen zum Waschen von Filterkuchen in Filterpressen, *Chemie Ingenieur Technik* 64 (1992) 1041–1044.
- [77] R.J. Wakeman, Washing thin and nonuniform filter cakes: effectsof wash liquor maldistribution, *Filtration and Separation* 35 (1998) 185–190.
- [78] J.H. Harker, J.R. Backhurst, J.F. Richardson, *Chemical Engineering*, 5th ed. 2, Butterworth-Heinemann, New York, 2013.
- [79] D. Gehrman, Trocknungstechnik, *Chemie Ingenieur Technik* 75 (2003) 1507–1514.
- [80] O. Kirscher, W. Kast, *Trocknungstechnik - Die wissenschaftlichen Grundlagen der Trocknungstechnik*, Springer, Berlin, 1992.
- [81] Evangelos Tsotsas, Volker Gnielinski, Ernst-Ulrich Schlünder, "Drying of Solid Materials," in: *Ullmann's Encyclopedia of Industrial Chemistry*, 2005, accessed 13 October 2015.
- [82] E.K. Sahni, B. Chaudhuri, Contact drying: A review of experimental and mechanistic modeling approaches, *International Journal of Pharmaceutics* 434 (2012) 334–348.
- [83] D. Gehrman, G. Esper, H. Schuchmann, *Trocknungstechnik in der Lebensmittelindustrie*, 1st ed., Behr's Verlag, Hamburg, 2009.
- [84] A.S. Mujumdar (Ed.), *Handbook of Industrial Drying*, 4th ed., CRC Press Taylor & Francis Group, London, New York, 2015.
- [85] V. Gnielinski, A. Mersmann, F. Thurner, *Verdampfun, Kristallisation, Trocknung*, Vieweg, Braunschweig, 1993.
- [86] M. Stieß, *Mechanische Verfahrenstechnik 2*, Springer, Berlin, Heidelberg, New York, 1993.
- [87] D. Geldart, Types of Gas Fluidization, *Powder Technology* 7 (1973) 285–292.
- [88] O. Molerus, Interpretation of Geldart's Type A, B, C, D Powdersby Taking Into Account Terparticle Cohesion Forces, *Powder Technology* 33 (1982) 81–87.

-
- [89] W.-C. Yang, *Handbook of Fluidization and Fluid-Particle Systems*, Marcel Dekker AG, New York, 2003.
- [90] K.R. Morris, S.L. Nail, G.E. Peck, S.R. Byrn, U.J. Griesser, J.G. Stowell, S. Hwang, K. Park, *Advances in pharmaceutical material and processing*, *Pharmaceutical Science & Technology Today* 6 (1998) 235–245.
- [91] F. Zeng, S. Zhu, F. Chen, Q. Gao, S. Yu, *Effect of different drying methods on the structure and digestibility of short chain amylose crystals*, *Food Hydrocolloids* 52 (2016) 721–731.
- [92] R.B. Keey, *Drying of Loose and Particulate Materials*, Hemisphere Publishing, New York, 1992.
- [93] C. Modugno, A.H. Paterson, J. McLeod, *Lactose Caking: Influence of the Particle Size Distribution and the Water Content*, *Procedia Engineering* 102 (2015) 114–122.
- [94] R. David, P. Marchal, J.-P. Klein, J. Villermaux, *Crystallization and precipitation engineering—III. A discrete formulation of the agglomeration rate of crystals in a crystallization process*, *Chemical Engineering Science* 46 (1991) 205–213.
- [95] K. Wohlgemuth, A. Kordylla, F. Ruether, G. Schembecker, *Experimental study of the effect of bubbles on nucleation during batch cooling crystallization*, *Chemical Engineering Science* 64 (2009) 4155–4163.
- [96] G. Ruecroft, D. Hipkiss, T. Ly, N. Maxted, P.W. Cains, *Sonocrystallization: The Use of Ultrasound for Improved Industrial Crystallization*, *Organic Process Research & Development* 9 (2005) 923–932.
- [97] S.M. Iveson, J.D. Litster, K. Hapgood, B.J. Ennis, *Nucleation, growth and breakage phenomena in agitated wet granulation processes: a review*, *Powder Technology* 117 (2001) 3–39.
- [98] K. Drauz, I. Grayson, A. Kleemann, H.-P. Krimmer, W. Leuchtenberger, C. Weckbecker, *Amino Acids*, in: *Ullmann's Encyclopedia of industrial chemistry*.
- [99] M.T. Musser, *Adipic Acid*, *Ullmann's Encyclopedia of Industrial Chemistry*, Wiley-VCH Verlag, Weinheim, 2005.
- [100] G. Caputo, R. Adami, E. Reverchon, *Supercritical Fluid Crystallization of Adipic Acid Using Urea as Habit Modifier*, *Crystal Growth & Design* 8 (2008) 2707–2715.
- [101] O. Narducci, A. Jones, E. Kougoulos, *Continuous crystallization of adipic acid with ultrasound*, *Chemical Engineering Science* 66 (2011) 1069–1076.

-
- [102] W. Kleppmann, Taschenbuch Versuchsplanung Produkte und Prozesse optimieren, 5th ed., Carl Hanser Verlag, München, 2008.
- [103] K. Backhaus, Multivariate Analysemethoden. Eine anwendungsorientierte Einführung, 12th ed., Springer Lehrbuch, Berlin, 2008.
- [104] A.C. Rencher, W.F. Christensen, Methods of Multivariate Analysis, 3rd ed., Wiley-VCH Verlag, 2012.
- [105] S. Heisel, Entwicklung eines Bildanalyse-Tools zur Bestimmung des Agglomerationsgrades von Kristallisaten, bachelor thesis, TU Dortmund University, Dortmund, 2013.
- [106] R.A. Granberg, D.G. Bloch, A.C. Rasmuson, Crystallization of paracetamol in acetone-water mixtures, *Journal of Crystal Growth* (1999) 1287–1293.
- [107] N. Faria, M. Pons, S. Feyo de Azevedo, F. Rocha, H. Vivier, Quantification of the morphology of sucrose crystals by image analysis, *Powder Technology* 133 (2003) 54–67.
- [108] M.-N. Pons, H. Vivier, J. Dodds, Particle shape characterization using morphological descriptors, *Particle & Particle Systems Characterization* 14 (1997) 272–277.
- [109] Z.Q. Yu, R.B. Tan, P.S. Chow, Effects of operating conditions on agglomeration and habit of paracetamol crystals in anti-solvent crystallization, *Journal of Crystal Growth* (2005) 477–488.
- [110] A. Ferreira, N. Faria, F. Rocha, S. Feyo de Azevedo, A. Lopes, Using Image Analysis to Look into the Effect of Impurity Concentration in NaCl Crystallization, *Chemical Engineering Research and Design* 83 (2005) 331–338.
- [111] A.-F. Blandin, A. Rivoire, D. Mangin, J.-P. Klein, J.-M. Bossoutrot, Using In Situ Image Analysis to Study the Kinetics of Agglomeration in Suspension 17 (2000) 16–20.
- [112] L.-M. Terdenge, S. Heisel, G. Schembecker, K. Wohlgemuth, Agglomeration degree distribution as quality criterion to evaluate crystalline products, *Chemical Engineering Science* 133 (2015) 157–169.
- [113] A. Ferreira, G. Pereira, J. Teixeira, F. Rocha, Statistical tool combined with image analysis to characterize hydrodynamics and mass transfer in a bubble column, *Chemical Engineering Journal* 180 (2012) 216–228.

-
- [114] X. Bai, C. Sun, Z. Fugen, Splitting touching cells based on concave points and ellipse fitting, *Pattern Recognition* (2009) 2434–2446.
- [115] G. Cong, B. Parvin, Model-based segmentation of nuclei, *Pattern Recognition* (2000) 1383–1393.
- [116] T. Kovacevic, A. Reinhold, H. Briesen, Shape identification of primary particles in crystal aggregates, 19th International Symposium on Industrial Crystallization (2014).
- [117] Ian M. Smallwood, *Solvent Recovery Handbook*, 2nd ed., Blackwell Science, Oxford, 2002.
- [118] R.M. Stephenson, Mutual Solubilities: Water-Ketone, Water-Ethers, and Water-Gasoline-Alcohols, *Journal of Chemical and Engineering Data* 37 (1992) 80–95.
- [119] J.A. Kossuch, Influence of gassing crystallization on the agglomeration degree of crystalline products, master thesis, TU Dortmund University, Dortmund, 2015.
- [120] A.N. Gaivoronskii, V.A. Granzhan, Solubility of Adipic Acid in Organic Solvents and Water, *Russian Journal of Applied Chemistry* 78 (2005) 404–408.
- [121] D. Wei, W. Cao, Solubility of Adipic Acid in Acetone, Chloroform, and Toluene, *Journal of Chemical and Engineering Data* 54 (2009) 152–153.
- [122] K. Henke, Experimentelle Untersuchungen zur Keimbildung bei der Kristallisation von Adipinsäure, diploma thesis, TU Dortmund University, Dortmund, 2008.

List of Figures

Figure 2.1:	Solubility, supersaturation, and metastable zone.....	4
Figure 2.2:	Limits of the metastable zone in dependence of the nucleation mechanism [8].....	5
Figure 2.3:	Impact of the filter cake formation on cake washing.....	13
Figure 2.4:	Drying curves: Moisture content in dependence of time (left), Drying rate in dependence of time (right)	15
Figure 2.5:	States of fluidized beds	17
Figure 3.1:	(I) Solubility of L-alanine in water [53], (II) SEM image of L-alanine crystallized out of water	20
Figure 3.2:	(I) Solubility of adipic acid in water, (II) SEM image of adipic acid crystallized out of water.....	20
Figure 3.3:	CSDs measured by laser diffraction of static dried L-alanine product batches filtered with Büchner funnel set up.....	22
Figure 3.4:	Self-constructed filtration system: (A) Overview, (B) Side view of filter cake, (C) Top view of filter cake	23
Figure 3.5:	CSDs measured by laser diffraction of static dried L-alanine product batches filtered with the self-constructed filtration system	24
Figure 3.6:	Self-constructed drying tube: (A) front view (B) interior view.....	25
Figure 3.7:	Central composite design for three factors (A, B, and C).....	28
Figure 3.8:	Schematic principle of Discriminant Factor Analysis (DFA) for two groups (displayed as blue and red dots) and two characteristic variables (X_1 , X_2).....	31
Figure 3.9:	Results of factor analysis: (I) factor matrix without processing, (II) with varimax algorithm rotated factor matrix, sorted by values, and an indicator threshold value of 0.5.....	32
Figure 4.1:	Schematic diagram of the agglomeration degree distribution (AgD) and crystal size distribution (CSD).....	36

Figure 4.2:	Characterization and comparison of AgDs by means of the characteristic values $d(Ag_{0.5})$ and $d(Ag_{0.9})-d(Ag_{0.5})$	36
Figure 4.3:	Flow chart to determine the AgD of a crystalline product batch.....	39
Figure 4.4:	Composition of the training sets T1, T2, and T3	41
Figure 4.5:	Influence of the number of image descriptors on mean PI (left) and mean δAg (right).....	46
Figure 4.6:	Transfer potential of variant 5 (5 image descriptors)	48
Figure 4.7:	Transfer potential of variant 12 (7 image descriptors)	49
Figure 4.8:	CSDs and AgDs of the crystalline product batches Ala-2 (I) and Ala-3 (II).....	54
Figure 4.9:	CSD and AgD of the crystalline product batches AA-1 (I) and AA-2 (II).....	56
Figure 4.10:	Setup of the measurement system for image recording of crystals in suspension using the QICPIC	60
Figure 4.11:	Schematic illustration of measures needed for the computation of the image descriptors number of concave points (nConc), maximal concavity depth (MaxDepth), and centroid distance (dCentroid).....	61
Figure 4.12:	Transfer potential of the discriminant function using image descriptor combination: elongation, solidity, area fraction, equivalent diameter, and number of concave points for L-alanine crystals in suspension.....	63
Figure 4.13:	CSDs and AgDs of the same L-alanine crystalline product batch analyzed with the scanner (dried product) and the QICPIC (resuspended product).....	64
Figure 4.14:	Averaged distribution of crystalline particles on the groups single crystal, agglomerates, and waste for the image descriptor combination D_{AA-0}	67
Figure 4.15:	Averaged distribution of crystalline particles on the groups single crystal, agglomerates, and waste for the image descriptor combination D_{AA-3}	67
Figure 5.1:	CSD and AgD of L-alanine/water measured directly after crystallization out of suspension with QICPIC.....	72

Figure 5.2:	SEM images of statically dried L-alanine crystals	75
Figure 5.3:	Ag and d_{90} - d_{10} of L-alanine crystalline product batches after crystallization and drying depending on the number of wash cycles and amount of wash liquid used	76
Figure 5.4:	CSDs and AgDs after static drying (50 °C, 30 g) in comparison to the results after crystallization.	78
Figure 5.5:	CSDs and AgDs of the star experiments of the DoE for static drying	82
Figure 5.6:	Contour plots for the significant factor interactions of fluidized bed drying	85
Figure 5.7:	CSDs and AgDs of crystalline product batches after fluidized bed drying: variation of the volume flow	87
Figure 5.8:	CSDs and AgDs of crystalline product batches after fluidized bed drying: variation of the amount of feed material	88
Figure 5.9:	Contour plots for the significant factor interactions of rotary tube drying	91
Figure 5.10:	CSDs and AgDs of crystalline product batches after rotary tube drying: comparison of center point experiments (dashed lines) with the star experiments (solid lines) of the amount of feed material.....	93
Figure 5.11:	CSDs and AgDs of crystalline product batches after rotary tube drying: variation of the rotational speed	95
Figure 5.12:	Ag and d_{90} - d_{10} of L-alanine crystalline product batches after crystallization, static drying, fluidized bed drying, and rotary tube drying	96
Figure 6.1:	CSD and AgD of adipic acid/water measured directly after crystallization out of suspension with QICPIC.....	100
Figure 6.2:	Impact of the amount of acetonitrile used for cake washing on the displacement of water out of the filter cake.....	103
Figure 6.3:	CSDs and AgDs after static drying at 22 °C in comparison to the results after crystallization measured with QICPIC. I: AA-ST1, two wash cycles with 70 mL acetonitrile each; II: AA-ST2, unwashed.....	105

Figure 6.4:	CSDs and AgDs after static drying at 50 °C in comparison to the results after crystallization measured with QICPIC. I: AA-ST3, two wash cycles with 70 mL acetonitrile each; II: AA-ST4, unwashed.....	106
Figure 6.5:	CSDs and AgDs of adipic acid product batches: (I) impact of gassing supersaturation, (II) impact of stirring rate.....	112
Figure 6.6:	Correlation between the width of the CSD (d_{90} - d_{10}) and the characteristic diameters d_{10} and d_{90} of all data points of the DoE	116
Figure 6.7:	Contour plots for the significant factor interactions for d_{90} - d_{10}	116
Figure 6.8:	Experimental results for d_{90} - d_{10} and Ag of all experiments.....	118
Figure A.1:	Corresponding cooling profiles of crystallization to the CSDs depicted in Figure 3.3 of static drying crystalline product batches	123
Figure A.2:	Corresponding concentration profiles of crystallization to the CSDs depicted in Figure 3.3 of static drying crystalline product batches	123
Figure A.3:	Transfer potential of variant 13 (8 image descriptors)	127
Figure A.4:	Transfer potential of variant 15 (14 image descriptors)	128
Figure A.5:	Transfer potential of variant 12+ (8 image descriptors)	129
Figure A.6:	Transfer potential of variant 13+ (9 image descriptors)	130
Figure A.7:	Classification results of the crystalline product batch Ala-2 depicted as trace plots for the image descriptors equivalent diameter, elongation, standard deviation of grayscale values, and equivalent diameter, solidity, standard deviation of grayscale values	131
Figure A.8:	Classification results of the crystalline product batch Ala-2 depicted as trace plots for the image descriptors equivalent diameter, elongation, area fraction, and equivalent diameter, solidity, area fraction.....	132
Figure A.9:	Classification results of the crystalline product batch Ala-2 depicted as trace plots for the image descriptors equivalent diameter, elongation, solidity and equivalent diameter, area fraction, standard deviation of grayscale values.....	133
Figure A.10:	Images of single crystals, agglomerates, and waste particles recorded with the QICPIC for the material system adipic acid/ water	133

Figure A.11:	Transfer potential for variant D_{AA-0}	134
Figure A.12:	Transfer potential for variant D_{AA-1}	135
Figure A.13:	Averaged distribution of crystalline particles on the groups single crystal, agglomerates, and waste for the image descriptor combination D_{AA-1}	135
Figure A.14:	Averaged distribution of crystalline particles on the groups single crystal, agglomerates, and waste for the image descriptor combination D_{AA-2}	136
Figure A.15:	Transfer potential for variant D_{AA-2}	136
Figure A.16:	Transfer potential for variant D_{AA-3}	137
Figure A.17:	CSDs and AgDs after fluidized bed drying (50 °C, 30 g, 31 m ³ /h) in comparison to the results after crystallization.	139
Figure A.18:	CSDs and AgDs after fluidized bed drying: star experiments for the volume flow	140
Figure A.19:	Solubility and averaged concentration as well as supersaturation profile of cooling crystallizations without gassing of adipic acid in water.....	144
Figure A.20:	Solubility of adipic acid in different solvents.....	144

List of Tables

Table 3.1:	Characteristic values of L-alanine product batches produced under same conditions for all process steps, filtered with Büchner funnel set up.....	23
Table 3.2:	Characteristic values of L-alanine product batches produced under same conditions for all process steps, filtered with the self-constructed filtration system.....	24
Table 4.1:	Washing and drying parameters of the crystalline product batches investigated for the development of the image analysis tool.....	37
Table 4.2:	Results of DFA for the data sets Ala-1a and Ala-2b in dependence of the training sets (1000 particles) used.....	43
Table 4.3:	Results of factor analysis for L- alanine data sets	44
Table 4.4:	Variants of image descriptor combinations	45
Table 4.5:	Characteristic values of CSD and AgD for the crystalline product batches Ala-2 and Ala-3	55
Table 4.6:	Characteristic values of CSD and AgD for the crystalline product batches AA-1 and AA-2	57
Table 4.7:	Composition of L-alanine trainings sets for QICPIC reference discriminant function	62
Table 4.8:	Characteristic values of the same crystalline product batch analyzed with the transmitted light scanner and the QICPIC	64
Table 4.9:	Composition of adipic acid (AA) trainings sets for QICPIC reference discriminant function	65
Table 4.10:	Image descriptor combinations of QICPIC discriminant functions tested for the material system adipic acid/ water.....	66
Table 4.11:	Averaged classification results for the image descriptor combinations $D_{AA-0} - D_{AA-3}$	66
Table 5.1:	Characteristic values of the L-alanine product batches directly after crystallization.....	72

Table 5.2:	Viscosity ratio, solubility of water, and wash results of potential wash liquids for the material system L-alanine/ water	73
Table 5.3:	Factors (A-B) and levels investigated for static drying	81
Table 5.4:	Effects on the responses for static drying	81
Table 5.5:	Factor levels and responses of the star experiments	83
Table 5.6:	Factors (A-C) and levels investigated for fluidized bed drying.....	84
Table 5.7:	Effects on the responses for fluidized bed drying.....	85
Table 5.8:	Factors (A-C) and levels investigated for rotary tube drying	90
Table 5.9:	Effects on the responses for rotary tube drying	90
Table 6.1:	Characteristic values of adipic acid product batches directly after crystallization.....	100
Table 6.2:	Viscosity ratio, solubility of water, and wash results of potential wash liquids for the material system adipic acid/ water	102
Table 6.3:	Factors (A-D) and levels investigated for gassing crystallizations of adipic acid	108
Table 6.4:	Effects of factors, factor interactions, and nonlinearities on the responses for gassing crystallization of adipic acid/ water.....	110
Table 6.5:	Factor levels and results of the responses d_{90} - d_{10} and A_g for product quality control	117
Table 6.6:	Adjustable range for A_g and d_{90} - d_{10} of gassing crystallizations in comparison of cooling crystallization results without gassing at 210 rpm	119
Table A.1:	Filtration/washing* and drying conditions of CSDs depicted in Figure 3.3 and Figure 3.5 of static dried L-alanine product batches	123
Table A.2:	Thermal history of L-alanine/water crystallizations	124
Table A.3:	Constant crystallization conditions of the material system L-alanine/water	124
Table A.4:	Thermal history of the adipic acid/water crystallizations	124

Table A.5:	Constant crystallization conditions of the material system adipic acid/water.....	124
Table A.6:	Constant gassing crystallization conditions of the adipic acid crystalline product batches AA-1 and AA-2.....	124
Table A.7:	Primary (numbers 1-8), secondary (numbers 9-18), and grayscale image descriptors (numbers 19-22)	125
Table A.8:	Composition of the training sets Ala-1a and Ala-2a.....	127
Table A.9:	Gassing experiments of the material system adipic acid/ water used for the creation of the training sets	134
Table A.10:	Solubility of L-alanine in different solvents measured two times	137
Table A.11:	Experimental design and results for static drying (L-alanine/ water).....	141
Table A.12:	Experimental design and results for fluidized bed drying (L-alanine/ water)	142
Table A.13:	Experimental design and results for rotary tube drying (L-alanine/ water)	143
Table A.14:	Experimental conditions and characteristic values of adipic acid product batches realized two times and analyzed after static drying with QICPIC	145
Table A.15:	Experimental design for gassing crystallization (adipic acid/ water).....	146
Table A.16:	Experimental results of the DoE for gassing crystallization (adipic acid/ water)	147

Curriculum Vitae

Personal Details

Name: Lisa-Marie Terdenge
Date of birth: November 6th, 1986
Place of birth: Recklinghausen, Germany
Nationality: German

Professional Experience

03/2012 – 05/2015 Scientific assistant and Ph.D. student
Laboratory of Plant and Process Design, TU Dortmund
University, Dortmund
08/2010 – 11/2010 Internship in the department of Chemical and Process
Engineering, BASF SE, Ludwigshafen
07/2006 – 09/2006 Internship in the field processing of metallic materials
Kreitzler Industriebühnen GmbH, Witten

Education

10/2006 – 11/2011 Academic studies of Biochemical Engineering
Department of Biochemical and Chemical Engineering,
TU Dortmund University, Dortmund
08/1997 – 06/2006 Secondary school, Gymnasium Essen-Überruhr, Essen
08/1993 – 07/1997 Primary school, Johann-Peter-Hebel Schule, Essen



Lisa-Marie Terdenge

In crystallization a high effort for optimization and process control is made to achieve the desired quality characteristics of crystalline products. The quality is defined by the crystal form and size, the crystal size distribution (CSD), and purity. The CSD e.g. is an important quality criterion for filterability and flowability. In general, the CSD is characterized by characteristic values, like median crystal size d_{50} or width of CSD $d_{90}-d_{10}$. However, no information about the particle morphology or the amount of agglomerates is given by these characteristic values. This lack of information in CSD can lead to misunderstand the crystallization process, especially when agglomeration takes place during solid-liquid separation or drying, and an off-line CSD measurement technique is used.

Therefore, in this thesis the agglomeration degree distribution (AgD) is introduced as new quality criterion to allow a quantitative characterization and comparison of crystalline product batches with different morphology. By using the AgD clear statements whether a material system tends to agglomerate during crystallization and/or downstream process can be made on basis of simple experiments.

Furthermore, in order to increase the understanding of agglomeration and to provide insights into the relevance for holistic process design, the agglomeration behavior of two material systems, characterized by different crystal habit and d_{50} , is systematically investigated.